



UNIVERSIDAD NACIONAL AUTÓNOMA DE MÉXICO

POSGRADO EN INGENIERÍA ELÉCTRICA

FACULTAD DE INGENIERÍA

DESARROLLO Y CARACTERIZACIÓN
DE UN PROTOTIPO DE DETECTOR DE
PARTÍCULAS CARGADAS EMPLEADO
EN ESTUDIOS DE HACES
RADIOACTIVOS

TESIS

QUE PARA OBTENER EL GRADO ACADÉMICO DE

**MAESTRA EN INGENIERÍA ELÉCTRICA
(INSTRUMENTACIÓN)**

P R E S E N T A

AVRIL ALICIA MEZA OLIVO

Director de Tesis: Dr. Roberto Ortega Martínez.
Tutor específico: Dr. Alfredo Galindo-Uribarri.

MÉXICO, D.F.

FEBRERO, 2012

RESUMEN

La presente Tesis de Maestría tiene su aplicación en, más no se limita a, el campo de la Física Nuclear, específicamente, en el estudio de las propiedades de núcleos radioactivos, producidos a partir de reacciones nucleares generadas mediante el uso de aceleradores de partículas.

Dentro de la Física Nuclear, la espectroscopía de rayos gamma ha demostrado ser una herramienta invaluable para lograr descubrimientos acerca de la estructura básica de la materia. Una de las técnicas experimentales más útiles para llevar a cabo espectroscopía nuclear en laboratorios dedicados al estudio de haces radioactivos alrededor del mundo, consiste en la *operación conjunta* de espectrómetros de rayos gamma de alta resolución y diversos sistemas auxiliares de detección de partículas, pues la combinación de ambos tipos de detectores permite explotar al máximo las capacidades de la espectroscopía de rayos gamma; proporcionando información muy detallada acerca de los haces radioactivos bajo observación. Ejemplos de los espectrómetros de rayos gamma más sofisticados en la actualidad son GRETINA en Estados Unidos [1] y AGATA Demonstrator Array en Europa [2].

Los estudios aquí reportados son de gran interés en el desarrollo de una nueva generación de *detectores de partículas cargadas*, que puedan funcionar como instrumentos auxiliares a las técnicas de espectroscopía de rayos gamma más actuales.

El objetivo a largo plazo de este proyecto consiste en contar con un instrumento que sea capaz de detectar en tiempo real las diversas partículas emitidas durante reacciones nucleares (generadas mediante aceleradores de partículas) que involucren haces radioactivos. Por lo tanto, dicho instrumento debe contar con características tales como: tamaño y masa pequeños (pues se pretende que funcione en el interior de un espectrómetro de rayos gamma y debe influir lo menos posible en la espectroscopía de rayos gamma), debe ser insensible a campos magnéticos en la mayor medida posible, debe tener buena resolución de energía, amplio rango dinámico (1-50 MeV) y debe proporcionar información de la posición con la que las partículas cargadas son emitidas en una reacción nuclear dada. Además, el sistema de adquisición y procesamiento de los datos provenientes del detector también debe diseñarse de tal forma que influya lo menos posible en la espectroscopía gamma.

En el presente trabajo, hemos propuesto y caracterizado un nuevo prototipo de detector de partículas cargadas basado en los principios de detectores de centelleo. Debido a las razones que se explican a lo largo de este texto, el prototipo propuesto consiste en el uso de un cristal centellador, inorgánico, “yoduro de cesio activado con talio” CsI(Tl); acoplado a un Fotomultiplicador de Silicio (SiPM, por sus siglas en inglés).

Dicho prototipo ha sido hasta ahora caracterizado utilizando únicamente isótopos radioactivos en reposo; es decir, fuera de la línea de operación de un acelerador de partículas. Esto debido a que el principal objetivo de esta Tesis consistió en verificar la capacidad de respuesta del SiPM a partículas cargadas, y estudiar su viabilidad para operar satisfactoriamente bajo las condiciones antes descritas. En términos generales, la investigación aquí reportada constituye el primer paso hacia la futura implementación y operación de un detector de partículas cargadas que funcione como instrumento auxiliar en espectroscopía nuclear de haces radioactivos. Esta primera investigación es esencial pues delimita los parámetros a considerar para la futura construcción del detector, dado que el arreglo que aquí proponemos no ha sido anteriormente empleado para esta aplicación. Dicha implementación y puesta en marcha del detector operando en tiempo real dentro de un acelerador de partículas es parte del trabajo futuro de este proyecto.

Por otro lado, la caracterización de nuestro prototipo ha sido llevada a cabo haciendo uso tanto de instrumentación analógica, como digital; por lo que esta Tesis aborda también un detallado estudio del procesamiento de señales aplicado en Física Nuclear; haciendo especial énfasis en las ventajas que el procesamiento digital proporciona para satisfacer los requerimientos de implementación y operación del prototipo.

De manera general, el procesamiento de pulsos provenientes de detectores de radiación se compone de las siguientes etapas: (1) pre-amplificación (o acondicionamiento) del pulso, (2) filtrado o “formador” del pulso, (3) discriminación de eventos y (4) almacenamiento y análisis de eventos.

Para efectos de esta Tesis, la etapa de filtrado del pulso ha sido instrumentada tanto analógica como digitalmente, dando así lugar a dos arreglos experimentales distintos.

El primer arreglo experimental (filtrado analógico) consistió en conectar la salida del preamplificador a un amplificador espectroscópico, seguido de un dispositivo denominado analizador multicanal para la discriminación y análisis de eventos.

En el segundo arreglo experimental (filtrado digital), la salida del pre-amplificador se conecta a un osciloscopio digital encargado de las funciones de digitalización, discriminación y adquisición de eventos; seguido de la conexión vía Ethernet hacia una computadora personal, donde, mediante el uso del software MATLAB®, diversos algoritmos de filtrado, y análisis de los datos fueron realizados.

Igualmente, para el desarrollo de esta Tesis, este segundo arreglo experimental fue suficiente para efectos de caracterización del prototipo, así como para el estudio de las técnicas de procesamiento digital de señales; sin embargo, una vez que el detector de partículas cargadas final sea construido; dicho procesamiento será implementado digitalmente mediante *procesadores digitales portables*, como son, por ejemplo, los denominados DSPs (Digital Signal Processors) o bien los FPGAs (Field Programmable Gate Arrays), dispositivos que se explican en el Capítulo 2. Dicha implementación digital, en conjunto con las propiedades intrínsecas del prototipo propuesto proporcionará al detector de partículas cargadas características tales como portabilidad (debido a su tamaño), sensibilidad a la posición, reducción en el ruido asociado a la electrónica e inmunidad a campos magnéticos, entre otras; permitiendo así la óptima operación del detector de partículas cargadas dentro de la línea de operación del acelerador de partículas.

Un tercer sistema de instrumentación fue probado: el sistema de procesamiento digital de pulsos desarrollado exclusivamente para el experimento internacional GRETINA [1]. Sin embargo, este digitalizador fue empleado con propósitos meramente didácticos, con el objeto de conocer los estándares de instrumentación utilizados en Física Nuclear; así como de adquirir una idea general de los *sistemas reales de gran escala* empleados en este tipo de experimentos; por lo que poco análisis de datos fue realizado con esta instrumentación.

Todos los experimentos y pruebas que componen esta Tesis fueron realizados en el complejo Holifield Radioactive Ion Beam Facility (HRIBF), perteneciente al Laboratorio Nacional de Oak Ridge (Oak Ridge National Laboratory), en Estados Unidos, y esta investigación está patrocinada por la Oficina de Física Nuclear del Departamento de Energía de los Estados Unidos de América.

El presente trabajo ha sido presentado en diversos congresos y seminarios estudiantiles, así como en el 22º Congreso General de la Comisión Internacional para Óptica (22nd

General Congress of the International Commission for Optics, ICO 2011), llevado a cabo en Puebla, México; en Agosto de 2011 (ver páginas 201-203 y Ref. [98]).

La información contenida en este texto se ha organizado de la siguiente manera:

En el Capítulo 1 se presenta una breve introducción acerca de la Física Nuclear de iones pesados, junto con los métodos experimentales más comúnmente usados en este campo, cubriendo algunas definiciones básicas concernientes a los detectores de radiación, sus propiedades generales, algunos de los tipos de detectores existentes; así como una breve descripción de las técnicas analógicas utilizadas en el procesamiento de las señales.

En el Capítulo 2 se presentan las etapas que componen el procesamiento de pulsos provenientes de detectores de radiación, iniciando con una descripción general de los bloques que integran cada etapa y las consideraciones electrónicas más importantes que deben tenerse en cuenta para su instrumentación. En este capítulo se da especial énfasis a las técnicas empleadas en el *procesamiento digital* de señales en aplicaciones de Física Nuclear, incluyendo una breve presentación de los dispositivos más comúnmente utilizados para implementar el procesamiento digital de pulsos, tales como ASICs (Application-Specific Integrated Circuits), los DSPs (Digital Signal Processors) y los FPGAs (Field Programmable Gate Arrays). Y finalmente se presenta una extensa comparación entre los métodos de procesamiento analógico y digital utilizados en aplicaciones de Física Nuclear.

El Capítulo 3 consiste en la descripción detallada del arreglo de partículas cargadas propuesto para fines de esta Tesis, así como de la instrumentación utilizada en la caracterización de dicho arreglo.

En el Capítulo 4 se presenta el análisis y discusión de los resultados obtenidos. Y finalmente, se proporcionan las conclusiones de esta investigación y el trabajo futuro.

**DEVELOPMENT AND CHARACTERIZATION OF A CHARGED-PARTICLE
PROTOTYPE DETECTOR TO BE USED IN STUDIES WITH RADIOACTIVE ION
BEAMS**

by

Avril Alicia Meza Olivo

A Thesis submitted in conformity with the requirements for the Degree of
Master in Electrical Engineering in Universidad Nacional Autónoma de
México.

February, 2012.

ABSTRACT

The present Master Thesis has its application in, but is not restricted to, the field of Nuclear Physics, mainly within the study of radioactive ion beams (RIBs) produced in nuclear reactions by means of particle accelerators.

In the field of Nuclear Physics, gamma ray spectroscopy has proven to be an invaluable tool to help discovering the basic structure of matter. The utilization of high resolution gamma ray spectrometers, operated in conjunction with a variety of associated particle detection systems, continues to be one of the most useful experimental techniques for nuclear spectroscopy at RIB facilities around the world, since the combination of both types of detectors allows to fully exploit gamma-ray spectroscopy capabilities for RIBs studies. GRETINA in the USA [1] and AGATA Demonstrator Array in Europe [2] are examples of state-of-the-art gamma ray spectrometers.

Studies reported here are of great interest in the development of a new generation of charged particle detectors, which will be able to work as auxiliary detectors associated to gamma ray spectroscopy techniques in order to achieve a deeper understanding on RIBs properties.

The long term objective of this project is the development of an instrument capable of detecting in real time the particles emitted by nuclear reactions (produced by particle accelerators) involving RIBs. Therefore, such an instrument must present features like: compactness (low mass and size is required since the detector will perform inside a gamma ray spectrometer and should not affect the gamma ray spectroscopy), insensitivity to magnetic fields, good energy resolution, wide dynamic range (~ 1 -50 MeV), and should be capable of providing information about the position/angle from which the charged particles are emitted by a given nuclear reaction. Additionally, the data acquisition and analysis system should be designed in order to affect as little as possible the gamma spectroscopy as well.

In this Thesis a new prototype of charged particle detector based on the principles of scintillation detection has been proposed and characterized. Because of reasons that will be presented in this text, this prototype consists of an inorganic crystal scintillator “thallium activated cesium iodide” CsI(Tl), coupled to a silicon photomultiplier (SiPM).

Up to now, this prototype detector has been characterized using radioactive isotopes at rest only. It means that no tests within a real time operation of a particle accelerator have been performed yet. This is because the main objective of this work was to verify the SiPM response capabilities for charged particle detection and to study the feasibility of successfully using it under the conditions already mentioned. In general terms, the research here reported represents the first step towards the future implementation and operation of a charged particle detector system able to perform as an auxiliary instrument for nuclear spectroscopy studies involving RIBs. The results presented here are of great interest for establishing the parameters that must be taken into account when implementing the final detector, since the array proposed here had not been used for such an application before. However, the real time operation of the detector, working under particle accelerator conditions, is part of the future work of this project.

On the other hand, the characterization of our prototype had been made by means of both analog and digital instrumentation systems. Therefore in this Thesis a detailed study of signal processing techniques used in Nuclear Physics radiation detectors is also presented, focusing on the advantages that digital processing methods provide in order to satisfy the implementation and operation requirements of the project.

From a general point of view, the blocks needed to process pulses coming from a radiation detector are: (1) pulse pre-amplification, (2) pulse shaping (or filtering), (3) event discrimination, and (4) events analysis.

For the purposes of this work, the pulse shaping stage was implemented in both analog and digital approaches; so that two different experimental setups beyond the pre-amplification stage were instrumented (the pre-amplification block used was the same for both cases).

The first instrumentation setup (analog filtering) consisted of connecting the pre-amplifier output to a spectroscopic amplifier, followed by a multichannel analyzer for discrimination and analysis of the events.

In the second approach (digital filtering) the pre-amplifier output was connected to a digital oscilloscope responsible for digitization; discrimination and acquisition of the pulses, followed by an Ethernet connection towards a PC, where, using the MATLAB® software, several filtering and analyzing algorithms were performed.

Again, for the purposes of this Thesis, this second instrumentation setup was good enough for characterizing the prototype as well as for a deep investigation of digital signal processing techniques. However, once the final charged particle detector is constructed, the pulse processing stages will be digitally implemented into portable devices called digital signal processors, by means of using either DSPs (Digital Signal Processors) or FPGAs (Field Programmable Gate Arrays). Such digital approach, together with the intrinsic properties of the prototype that we have developed, will provide the detector features like portability, position sensitivity, electronic noise reduction, and immunity to magnetic fields, among others, thus making it suitable to perform under the particle accelerator operation conditions.

A third instrumentation system was tested: the digitizer module designed for the GRETINA experiment [1]. However, this system was tested for educational purposes only, in order to learn about the instrument standards employed in Nuclear Physics, and also to get a general idea about the real large-scale systems developed for this kind of experiment, so few tests were carried out using this digitizer.

All the tests and experiments subject of this Thesis were developed at the Holifield Radioactive Ion Beam Facility (HRIBF), in Oak Ridge National Laboratory (ORNL), located in Oak Ridge, TN, USA, and this research was sponsored by the Nuclear Physics Office of the USA Department of Energy.

The present work has been presented in several student congresses and seminars, as well as in the 22nd General Congress of the International Commission for Optics, ICO 2011, held in Puebla, México; in August 2011 (see pages 201-203 and Ref. [98]).

The information contained in this text is organized as follows:

In Chapter 1, a brief introduction to Heavy-Ion Nuclear Physics is presented, together with the experimental methods more commonly used in this field. There are given some basic definitions regarding to radiation detectors, their general properties, some types of radiation detectors, and a brief description of analog instrumentation techniques used.

Chapter 2 involves a detailed study of the signal processing techniques applied to pulses coming from a radiation detector, beginning with an overview of the processing blocks and the major electronics considerations to take into account for their correct

instrumentation. Next a discussion about digital processing of pulses coming from radiation detectors is given. And finally, an extensive comparison between analog and digital approaches for nuclear pulse processing applications is presented.

In Chapter 3 the description of the prototype proposed for charged particle detection can be found, as well as the details on the instrumentation used for the characterization of the array.

Chapter 4 analyzes and discusses the obtained results, and finally, the conclusions and future work are presented.

TABLE OF CONTENTS

Resumen	ix
Abstract	xv
List of figures	xxiii
List of tables	xxvii

CHAPTER 1: AN OVERVIEW OF DETECTION SYSTEMS FOR HEAVY-ION NUCLEAR

PHYSICS EXPERIMENTS 1

1.1 Introduction	2
1.2 Radioactivity	4
1.3 Radioactive Ion Beams	5
1.4 Experimental Methods.....	8
1.4.1 Radiation interaction with matter	8
1.4.2 General properties of radiation detectors.....	13
1.4.2.1 Simplified detector model	13
1.4.2.2 Modes of detector operation	14
1.4.2.3 Differential pulse height spectra	18
1.4.2.4 Energy resolution	19
1.4.2.5 Detection efficiency	21
1.4.3 Scintillation detectors.....	22
1.4.4 Gas detectors.....	27
1.4.5 Solid-state detectors	28
1.4.6 Pulse-shape analyses.....	30
1.4.7 Comparison between detector types	31
1.4.8 Analog electronics: high-resolution energy measurements.....	32
1.4.9 Analog electronics: timing measurements.....	35
1.5 Requirements for future detection systems	36

CHAPTER 2: SIGNAL PROCESSING FOR NUCLEAR PHYSICS	39
2.1 Overview of pulse processing	39
2.1.1 Major electronic considerations	42
2.1.2 Device Impedances	43
2.1.3 Noise considerations.....	44
2.1.4 Dependence of noise on shaping time and capacitance.....	48
2.2 Instrument Standards.....	49
2.3 Pulse Shape Discrimination.....	50
2.4 Digital Pulse Processing.....	51
2.4.1 Analog-to-Digital conversion.....	52
2.4.1.1 Spectroscopy Analog-to-Digital conversion	60
2.4.2 Digital Shaping or Filtering	64
2.4.3 Pulse Shape Analysis.....	67
2.4.4 Baseline Restoration.....	68
2.4.5 Digital Pulse Processors.....	68
2.5 Comparison between Analog and Digital Pulse Processors.....	70
2.5.1 Simplified schematics	70
2.5.2 Advantages and Disadvantages of Digital Filtering	72
CHAPTER 3: ARRAY FOR LIGHT CHARGED PARTICLE DETECTION	79
3.1 Introduction	79
3.2 4π Gamma ray spectrometers and charged particle detectors	83
3.3 Prototype proposed	85
3.3.1 Why using a CsI(Tl) scintillator	86
3.3.2 Why using a SiPM	88
3.3.3 Selecting specific CsI(Tl) scintillator and specific SiPM	94
3.3.4 Optical coupling	97
3.3.5 Radioisotope sources tested	97
3.3.6 Charged particle detection experimental setup.....	100
3.3.7 Electronics: Analog filtering setup	102
3.3.8 Electronics: Digital filtering setup	108
3.3.9 Electronics: GRETINA digitizer.....	117

CHAPTER 4: RESULTS AND DISCUSSION	119
4.1 SensL Silicon Photomultiplier (SiPM) features	119
4.2 Performance of the Prototype for charged particle detection.....	120
4.2.1 Calibration on dark noise	120
4.2.2 Dynamic Range	125
4.2.3 Resolution at different energies	127
4.2.4 Linearity	131
4.2.5 Pulse shape discrimination.....	132
4.2.6 Sensitivity to the environment.....	133
CONCLUSIONS AND FUTURE WORK	135
Glossary.....	139
References	151
Appendix A: Counting Statistics	155
Appendix B: Coaxial cables.....	165
Appendix C: NIM, CAMAC, and VMEbus Instrument Standards.....	175
Appendix C: Guide to the safe handling of radioactive materials in research	183

LIST OF FIGURES:

1.1.	Schematic drawing comparin the two main RIB production techniques.....	6
1.2.	Schematic layout of the Holifield Radioactive Ion Beam Facility, HRIBF, an ISOL facility at Oak Ridge National Laboratory.....	7
1.3.	Specific energy loss normalized to particle energy (arbitrary units) along the particle track in silicon.	11
1.4.	(a) The assumed current output form a hypothetical detector. (b) The signal voltage $V(t)$ for the case of a small time constant load circuit. (c) The signal voltage $V(t)$ for the case of a large time constant load circuit.	16
1.5.	Example of differential pulse height spectra for an assumed source of pulses.	18
1.6.	Definition of detector resolution.....	20
1.7.	Example of the full-energy peak in a differential pulse height spectrum	22
1.8.	The emission spectra of several common inorganic scintillators.....	24
1.9.	Typical photomultiplier structure.....	26
1.10.	Simplified schematic of a charge preamplifier.....	29
1.11.	Example of shaping of the output of a charge preamplifier used in order to achieve a better signal-to-noise ratio.	33
1.12.	Schematic representation of the CFD working principle	36
2.1.	Schematic diagram of the detector and electronics.....	40
2.2.	Schematic of simple signal processing electronics.....	41
2.3.	Device impedances: Idealized input and output configuration.....	43
2.4.	Sketches of the effect of low-frequency and high-frequency noise on signal pulses of constant amplitude	45
2.5.	Variation of the contribution of series and parallel noise sources as a function of the shaping time in the pulse processing electronics.....	48

2.6.	Series and parallel noise behavior of two detectors that are identical except for their capacitance values.....	49
2.7.	Quantization error.....	55
2.8.	Block diagram of a 3-bit flash ADC.....	57
2.9.	Analogy to the operation of a subranging ADC in which magnifiers are used in sequence to expand the analog voltage scale	59
2.10.	The elements of a single subranging stage or module	60
2.11.	Block diagram of a linear ramp (Wilkinson type) ADC	62
2.12.	Operational sequence for a successive approximation ADC	63
2.13.	An illustration of a digital transversal filter	65
2.14.	Example of a simple digital filter that produces a triangular-shaped pulse from a step input.....	66
2.15.	Schematic of a simple analog pulse shaper	71
2.16.	Simplified schematic of an “ideal” digital pulse processor	71
2.17.	Pulse shapes in analog and digital pulse processors	72
2.18.	Plots of differentiator output for analog and digital shaping	74
2.19.	Plot showing pulse shapes from three different pulse shapers	75
3.1	Tracking Principle assuming that full energy gamma ray is deposited. Source location and interaction points are known	81
3.2	Doppler broadening effect within a nuclear reaction.....	82
3.3	Physical disposition of GRETINA (left) and Gammasphere (right) 4π gamma ray spectrometers	83
3.4	Prototype for charged particle detection consisting of a CsI(Tl) scintillator optically coupled to a SiPM for the electronics read out	86
3.5	Schematic diagram of an array of passively quenched Geiger-mode APDs	91
3.6	Circuit diagram for a passively quenched Geiger-mode APD (left) and the typical quench and reset times of a Geiger pulse calculated for different resistor values R_{load} (right)	92

3.7	(a) A SiPM configuration.	
	(b) The dark noise amplitude spectrum	94
3.8	(a) 4 side tileable SPMArray mounted onto a pin socket.	
	(b) Top view of the SPM pixel layout in the SPMArray4 package	95
3.9	SPMArray4 SensL evaluation kit	96
3.10	Penetration of matter of alpha particles and gamma rays	100
3.11	Schematic of the experimental setup for charged particle detection	100
3.12	(Left): SensL evaluation kit fixed to foam rubber into the dark box.	
	(Right): Dark box containing the experimental setup	101
3.13	Schematic of the analog filtering electronics setup.....	102
3.14	Single channel pre-amplification schematic.....	103
3.15	MCA800A block diagram	106
3.16	Plot of a Cs-137 pulse height distribution taken with the MCA8000A	107
3.17	Schematic of the digital filtering electronics setup.....	108
3.18	Alpha source pulse and dark current pulse taken at a sampling frequency of 50 MSa/s	110
3.19	Digital Pulse Processing stages.....	114
3.20	Identification of alpha particles and gamma rays with a CsI(Tl) crystal coupled to a SiPM	116
3.21	Analog and Digital electronics setups	117
3.22	Gretina digitizer module into a VMEbus crate.....	118
4.1	Photoelectron spectrum obtained over the peak voltage of dark current pulses ..	122
4.2	Voltage on the oscilloscope as a function of the SiPM micro-pixels fired	122
4.3	Photoelectron spectrum obtained over the peak current of dark current pulses ..	123
4.4	(a) Experimental current at the output of the pre-amplifier.	
	(b) Theoretical current at the input of the pre-amplifier	124
4.5	Dynamic range for 1 pixel of the SensL SiPM	126
4.6	Dynamic range for the total 16 pixels of the SensL SiPM	127

4.7	Energy spectrum for Cf-252	128
4.8	Energy spectrum for Cm-244	128
4.9	Energy spectrum for Am-241	128
4.10	Energy spectrum for triple alpha source	128
4.11	Energy spectrum for Cs-137	128
4.12	Energy spectrum for Co-60	128
4.13	Energy spectrum for Cs-137 taken with the MCA8000A	130
4.14	Energy spectrum for the triple alpha source taken with the MCA8000A.....	130
4.15	Energy spectrum for Co-60 taken with the GRETINA digitizer	130
4.16	Linearity over the gamma rays and alpha particles sources.....	131
4.17	Identification of alpha particles and gamma rays detected by the CsI(Tl)-SiPM array.	132
A.1	Distribution function for two sets of data with differing amounts of internal fluctuation.....	156
A.2	Comparison of the discrete and continuous forms of the Gaussian distribution	163
A.3	A plot of the general Gaussian curve	164
B.1	Construction of a standard coaxial cable	165
B.2	Sketch illustrating ground connections in a simple system.....	168
B.3	Application of a step voltage V_s to a coaxial cable terminated in R_t	171
C.1	Pin assignments for the NIM standard connector between bin and module	176
C.2	Diagram of the CAMAC dataway.....	179
C.3	Functional modules and busses defined by the VMEbus standard	181

LIST OF TABLES:

1.1.	Properties of inorganic scintillators commonly used in Nuclear Physics.....	25
1.2.	Simplified comparison between the different detector types discussed in the text	32
1.3.	Parameters describing the behavior of a $CR-RC$ and $CR-RC^4$ shaping networks.....	34
2.1.	Some examples of Fast Analog-to-Digital Converters	58
2.2.	Noise indices and pulse duration (FWHM) for three common shaping amplifiers	76
3.1.	Relative signal yields of different types of radiation sensors coupled to a CsI(Tl) crystal, compared to an NaI(Tl) scintillator coupled to a Bi-alkali PMT	95
3.2.	Elements of the evaluation kit provided by SensL.....	96
3.3.	Radioisotope sources tested	98
3.4.	Main characteristics of the ORTEC 572 spectroscopic amplifier	105
4.1.	Energy resolution for different radioisotope sources	130
B.1	Properties of coaxial cables	166
B.2	Reflection conditions created by various terminations at the end of a coaxial cable with characteristic impedance Z_0	172
C.1	NIM Standard Logic Levels	176
C.2	NIM Fast Logic Levels for 50-ohms systems.....	176

CHAPTER 1: AN OVERVIEW OF DETECTION SYSTEMS FOR HEAVY-ION NUCLEAR PHYSICS EXPERIMENTS

The birth of Nuclear Physics can be traced back to the works of Becquerel and of Rutherford, who discovered radioactivity (Becquerel, 1896) and proposed a theory where the atom has a massive charged core, the nucleus (Rutherford, 1911). Few years later Quantum Mechanics was developed (Schrödinger, 1926) and the first machines able to accelerate nuclei were built (Cockcroft and Walton 1930, Van de Graff 1931).

These and other experimental and theoretical findings made it possible to begin a systematic study of the nucleus that is still under way. Physicists' current knowledge of nuclei covers many aspects of nuclear behavior (radioactivity, energy spectra, nuclear reactions, stellar nucleosynthesis) and it has found also several practical applications in everyday life. Nevertheless, the difficulty of having a unique theory able to explain completely the behavior of nuclear matter still challenges both theoretical and experimental physicists. From an experimental point of view the goal is to perform high "quality" measurements (high resolution and granularity, low thresholds, among others) that can be used to verify and improve the existing theories.

Experimental systems are based upon arrays of various detector types able to measure the characteristics of the incoming particles (for example energy, charge). For decades the electrical output of a particle detector has been analyzed using (rather sophisticated) analog methods, and using digital electronics only for final data conversion, acquisition and storage.

In the everyday world people are fully accustomed to a digital manipulation of various kinds of information: a few examples are mobile communications, digital entertainment systems, media broadcasting and data measurement and storage. In these applications some "analog" information (i.e. audio, video) is converted very soon into a digital data stream and subsequently processed and/or transmitted (and possibly converted back to "analog").

In the last few years these technologies have reached such a development status to make them attractive for the nuclear physics field. The electrical output of a particle detector

can be digitized and the corresponding data properly processed to extract all the information needed. If successful, this approach would allow a major renovation in the organization of large experiments, due to the important electronic simplification and to the greater flexibility of these methods with respect to the standard analog methods. Moreover, because of the widespread of these technologies in the consumer market, many industrial companies are actively developing various components related to digital information manipulation, thus lowering the general cost of these systems.

1.1 INTRODUCTION

As in many other fields, in Nuclear Physics the development of new detection methods or the improvements of the existing ones is strictly related to the precise measurement of certain observables that are relevant for the currently open topics.

In this chapter a brief introduction regarding few of the main open topics in Nuclear Physics is given, focusing on the experimental features needed in future experiments in order to improve significantly the existing knowledge in these areas. The commonly used detector types in Nuclear Physics are then described, and some details are given on the detection processes that are often the limiting factor for the achievable performances. The standard analog-electronics methods used to process the output signals of these detectors are also briefly discussed. In the last section a brief overview of the detector/electronic improvements that would be needed in order to meet the theoretical needs is presented. Some of the motivations that lead to the development of a new experimental method based on fast signal processing are also discussed.

Here and in the following, the expression “Heavy-Ion Nuclear Physics” will be used to describe Nuclear Physics studies where the properties of heavy nuclei or of their decay products are of interest, with beam energies generally lower or of the order of ≈ 100 AMeV (Mega electron-Volts per nucleon).

Nuclear Physics in the next decade

In the last 50 years a number of accelerators for the study of nuclear properties have been realized and used all over the world, frequently employing an electromagnetic acceleration. The desired energy is usually reached with two or more consecutive

accelerating stages, each of them tailored to the energy range to be covered by the specific stage. Up to now most of these methods have been restricted to accelerate stable nuclei only, so that a limited region of the nuclear chart has been explored, namely nuclei lying close to the stability valley in the Z (atomic number) versus N (number of neutrons within a nucleus) plane.

The study of Heavy-Ion Nuclear Physics based on accelerators can be roughly divided into two areas, namely *Nuclear Structure* and *Nuclear Reactions*. In Nuclear Structure a study of the properties of nuclei at low excitation energy is performed, i.e. the nucleus is treated as a bounded quantum system where energy levels can be, for example, studied by means of the gamma excitation processes. A proper description of nuclei must include quantities like the mass (or the binding energy), the lifetime (if not stable), and quantum numbers like spin, orbital angular momentum, etc., of both the ground state and excited levels. In Heavy-Ion Nuclear Reactions with $E \geq 15$ AMeV, the dynamical/thermo-dynamical properties of the nuclear matter are studied. Typically the use of colliding heavy nuclei permits to create excited nuclear matter, which is usually treated as a fluid described by an Equation of State (EoS).

Both in structure and reaction studies the various nuclei and nuclear matter properties are expected to depend upon the Z/N ratio of the involved nuclei. This prediction has been indeed experimentally observed for decades, although due to the limited region of the *nuclear chart* available to experiments, a deeper investigation of these properties is still needed.

The study of nuclear properties is relevant also for astrophysical motivations, for example to understand the nucleosynthesis of various light and heavy elements that are found in nature. These processes involve nuclei that play an important role in the stellar environment, but that are unstable in ordinary conditions, thus making difficult (often impossible) the experimental study of their properties using the today available stable beams. The study of excited nuclear matter as a function of the Z/N ratio would also allow a deeper understanding of cosmic entities like neutron stars.

These and other motivations have led to the development of new generation accelerators where the production of radioactive (i.e. unstable) nuclear beams is possible, using a secondary production from a primary stable beam. This comes at the price of a generally low radioactive-beam intensity, mainly due to the two-step mechanism used (production

of a stable beam and “conversion” to the radioactive one). These machines will allow the investigation of nuclear matter far from the stability region, thus considerably extending our knowledge of nuclear matter. Several open topics in Heavy-Ion Nuclear Physics will benefit from such machines.

Among the major questions of present day nuclear structure, nuclear astrophysics and applications are:

How do protons and neutrons make stable nuclei and rare isotopes?

What is the origin of simple patterns in complex nuclei?

What is the EoS of matter made of nucleons?

What are the heaviest nuclei that can exist?

When and how did the elements from iron to uranium originate?

How do stars explode?

What is the nature of neutron star matter?

How can our knowledge of nuclei and our ability to produce them benefit humankind?

1.2 RADIOACTIVITY

Radioactivity was first discovered in 1896 by the French scientist Henri Becquerel. A radioactive nucleus is unstable, and can thus spontaneously stabilize to a less-excited system. The resulting transformation might alter the structure of the nucleus and results in the emission of either a photon or a particle such as an electron or an alpha particle. Other less familiar types of radioactive decay include cluster decay (emission of a heavy-ion like ^{14}C , ^{20}O , ^{24}Ne), spontaneous fission, beta delayed particle emission, and two-proton radioactivity.

The activity of a radioisotope source is defined as its rate of decay and is given by the fundamental law of radioactive decay

$$\left. \frac{dN}{dt} \right|_{\text{decay}} = -\lambda N \quad (1.1)$$

Where N is the number of radioactive nuclei and λ is defined as the decay constant. The historical unit of activity has been the curie (Ci), defined as exactly 3.7×10^{10} disintegrations/second, and owes its definition to its origin as the best available estimate of the activity of 1 gram of pure ^{226}Ra .

1.3 RADIOACTIVE ION BEAMS (RIBs)

The RIB can be considered as a tool that allows us to study the shell structure and the gap evolution when the number of neutrons and protons changes. Access to new regions in the nuclear chart with Z/N very different from the ones that occur at the valley of stability will be possible. Approximately 280 stable nuclei are known and close to 3000 have been created and studied in the laboratory from about 7000 that have been predicted to exist and decay radioactively [3]. This means that there is still a vast territory to be explored.

The acceleration of unstable nuclei has required the development of very specialized equipment. Several RIB facilities in the world are now operating, under construction, or proposed. Below there is a short review on two of the main acceleration schemes used with radioactive ion beams.

Beam Production

The production of a RIB is mainly achieved by either two ways: the Projectile Fragmentation Method (PFM) or the Isotope Separator On-Line (ISOL) technique (Fig. 1.1). The PFM requires one accelerator where the radioactive fragments are produced from collisions between heavy-ion projectiles and light-target nuclei and selected by electromagnetic beam line components [4]. The ISOL method requires two accelerator systems, a driver accelerator to produce radioactive atoms at rest and a post accelerator to accelerate them to energies of interest. The two accelerators are coupled by a target-ion source (TIS) and a high-resolution mass separator.

In the PFM beams are inherently weak and poorly defined spatially and in terms of energy. One of the main advantages of the PFM is that it is independent of the chemistry of the ions involved (a major challenge in the ISOL method). Another advantage is that ions with very short-lives can be studied with the PFM.

The next section will focus to the production and use of RIBs by the ISOL technique at the Holifield Radioactive Ion Beam Facility (HRIBF) at Oak Ridge National Laboratory in the USA.

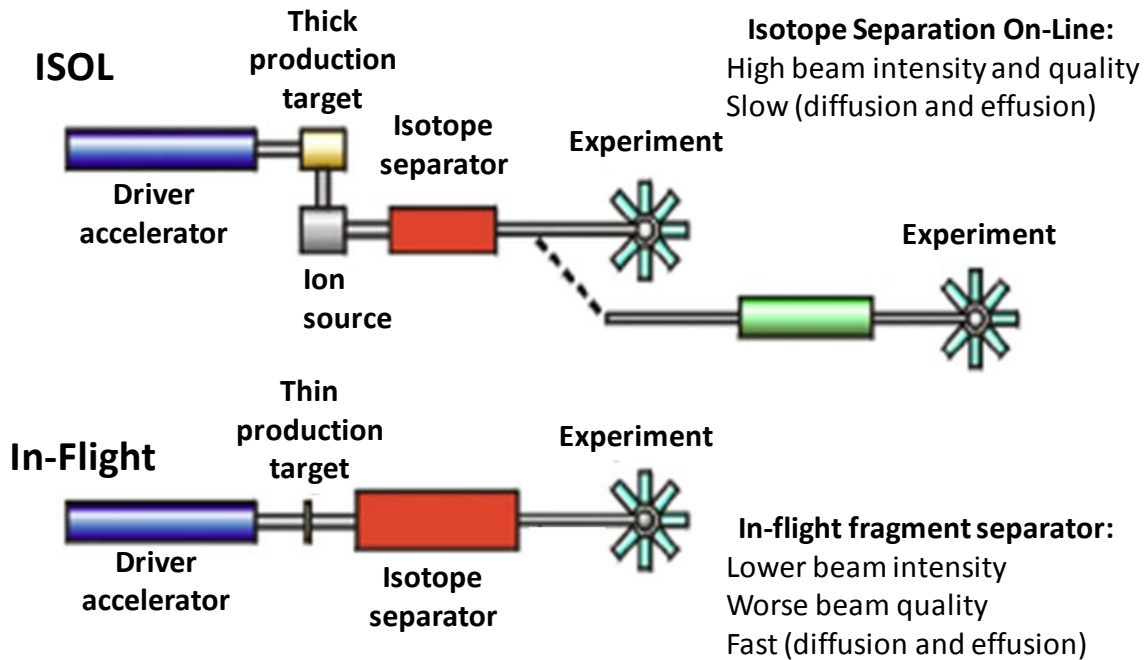


Figure 1.1: Schematic drawing comparing the two main RIB production techniques.

An example of an ISOL Facility: HRIBF

The production of each RIB species with the ISOL technique is a research project itself and constitutes one of the main challenges of RIB science. High efficiencies are required in each step of the production, ionization, separation and transportation.

In general, the ISOL method requires two steps. In the first one radioactive species of interest are produced in reactions induced by an intense charged-particle beam (protons, deuterons and alphas) from an accelerator or by neutrons (e.g. from a reactor). The method involves a thick target maintained at high temperatures ($T \sim 2,500 \text{ }^\circ\text{C}$) to promote the rapid transfer to the actual ion source. Once ionized in an ion source the ions can be extracted by electric fields and then mass analyzed with magnets before its injection into a post-accelerator which takes them to the energy required by the experiment.

An exciting nuclear structure and nuclear astrophysics program is pursued at the HRIBF, at Oak Ridge. HRIBF is an ISOL facility (Fig. 1.2), where the Oak Ridge Isochronous Cyclotron

(ORIC) serves as the driver, accelerating intense beams (tens of μA) of light ions for the production of radioactive isotopes, and the folded-geometry 25 MV tandem accelerator serves as a post accelerator for the RIBs. This accelerator is the highest operating voltage electrostatic accelerator in the world capable of producing beams of 0.1 up to 15 AMeV for light nuclei and up to 5 AMeV for heavier masses. HRIBF is the first facility to produce post-accelerated beams of heavy neutron-rich nuclei opening important physics opportunities. A very important element at HRIBF is the RIB injector which consists of various components including the RIB production target/ion source (TIS) and two mass separation stages. In order to avoid excessive losses through radioactive decay of short lived nuclei, prompt diffusion release and transport of the product to the ion source in a time period commensurate with the life-time of the species is required. Various target/ion sources have been designed to operate with the highest possible efficiency [5-7].

Compared to conventional stable heavy ion beams (SIBs), RIB intensities are several orders of magnitude lower, particularly for those further from stability. Therefore it is most important to optimize the beam transport in every stage to provide enough RIB intensity for physics experiments. The field of RIB Physics demands a closer interaction between experimenters and accelerator operations staff to fully exploit these exotic beams.

Radioactive beam physics represents one of the frontiers in nuclear science. Examples of current and future facilities using the PF method are FAIR in Germany, RIKEN in Japan and NSCL and FRIB in the USA. The ISOL method is or will be used at facilities that include HRIBF at ORNL in USA, ISAC-TRIUMF in Canada, SPIRAL-2 in France, SPES in Italy, KoRIA in South Korea, BRIF in China, HIE-ISOLDE at CERN and EURISOL in Europe [8].

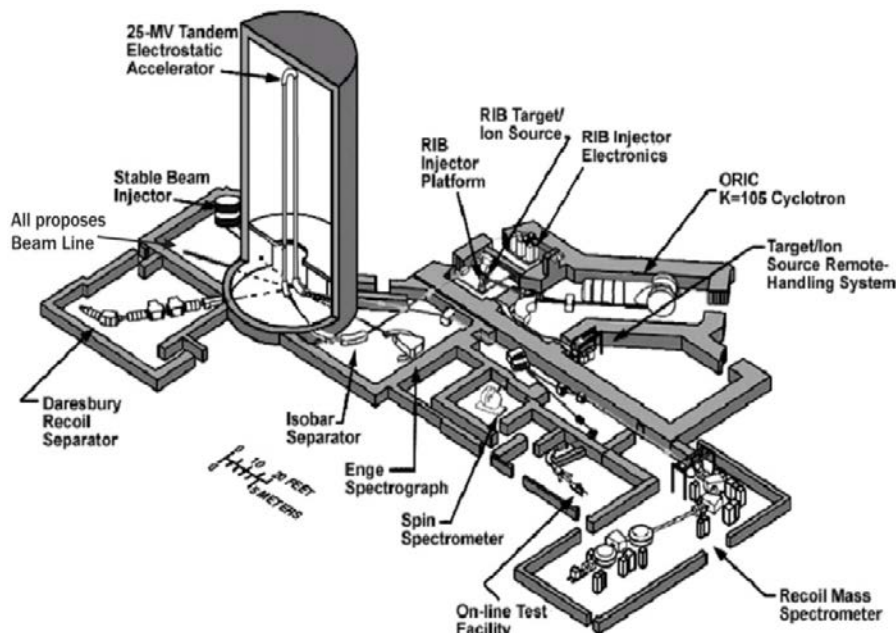


Figure 1.2: Schematic layout of the Holifield Radioactive Ion Beam Facility, HRIBF, an ISOL facility at Oak Ridge National Laboratory.

1.4 EXPERIMENTAL METHODS

In this section some basic definitions as well as a brief overview of the experimental methods that are commonly used in Nuclear-Physics experiments will be given. The discussion will be limited to the main properties of detectors and analog systems that are relevant for the purposes of this Thesis. After a description of the principal interaction properties of radiation and the main general properties of radiation detectors, a brief description of the commonly used detectors is given, as well as of the standard analog electronics used to process their signals.

1.4.1 RADIATION INTERACTION WITH MATTER

The principle of operation of all the nowadays commonly used radiation detectors is based on the conversion of the energy deposited by the impinging radiation in the active volume of the detector into some electronic signal. This signal can then be properly analyzed to extract the desired information.

The detailed understanding of the interaction processes between the radiation and the detector material is thus the basis for the design and the use of radiation detectors. The principal radiation types are charged particles, gamma rays and neutrons. This Thesis work focuses mainly on heavy charged particles and gamma ray detectors.

A. Charged Particles

The interaction with a medium causes an energy loss of the impinging charged particle which is slowed down from its original energy E and possibly stopped inside the material. The main mechanism leading to energy loss is the Coulomb interaction between the particle and the negative charged cloud of the orbital electrons of the absorber atoms.

Other mechanisms like electromagnetic or strong interactions with the nuclei are present, although less significant for the purpose of particle detection (but they may be important in particular experimental conditions and definitely in High-Energy Physics). The energy transferred from the particle to the absorber can be so low to excite atoms and/or molecules (*excitation processes*) or high enough to produce *ionization*. The energy deposited in the detector can thus be found either as atomic/molecular excited states, which subsequently de-excite with the emission of low-energy photons (mainly in the

visible range), or as an electron-ion pair (electron-hole in semiconductors) resulting from the ionization processes.

Other non-irradiative de-excitation processes do exist but they will be neglected in the present discussion.

The *linear stopping power* S for a charged particle in a given absorber is simply defined as the differential energy loss for that particle within the material divided by the corresponding differential path length:

$$S = -\frac{dE}{dx} \quad (1.2)$$

The value of S along a particle track is also called its *specific energy loss* or, its “rate” of energy loss. For particles with a given charge state z , S increases as the particle velocity is decreased. The classical expression that describes the specific energy loss of a heavy charged particle (with mass $m \gg m_e$, where m_e is the electron mass) is approximately described by the Bethe-Bloch formula [9, 10]:

$$-\frac{1}{\rho} \frac{dE}{dx} \propto \frac{z^2}{\beta^2} \frac{Z}{A} \left[\log \frac{2m_e \beta^2 c^2}{I(1-\beta^2)} - \beta^2 \right] \quad (1.3)$$

where z is the charge of the particle, $v = \beta c$ its speed, ρ , Z , A , and I are the density, charge, mass and empirical ionization constant of a mono-elemental absorber, respectively.

This formula describes the energy loss of heavy charged particles at non-relativistic energies and for energies greater than the shell energies of the absorber.

As expressed in Eq. 1.3, the energy loss exhibits a strong dependence on the charge and the velocity of the particle, with a moderate dependence on its mass. When comparing different charged particles of the same velocity, the only factor that may change outside the logarithmic term in Eq. 1.3 is z^2 , which occurs in the numerator of the expression. Therefore, particles with the greatest charge will have the largest energy loss. Alpha particles, for example, will lose energy at a rate that is greater than protons of the same velocity but less than that of more highly charged ions. In comparing different materials as absorbers, dE/dx depends primarily on the term $\rho = NZ$ which represents the electron

density of the absorber. High atomic number, high-density materials will consequently result in the greatest linear stopping power.

Examples of specific energy loss for various particles along their track in a silicon absorber are shown in Fig. 1.3. It is possible to note that the energy deposited along the particle track exhibits a sharp maximum, the Bragg peak. There also exists a well defined distance R (the range of the charged particle) that represents the minimum detector thickness needed to absorb the incoming particles. The range depends on particle type and energy; for example, see Fig. 1.3, the range in silicon for 3 MeV protons is about 90 μm , whereas for a 40 MeV ^{12}C (having the same β) is about 45 μm .

When the detector thickness is greater than the particle range the particle deposits its full energy and it consequently stops within the detector. In the opposite case the particle deposits only a fraction of its energy in the detector and emerges with a non-zero residual energy. The deposited fraction of the full energy thus depends on particle type and energy; the correlation between the deposited and the residual energy is the basis of the ΔE - E particle identification method, discussed in [13].

The time required to stop a charged particle in an absorber is usually referred to as its *stopping time* and can be deduced from its range R and average velocity. For non-relativistic particles of mass m and kinetic energy E , the stopping time [13] is:

$$T \cong 1.2 \times 10^{-7} R \sqrt{\frac{m_A}{E}} \quad (1.4)$$

where T is in seconds, R in meters, E in MeV, and m_A is the particle mass in atomic mass units.

These considerations are valid when the mass of the incoming particle is much greater than the electron mass, as for example with nuclei. The energy loss of electrons in matter deserves its own discussion; see [11].

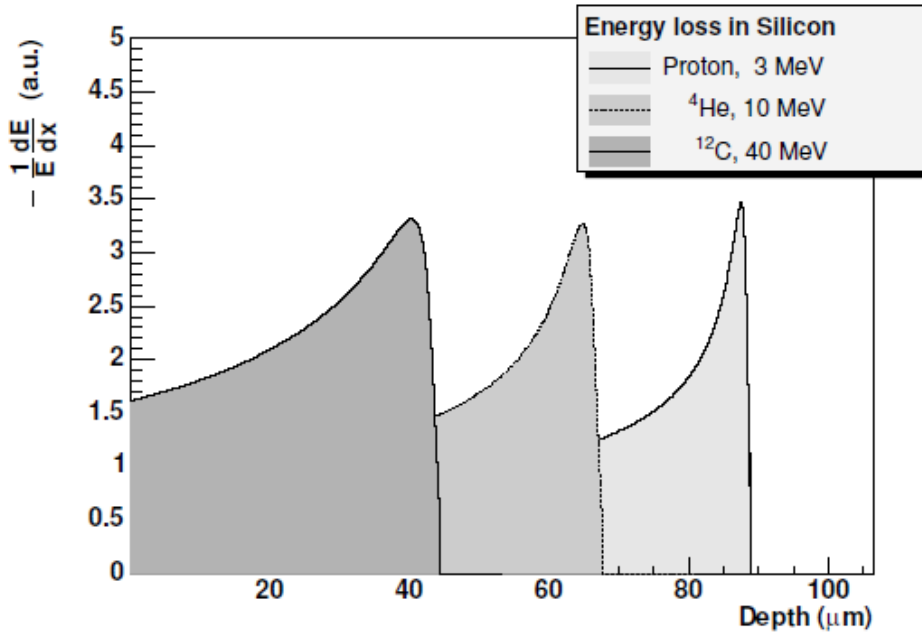


Figure 1.3: Specific energy loss normalized to particle energy (arbitrary units) along the particle track in silicon. Note the strong dependence on particle charge and energy.

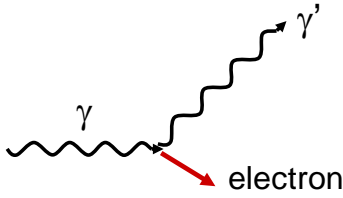
B. Gamma Interactions

There are three main interaction mechanisms that are relevant for the purposes of gamma rays detection: *photoelectric absorption*, *Compton scattering*, and *pair production*. In all these processes an absorber electron receives part or all of the gamma ray photon energy and it is the particle actually detected. The gamma ray photon might undergo abrupt changes, it can either disappear entirely or might be scattered through a significant angle. This behavior is in marked contrast to the charged particles discussed before, which slow down gradually through continuous, simultaneous interactions with many absorber atoms.

Photoelectric absorption

γ electron In the photoelectric absorption process the photon is completely absorbed in the interaction with a detector atom and this causes the ejection of a high-energetic electron from the atom (*photoelectron*). The full incident energy of the gamma ray is thus released in the detector.

Compton scattering



In Compton scattering an incoming photon with energy E_γ undergoes a scattering with an electron. If ϑ is the scattering angle, the photon energy E'_γ after the scattering is given by:

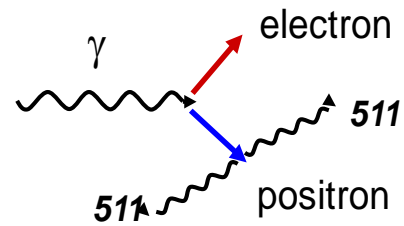
$$E'_\gamma = \frac{E_\gamma}{1 + \frac{E_\gamma}{m_e c^2} (1 - \cos \theta)} \quad (1.5)$$

where m_e is the electron mass.

The deposited energy in the detector is thus $E_{det} = E_\gamma - E'_\gamma$. The cross section of this process is described by the Klein-Nishina formula [12]. It is possible to recognize that only a fraction of the total γ energy is released in the detector. In the case of the scattered photon escaping from the detector this causes the formation of a “Compton continuum” in the experimental spectra.

Pair Production

For gamma energies E_γ greater than $2m_e c^2$ (twice the rest-mass energy of an electron = 1.02MeV), the pair production is an energetically possible process, although this effect is important only for $E_\gamma \geq 5-10$ MeV. The full gamma energy is released in the detector as kinetic energy of the electron-positron pair and their subsequent annihilation (although one or both of the emitted gamma rays can escape the detector, causing a continuum and single or double “escape peaks”).



These three processes are not exclusive, although their relative importance varies greatly with the gamma energy and the charge Z of the absorber. Often a gamma ray undergoes several interactions before escaping or being completely absorbed in the detector (for example a Compton scattering followed by a photoelectric absorption).

1.4.2 GENERAL PROPERTIES OF RADIATION DETECTORS [13]

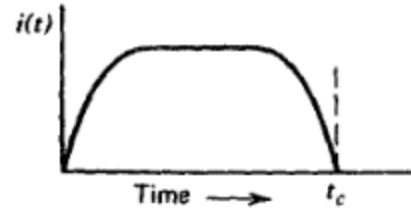
Before discussing different types of radiation detectors individually, first are outlined some general properties that apply to all types. Some basic definitions of detector properties, such as efficiency and energy resolution, together with some general modes of operation and methods of recording data that will be helpful in categorizing detector applications.

1.4.2.1 Simplified Detector Model

Consider a hypothetical detector that is subject to some type of irradiation. Focusing on the interaction of a single particle or quantum of radiation in the detector, which might, for example, be a single alpha particle or an individual gamma ray photon. In order for detector to respond at all, the radiation must undergo interaction through one of the mechanisms discussed in §1.4.1. As indicated by Eq. 1.4, the time of interaction or stopping time is very small (typically a few nanoseconds in gases or a few picoseconds in solids). In most practical situations, these times are so short that the deposition of the radiation energy can be considered instantaneous.

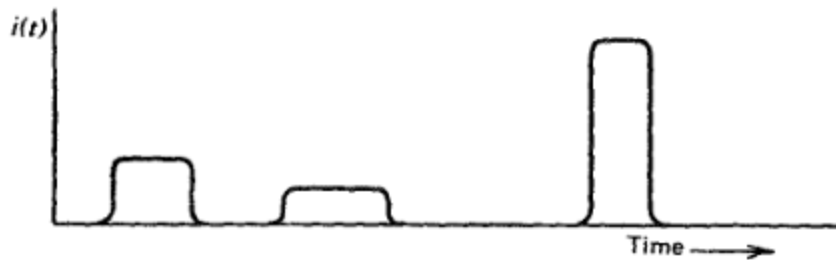
The net result of the radiation interaction in a wide category of detectors is the appearance of a given amount of electric charge within the detector active volume. The simplified detector model assumes that a charge Q appears within the detector at time $t=0$ resulting from the interaction of a single particle or quantum of radiation. Next, this charge must be collected to form the basic electrical signal. Typically, collection of the charge is accomplished through the imposition of an electric field within the detector, which causes the positive and negative charges created by the radiation to flow in opposite directions. The time required to fully collect the charge varies greatly from one detector to another. For example, in *gas detectors* the collection time can be as long as few milliseconds, whereas in semiconductor diode detectors the time is a few nanoseconds. These times reflect both the mobility of the charge carriers within the detector active volume and the average distance that must be traveled before arrival at the collection electrodes. Therefore it is first considered a model of a prototypal detector whose response to a single particle or quantum of radiation will be a current that flows for a time equal to the charge collection time.

The sketch on the right illustrates one example for the time dependence the detector current might assume, where t_c represents the *charge collection time*. The time integral over the duration of the current must simply be equal to, the total amount of charge generated in that specific interaction.



$$\int_0^{t_c} i(t)dt = Q$$

In any real situation, many quanta of radiation will interact over a period of time. If the irradiation rate is high, situations can arise in which current is flowing in the detector from more than one interaction at a given time. For the present discussion it is assumed that the rate is low enough so that each individual interaction gives rise to a current that is distinguishable from all others. The magnitude and duration of each current pulse may vary depending on the type of interaction, and a sketch of the instantaneous current flowing in the detector might then appear as shown below.



It is important to recall that, because the arrival of radiation quanta is a random phenomenon governed by Poisson statistics (see Appendix A), the time intervals between successive current pulses are also randomly distributed.

1.4.2.2 Modes of detector operation

There are three general modes of operation of radiation detectors: *Pulse mode*, *Current mode*, and *Mean square voltage average (MSV)*. Pulse mode is the most commonly applied of these, but current mode also finds many applications. MSV mode is limited to some specialized applications that make use of its unique characteristics. Although the three modes are operationally distinct, they are interrelated through their common

dependence on the sequence of current pulses that are the output of the simplified detector model.

In pulse mode operation, the measurement instrumentation is designed to record each individual quantum of radiation that interacts in the detector. In most common applications, the time integral of each burst of current, or the total charge Q , is recorded since the energy deposited in the detector is directly related to Q . All detectors used to measure the energy of individual radiation quanta must be operated in pulse mode. Such applications are categorized as *radiation spectroscopy* and the studies carried on in this Thesis belong to this category.

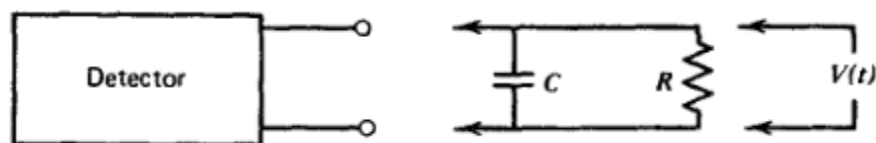
In other circumstances, a simpler approach may suit the needs of the measurement: All pulses above a low-level threshold are registered from the detector, regardless of the value of Q . This approach is often called pulse counting. It can be useful in many applications in which only the intensity of the radiation is of interest, rather than the incident energy distribution of the radiation.

At very high event rates, pulse mode operation becomes impractical or even impossible. The time between adjacent events may become too short to carry out an adequate analysis, or the current pulses from successive events may overlap in time. In such cases, one can revert to alternative measurement techniques that respond to the time average taken over many individual events. This approach leads to the remaining two modes of operation: current mode and MSV mode.

For the purposes of this Thesis, only the pulse mode operation will be presented. Deep information about current and MSV modes can be found in [13].

Pulse mode operation

The nature of the signal pulse produced from a single event depends on the input characteristics of the circuit to which the detector is connected to (usually a preamplifier). The equivalent circuit can often be represented as:



Here R represents the input resistance of the circuit, and C represents the equivalent capacitance of both the detector itself and the measuring circuit. For example, if a preamplifier is attached to the detector, then R is its input resistance and C is the summed capacitance of the detector, the cable used to connect the detector to the preamplifier, and the input capacitance of the preamplifier itself. In most cases, the time-dependent voltage $V(t)$ across the load resistance is the fundamental signal voltage on which pulse mode operation is based. Two separate extremes of operation can be identified that depend on the relative value of the time constant of the measuring circuit. From simple circuit analysis, this time constant is given by the product of R and C , or $\tau = RC$.

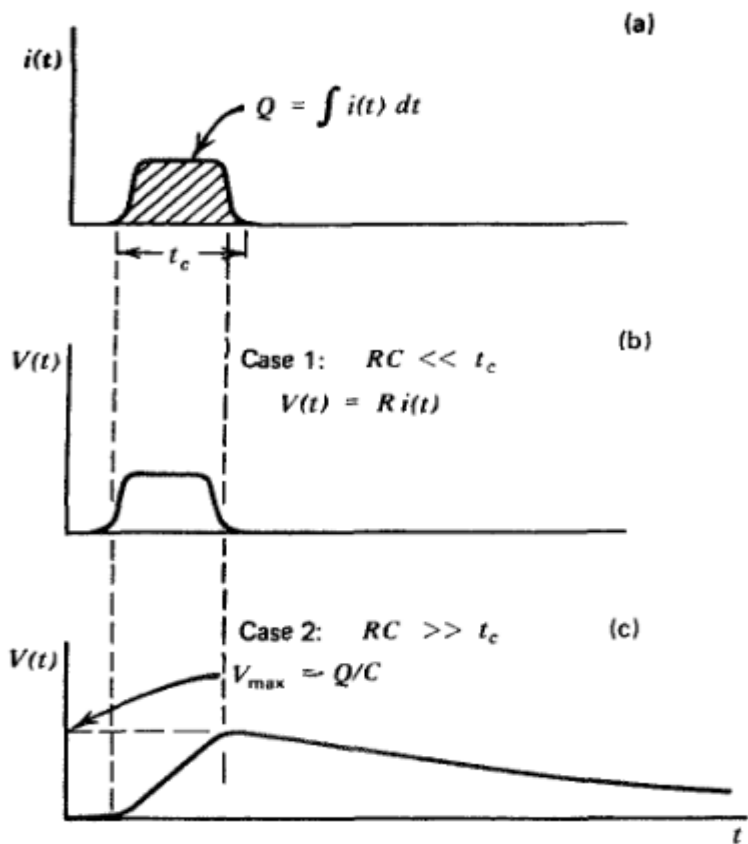


Figure 1.4: (a) The assumed current output form a hypothetical detector. (b) The signal voltage $V(t)$ for the case of a small time constant load circuit. (c) The signal voltage $V(t)$ for the case of a large time constant load circuit.

Case 1. Small RC ($\tau \ll t_c$)

In this case the time constant of the external circuit is kept small compared to the charge collection time, so that the current flowing through the load resistance R is essentially

equal to the instantaneous value of the current flowing in the detector. The signal voltage $V(t)$ produced under these conditions has a shape nearly identical to the time dependence of the current produced within the detector as illustrated in Fig. 1.4b. Radiation detectors are sometimes operated under these conditions when high event rates or timing information is more important than accurate energy information.

Case 2. Large RC ($\tau \gg t_c$)

It is generally more common to operate detectors in this case. Here very little current will flow in the load resistance during the charge collection time and the detector current is momentarily integrated on the capacitance. If we assume that the time between pulses is sufficiently large, the capacitance will then discharge through the resistance, returning the voltage across the load resistance to zero. The corresponding signal voltage $V(t)$ is illustrated in Fig. 1.4c. In this case of pulse-type operation of detectors the time required for the signal pulse to reach its maximum value is determined by the charge collection time within the detector itself. No properties of the external circuit influence the *rise time* of the pulses. On the other hand, the *decay time* of the pulses, or the time required to restore the signal voltage to zero, is determined only by the time constant of the load circuit. The conclusion that *the leading edge is detector dependent and the trailing edge circuit dependent* is a generality that will hold for a wide variety of radiation detectors operated under the conditions in which $RC \gg \tau_c$. Also, the amplitude of the signal pulse shown as V_{max} in Fig. 1.4c is determined simply by the ratio of the total charge Q created within the detector during one radiation interaction divided by the capacitance C of the equivalent load circuit. Because this capacitance is normally fixed, the amplitude of the signal pulse is directly proportional to the corresponding charge generated within the detector and is given by the simple expression:

$$V_{max} = \frac{Q}{C} \quad (1.6)$$

Thus the output of a detector operate in pulse mode normally consists of a sequence of individual signal pulses, each representing the results of the interaction of a single quantum of radiation within the detector. A measurement of the rate at which such pulses occur will give the corresponding rate of radiation interaction within the detector. Furthermore, the amplitude of each individual pulse reflects the amount of charge generated due to each individual interaction.

Pulse mode operation is the more common choice for most radiation detector applications because of several inherent advantages over current mode. First, the sensitivity that is achievable is often many factors greater than when using current or MSV mode because each individual quantum of radiation can be detected as a distinct pulse. Lower limits of detectability are then normally set by background levels. In current mode, the minimum detectable current may represent an average interaction rate in the detector that is many times greater. The second and more important advantage is that each pulse amplitude carries some information that is often a useful or even necessary part of a particular application, such as the case of this Thesis. In both current and MSV mode operations, this information on individual pulse amplitudes is lost and all interactions, regardless of amplitude, contribute to the average measured current.

1.4.2.3 Differential pulse height spectra

If we examine a large number of pulses when operating a radiation detector in pulse mode, their amplitudes will not all be the same. Variations may be due either to differences in the radiation energy or to fluctuations in the inherent response of the detector to mono-energetic radiation. The *pulse amplitude distribution* is a fundamental property of the detector output that is routinely used to deduce information about the incident radiation or the operation of the detector itself.

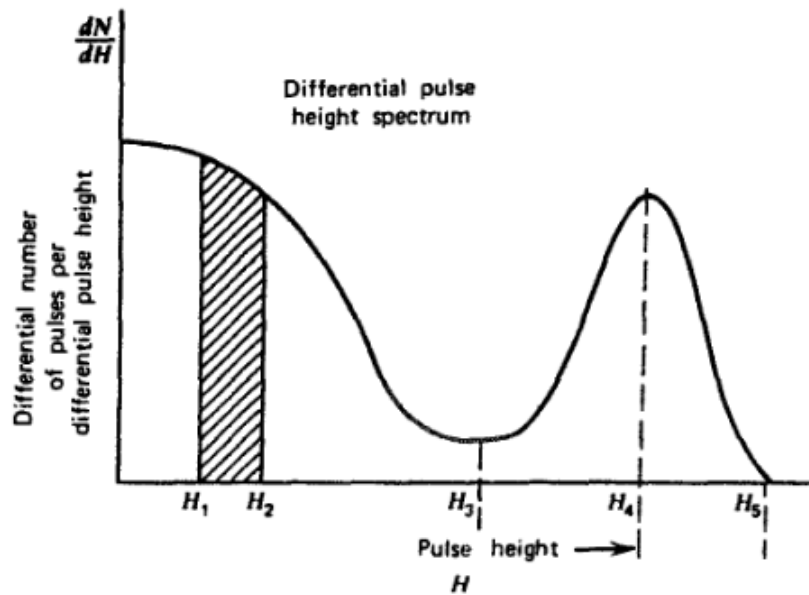


Figure 1.5: Example of differential pulse height spectra for an assumed source of pulses.

The most common way of displaying pulse amplitude information is through the *differential pulse height distribution*. Figure 1.5 gives a hypothetical distribution for purposes of example. The abscissa is a linear pulse amplitude scale that runs from zero to a value larger than the amplitude of any pulse observed from the source. The ordinate is the differential number dN of pulses observed with an amplitude within the differential amplitude increment dH , divided by that increment, or dN/dH . The horizontal scale then has units of pulse amplitude (Volts), whereas the vertical scale has units of inverse amplitude (Volts^{-1}). The number of pulses whose amplitude lies between two specific values, H_1 and H_2 , can be obtained by integrating the area under the distribution between those two limits, as shown by the hatched area in Fig. 1.5:

$$\text{Number of Pulses with Amplitude between } H_1 \text{ and } H_2 = \int_{H_1}^{H_2} \frac{dN}{dH} dH \quad (1.7)$$

The total number of pulses N_0 represented by the distribution can be obtained by integrating the area under the entire spectrum:

$$N_0 = \int_0^{\infty} \frac{dN}{dH} dH \quad (1.8)$$

The physical interpretation of differential pulse height spectra always involves areas under the spectrum between two given limits of pulse height. The value of the ordinate itself (dN/dH) has no physical significance until multiplied by an increment of the abscissa H .

1.4.2.4 Energy Resolution

A formal definition of detector energy resolution is shown in Fig. 1.6. The differential pulse height distribution for a hypothetical detector is shown under the same assumption that only radiation for a single energy is being recorded. The *full width at half maximum* (FWHM) is illustrated in the figure and is defined as the width of the distribution at a level that is just half the maximum ordinate of the peak. So that, any background or continuum on which the peak may be superimposed is negligible or has been subtracted away.

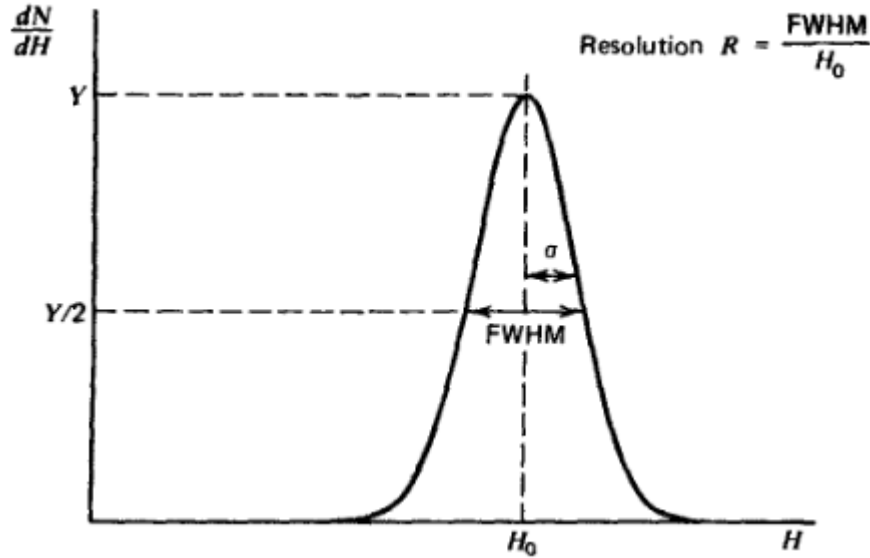


Figure 1.6: Definition of detector resolution. For peaks whose shape is Gaussian with standard deviation σ , the FWHM is given by 2.35σ .

The energy resolution of the detector is defined as the FWHM divided by the location of the peak centroid H_0 . The energy resolution R is thus a dimensionless fraction conventionally expressed as a percentage. Semiconductor diode detectors used in alpha spectroscopy can have an energy resolution less than 1%, whereas scintillation detectors used in gamma-ray spectroscopy normally show an energy resolution in the range of 3-10%. The thinner the figure for the energy resolution, the better the detector will be able to distinguish between two radiations whose energies lie near each other. An approximate rule of thumb is that it should be possible to resolve two energies that are separated by more than one value of the detector FWHM.

There are a number of potential sources of fluctuation in the response of a given detector that result in imperfect energy resolution. These include any drift of the operating characteristics of the detector during the course of the measurements, sources of *random noise* within the detector and instrumentation system, and *statistical noise* arising from the discrete nature of the measured signal itself. The third source is in some sense the most important because it represents an irreducible minimum amount of fluctuation that will always be present in the detector signal no matter how perfect the remainder of the system is made. Any other source of fluctuations in the signal chain will combine with the inherent statistical fluctuations from the detector to give the overall energy resolution of the measuring system. It is sometimes possible to measure the contribution to the overall FWHM due to a single component alone. For example, if the detector is replaced by a

stable pulse generator, the measured response of the remainder of the system will show a fluctuation due primarily to *electronic noise*. If there are several sources of fluctuation present and each is symmetric and independent, statistical theory predicts that the overall response function will always tend towards a Gaussian shape (see Appendix A), even if the individual sources are characterized by distribution of different shape. As a result, the Gaussian function is widely used to represent the response function of detector systems in which many different factors may contribute to the overall energy resolution. Then the total quadratic FWHM will be the sum of the quadratic FWHM values for each individual source of fluctuation:

$$(\text{FWHM})_{\text{overall}}^2 = (\text{FWHM})_{\text{statistical}}^2 + (\text{FWHM})_{\text{noise}}^2 + (\text{FWHM})_{\text{drift}}^2 + \dots$$

Each term on the right is the square of the FWHM that would be observed if all other sources of fluctuation were zero.

Noise influence on the Nuclear Physics instrumentation is further discussed in Chapter 2.

1.4.2.5 Detection Efficiency

All radiation detectors will, in principle, give rise to an output pulse for each quantum of radiation that interacts within its active volume. For primary charged radiation such as alpha or beta particles, interaction in the form of ionization or excitation will take place immediately upon entry of the particle into the active volume. After traveling a small fraction of its range, a typical particle will form enough ion pairs along its path to ensure that the resulting pulse is large enough to be recorded. Thus, it is often easy to arrange a situation in which a detector will see every alpha or beta particle that enters the active volume. Under these conditions, the detector has a *counting efficiency* of 100%.

On the other hand, uncharged radiation such as gamma rays or neutron must first undergo a significant interaction in the detector before detection is possible. Because these radiations can travel large distances between interactions, detectors are often less than 100% efficient. It then becomes necessary to have a precise figure for the detector efficiency in order to relate the number of pulses counted to the number of neutrons or photons incident on the detector.

From the experimental point of view, it is often used an efficiency named *peak efficiency*, because the number of full energy events is not sensitive to some perturbing effects such as scattering from surroundings objects or spurious noise, whereas *total efficiency* values may be influenced by variable conditions. The peak efficiency assumes that only those interactions that deposit the full energy of the incident radiation are counted. In a differential pulse height distribution, these full energy events are normally evidenced by a peak that appears at the highest end of the spectrum. Events that deposit only part of the incident radiation energy then will appear farther to the left in the spectrum. The number of full energy events can then be obtained by simply integrating the total area under the peak, shown as the hatched area in Fig. 1.7.

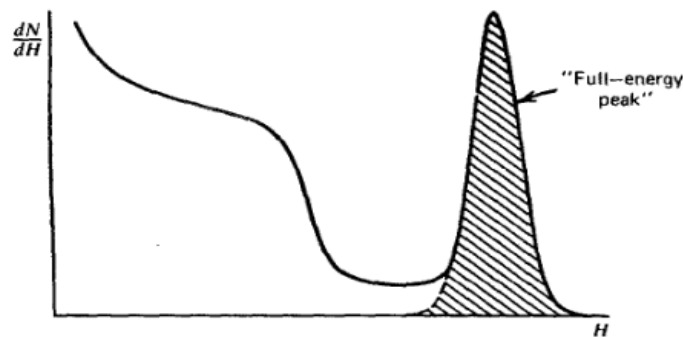


Figure 1.7: Example of the full-energy peak in a differential pulse height spectrum.

Given the most important general properties of radiation detectors, now a brief discussion of main types of radiation detectors subject of this Thesis is presented.

1.4.3 SCINTILLATION DETECTORS

The principle of operation of scintillation detectors is based on the collection of the photons emitted by the material following the detection of a charged particle. The mechanisms leading to the emission of photons after the initial energy deposit vary depending on the scintillator type (for example whether organic or inorganic), but all share the characteristic of producing one or more photons in the visible or near-visible range. The final number of visible photons is proportional to the energy loss of the detected particle in the material.

Many scintillator materials exist differing for scintillation efficiency, light emission wavelength, time constant of the de-excitation processes, ease of manufacturing, and density (hence stopping power, see Eqs. 1.2 and 1.3). For a general review see [13].

The ideal scintillation material should possess the following properties:

1. Conversion of the kinetic energy of charged particles into detectable light with high scintillation efficiency.
2. This conversion should be linear – the light yield should be proportional to deposited energy over as wide a range as possible.
3. The medium should be transparent to the wavelength of its own emission for good light collection.
4. The decay time of the induced luminescence should be short so that fast signal pulses can be generated.
5. The material should be of good optical quality and subject to manufacture in sizes large enough to be of interest as a practical detector.
6. Its index of refraction should be near that of glass (~ 1.5) to allow efficient coupling of the scintillation light to a light sensor.

No material simultaneously meets all these criteria, and the choice of a particular scintillator is always a compromise among these and other factors. The light output of a scintillation detector is usually characterized by an exponential decay, due the de-excitation of the scintillator material. Depending on the details of the excitation and de-excitation processes, more than one decay time constant may be present in the output signal.

Common material choices in Nuclear Physics are thallium activated sodium iodide NaI(Tl), thallium activated cesium iodide CsI(Tl) (good efficiency and energy resolution but with relatively long decay times, of the order of few μ s) and fast plastic scintillators (low efficiency and poor energy resolutions but with fast decay times, of the order of few ns).

The emission spectrum of the light produced by some inorganic scintillators is shown in Fig. 1.8. To make full use of the scintillation light, the spectrum should fall near the wavelength region of maximum sensitivity for the device used to detect the light.

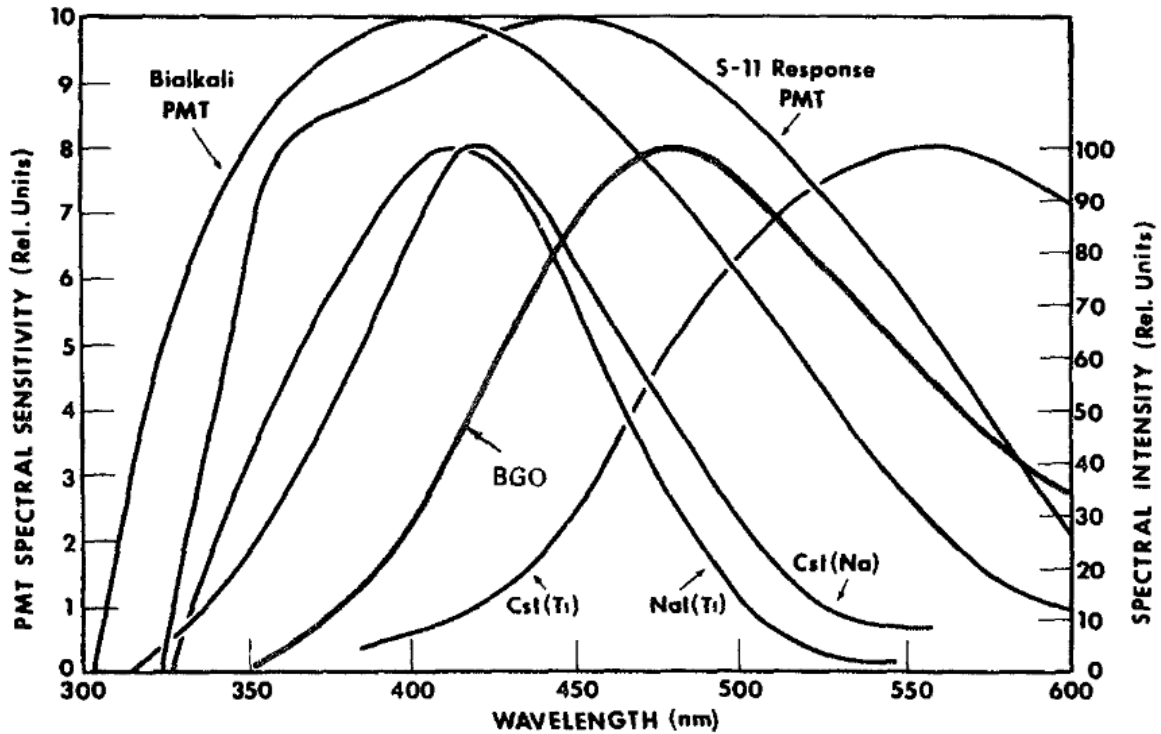


Figure 1.8: The emission spectra of several common inorganic scintillators. Also shown are the response curves for two widely used photo-cathodes. (Primarily from Scintillation Phosphor Catalog, The Harshaw Chemical Company. The emission spectrum for BGO is from Ref. 14).

The scintillation properties at room temperature of a collection of NaI(Tl), CsI(Tl) and CsI(Na) are compiled in Tab. 1.1. The fourth column represents the decay times. As shown, CsI(Tl) and CsI(Na) present two decay components. Percentages listed represent the relative yields of the components shown. The fifth column is an estimate of the total number of scintillation photons produced over the entire emission spectrum from the deposition of 1 MeV of energy by fast electrons. There is considerable variability in published values for a given material, most likely because of differences in impurity levels or variations in the optical quality of the samples. The sixth column compares the relative pulse amplitude when the scintillator is excited by fast electron (or gamma rays) and coupled to a glass end-window photomultiplier tube (UV sensitive) with a bi-alkali photocathode. The variability of photocathode may also introduce additional variations in these values.

For common inorganic scintillators, the light yield is more nearly proportional to deposited radiation energy than is typically observed in organic scintillators.

Table 1.1: Properties of inorganic scintillators commonly used in Nuclear Physics.

Scintillator	Wavelength of Max. Emission (nm)	Refractive Index	Decay Time (μ s)	Abs. Light Yield in Photons/MeV	Relative Pulse Height Using Bialk. PMT	Ref.
NaI(Tl)	415	1.85	0.23	38,000	1.00	15, 16
CsI(Tl)	540	1.80	0.68(64%), 3.34 (36%)	54,000	0.49	17-19
CsI(Na)	420	1.84	0.46, 4.18	39,000	1.10	20

Extensive study of the properties of these three inorganic scintillators is presented in Chapter 3.

In order to obtain an electric signal output, the scintillation photons coming from the detector must be collected and converted. A common conversion device is the *photomultiplier tube* (PMT), and the collection is usually enhanced using properly shaped detectors and/or light guides (taking advantage of reflection and diffusion of photons at interfaces).

The structure of a typical PMT is shown in Fig. 1.9. The photons produced by the scintillation process hit the photocathode. The purpose of the photocathode is the conversion of as many of the incident photons as possible into low-energy electrons. This process can be thought as a two step process: first the photon is absorbed by the photocathode, thus transferring its energy to a free electron of the material. Then the electron migrates and, if it reaches the surface of the photocathode, it may escape from the material. The combined efficiency of these processes is quite low and thus for a given number of incident photons only few photoelectrons are produced. Taking into account the various efficiencies, it is possible to estimate that the generation of a photoelectron requires – on average – an incident energy of about 100–500 eV, depending on the used scintillator. This means that the Poissonian fluctuations in the photoelectron number are often the main factor limiting the achievable energy resolution of the detector-phototube system. The current pulse due to photoelectrons would be very small and thus unfeasible for direct measurement. This problem is solved by the electron multiplier structure of Fig. 1.9. The photoelectrons are accelerated by the imposed electric field in the volume between the photocathode and the first dinode. When they strike the first dinode the acquired energy is high enough to produce a secondary electron emission from the

dinode. Typically 3–5 secondary electrons are produced for each primary photoelectron. The secondary electrons are then accelerated towards the next dinode where a further multiplication occurs. This process is repeated several times (12 in Fig. 1.9) until a measurable signal is obtained and output to the anode. This electrode arrangement allows an almost noise-free amplification of the original signal, still retaining the time structure of the original photon burst (if the transit time spread of the photomultiplier can be neglected). The average gain achieved by a PMT is 10^6 .

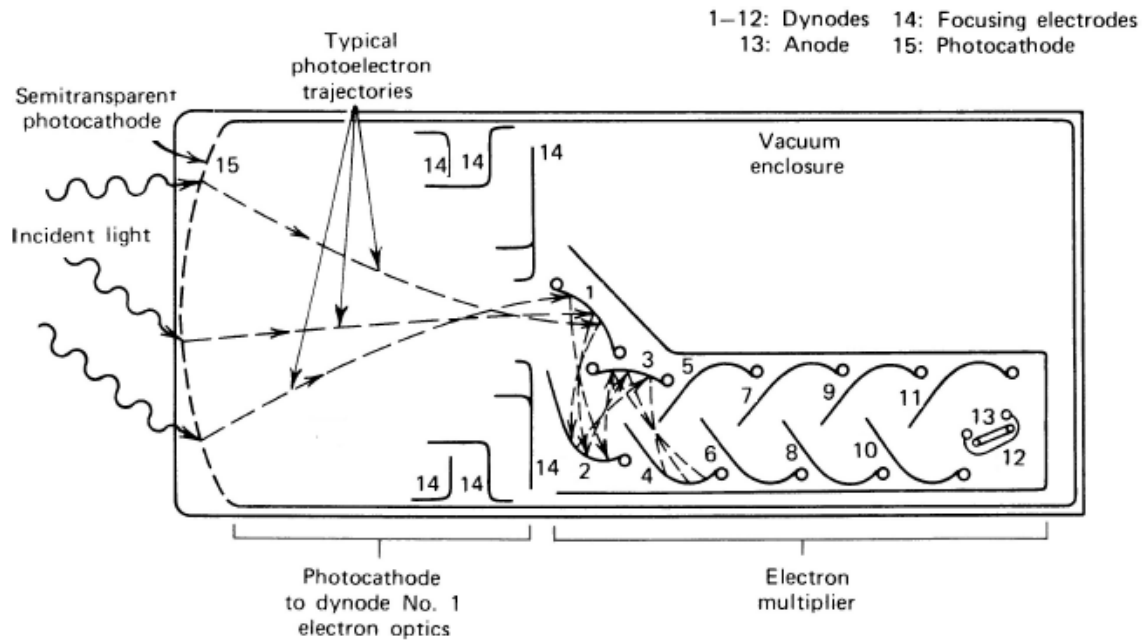


Figure 1.9: Typical photomultiplier structure. The photons hit the photocathode causing the emission of a small number of photoelectrons that is subsequently amplified by the dynodes.

Other devices like photodiodes can be used in place of a photomultiplier for the scintillation photons detection. Their principle of operation is the same of solid-state detectors, that are described in §1.4.5. These devices do not usually provide an amplification of the current (with the exception of avalanche photodiodes) and are characterized by inferior noise properties with respect to phototubes. On the other hand, their very compact size, easy handling and substantial immunity from magnetic fields make photodiodes attractive for the readout of scintillation detectors in some applications.

During the last few years, a strong development of an array of avalanche photodiodes, called Silicon Photomultiplier (whose characteristics are deeply presented in Chapter 3), have led to considering these devices as a good alternative for scintillation detectors, instead of the use of PMTs, up to now, they have been used mainly in applications for gamma ray spectroscopy. However, their performance as good charged particle scintillation detector is subject of study within this Thesis and will be extensively discussed in Chapter 3.

Scintillation detectors are commonly used for the detection of energetic light particles and for covering large areas (or angular regions) with a moderate cost. Fast scintillators are used in those applications where the definition of the arrival time of the particle is of paramount importance, at the expense of a much lower energy resolution.

1.4.4 GAS DETECTORS

In gas detectors the energy loss mechanism leading to the formation of ion-electron pairs (§1.4.1) is exploited. The active volume of the detector is filled with a particular gas mixture at low pressure, which is the medium where incoming charged particles deposit part of their energy creating ion-electron pairs. The number of created pairs is proportional to the energy deposited by the incoming particle, and, on the average, about 20–40 eV are required for the production of a pair (this value depends on the used gas mixture and on the particle type).

An electric field is applied over the gas volume, in order to separate ions and electrons and avoid recombination. With such an arrangement, ions and electrons start drifting inside the detector volume in opposite directions, thus inducing a current on the collecting electrodes.

The ion drift velocity is several orders of magnitude smaller than the electron one, and in many applications only the faster signal coming from the electron drift is used for measurement. Depending on the applied voltage and pressure the drift velocity of electrons may become high enough to generate a secondary ionization in the gas. This effect is called “gas multiplication” and it is often used to obtain a higher-level signal as output of the gas detector.

There exist many gas-detector configurations which cover the various needs met in both Nuclear and Particle Physics. This detector type is characterized by low detection thresholds, good timing properties, position sensitivity and poor energy resolution.

From the practical point of view the handling of a gas filled detector within an experiment that operates under vacuum needs particular care.

1.4.5 SOLID-STATE DETECTORS

The principle of operation of solid-state detectors closely resembles the one discussed for gas detectors.

The incoming particle deposits part of its energy into the detector material, which is a high-purity semiconductor junction (usually silicon or germanium); the ionization produces a number of electron-hole pairs proportional to deposited particle energy. About 3.6 eV are required for each electron-hole pair, thus making the contribution to the energy resolution due to fluctuations in the number of carriers much smaller than the previously discussed detector types, taking also into account that the effective fluctuations are reduced with respect to the pure Poissonian case by the Fano factor [21].

A bias voltage is applied to the semiconductor junction in order to separate electrons and holes and avoid recombination. Drift velocities of holes and electrons are of the same order of magnitude, and thus both charges give an important contribution to the overall current pulse while drifting towards the collecting electrodes.

The current output from the detector is usually processed with a *charge-sensitive preamplifier* as the one depicted in Fig. 1.10. The preamplifier integrates the current $i(t)$ over the capacitor C , whereas the resistor R is used to bring back to zero the output of the integrator with a decay time $\tau_{pre} = RC$ (much longer than the current signal duration). As discussed in §1.4.2.2, for times $t \ll \tau_{pre}$ the resulting signal is thus very similar to a step but for a non-zero rise time, given the finite duration of the current signal.

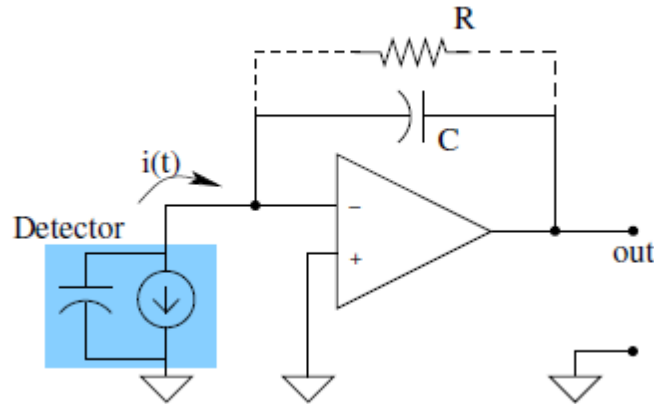


Figure 1.10: Simplified schematic of a charge preamplifier. The current pulse coming from the detector is integrated on the capacity C . The resistor R is used to bring back the output to zero over long times with a time constant equal to RC .

Due to the high intrinsic resolution of these detectors, the preamplifier noise often gives a non negligible contribution to the attainable final resolution, especially in those cases where the measurement of low-energy particles or gamma rays is of interest. Taking into account the various noise sources of the schematic in Fig. 1.10, the dark current noise of the detector and the bias resistor noise, the spectral noise density [22] of the preamplifier can be approximately described by the following expression:

$$\varpi(\omega) = a \cdot \frac{\tau_{pre}^2}{1 + \tau_{pre}^2 \omega^2} + b \approx \frac{a}{\omega^2} + b \quad (1.9)$$

where a and b are constants that depend on the detector-preamplifier system (the last approximation derives from considering the practical case of very large τ_{pre}). The b term increases with the detector capacitance, thus causing a higher *white noise* contribution for high capacitance detectors.

Typical values found in high-resolution germanium-based systems are $\tau_{pre} = 0.1 - 1$ ms, with a final contribution from the preamplifier noise to the achievable resolution of the order of 0.5–1 keV. A deeper discussion of the noise properties of these systems is given in §1.4.8, and in Chapter 2.

These detectors are usually employed where a high-resolution energy measurement is needed, with the added bonus of good quality timing properties. Germanium detectors

can be fabricated with relatively large active volumes (about 300 cm³) and are used for high resolution gamma ray spectroscopy applications. Silicon detector sizes are more limited (about 50–100 cm² with 100–500 μm thickness) and they are normally employed for charged particle detection.

1.4.6 PULSE-SHAPE ANALYSES

The ionization density, proportional to the specific energy loss dE/dx , varies greatly for different particles. In general the presence of a high ionization density produces a reduction of the final signal amplitude (generally indicated as “quenching”) and a distortion of the shape of the current pulse with respect to the low-ionization case. As a consequence, while the total charge of the output pulse is (or should be) proportional to the particle energy regardless of its type, these (and other) factors lead to a dependence of the pulse shape on the particle type.

A typical example is the response of the CsI(Tl) scintillator. Its current output can be schematized as the sum of two exponentially decaying pulses with different decay times as shown in Tab. 1.1. The relative weight of these two exponentials is related to the initial specific ionization density, and this finally gives a dependence on the particle charge and mass. The pulse-shape dependence on the particle type can be effectively used as an experimental tool for determining, with a single detector, not only the particle energy but also its type. This point will be deeper discussed in Chapter 3, since is also subject of analysis of the present work.

Commonly used detectors with notable pulse shape properties are scintillation detectors (mainly CsI), that have been used since several years in large Nuclear Physics experiments.

Recently, interest has grown in the application of pulse shape analyses (PSA) to silicon detectors for identification of the detected charged particles.

A different application of pulse shape analysis can be found in coaxial germanium detectors, where a dependence of the pulse shape on the interaction point is observed (due to the high inhomogeneous electric field inside the detector). International collaborations [23, 24] are actively working in this field with the goal of reconstructing the interaction point using segmented large-volume germanium detectors and digital-sampling methods.

1.4.7 COMPARISON BETWEEN DETECTOR TYPES

Depending on the particular application, the energy and the type of the particles to be detected, and the possible need for good energy and/or timing measurements, a particular detector type can be chosen. Often no single detector is able to satisfy all the experimental requirements and then two or more different types are used, trying to match their characteristics and to cover the needed detection range.

The comparison between each detector properties is not trivial, and would deserve a much deeper discussion. However, in order to describe better the range of applicability of each detector, in Tab. 1.2 a very simplified comparison is presented.

It is possible to appreciate that the low energy needed for the creation of an electron-hole pair makes solid-state detectors the option of choice for high-resolution energy measurements. The timing performances of the various detector types are similar (although they may vary significantly depending on the particular detector used), except for the case of fast plastic scintillators where the resolution can be as good as 10–30 ps. As a general rule of thumb, the timing properties deteriorate with the increase of the detector size.

Silicon detectors can be used to measure charged particles in a very wide charge range, whereas gas detectors have high efficiency only for highly ionizing particles and scintillation detectors are commonly used only in light charged particle detection applications (besides gamma ray detection).

Pulse-shape applications are well established in the case of inorganic scintillation detectors, whereas studies are still under way for solid-state devices. Gas detectors are the option of choice in very specific applications where a large area/volume coverage is needed. The price for a given angular coverage using solid-state detectors is generally higher than that of scintillation or gas ones. Whereas the resolution figures reported in Tab. 1.2 refer to ≈ 1 MeV energies, Nuclear Physics experiments usually operate over wide dynamic ranges, so that other experimental factors (like detector homogeneity, quenching, among others) are usually limiting the finally attainable energy resolution performances.

Table 1.2: Simplified comparison between the different detector types discussed in the text. Only the gross average properties of each detector type when used in a standard configuration have been reported.

	Scintillator	Gas	Solid-state
Energy/carrier	100-500 eV	20-40 eV	~3 eV
Energy resol. @ 1MeV	100-500 keV	20-50 keV	20-10 keV
Timing resol. @ 1MeV	~0.03-1 ns	0.1-1 ns	0.1-2 ns
Pulse shape	Y	N	Y/N
Area limits	100 cm ²	m ²	cm ²
Easy to handle	Y	Y/N	Y
Cost/cm2	\$	\$	\$\$

A typical Nuclear Physics experiment will use two or more detector types in order to reach its detection goals.

1.4.8 ANALOG ELECTRONICS: HIGH-RESOLUTION ENERGY MEASUREMENTS

For all the discussed detector types, the current output of the system is characterized by an amplitude (or an integral) proportional to the energy deposition of the detected particle. An accurate measure of this quantity thus allows, with proper calibration, the determination of the particle energy.

Solid-state detectors are the most demanding detectors in terms of electronic signal-to-noise-ratio (SNR – see Glossary -). The following discussion will thus focus on the use of analog electronics to extract the amplitude information on such signals, although many of the presented solutions can be applied to other detectors with small modifications. A careful optimization of the electronic processing chain is usually needed only for solid-state detectors when used for low-energy particle or gamma ray detection, whereas for high-energy particles as well as gas and scintillation detectors the choice of the signal processing methods and parameters is less critical.

As discussed in §1.4.5, silicon and germanium detectors are usually connected to charge-sensitive preamplifiers, whose output spectral noise density (given in Eq.1. 9) is the sum of a white component (b term) and a non-white one (a term) with a $1/\omega^2$ behavior. A filter is applied to the step-like output coming from the charge preamplifier in order to increase the SNR (see §2.1.3) of the signal. The peak of the filtered signal is measured using

Charge-to-Digital Converters (QDCs) or Peak-Sensing converters [13]. An example of signal shaping is presented in Fig. 1.11.

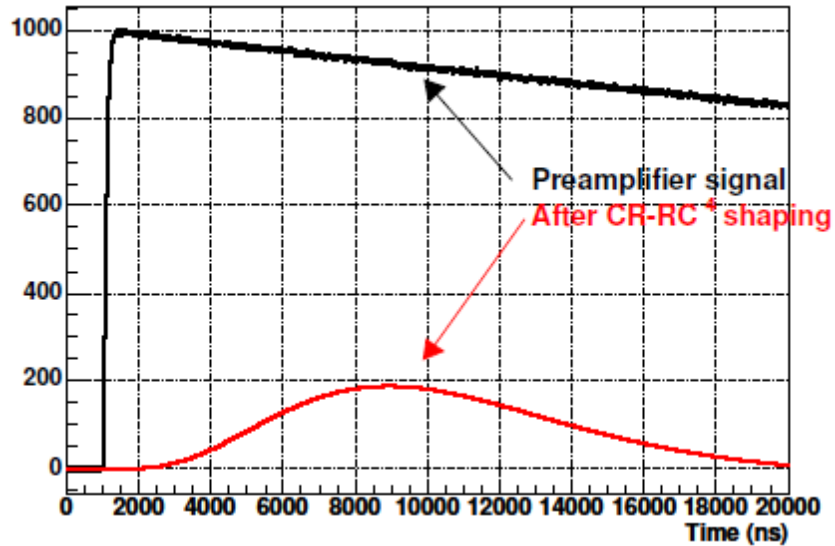


Figure 1.11: Example of shaping of the output of a charge preamplifier used in order to achieve a better signal-to-noise ratio. A $CR-RC^4$ network has been considered in this example.

Extensive work about the “optimal” signal-processing electronic chain to be used in this and similar experimental configurations can be found in the literature (see for example [25, 26]). It is found that the best SNR for a signal with these properties is achieved using an “infinite-cusp shaping” [26], which is a shaping network with an infinite output response (i.e. infinite duration in the time domain) characterized by a sharp cusp. Various practical considerations lead to the use of different shaping networks, whose performances are then usually measured as ratios with the infinite cusp one.

In Tab. 1.3 the SNR of two common configurations is reported: the $CR-RC$ shaping (a differentiation, CR , followed by a low-pass RC) and the $CR-RC^4$ (a differentiation, CR , followed by four low-pass RC networks). A deep discussion about analog shaping configuration commonly used in Nuclear Physics can be found in [13]. And a general discussion about analog filtering techniques can be found in [27].

In both configurations a single parameter $\tau_{sha} = RC$ (the shaping time) is used to select the desired frequency band. In Tab. 1.3 the time response of the filter $G_{step}(t)$ to a step and the time $t_{maximum}$ (the time at which the shaped signal reaches its maximum) obtained with a step signal as input are also reported.

Table 1.3: Parameters describing the behavior of a CR–RC and CR–RC⁴ shaping networks. See text for details.

Parameter	CR–RC	CR–RC ⁴
SNR/SNR _{cusps}	0.736	0.858
Step response G _{step} (t)	$\frac{t}{\tau_{sha}} \exp\left(-\frac{t}{\tau_{sha}}\right)$	$\frac{1}{24} \frac{t^4}{\tau_{sha}^4} \exp\left(-\frac{t}{\tau_{sha}}\right)$
t _{maximum}	τ_{sha}	4 τ_{sha}
α	1/8	35/512
β	1/8	5/512
γ	1/e	32/3 exp(-4)

The total output variance of the shaping filter \mathcal{F} (assuming a perfectly noiseless filtering network) can be computed from the filter transfer function $H_F(\omega)$ and from the input spectral noise density $\varpi(\omega)$ (see Eq. 1.9) as:

$$\sigma_{sha}^2 = \frac{1}{2\pi} \int_0^\infty \varpi(\omega) |H_F(\omega)|^2 d\omega \quad (1.10)$$

The following expression (normalized to signal output) is obtained:

$$\sigma_{sha}^2 = \frac{1}{\gamma^2} \left(\alpha a \tau_{sha} + \frac{\beta b}{\tau_{sha}} \right) \quad (1.11)$$

where γ is the shaped signal amplitude for $t = t_{maximum}$, α and β are numerical constants. The values of α , β and γ for the two considered filters are reported in Tab. 1.3.

Differentiating Eq. 1.11 with respect to τ_{sha} allows the determination of the optimal choice of τ_{sha} for a given a , b :

$$\tau_{sha}^{opt} = \sqrt{\frac{\beta b}{\alpha a}} \quad (1.12)$$

which gives the following equivalent expressions for the optimal resolution:

$$\sigma_{sha,opt}^2 = \frac{2}{\gamma^2} \alpha a \tau_{sha}^{opt} = \frac{2}{\gamma^2} \frac{\beta b}{\tau_{sha}^{opt}} = \frac{2}{\gamma^2} \sqrt{\alpha a \beta b} \quad (1.13)$$

The above discussion is based on the assumption of a fixed-shape step-like input signal. Whereas this approximation is usually valid for real signals when the signal rise time is much smaller than the shaping constant τ_{sha} , the presence of signals with different shapes gives an additional contribution to resolution worsening. Signals with the same amplitude but different shapes are treated in a different way by the shaping filter and thus the final maximum of the shaped signal depends not only on particle energy but also on signal shape. This effect causes a reduced amplitude for slower signals and it is commonly referred to as “ballistic deficit”. Further information about analog pulse processing is given in §2.1 and in [13].

1.4.9 ANALOG ELECTRONICS: TIMING MEASUREMENTS

Timing electronics is usually employed to perform coincidence measurements (for example to measure the *time of flight* of a particle) or to obtain information about the shape of the signal.

A commonly used method is the “constant fraction timing” (CFD), schematically shown in Fig. 1.12. Two copies of the original input signal of Fig. 1.12a are produced, one inverted and attenuated by a fraction f and the other delayed by a time amount δ ; a final signal is obtained summing the two signals, as shown in Fig. 1.12d.

The desired time mark is generated in correspondence to the zero crossing of the final signal. It is easily shown that, if the signals of interest are characterized by a linear rise and have a fixed shape, the obtained time reference is independent of the final amplitude of the original signal, and it is equal, apart from an offset, to the time where the original signal reaches a fraction of its amplitude (hence the name of the method). The method works properly when the delay δ is greater than the time needed by the signal to reach its asymptotic value (loosely speaking, its rise time).

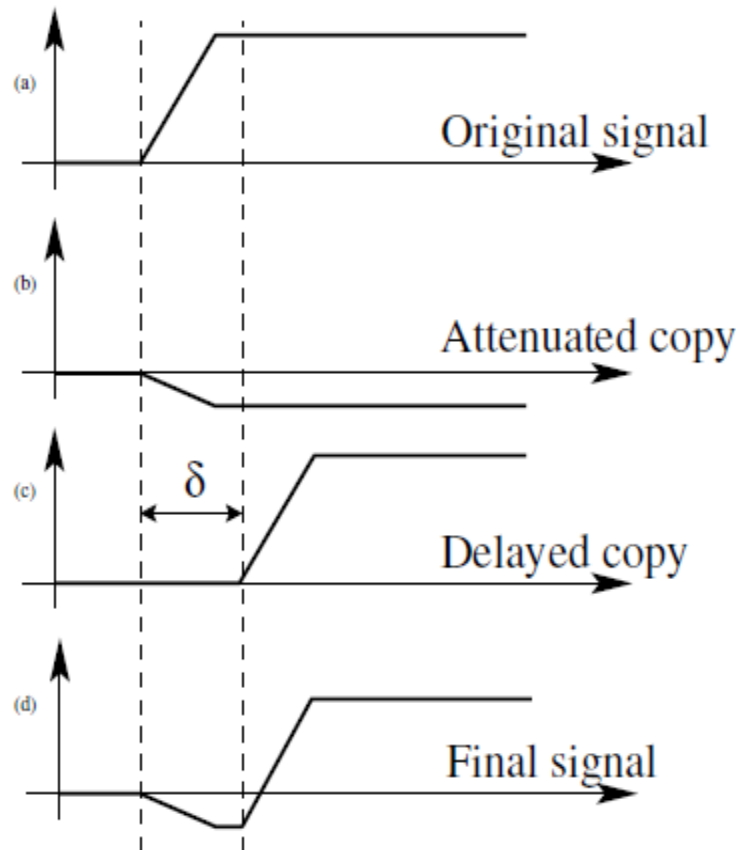


Figure 1.12: Schematic representation of the CFD working principle. One inverted and attenuated and one delayed copy of the original signal are summed to obtain a final signal characterized by a zero-crossing.

As a variant of this method, in Amplitude and Rise time Compensated CFD the delay δ is chosen as short as possible taking into account the experimental noise. It is possible to show that this modification allows a time measurement with the same desirable properties of CFD timing plus a compensation for the possibility of different rise times. This compensation effect is exact for linear signals and only approximate for real signals with a non-linear onset.

1.5 REQUIREMENTS FOR FUTURE DETECTION SYSTEMS

In the previous sections an overall description of the current status of experimental methods used in Nuclear Physics has been presented. It is important to note that, in order to take full advantage of the future radioactive nuclear beam facilities, these methods need to be enhanced or possibly replaced with new techniques. These improvements, if

possible, will allow a high-resolution determination of the various measurable quantities that are needed for enhancing our knowledge of nuclear matter. As discussed in §1.1.

For nuclear dynamics and thermodynamics studies the detection over the full solid-angle of charged particles that are emitted during the collision is of paramount importance. A one-unity resolution for charge and mass determination and a precise measurement of the velocity of each particle is needed in order to fully characterize each event, and this in turn requires high granularity, good timing measurements and isotopic identification of the detected particles.

For nuclear spectroscopy studies high granularity is needed for the requested angular-correlation accuracy and for high-resolution energy measurements, where an important effect due to Doppler shift of the emitted by the moving source is expected. The use of ancillary detectors for the detection of light charged particles ($Z \leq 4$) is also envisaged. The gamma ray energies involved in these applications are of the order of 10 keV–10 MeV, with a needed electronic energy resolution of about 1 keV. Electronic timing with a resolution of the order of few nanoseconds should be adequate for the purposes of these experiments.

As already discussed, a requirement that is common to many applications is the need of high granularity that in turn translates into the necessity of using a very high number of electronic channels. This means that the size, power dissipation, and cost of each channel must be low enough to allow a practical implementation of the system. Modularity and flexibility are also important issues in systems where the final number of acquisition channels is of the order of 10^4 or more.

Another common requirement is a high efficiency for the experimental apparatus. A full 4π solid angle coverage is needed in order to have full event-by-event reconstruction.

In this Thesis a detailed study of pulse processing techniques has been performed, making an extensive comparison between analog and digital instrumentation involved for these purposes, focusing to the advantages of using digital methods for both, energy and timing measurements.

These methods were carried out in off-line basis, meaning that no digital processors were used yet to perform operations in real time for portable applications. Nevertheless, the

acquired knowledge and the algorithms here developed are expected to be implemented on such real time processors, that would be able to satisfy most (if not all) of the requirements for future detection systems. For example, studies about using sampling systems in spectroscopy measurements for Doppler shift corrections (using segmented germanium detectors) are in progress.

Another key point covered by this Thesis focuses on particle detection methods. We have tested the performance of a scintillator detector based on CsI(Tl) and coupled to a Silicon Photomultiplier for light charged particle detection purposes, and its applicability in the next generation gamma-ray spectroscopy experiments.

CHAPTER 2: SIGNAL PROCESSING FOR NUCLEAR PHYSICS

In this chapter, a detailed study of the pulse processing techniques used for measurements in Nuclear Physics will be presented.

Firstly an introduction on signal processing stages will be given, describing the major electronic considerations to take into account for processing pulses coming from radiation detectors, focusing on signal/noise considerations. Then the main instrumentation standards developed for Nuclear Physics applications are presented, followed by an introduction to the pulse processing discrimination importance for particle identification purposes, which will be deeply discussed in Chapter 3. In §2.3 a detailed study of *digital* signal processing techniques is carried out, involving the analog-to-digital conversion, digital shaping, pulse shape analysis and baseline restoration stages. Also, brief introduction to the more common digital signal processors used for implementing the pulse processing tasks, such as ASICs (Application-Specific Integrated Circuits), DSPs (Digital Signal Processors) and FPGAs (Field Programmable Gate Arrays) is given, and finally in this chapter, a comparison between analog and digital approaches for pulse processing in Nuclear Physics applications is presented.

2.1 OVERVIEW OF PULSE PROCESSING [13]

The basic components in a typical signal processing chain are shown in Fig. 2.1: An incident quantum interacts in the detector and deposits energy that is converted into a current pulse. The total charge is usually too small to be sensed directly. The current is sent to a *pre-amplifier*, an interface between the detector and the subsequent processing electronics. The preamplifier usually has a charge-sensitive configuration (as the one depicted in §1.4.5), integrating the transient current pulse to produce a voltage step ΔV proportional to Q . The *shaping amplifier* converts the preamplifier output signal into a form suitable for measurements, producing an output voltage pulse with pulse height V_{peak} proportional to the deposited charge Q . Since the size of Q reflects the energy deposited by the incident quantum in the detector, the pulse height distribution is then recorded to provide information about the energy distribution of the incident radiation.

The output of the shaping amplifier should return rapidly to the *baseline* to prevent pulses from overlapping and a resulting distortion of the measurement. The output must return to true zero between pulses so that the peak is referenced to the correct baseline. The amplifier also filters high- and low-frequency noise to improve the signal-to-noise ratio. Both the noise filtering and return to baseline change the time profile or shape of the pulse, hence the name shaping amplifier.

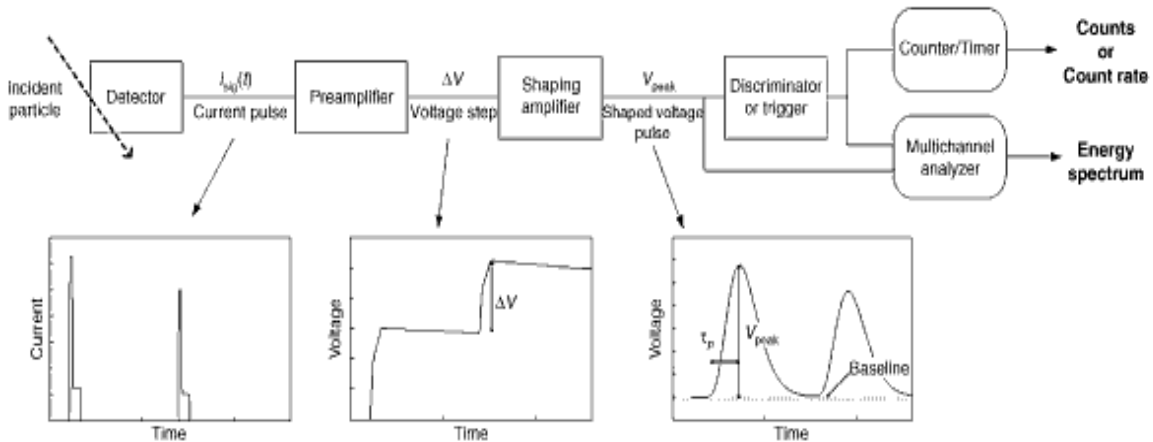


Figure 2.1: Schematic diagram of the detector and electronics. Typical outputs from each stage of the processing electronics (for two pulses) are also sketched.

The amplifier is characterized by a *shaping time constant* that is related to the duration of the pulse produced at its output. Since radiation interactions usually occur at random time intervals, there is always some probability that two pulses will overlap in time, resulting in distorted outputs. Short shaping times are desirable to minimize the overlap or pulse pile-up. However, since a short shaping time passes more broadband *electronic noise*, this choice may result in a greater influence of noise on the information carried by the pulse amplitude. This trade-off is fundamental in shaping amplifiers. Shaping amplifiers with multiple choices of shaping techniques may offer better performance in this trade space, but at the cost of more complexity, more power, and so on. Shaping amplifiers also differ in how well they maintain the baseline relative to the true zero.

The shaped pulse is sent to circuits that select pulses for further processing. This selection may be very simple – for example, an *integral discriminator* selects all pulses with pulse height above a certain threshold. A *differential discriminator*, also called a *single channel analyzer*, selects pulses with peak amplitude between upper and lower thresholds. More complex logic may reject events that pile up or exhibit distorted pulse shapes. Many systems have components that require detectors to be triggered within a narrow time interval as part of selection logic.

Selected events are then processed by circuits that produce a result that depends on the accumulation of many individual pulses over a defined measurement time. The simplest example is a counter, which counts the number of selected events over a finite time period. A more complex example is a *multichannel analyzer*, or MCA. The MCA measures the pulse height for each of a series of selected events, assigning the height to one of many pulse height ranges or channels. It then increments a counter (or memory register) for the appropriate channel. At the end of the measurement, the result is a histogram containing the number of pulses that deposited energy within each of its amplitude bins. The output histogram is called the *pulse height spectrum*. It consists of digital values that can be displayed, stored, or transmitted for further processing and analysis.

Figure 2.2 shows the schematic of a simple system implementing these functions. The detector could be, for example, a solid-state detector as described in §1.4.5. Radiation interacting in its sensitive volume creates electron-hole pairs that move under the applied electric field to the appropriate electrodes, generating a current pulse by their motion. This pulse of current is integrated onto the feedback capacitor C_F , producing pulses $\Delta V = Q/C_F$. In a typical application, the input charge per pulse is in the order of femtocoulombs, C_F is in picofarads, and ΔV in millivolts. The feedback resistor R_F restores the input to ground with a very long time constant, $R_F C_F$, usually set to hundreds of microseconds. The result is usually called a *tail pulse*, with rapid rise and very slow return to baseline. In Fig. 2.2, two of these pulses closely spaced in time are sketched at the output of the preamplifier. The figure represents the return to baseline as very long compared with the time scale illustrated, so the two pulses superimpose in something resembling a staircase output.

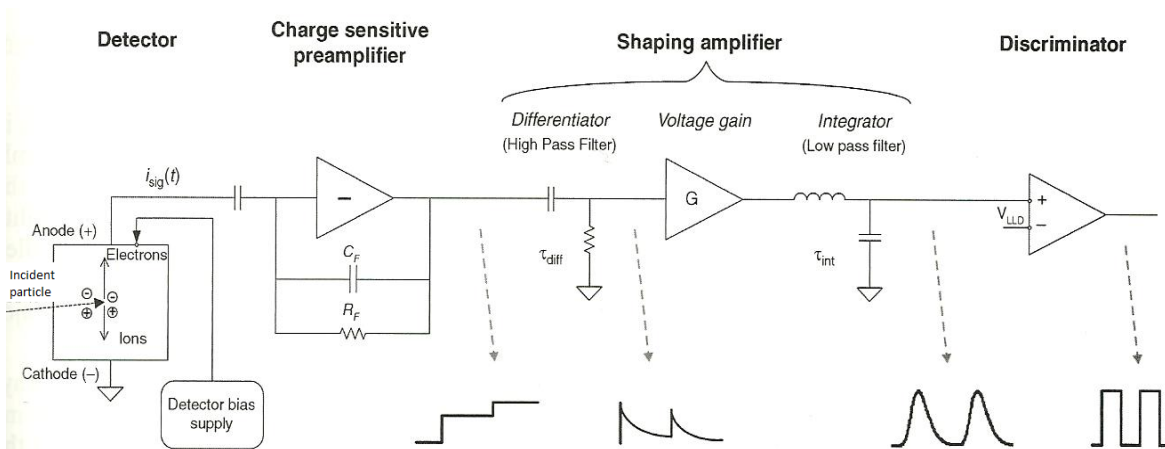


Figure 2.2: Schematic of simple signal processing electronics. This circuit is suitable for use in many applications and is conceptually similar to more complex circuits.

Because the preamplifier output pulses superimpose one on another in time, the first stage of the shaping amplifier is a *high-pass filter* or *differentiator*. This stage passes the rising edge from the preamp, but then the signal returns rapidly to baseline so that subsequent pulses can be accurately processed. These differentiated pulses are amplified to voltages required by subsequent circuits. High-frequency noise is present along with the signal, so the amplified pulse is then passed to a low-pass filter or integrator to improve the signal-to-noise ratio and to make it easier to measure the peak height. The shaped pulse has a rise time of order τ_{int} and a fall time of order τ_{diff} . These are usually set to equal values yielding the shaping time constant τ . The shaped pulse then has duration of order τ , and a bandwidth of order $1/\tau$. The final unit shown in Fig. 2.2 is a *discriminator* that outputs a logic pulse for each shaped pulse exceeding its set threshold. These logic pulses can then be passed on to a simple counter or further processed.

2.1.1 MAJOR ELECTRONIC CONSIDERATIONS

The objective of the pulse processing is to measure the detector signal with no distortion and with minimum influence from electronic noise. In real instrumentation, the pulse processing will affect the measurements in ways that can be as important as the function of the detector itself. There are five general categories to take into account when choosing parameters of the electronic system and usually it is necessary to trade-off performance in one or more of these general categories:

1. One of the distinguishing characteristics of radiation applications from other fields in electrical measurements is that in most cases the events in the detector are randomly distributed in time. Some time intervals between events will always be short (see the discussion of interval distribution in Appendix A). This characteristic opens the possibility that two pulses closely spaced in time may interfere with each other, a process called pulse pile-up. At high counting rates, these effects may become serious and require user choices in the processing of the pulses that minimize their pile-up.
2. Electronic noise, defined as any unwanted fluctuations in the processed signal, is always present at some level in any electrical measurement. Noise considerations often become a dominant concern in the processing of pulses from radiation detectors because of the small-amplitude signals that they intrinsically produce. The choices made in processing these pulses, most critically in the preamplifier and shaping amplifier, can strongly affect the SNR of the recorded pulses, and thus the energy resolution that is achieved.

3. Measurements of the pulse amplitude are ideally made with respect to a true zero baseline. However, there are often conditions that may tend to displace the actual baseline either above or below true zero. Strategies can be chosen to eliminate or minimize this baseline shift to best preserve the accuracy of the pulse amplitude measurement.
4. Sometimes there are conditions in which the amplitude of pulses produced by the processing system may drift over the course of the measurement due to changes in temperature, supply voltages, or other environmental factors. This drift, if significant, will cause a deterioration of the recorded energy resolution. Techniques to minimize these effects in recorded pulse height spectra are called methods of *spectrum stabilization*.
5. There are many applications in which the precise time of occurrence of an event in a detector is of importance, such as the sensing of coincident events in multiple detectors. Units known as *triggers* are designed to produce a timing pulse that is closely coupled to the true time of interaction in the detector. The ideal trigger produces its output at a time that is independent of the amplitude of the input pulse, independent of its shape, and unaffected by noise.

2.1.2 DEVICE IMPEDANCES

A basic concept in the processing of pulses from radiation detectors is the impedance of the devices that comprise the signal-processing chain. A simplified representation of the input and output configurations of a typical component is shown in Fig. 2.3. Both the input and output impedances can in general involve capacitive or inductive components, but for the sake of simplicity, a purely resistive impedance will be assumed.

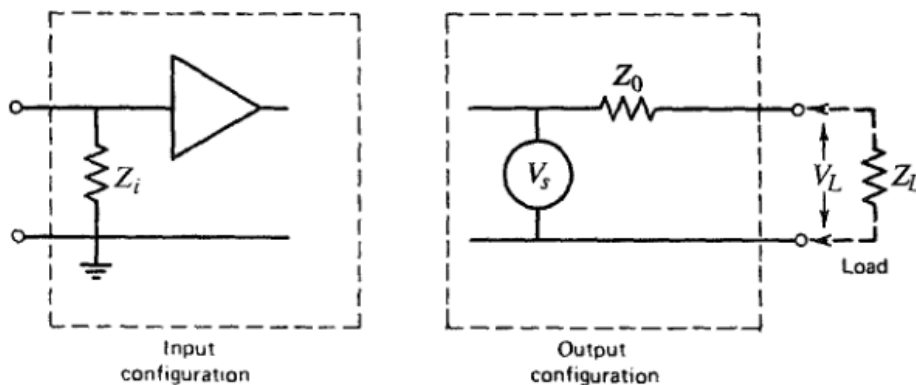


Figure 2.3: Idealized input and output configuration. For the input configuration, the triangle represents an ideal operational amplifier with infinite input impedance. Therefore, the effective device input impedance is Z_i . For the output configuration, Z_o represents the output impedance in series with an ideal voltage generator V_s .

The input impedance Z_i represents the extent to which a device loads a given signal source. A high input impedance will draw very little current from the source and therefore present only a very light load. For example, the input impedance of an oscilloscope is always very high to avoid perturbing the signals that are being inspected. For most applications, input impedances of devices are kept high to avoid excessive loading, but other factors may sometimes dictate situations in which the input impedance must be low enough to load the source significantly.

The output impedance can be thought of as an internal resistance in series with a voltage generator representing the output stage of a given component (see Fig. 2.3). For most applications, one would ideally want this output impedance to be as low as possible to minimize the signal loss when the output is loaded by a subsequent component. In Fig. 2.3, the voltage V_L appearing across a loading Z_L is given by the voltage-divider relation

$$V_L = V_S \frac{Z_L}{Z_0 + Z_L} \quad (2.1)$$

The open circuit or unloaded ($Z_L \rightarrow \infty$) voltage appearing at the output of the device is simply V_S . To preserve maximum signal level, one normally wants V_L to be as large a fraction of V_S as possible. If the output impedance is low compared with the load ($Z_0 \ll Z_L$), then $V_L \approx V_S$ and essentially all the signal voltage is transmitted to the load. If the output impedance is equal to the load ($Z_0 = Z_L$), then $V_L = V_S/2$ and only half the unloaded output voltage of the device appears across the load. Output stages with low output impedance thus are often an important design goal.

When devices are interconnected in a signal chain, the load Z_L presented to a given component is the input impedance of the following one. If all output impedances are low compared with input impedances, the maximum signal level is preserved throughout the chain. This condition is often realized in normal detector pulse processing systems. If very fast pulses are being handled, however, considerations involving reflection in coaxial cables can dictate impedance-matching conditions in which the output/input impedance ratio is not always small, and some signal attenuation will occur. Further information regarding cable reflections can be found in Appendix B.

2.1.3 NOISE CONSIDERATIONS

By definition, noise is any undesired fluctuation that appears superimposed on a signal source. Figure 2.4 is a graphical representation of the way in which a random noise

component can degrade the information carried by the amplitude of pulses from a radiation detector. There are only outlined some of the most important consideration regarding noise sources and the practical steps that can be taken to minimize their influence on measured pulse height spectra.

Intrinsic noise is the noise originated within the devices that constitute a circuit. There will be spontaneous fluctuations in both voltage and current at the preamplifier input, resulting from the physics of the devices and materials that make up the preamplifier input circuit, including the detector. This discussion is limited only to a few of the more important considerations. Electric current can be written $I = env$, where e is the charge on an electron, n is the number of carriers, and v is their mean velocity. Quantum effects cause spontaneous fluctuation in both the number and velocity of carriers, causing intrinsic noise. For example, all semiconductor detectors have a *leakage current*. In the absence of a radiation signal, a small number of carriers continuously pass through the diode junction. This number is subject to statistical fluctuations, termed *shot noise*, which are indistinguishable from fluctuations in the signal current. As another example, even in a device with no net current where the mean velocity of the carriers is zero, the carriers undergo Brownian thermal motion. The RMS thermal velocity is not zero, giving rise to a fluctuating instantaneous current called *thermal* or *Johnson noise*.

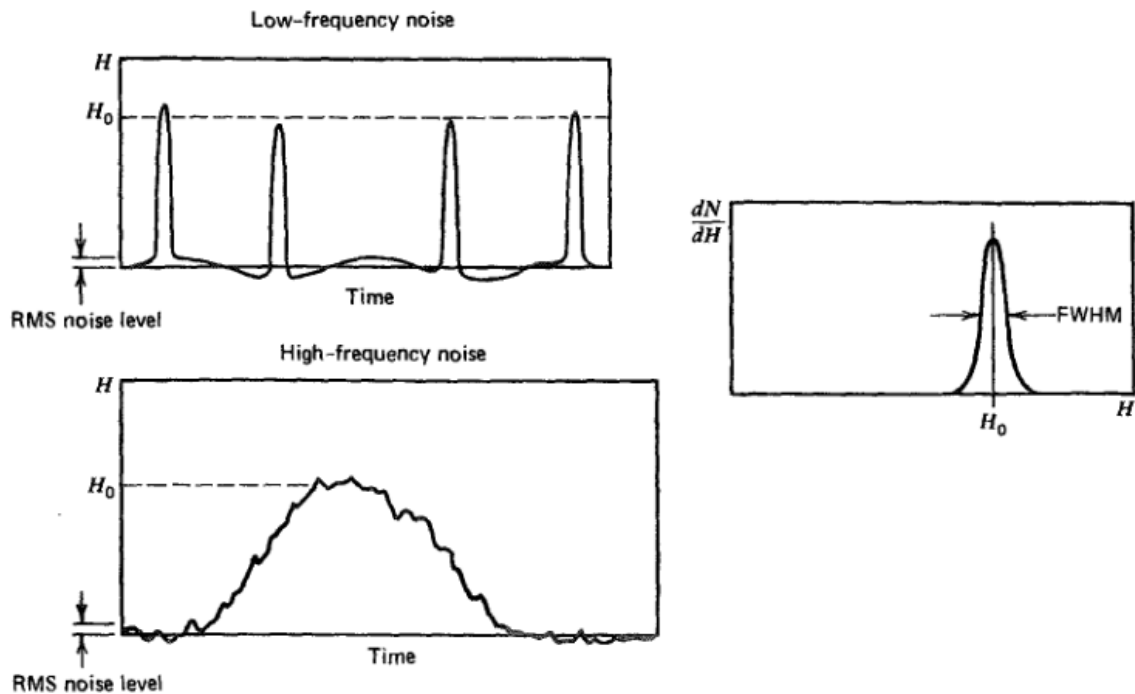


Figure 2.4: Sketches of the effect of low-frequency and high-frequency noise on signal pulses of constant amplitude. The effect is to broaden the peak recorded in the differential pulse height spectrum for the pulses. The FWHM of the peak of Gaussian-distributed noise will be equal to the RMS noise level multiplied by a shape factor of 2.35, provided noise is the only factor in the broadening peak.

Extrinsic noise or interference is originated in devices outside the circuit and couples into the circuit. There are many possible sources of interference in radiation detection, including *ground noise* arising from currents flowing in the ground path of the circuit, power line pick-up arising from the ac currents flowing in power lines (see Appendix B for grounding and picking-up noises), *crosstalk* from digital circuitry into analog circuits, and various other sources. In many measurements, interference effects such as ground loops may dominate the noise in nuclear instrumentation, so interference is a very important practical topic. Some useful tips against interference are:

- Pre-amplify the signal as close to the detector as possible. Once the signal amplitude is well above any interference, longer wires can be used for connection to later amplification stages.
- Shield the pre-amplifier with a metal enclosure to reduce electromagnetic interference on the signal lines. Use shielded cables to carry power and signals between enclosures (Appendix B).
- Arrange a second wire close to the signal-carrying wire so that it picks-up essentially the same interference but is not connected to the signal source. Differential amplification will then cancel most of the interference.
- If the signal and the unwanted noise contain significantly different frequency content, frequency filtering can help removing the noise while retaining as much of the signal as possible.

Another source of spurious pulses occurs if there are discharges or micro-breakdowns across capacitors or insulators that isolate high voltage, particularly under conditions in which their surfaces are exposed to high humidity. Since nearly all detectors require a voltage for their operation, such discharges are a possible cause of occasional pulses [28] that have nothing to do with radiation interactions in the detector.

The important sources of noise occur near the beginning of the signal chain where the signal level is at minimum. Noise generated at this point undergoes the same amplification as the signal, whereas noise generated further along the signal chain is usually much smaller than the signal. Therefore, discussions of electronic noise sources generally center on the preamplifier and, most importantly, its input stage. Noise sources can be categorized into those that are effectively in parallel with the input and those that are in series with the signal source. Sources of *parallel noise* include the fluctuations in the leakage current within the detector itself and in the gate-source current of the *field effect transistor* (FET) in the input stage of the preamplifier. *Series noise* sources involve the contribution of Johnson noise associated with series resistances and the thermal noise of

the FET. The frequency spectrum of both series and parallel noise is very broad, and for some analytical purposes it is often assumed that a “white” or uniform distribution in frequency holds.

In contrast, the frequency spectrum of the signal is confined to a much narrower band. For example, the signal from a detector whose charge collection time is about a microsecond can never contain useful information on a time scale of nanoseconds. Therefore, low-pass filtering of the output of such a detector will eliminate the contribution of high-frequency noise but will not affect the information-carrying components of the signal. Similarly, low-frequency power line pick-up is a noise source that can potentially degrade the signal, but high-pass filtering can remove this component without substantially affecting the signal pulse shape from most detectors. Therefore, the pulse-shaping role traditionally carried out by the linear amplifier actually amounts to selective filtering to remove as much broad spectrum noise as possible without severely attenuating the useful signal components. The pulse shaping is normally carried out through a combination of differentiating and integrating circuits, which corresponds to high-pass and low-pass filtering operations respectively.

The amount of noise added by the preamplifier-amplifier combination is often expressed in terms of the *equivalent noise charge* (ENC), defined as the amount of charge that, if applied suddenly to the input terminals of the system, would give rise to an output voltage equal to the RMS level of the output due only to noise. Formally the ENC is expressed in absolute units of charge, or coulombs. However, it has become common to divide this value by the unit charge of an electron (1.6×10^{-19} C) to express it in units of electron charges. For example, the electronic noise in a given system may be expressed as “100 electrons”, equivalent to 1.6×10^{-17} C.

For a specified type of detector, the contribution of electronic noise to the FWHM of peaks in the energy spectrum can be calculated from the ENC. In Fig. 2.4, the FWHM is equal to 2.35 multiplied by the RMS value of the noise level, or 2.35 times the ENC value. To convert to energy units one must also multiply by ϵ , the deposited energy required to create one charge carrier. In silicon at room temperature, $\epsilon = 3.62$ eV, so the relationship becomes:

$$FWHM \text{ (eV silicon)} = 2.35 \times 3.62 \text{ eV} \times ENC \text{ (electrons)} = 8.51 \text{ ENC (electrons)}$$

Thus the previous example of an ENC of 100 electrons predicts a peak width contribution (FWHM) caused by electronic noise in silicon detectors of 851 eV.

2.1.4 DEPENDENCE OF NOISE ON SHAPING TIME AND CAPACITANCE

The importance of various sources of electronic noise in the measured signal-to-noise ratio depends on choices made in the filtering or shaping operation. One of the important choices in spectroscopic amplifiers is a wide range of possible shaping times. Figure 2.5 shows that the contribution of series noise mentioned in the previous section tends to become less important as the shaping time is increased. On the other hand, sources of parallel noise become more important. There is another category of noise sources that are generally grouped together under the term $1/f$ noise that includes, for example, the effects of capture and release of charges in the input FET. This latter category contributes to the electronic noise in a manner that does not change with the choice of the shaping time.

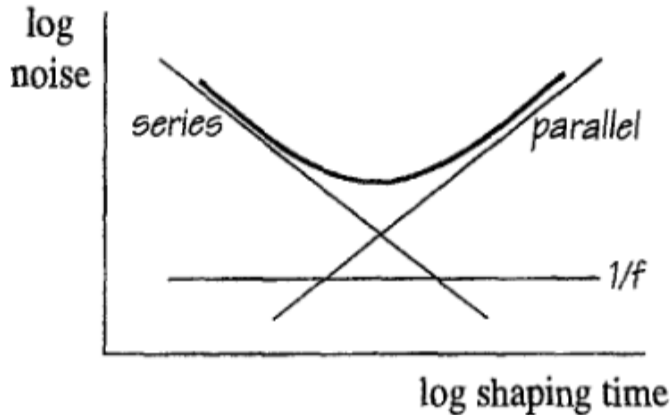


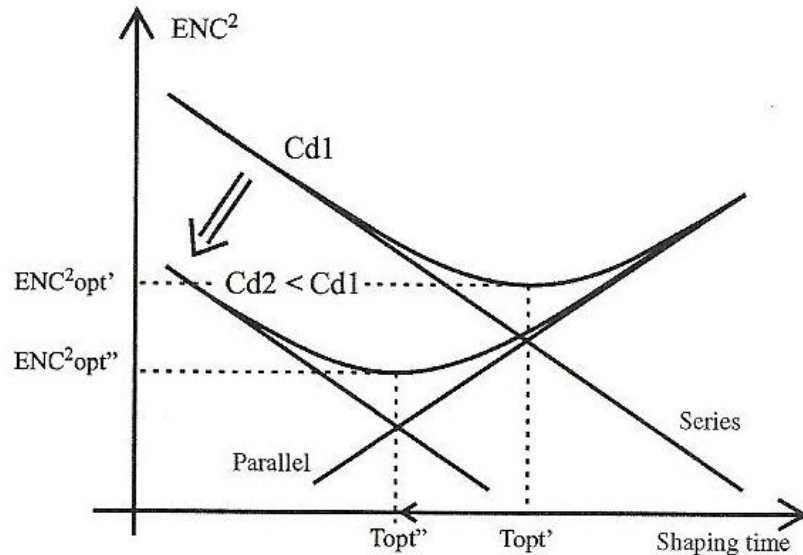
Figure 2.5: Variation of the contributions of series and parallel noise sources as a function of the shaping time in the pulse processing electronics. The minimum in the total occurs at the shaping time that results in equal contributions from series and parallel noise. The $1/f$ noise contribution is unaffected by the shaping time.

Considering the effect of all three sources of noise (which will be combined in quadrature), the overall electronic noise contribution will go through a minimum as the shaping time is increased from a small value. This optimum shaping time will generally occur at the point where the series and parallel noise contributions are equal. An experimental optimization of the shaping time can be done by measuring the pulse height resolution of the system as the shaping times are varied, carrying out these measurements at a counting rate equivalent to that expected in the application itself.

The contribution of series noise as a fraction of the signal increases with detector capacitance, while the relative contribution of parallel noise remains independent of this capacitance. In Fig. 2.6, the series and parallel noise behavior of two almost identical detectors is plotted, with the only difference being the detector capacitance value. Two important points are illustrated by this figure. First, because of its lower series noise, the detector with lower capacitance achieves a lower overall noise figure at its minimum.

Thus minimizing capacitance is a dominant consideration in detector choice and design when the lowest level of electronic noise is important. A second point is that the optimum shaping time at which the minimum is achieved is shorter for the detector with lower capacitance. All other factor being equal, the detector with lower capacitance can therefore be operated at higher counting rates before pulse pile-up reaches a given level of severity.

Figure 2.6: Series and parallel noise behavior of two detectors that are identical except for their capacitance values. The higher-capacitance detector (labeled as Cd1) reaches its minimum noise performance at an optimum shaping time labeled T_{opt}' . The detector with lower capacitance reaches a lower noise level at a shorter optimum shaping time.



2.2 INSTRUMENT STANDARDS [13]

Before the widespread use of solid-state circuitry, most electronic instrumentation used for nuclear measurements consisted of vacuum tube circuits housed in a self-contained chassis and required only connection to a power line. To facilitate mounting in a vertical stack, much of this equipment was built to fit a frame commonly known as the standard *19-in. relay rack*. Individual chassis are screw mounted one above the other in a relay rack, and widespread use persists to this day for the convenient mounting of nuclear electronic components. Some bulky units such as high-voltage power supplies continue to be manufactured in the full 19-in. width, but the advent of solid-state circuitry has led to more compact packaging in which only a fraction of the full width needs to be occupied by a single electronic unit.

It has become common in practice to manufacture most nuclear electronics in standard modules, a number of which can fit into a housing called a bin or *crate*, which occupies the full 19-in. width. Two important international standards, the NIM (Nuclear Instrument

Module) and the CAMAC (Computer Automated Measurement And Control) standards, have become widely accepted, and now virtually all modular nuclear electronics are manufactured according to one of them. These systems have resulted in a great simplification for the user, and one can quite generally intermix components and bins from different manufacturers with assurance that those adhering to a common standard will be mutually compatible. The NIM system is usually better suited for small-scale linear pulse processing normally encountered in the routine application of radiation detectors. The more costly CAMAC system, which is strongly oriented towards large digital systems and computing interfacing, is usually necessary only when large-scale signal processing involving many detectors or logical operation is required. A third common standard, called VMEbus, has evolved from specifications originally designed for computer interfacing, and some nuclear instrumentation is now available in that format as well.

As a self-contained system, each of these standards shares the following attributes:

- The basic dimensions for the bin and modules are specified so that all modules and bins within a given system are mechanically interchangeable.
- The philosophy generally adopted is that only the bin (or crate) will be connected to the laboratory ac power, and it will contain the necessary power supplies to generate all the dc supply voltages required by all modules contained within that bin. Individual modules therefore do not contain their own power supplies, but draw power from the bin in which they are located.
- The connector interface between the module and bin must therefore be standardized both electrically and mechanically, so that any standard module can draw its required power when plugged into any one of the available bin locations.
- Specifications are included for the polarity and span of both logic and linear pulse of various types.

See Appendix C for further information about NIM, CAMAC, and VMEbus Instrumentation standards.

2.3 PULSE SHAPE DISCRIMINATION [13]

The usual information carried by a linear pulse is its amplitude (and time of occurrence). There are occasions in nuclear measurements, however, when the shape of the pulse also assumes some importance. Most shape differences arise because of differences in the time profile of the current produced in the detector by a radiation interaction. If a fast

linear pulse is generated with a short collection time constant at the detector, the shape of the pulse is a reproduction of the time history of this current and will therefore directly reproduce these differences. In the more common application, the linear tail pulse obtained by collecting this current across a large time constant will show changes only in its leading edge characteristics. Therefore, pulse shape discrimination (PSD) methods designed to sense the difference between such events are sometimes also called *rise time discrimination* methods.

Sensing differences in pulse shape can serve a useful purpose when applied to the output of a number of different detector types. One of the applications of PSD is of great interest for this Thesis: the separation of various particle types in scintillators such as CsI(Tl), as will be explained in Chapter 3.

There are two general approaches that have been used to carry out pulse shape discrimination measurements. The first is based on electronic methods of sensing the differences in the rise time of an output pulse, while the second derives a signal based on integrating the total charge over two different time periods. As will be also discussed in Chapter 3, for this Thesis we have used the second approach. This method is based on independent measurements of the integrated charge over two different time regions of the pulse. The ratio of these signals will be approximately constant for pulses of common shape, independent of pulse amplitude. The implementation of this approach can either be carried out with analog circuitry (for example, as in [29-31]) or using digital techniques [32-38]. We have chosen digital techniques explained in Chapter 3.

2.4 DIGITAL PULSE PROCESSING [13]

Beginning in the early 1990s the development of high-speed analog-to-digital converters (ADCs) with good resolution opened a new possibility for the digital processing of pulses from detectors. A number of commercially available spectroscopic systems now incorporate digital processing in place of the traditional analog approach, and they demonstrate significant advantages over analog systems in some circumstances, as will be presented later on.

With sufficiently fast and accurate ADCs, all the information in a single analog pulse from a detector and preamplifier can be preserved by taking multiple samples of the pulse amplitude during the duration of the pulse and converting the samples into a sequence of digital values. Many samples are required during the charge collection time of the

detector if the full shape information is to be preserved, so very fast ADCs are needed. The pulse characteristics are conveyed by a string of numbers that can then be manipulated using standard digital operations such as addition, multiplication, and so on. Combinations of these operations can emulate the standard shaping (or filtering) steps or differentiation and integration, and produce pulse shapes that are similar to those that have proven useful in analog shaping. These digital shapers (or filters) have the same effect as the equivalent analog processes in determining the overall width of the shaped pulse as well as in enhancing its signal-to-noise characteristics.

There are a number of potential advantages to digital signal processing. It offers an unlimited flexibility in the choice of shaping parameters since these are only inputs to be set into the software or firmware routines that carry out the digital operations. Digital processing allows a more detailed analysis when dealing with signals from multiple outputs configured on the same detector, usually as strips or pixels. While only one electrode normally collects the charges from an interaction point and produces a pulse proportional to the total collected charge, transient signal can appear at nearby outputs. By digitally analyzing the amplitude and shape of these signals, position information can be obtained by interpolation to a finer resolution than the pitch of the electrodes [39].

Another advantage of the digital approach is stability. After the conversion to digital data, there can be no further change in that information, and subsequent processing will be totally immune from the drifts that can take place in analog processors because of temperature or line voltage changes. In contrast with analog circuits, digital manipulations introduce no further noise into the system and are perfectly linear. It is also possible to introduce time delays in the pulse processing system in the form of “first in, first out” (FIFO) registers that, in contrast to analog delays, introduce absolutely no distortions in the digitized pulse shape. One potential disadvantage arises when fast timing information is important. Using simple threshold sensing, digital systems are limited in timing accuracy to the nearest period of the sampling frequency. Some more complex techniques based on applying digital filters can do better, but simpler analog timing methods will often yield more precise timing information when very fast detectors are involved.

2.4.1 ANALOG TO DIGITAL CONVERSION

The first and critical step in digital pulse processing is the conversion of the analog pulse waveform into digital data. In this section the general principles of ADCs are first introduced, then a discussion on the types known as *Flash* and *subranging* ADCs that are of most importance in the digital shaping of pulses, and finally, the types of *successive*

approximation and *linear ramp* ADCs that are of greater interest for use in multichannel analyzers are also presented.

The basic function of an ADC is to produce a digital code (or number) at its output that is proportional to an analog voltage supplied to its input. The analog-to-digital conversion procedure is usually triggered by some logic signal that fixes the time t at which the conversion occurs. A very common configuration is realized using a periodic logic signal (clock) with a fixed frequency f_s (sampling frequency) to trigger the conversions. In this way the time slice between two successive conversions (or samples) is fixed and equal to $\tau_{clk} = 1/f_s$ (sampling period). For example, a 100 MHz clock will produce 100 megasamples per second (MSPS), or one sample every 10 ns.

Whereas the amplitude of the analog input signal can assume any value, the digital output from the ADC can assume only a finite number of values (that is usually a power of 2). The converter can thus only approximate the continuous input value with its discrete output. For example the output of a 12 bit converter can only assume integer values ranging from 0 to $2^{12} - 1 = 4095$. This fixes also the minimum change in the input that can be measured (in our example $1/4096$ of the full ADC input range). The smallest digital unit is usually referred to as *least significant bit* (LSB).

In an ideal ADC, each conversion of input voltage to output codes is independent, perfectly linear, and occurs instantly. Nevertheless, the characteristics of an ideal ADC are not met in the case of real ADCs, and non-idealities limit both the maximum sampling frequency and the linearity and accuracy of the conversion. Regardless of ADC type, some general properties are defined below.

Linearity

The ideal ADC would perform a perfectly linear conversion of analog voltage to code value, so that a plot of input voltage versus code number would be a simple straight line. Because of the discrete nature of the output code, there will actually be a small range of input voltages for each output code value, so the midpoint of this range is technically the quantity that should be plotted versus the code number.

Integral non-linearity

The integral non-linearity of a converter measures the maximum deviation of the measured curve from the ideal straight line behavior. A typical absolute value is 0.2–1 LSB.

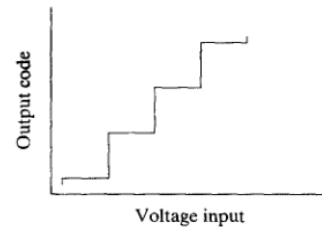
Differential non-linearity

A more sensitive measure of linearity can be carried out using a voltage generator that produces a slowly varying output that follows a perfect ramp or triangle shape. Then the time that the input voltage is within the range corresponding to any given output code should be constant, and the same number of conversions should take place for every code value. A plot of the number of recorded conversions versus the code number should then be constant across the entire output code scale. Deviations from the average constant value are quoted as the *differential non-linearity* (DNL), a typical value is 0.2-0.5 LSB

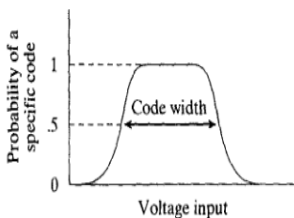
In the case of an ADC with a DNL greater than 1 LSB some valid digital codes cannot be produced by the device (because they would overlap with some neighbor wide bit). This undesired effect is referred to as the presence of missing codes. Typically the absence of missing codes is guaranteed.

Channel profile and Code width

Assume that an analog voltage perfectly controllable (such as that mentioned in the previous section) is supplied to an ADC. As this voltage is smoothly varied, the output code should switch abruptly between adjacent values. A plot of the output versus input should look like the sketch on the right.



The vertical scale is shown in increments of one LSB of the output code. As a result of noise and other non-ideal behavior, the transitions between output codes are not exactly vertical as idealized above. If we focus on a single output code, then a precise calibration will reveal the following typical result for a “channel profile”:



The “code width” is defined as the range of analog input voltages beginning and ending with the 0.5 probability level on the channel profile. Ideally, all code widths are the same, and any variations that are “too wide” will collect more conversions than those that are “too narrow” in the test involving ramp or triangular inputs.

ADC Resolution or bit depth

This number defines the maximum number of increments (or channels) into which the input voltage can be sorted. A 12-bit ADC will generate 2^{12} , or 4096, discrete codes (or channels of resolution), over its input range. Thus a 12-bit ADC will offer a “digital resolution” of $1/4096$ or just under 0.025%. The number of bits needed in a specific case is largely dependent on the signal-to-noise ratio of the input. If the noise level is several percent, then choosing an ADC with more than 8 bits will only result in digitizing meaningless noise fluctuations. Conditions with higher signal-to-noise ratios will demand greater bit depth.

There is a “quantization error” ϵ associated with an ideal conversion process that becomes smaller with a larger bit depth. As shown in Fig. 2.7, a zero value for ϵ corresponds to an analog voltage at the midpoint of a channel, and ϵ becomes \pm half of the code width at the extreme edges of the channel.

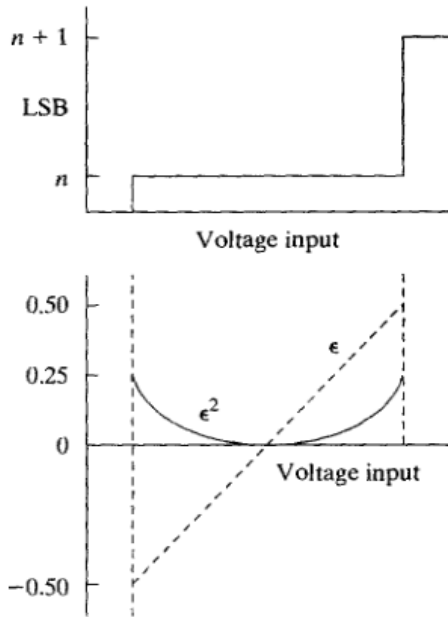


Figure 2.7: Quantization error. The top plot shows the ideal conversion between analog voltage input and the output code of an ADC. The bottom plot shows the quantization error ϵ (in units of code width), together with the square of its value ϵ^2 .

The RMS value of this ideal quantization error can be calculated from the integration:

$$\langle \epsilon^2 \rangle = 2 \int_0^{0.5} x^2 dx = \frac{1}{12}$$

$$\epsilon \equiv \sqrt{\langle \epsilon^2 \rangle} = \frac{1}{\sqrt{12}} \quad (2.2)$$

in units of the code width.

Deeper discussion on quantization error can be found in [40].

Effective number of bits

In the case of a noiseless constant input signal an ideal AD converter should produce a constant conversion code. This is not the case of real ADCs, which outputs a digital data stream of different samples fluctuating around the nominal value. If the noise is at a high enough level, it can reduce the significance of the LSBs in the converted code. The amount of this fluctuation can be quantified with the “effective number of bits” (ENOB, in general a non-integer quantity), and is defined as [41]:

$$ENOB = N - \log_2(RMS_{noise} / \varepsilon) \quad (2.3)$$

where N is the number of digitized bits and ε is the ideal quantization error given above. RMS_{noise} is the measured RMS deviation of the converted code from a precisely known but variable input voltage that is swept over the ADC range. At a minimum, this measurement will include the ideal quantization error, so the logarithm term is zero if no other sources of noise are significant. Then $ENOB = N$, and a 12-bit ADC would deliver 12 fully significant bits. However, if additional noise is present to the extent that the RMS_{noise} is twice ε , then the same ADC really produces only 11 effective bits. The noise level, and thus the value of ENOB, can be expected to vary with operating parameters such as sampling frequency and the rate of change of the input voltage.

Typical values for high-speed ADCs are 1–2 bits below the “physical” number of bits (for example a 12 bit converter can have 10–11 effective bits). An equivalent quantity to state the effective number of bits is the signal-to-noise ratio (SNR), usually given in decibels. The following holds:

$$SNR(dB) = 6.02 \cdot ENOB + 1.76dB \quad (2.4)$$

For many applications this effect can be schematized as an additional *white noise* source fed into the input of an otherwise perfect ADC. A full discussion (together with some useful conversion formulas) is given in [42].

Only the principal parameters describing the performances of real ADCs have been presented here: for a detailed discussion see [43, 44].

The circuit used to perform the desired analog to digital conversion varies greatly depending on the requested performances: the key parameters are mainly the sampling frequency f_s and the resolution of the converter. The principal conversion techniques in digital pulse processing are presented below. A full discussion of AD conversion methods can be found also in [43, 44].

Flash ADCs

The basic layout, shown in Fig. 2.8, consists of a stack of threshold comparators, each set to a progressively higher voltage level. These reference voltages are conventionally provided via a resistive voltage divider with equal resistance values between each comparator. An n -bit flash ADC requires 2^n comparators, and the increasing complexity for large values of n limits contemporary flash ADCs to no more than 8 to 10 bits (256 to 1024 codes).

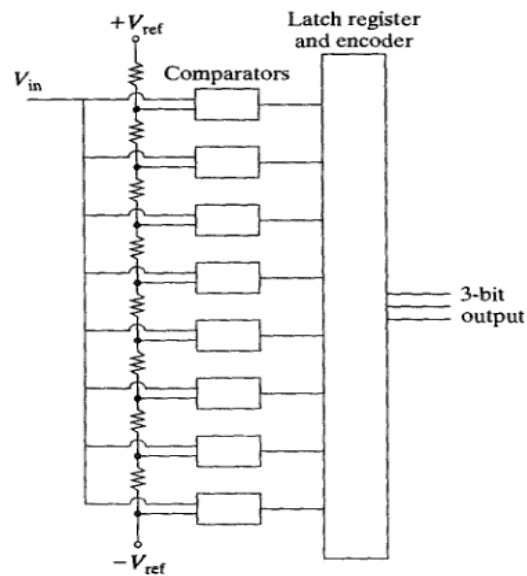


Figure 2.8: Block diagram of a 3-bit flash ADC. Each additional bit of resolution doubles the required number of comparators.

The input voltage is presented in parallel to all comparators, and all those with reference voltage below that of the input will produce a logic '1' output. Otherwise will produce a logic '0'. The resulting pattern of logic levels is read by the *latch register* and converted to a corresponding binary number by the encoder. The readout frequency is controlled by clock pulses and is as high as 3000 MHz in the sample of present-day designs shown in Tab. 2.1.

Because of the possible drift and instability in the large number of analog voltage comparisons that are required, the differential nonlinearity of flash ADCs is often fairly

poor. In the extreme, some output codes may actually be missing. To improve this weakness, some applications employ ADCs with higher resolution than actually required so that the LSBs can be discarded.

Table 2.1: Some examples of Fast Analog-to-Digital Converters.

Manufacturer	Model	Resolution (bits)	DNL (typ) LSB	Sample Rate (MSPS)	Power Consumption (mW)
Flash ADCs					
Intersil	HI1276	8	0.3	500	2800
Maxim	MAX109	8	0.25	2200	6800
National	ADC085000	8	0.2	3000	1900
Subranging (Multipass or Pipelined) ADCs					
Analog Devices	AD9626	12	0.3	250	390
	AD9211	10	0.1	300	468
	AD9481	8	0.35	250	619
Texas Instruments	ADS6129	12	1	250	687
Maxim	MAX1215	12	0.3	250	619800
National	ADC11DV200	11	0.32	200	450

Subranging ADCs

The limitations of flash ADCs have led to the widespread use of an alternative architecture for fast ADCs applied in digital pulse processing. The *subranging ADC* defines a series of expanding scales to allow a greater resolution and lower power consumption while retaining the high-frequency sampling characteristic of flash ADCs. Figure 2.9 illustrates, by analogy, the implemented process. At the first stage, a coarse determination is made with a flash ADC (in this case, to a resolution of 3 bits) of the most significant bits of the eventual converted digital value. This initial measurement determines the position of the “magnifying glass” that is placed over the region including the voltage signal to measure. In the case of the example, the lens has a magnifying power of x8 that allows a closer examination of the “subrange” of the first scale. Now the voltage is digitized on a finer scale, again to 3 additional bits in the example. Once more, the result of this digitization repositions the “magnifying glass” to allow another digitization to an additional 3 bits, now involving only a very small range of the analog voltage. The result from this last digitization provides the least significant bits of the conversion. Combining the results

from the three stages produces a 9-bit code that is the output of the unit. The subranging approach allows a considerable reduction in the number of comparators needed to carry out the conversion. In this example, three 3-bit flash ADCs were used to complete a 9-bit conversion. Since each of these ADCs involves 2^3 (or 8) comparators, a total of 24 are needed. If the same process were done in a single flash ADC, it would require 2^9 (or 512) comparators. This reduction leads to a decreased power consumption in subranging units (see Tab. 2.1) that is beneficial to promote stability and to facilitate use in battery-powered portable instrumentation.

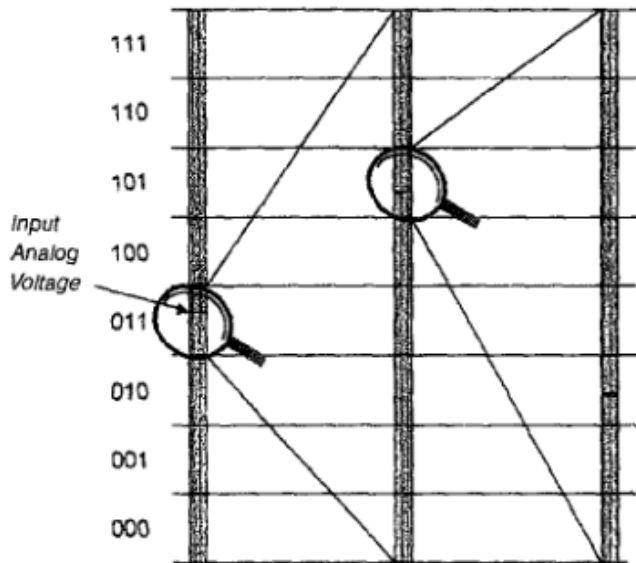


Figure 2.9: Analogy to the operation of a subranging ADC in which magnifiers are used in sequence to expand the analog voltage scale. For the example shown, a sequence of three 3-bit analog-to-digital conversions produces the 9-bit binary code of 011101010, or 243 on a decimal scale of 0-511.

Figure 2.10a shows the architecture of a module that carries out one stage of the process described above. At each clock cycle, the input voltage is momentarily held by a *track-hold* (T/H) circuit. A flash ADC carries out a digitization to n bits ($n = 3$ in this example), and that value serves as the digital output of the stage. That same value is supplied to a digital-to-analog converter (DAC) and subtracted from the input voltage. The analog difference is sent through an amplifier with gain of G corresponding to the magnification factor ($G = 8$ in the example above), and the amplified analog voltage is passed on to the next stage. A number of such modules can now be combined in a “multipass” or “pipelined” arrangement illustrated in Fig. 2.10b, with all stages synchronized by a common clock. The digital outputs of all the modules are combined in a logic block that typically includes functions of bit alignment, error correction, and self-calibration to form the overall digital result. Because of the serial operation of the individual stages, the final result is produced a number of clock cycles following the appearance of the corresponding analog input. This “latency time” is the same for all samples and introduces some delay between input

and output, but it does not affect the frequency of the conversions. Examples of some representative commercially available multipass or pipelined ADCs are given in Tab. 2.1. Units have been developed with resolutions of up to 16 bits and with conversion frequencies of up to a few hundred MHz.

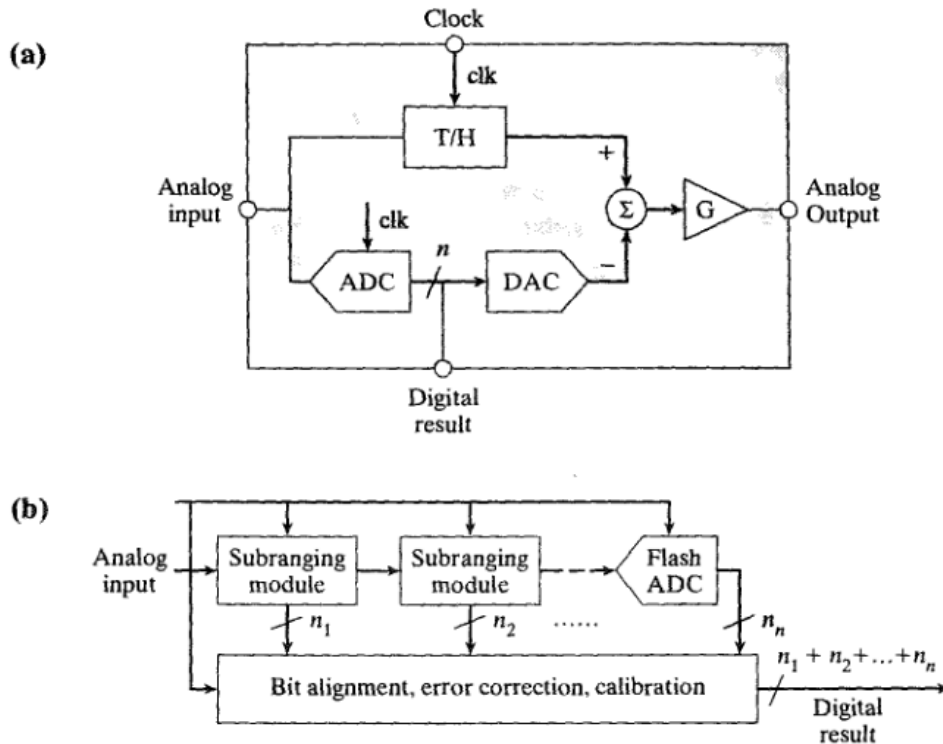


Figure 2.10: (a) The elements of a single subranging stage or module. T/H is a track-and-hold circuit, ADC is a flash ADC, DAC is a digital-to-analog converter, Σ is an analog summing unit, and G represent the gain of an analog amplifier. (b) The combination of multiples subranging modules in a fast pipelined ADC.

As mentioned before, Flash and Subranging ADCs are mostly applied for the shaping or filtering stage of the digital processing of pulses from radiation detectors. Next successive approximation and linear ramp ADCs will be presented, which are widely applied in the multichannel analyzer circuits used for spectroscopy purposes in Nuclear Physics.

2.4.1.1 Spectroscopy Analog-to-Digital Converter

As presented in section §2.1, a MCA is a circuit designed for measuring the pulse height for each of a series of events from radiation detectors already shaped and discriminated by means of either analog or digital techniques. At the end of these pulse height measurements, the MCA outputs a histogram containing the number of pulses that deposited energy within each of its amplitude bins. This histogram in radiation detectors is

no more than the energy spectrum of the radiation incident in the detector. Therefore, MCAs are great instruments for radiation spectroscopy purposes.

The analog-to-digital conversion performed within multichannel analyzers is usually referred to as *spectroscopy analog-to-digital conversion*.

The *conversion gain* of a spectroscopy ADC specifies the number of channels over which the full amplitude range will be spread. For example, at a conversion gain of 2048 channels, a 0 to 10 V full input scale ADC will store a 10 V pulse in channel 2048, whereas at a conversion gain of 512, that same pulse would be stored in channel 512. On many ADCs, the conversion gain can be varied for the purposes of the specific application. The resolution of an ADC must be at least as good as the largest conversion gain at which it will be used.

The conversion speed of the ADC is the critical factor in determining the overall speed of the MCA. Therefore, a fast conversion is desirable, but practical limitations restrict the speeding up of the conversion before the linearity begins to suffer. The fastest ADCs, the flash or subranging type discussed in the previous section are rarely used in MCAs because of their poor differential linearity. Two other types dominate: linear ramp converters and successive approximation ADCs. The first one of these, although the slowest, generally has the best linearity and channel profile specifications compared with the other types and has gained the most widespread application. Successive approximation ADCs offer faster conversion times, but generally with poorer linearity and channel uniformity.

The linear Ramp Converter (Wilkinson type)

The block diagram of the linear ramp converter is illustrated in Fig. 2.11. The peak amplitude of the input pulse is supplied to a comparator circuit that continuously compares the amplitude with that of a linearly increasing ramp voltage. The ramp is conventionally generated by charging a capacitor with a constant-current source that is started at the time the input pulse is presented to the circuit. The comparator circuit outputs a gate pulse that begins at the same time that the linear ramp is initiated. The gate pulse is maintained “on” until the comparator senses that the linear ramp has reached the amplitude of the input pulse. The gate pulse produced is therefore a variable length, which is directly proportional to the amplitude of the input pulse. This gate pulse is then used to operate a linear gate that receives periodic pulses from a constant-frequency clock as its input. A discrete number of these periodic pulses pass through the gate during the period it is open and are counted by the address register. Because the gate is opened

for a period of time proportional to the input pulse amplitude, the number of pulses accumulated in the address register is also proportional to the input amplitude. The desired conversion between the analog amplitude and a digital equivalent has therefore been carried out.

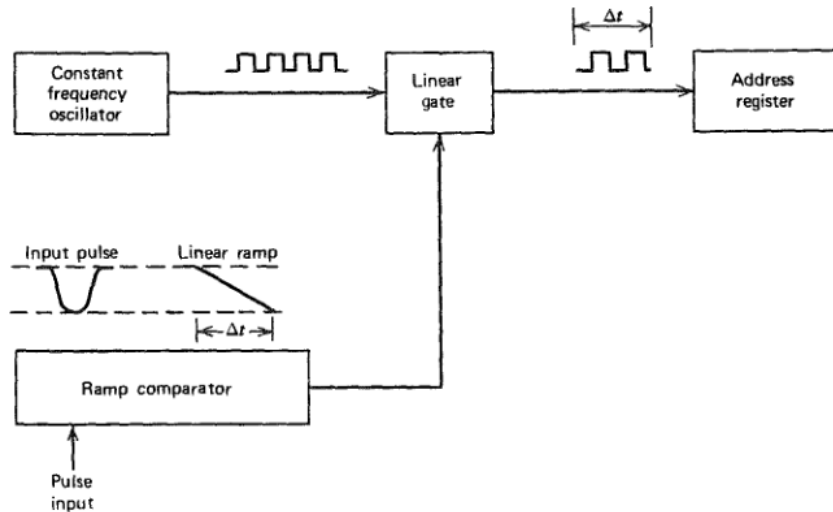


Figure 2.11: Block diagram of a linear ramp (Wilkinson type) ADC.

Because the clock operates at a constant frequency, the time required by a Wilkinson-type ADC to perform the conversion is directly proportional to the number of pulses accumulated in the address register. Therefore, under equivalent conditions, the conversion time for large pulses is always greater than for small pulses. Also, the time required for a typical conversion will vary inversely with the frequency of the clock. Clock frequencies of 100 MHz or higher are representative of present-day commercial designs.

The Successive Approximation ADC

The second type of ADC in common use is based on the principle of successive approximation. Its function can be illustrated by the series of logic operations shown in Fig. 2.12. In the first stage, a comparator is used to determine whether the input pulse amplitude lies in the upper or lower half of the full ADC range. If it lies in the lower half, a zero is entered in the first bit (*most significant bit* MSB) of the binary word that represents the output of the ADC. Otherwise, the circuit effectively subtracts a value equal to one-half the ADC range from the pulse amplitude, passes the remainder on to the second stage, and enters a one in the MSB. The second stage then makes a similar comparison, but only over half the range of the ADC. Again, a zero or one is entered in the next bit of the output word depending on the size of the remainder passed from the first stage. The

remainder from the second stage is the passed to the third stage, and so on. If 10 such stages are provided, a 10-bit word will be produced that will cover a range of 2^{10} or 1024 channels.

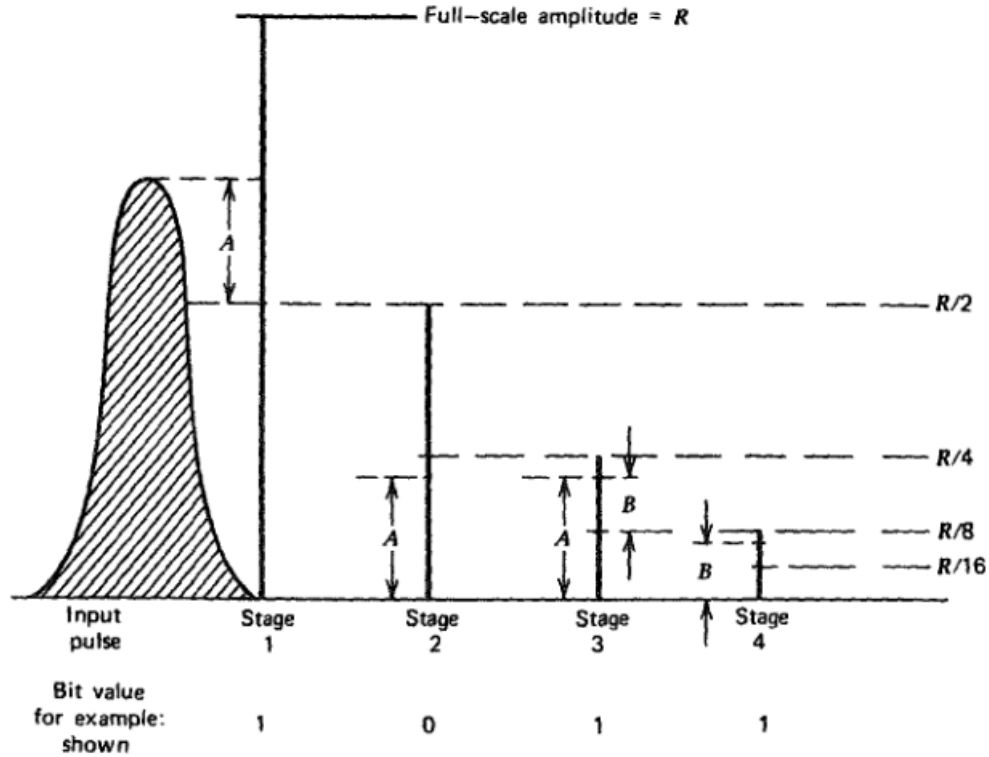


Figure 2.12: Operational sequence for a successive approximation ADC. Four stages are shown that generate the four-bit word shown at the bottom as the digital input.

In its most common circuit implementation, the successive approximation ADC makes multiple use of a single comparator that has two inputs: one is the sampled and held input voltage and the other is produced by a digital-to-analog converter (DAC). For the first-stage comparison, the input to the DAC is set to a digital value that is half the ADC output range. Depending on the result of the initial comparison, the second-stage comparison is then carried out with the digital input to the DAC set to either 25 or 75% of the range, and so on. In this way, analog subtractions are avoided but the functional operation is equivalent to that described above.

For a given successive approximation ADC, the conversion time is constant and independent of the size of the input pulse. For typical converters with a 10-bit output, the conversion time can be a few microseconds or less. The major disadvantage of typical successive approximation ADCs is a more pronounced differential non-linearity compared with linear ramp ADCs. Some refinements to their design are covered in Refs. [45-47].

During this Thesis, the multichannel analyzer from AMPTEK MCA8000A was used, which implements a 16-bit successive approximation ADC with 14 effective number of bits, so that achieves up to 16,384 conversion gain channels. Details on the hardware are given in Chapter 3.

2.4.2 DIGITAL SHAPING OR FILTERING

A. Linear Time-Invariant filters

Most of the pulse shaping operations involve what are known as “linear time-invariant filters.” Their definition incorporates the restriction that the properties of the filter are fixed and do not change with time. A “transversal filter” or “finite impulse response” filter (FIR), is by definition limited to using input data over the restricted time range $L < t < 0$, where L is the length of the filter. This time range reaches backward from the present time simply because only data that have already occurred can contribute to the output at a specific instant. The mathematical expression of the filtering process then takes the form of the convolution integral:

$$S(t) = \int_{t-L}^t V(t')H(t-t')dt \quad (2.5)$$

Where $H(t)$ is the *impulse response function of the system*. This function reflects the operations carried out by the analog shaping networks in conventional linear amplifiers. These definitions apply to cases in which the input data is an analog function. For the digital case, if a series of values $V(i)$ is assumed as the sampled input data, starting at $i = 0$ (where the time period between each sample represents the sampling period of the ADC), the impulse response function now becomes a discrete set of weighting factors $H(0), \dots, H(L)$. If the filter is of finite length L , then the values of $H(i)$ are 0 for values of $i < 0$ or $i > L$. The convolution process equivalent to Eq. 2.5 then can be written:

$$S(j) = \sum_{i=j-L}^{i=j} V(i)H(j-i) \quad (2.6)$$

where $S(j)$ now represents the discrete series of output values produced by the digital filtering process. An example for which the filter consists of four weighting factor, $H(0), \dots, H(3)$ (the length of the filter is $L = 3$). Values of $H(i)$ are by definition 0 outside this range. The input consists of the digital samples $V(i)$, assuming that the data begin at $i = 0$.

Evaluating the sum given in Eq. 2.6 for this example then gives, starting with the first nonzero output value ($j = 0$):

$$S(0) = \sum_{i=-3}^{i=0} V(i)H(-i) = V(0)H(0)$$

for $j = 1$:

$$S(1) = \sum_{i=-2}^{i=1} V(i)H(1-i) = V(0)H(1) + V(1)H(0)$$

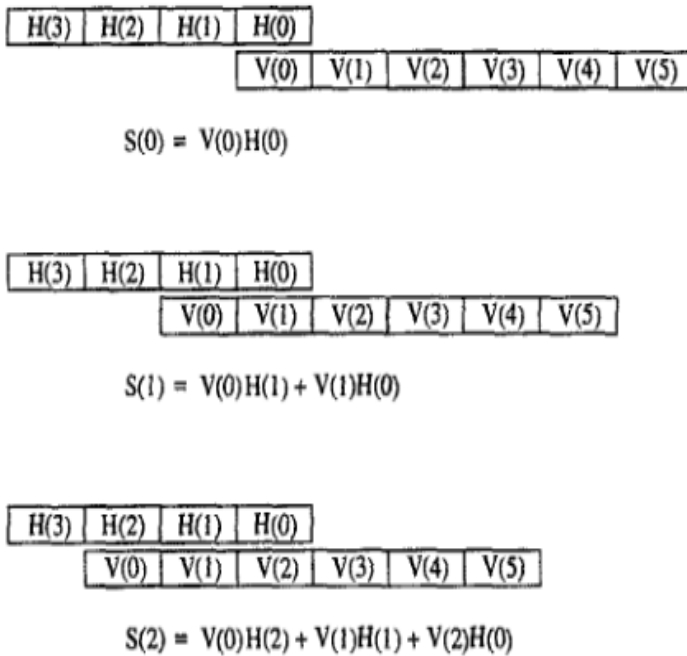


Figure 2.13: An illustration of a digital transversal filter. The filter elements are shown (right to left) along the top line of each step, with the digitized data analog the lower line. The output is formed by multiplying factors that are aligned and summing.

The process continues producing output values for each succeeding value of j , the number of terms in the summation reaching four at $j = 3$, and remaining at four for all higher values of j until the end of the input data sequence is approached. This example is illustrated in Fig. 2.13. As shown, the first nonzero value is for $j = 0$. Each successive value of the output is obtained by displacing the string of input values one step sequentially to the left and again carrying out the multiplication and summation. This process can be visualized as “pulling” the set of weighting functions through the sequence of input data (or pushing the data through the filter), advancing one step at a time to produce the sequential output values.

B. Triangular shaping

Figure 2.14 illustrates the operation of an “ideal” *digital pulse processor*. The preamplifier signal is digitized directly, using a fast ADC. In place of a *CR* differentiator, or high-pass filter, the digital differentiator adds each successive ADC input and subtracts the sample obtained k clock cycles previously.

For a step input from a preamp, the result is a square signal that is k clock cycles long. The integrator, or low-pass filter, is a sum or integral of the differentiator outputs, producing a triangular output. This output is now a true triangle, not the near triangle that can be synthesized using analog techniques.

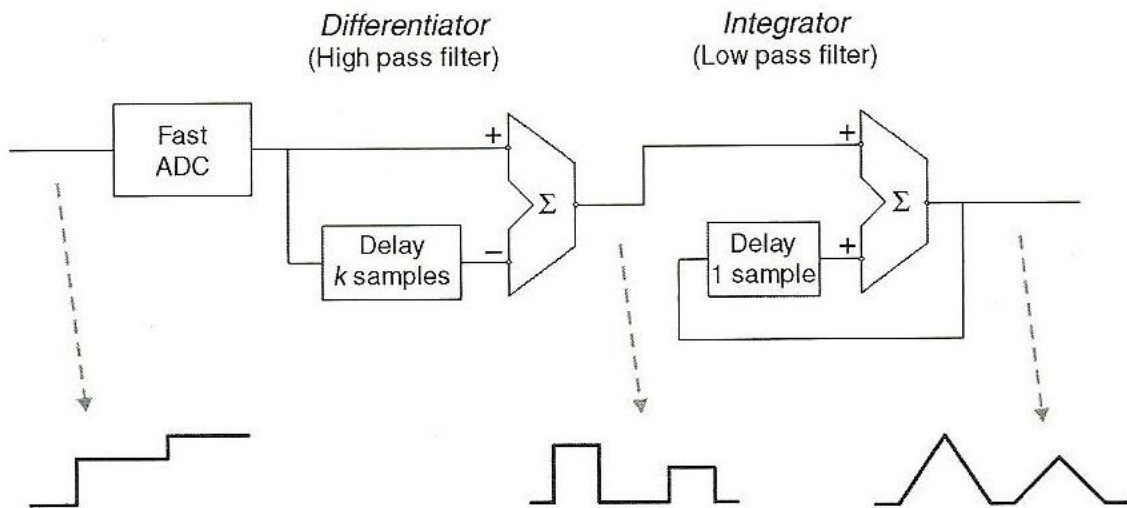


Figure 2.14: Example of a simple digital filter that produces a triangular-shaped pulse from a step input.

The digital approach has some very clear advantages over analog systems. First, the triangular output shape provides better pile-up and signal-to-noise performance than the analog shapers. The output pulse duration at the baseline is clearly equal to twice its FWHM. This width is shorter than the semi-Gaussian analog equivalent. It can be shown that the noise-filtering performance is superior to that of a semi-Gaussian shape with the same duration. Thus this digital processor provides both reduced pile-up and better noise filtering.

In the analog shaper, an impulse input leads to an exponential tail from the differentiator which takes infinite length of time to return to zero. This behavior is termed an “infinite impulse response,” or IIR. The output is negligible after a finite time, but is measurably non-zero for quite a long time. This prolongation affects pile-up and also baseline shift,

resulting from the IIR of the analog differentiator. In the digital shaper, an impulse response leads to the rectangular response from the differentiator, and the response goes to zero after k samples. It has a “finite impulse response” (FIR), meaning that any input has zero effect after a finite time. This behavior is fundamentally different from the analog shaper. Whatever happens at the input to the digital processor, the consequence on the output is zero after some time period. This property significantly improves the performance of the digital system at high count rates, reducing pile-up, baseline shifts, and so on.

C. Adaptive Filtering

Since digital pulse processing systems are controlled through software, it is possible to easily customize the filter weighting functions to suit the circumstances of the measurement. The choice of the optimum shaping method depends on the magnitude and nature of the noise that is present with the signal. Systems have been designed [48-51] that sample the detailed character of the noise present with the signal and then choose a weighting function that is optimal for the measured results. This is one example of *adaptive* filtering that exploits the flexibility of the digital system to easily adjust the shaping parameters.

Another example of adaptive filtering is applied to systems in which the counting rate changes substantially during a measurement. An adaptive filtering approach allows changing the width of the shaping function as a function of counting rate, thus adjusting automatically to these changing conditions.

2.4.3 PULSE SHAPE ANALYSIS

As mentioned in §2.3, there are several applications in which the detailed time profile of the current pulse reveals additional information about the nature of the event in the detector. Examples are in distinguishing one type of radiation from another, measuring the spatial position of an event, or distinguishing pulses that arise from a multiple gamma ray interactions from those that are due to a single interaction only. Sophisticated algorithms can be used to inspect the string of digital data representing each individual pulse so that rather subtle differences among them can be distinguished. As these operations become more complex, however, it is increasingly difficult to carry them out entirely in real time at high counting rates because of the limited time available between signal pulses. In such cases, the digital data can be sent to a memory and the processing completed off-line after the measurement.

2.4.4 DIGITAL BASELINE RESTORATION

In digital pulse processing systems, the baseline restoration process can be accomplished by digitally sampling the baseline between pulses and then subtracting an appropriate value from the measured pulse amplitude [52]. Independent baseline estimates can be obtained for each pulse that is processed or, alternatively, a common estimate applied to a series of pulses between more widely spaced samples of the baseline. Ideally, one would like multiple digital measurements of the baseline to be taken for a given sample to enhance its accuracy, requiring a relatively long time interval between pulses. Long intervals occur less frequently than short ones, so there must be a trade-off between the accuracy of the baseline measurement and the frequency with which they can be made.

2.4.5 DIGITAL PULSE PROCESSORS

For a long time, the close to optimal filtering stage of, pulse processing, was only possible to perform with analog components. For example, classical spectrometry amplifiers with Gaussian pulse shaping have been used for more than 40 years.

Due to the development of fast analog to digital converters (ADCs), field programmable gate arrays (FPGAs), and digital signal processors (DSPs) during the last few decades, it has become possible to digitize pulses after preamplifier stage, and process them in a real time. Therefore, the digital electronics, which was limited to the control of the acquisition process and data storage, has become feasible for signal processing as well. This immediately opened possibilities to design instruments with relatively high component density at a reasonable cost per channel. Such instruments could implement many analog processing functions like pulse discrimination, pulse amplitude filtering, pile-up correction, and base-line restoration.

The development of digital signal processors has been driven by the following consideration: utilizing data parallelism and allowing application-specific specialization, while keeping functional flexibility and minimizing power consumption. The selection of a specific processor will deal with different trade-offs in terms of performance, cost, power and flexibility. While application-specific integrated circuits (ASICs) and programmable digital signal processors (DSPs) remain the solution of choice for many digital signal processing applications, new system implementation are increasingly based on field programmable gate arrays (FPGAs).

A. Application-specific integrated circuits (ASICs)

ASICs have a significant advantage in area and power, and for many high-volume designs the cost-per-gate for a given performance levels is much lower than that of high speed FPGA or DSP: However, the inherently fixed nature of ASICs limits their flexibility, and the long design cycle may not justify the cost for low-volume or prototype implementation unless the design would be sufficiently general to adapt to many different applications.

B. Digital signal processors (DSPs)

DSPs have features designed to support high-performance, repetitive, numerically complex sequential tasks. Single-cycle multiply-accumulate and specialized execution control on cheap memory, and the execution of several operations with one instruction are the features that accelerate performance in state-of-the-art DSPs [53]. The peak performance of the DSP relies heavily on pipelining. However, parallelism in DSP is not very extensive; DSP is limited in performance by the clock rate, and the number of useful operations it can perform per clock cycle.

C. Field Programmable Gate Arrays (FPGAs)

Until fairly recently, FPGAs lacked the gate capacity to implement demanding DSP algorithms and did not have good tool support for implementing DSP tasks. They were also perceived as being expensive and high power demanding. However, with the introduction of new DSP-oriented products from Altera [54] and Xilinx [55], high throughput and design flexibility have positioned FPGAs as a solid silicon solution over traditional DSP devices in high-performance signal processing applications.

Since FPGAs can be reconfigured in hardware, they offer complete hardware customization while implementing various DSP applications. FPGAs also have features that are critical to DSP applications, such as embedded memory, DSP blocks, and embedded processors. Recent FPGAs provide up to 96 embedded DSP blocks, thus improving over 30 times what is provided by the fastest DSPs.

Over the last years, several companies have gradually developed very compact digital systems that comprise detector, preamplifier, and digital pulse processor all in one. Comparative studies of these systems [56-58] have confirmed the equal or better performance of digital systems over analog systems in terms of stability, resolution, differential non-linearity and throughput.

2.5 COMPARISON BETWEEN ANALOG AND DIGITAL PULSE PROCESSORS

A Digital Pulse Processor (DPP) performs the same functions as an analog shaping amplifier but has intrinsic performance advantages which have led to its widespread adoption where both the lowest noise and the highest count rates are needed. Although the function of the DPP is the same as an analog shaper, the implementation is different and some of the concepts and terminology are different. Analog and digital shapers will be compared, to aid in the understanding of digital processors, and to explain their advantages and disadvantages.

2.5.1 SIMPLIFIED SCHEMATICS

Figures 2.15 and 2.16 show simplified schematics of analog and digital shaping amplifiers, respectively. Both have the same detector and charge sensitive preamplifier circuits. In both cases, the preamplifier produces an output which consists of small steps, millivolts in height. In both cases, the preamp pulses are differentiated so that the step voltage can be measured. An integrator (low pass filter) improves the signal-to-noise ratio. In both cases, the output pulses are digitized and a histogram of the pulse heights is stored in memory. These key elements are the same in both systems.

The analog system shown in Fig. 2.15 yields the pulse shapes shown in Fig. 2.17 (left). The differentiator is an RC high pass filter. It passes the rising edge from the preamp, and then the voltage decays exponentially back to baseline with time constant τ_{diff} . The integrator is a low pass filter with response time τ_{int} . There are many types of shaping amplifiers (semi-Gaussian, pseudo-Gaussian, quasitriangular, etc) which use different low pass filters. The more sophisticated using complex pole-pairs have a rapid return to baseline with a more symmetric shape. The baseline restorer (BLR) keeps the baseline from which the peak is measured at a constant value. An analog peak detection and hold circuit captures this peak height, which is then digitized. This single digital sample represents the pulse, so the ADC must be very linear but need not be very fast, since it digitizes only one sample per pulse [59].

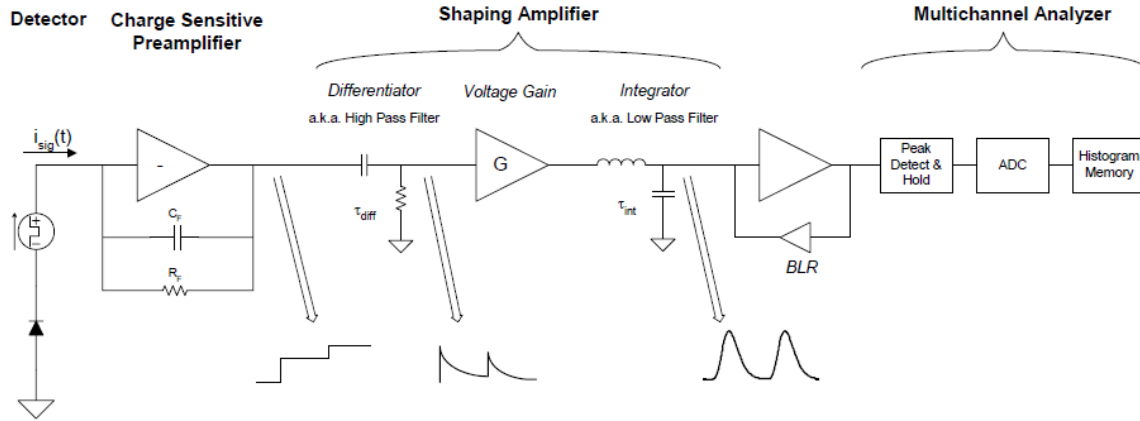


Figure 2.15: Schematic of a simple analog pulse shaper (with CR-RC² shaping).

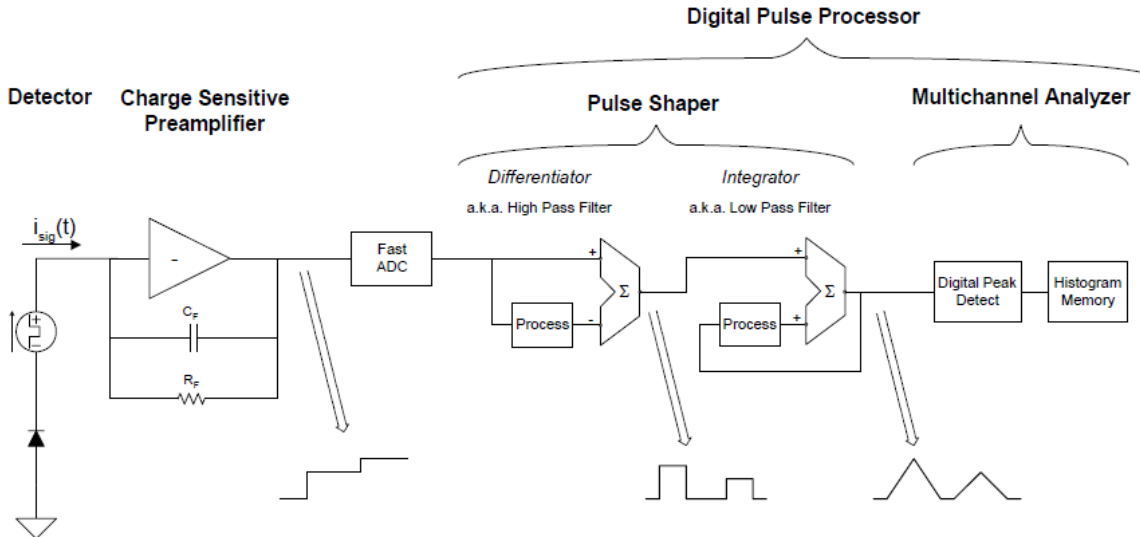


Figure 2.16: Schematic of a simple an "ideal" digital pulse processor.

In the "ideal" digital system shown in Fig. 2.16, the preamplifier signal is digitized directly, using a fast ADC. This is differentiated using a discrete differencing circuit. This is sent to a low pass filter which integrates the differentiator output. The two blocks labeled "process" represent algorithms which are applied to the inputs and which differ from one digital processor to another. With the most common low pass filter, the result is a triangular output. Trapezoidal pulses are also easily synthesized, along with more complex shapes such as the cusp. The values are already digitized, so a digital peak detect is used and this value sent to the histogram memory. The output of the integrator may also be sent to a DAC, so the user can view the pulses on an oscilloscope, but the system need not to generate an analog shaped pulse. The pulse shapes are shown in Fig. 2.17 (right).

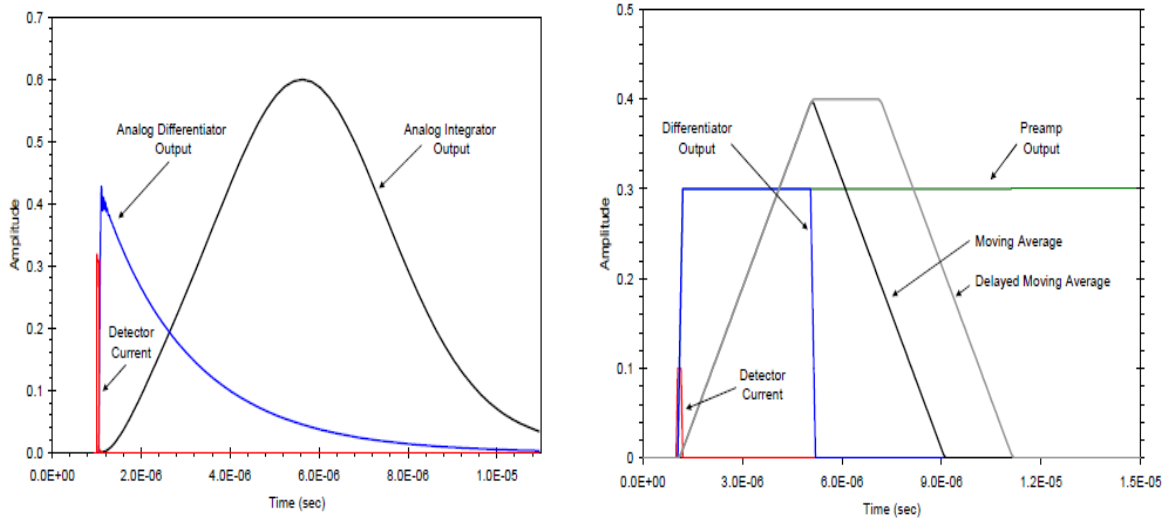


Figure 2.17: Left: Pulse shapes in an analog pulse shaper. These are for a quasi-triangular shaper using complex poles, which most closely approximates a triangle. Right: Pulse shapes in a digital pulse processor with triangular and trapezoidal shapes.

2.5.2 SUMMARY: ADVANTAGES AND DISADVANTAGES OF DIGITAL FILTERING

A digital processor has a few key advantages, summarized here then explained more below. A DPP has better performance (both lower noise and higher count rate capability), greater flexibility for tailoring to a specific application, and greater stability and reproducibility.

1. Researchers derived long ago the ideal filters for use in nuclear electronics, to give the best signal-to-noise ratio at a given count rate. The ideal transfer function cannot easily be produced in practical op-amp circuits but digital processors more closely approximate the ideal.
2. There is no dead time associated with the peak detect and digitization, so a digital processor has considerably higher throughput than an analog system. Further, since it has a finite impulse response, pile-up and other pulse overlap effects are reduced. The digital processor's performance advantage is particularly good at high count rates.
3. In an analog pulse processor, most parameters are determined by resistors and capacitors. It is impractical to have many different configuration options in an analog system. In a digital system, one can have far more shaping time constants, BLR options, etc, so the user can readily tailor a system to the needs of an application, resulting in better performance.
4. Because the analog system relies on resistors and capacitors, its stability is limited to the stability of these components and its reproducibility to their tolerances. In a

digital system, the stability and the reproducibility are much better, because they derive from a few very accurate references, e.g. the crystal oscillator to set timing.

There are disadvantages to a digital processor. First, it tends to dissipate more power: an ADC which suitable speed and precision dissipates more power than many analog designs. Second, the design is more complicated than that of an analog shaping amplifier.

Advantages of Digital Filtering

Finite Impulse Response

As mentioned in previous sections, in the analog shaper an impulse input leads to an exponential tail from the differentiator, which leads to an infinite impulse response (IIR). The output is negligible after a finite time, of course, but it is measurably nonzero for a long time, typically many times the nominal “width” of the pulse. Subsequent pulses “ride up” on the tail of earlier pulses. Since the DC output of the high pass filter is obviously ground, the baseline shifts with count rate: the long term average of the pulses is very important and is affected by this long duration but small amplitude tail. So both peak pile-up and baseline shifts result from the IIR of the analog differentiator.

In the digital shaper, an impulse response leads to a finite impulse response (FIR), meaning that any input has zero effect after a finite time. This significantly improves the performance of the DPP at high count rates, reducing pile-up, baseline shifts, etc.

Restoration of Flat Top

In the analog shaper, the preamp is nominally a step: a fast rise and then a flat top. The differentiator passes the step but then immediately begins to decay. If the rising edge is slow, then the pulse does not reach full amplitude, as shown in Fig. 2.18 (left). The loss of pulse height with rise time is termed ballistic deficit and affects resolution when the rise time varies from one pulse to the next.

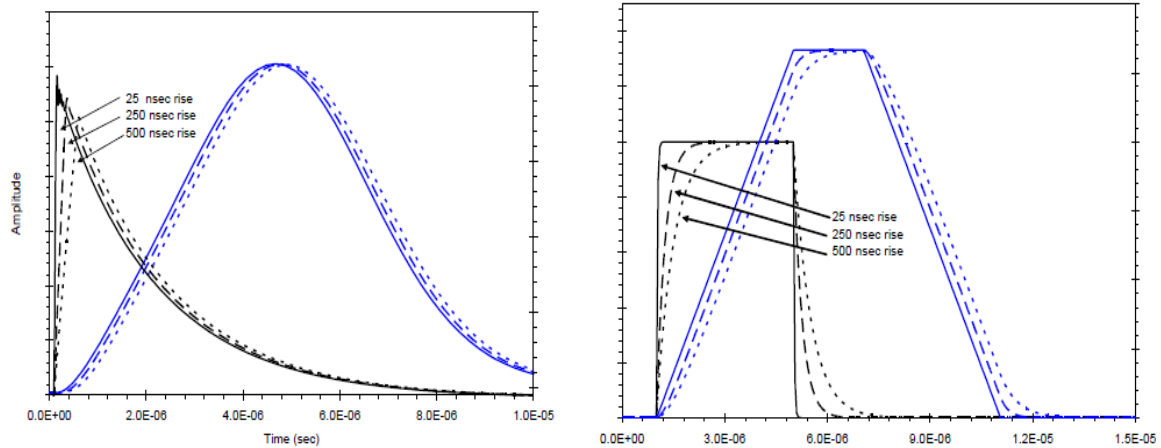


Figure 2.18: Plots of differentiator output for analog (left) and digital (right) shaping.

The problem arises because the analog “differentiator” does not pass the actual derivative and so does not pass the flat top. The advantage of the digital differentiator is that it actually implements a differencing operation, the digital true derivative, so it passes the actual flat top, as seen in Fig. 2.18 (right). The rising edge and flat top have the same shape as the preamp pulse. The digital processor is therefore immune to ballistic deficit, for rise times shorter than the flat top duration.

Pile-Up

Figure 2.19 shows the output pulse shapes from three different pulse shapers, all adjusted to give the same pulse duration when measured as full width at half maximum. The red curve shows the output of the simplest shaper, an analog $RC-CR$. The blue shows the shape from a high end analog shaper, a quasitriangular shaping amplifier using 6 poles of low pass filtering (three complex pole pairs). The black curve is from a digital trapezoidal shaper. The most important thing to notice is that, although they have the same FWHM pulse duration, the digital shaper will exhibit no pile-up at all if two pulses are separated by more than $(\tau_{peak} + \tau_{flat})$. The two analog shapers have exponential tails extending to many times the FWHM duration. Pulses overlapping during this time will pile-up.

There are two advantages to the digital shaping. First, the digital shaper has less pile-up (even with the same FWHM duration). Second, the pile-up timing for the digital system is very clear: due to the pulse symmetry, there is no pile-up after a fixed time. The analog shapers must use a pile-up rejection interval much longer than the peaking time, reducing throughput, i.e. the dead time due to the pulse shaping is longer in the analog system. Therefore, the digital system has both less pile-up and higher throughput with pile-up rejection used than the analog shapers.

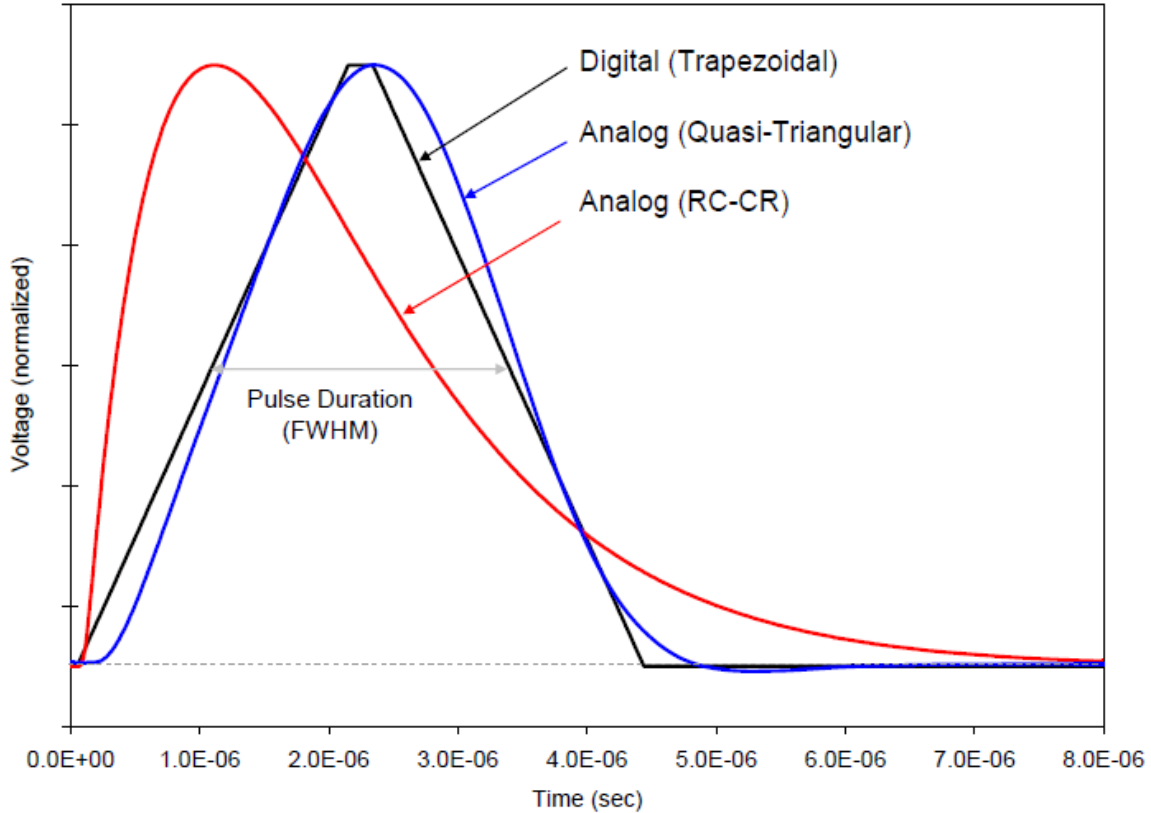


Figure 2.19: Plot showing pulse shapes from three different pulse shapers. All have essentially the same pulse duration, when specified as the full width at half maximum.

Signal to Noise Ratio

As mentioned in §1.4.8, researchers long ago concluded that, for a fixed pulse duration, the true triangle provides an optimum signal to noise ratio when series noise is dominant and the cusp when parallel noise is dominant [60]. Analog shapers approximate the triangle but the digital processor has a transfer function much closer to this ideal. The equivalent noise charge ENC for a radiation detection system is characterized by noise indices for series and parallel noise generators, A_s and A_p , for a given peaking time τ_{peak} . The noise can be written:

$$ENC^2 = (2qI_{leak} + R_p)(A_p \tau_{peak}) + (e^2_{pink} C_{in}^2) + \left(\frac{4kT}{(2/3)g_m} \right) \left(C_{in}^2 \frac{A_s}{\tau_{peak}} \right) \quad (2.7)$$

where I_{leak} is the leakage current through the detector, R_p is the resistance in parallel with the detector, C_{in} is the total input capacitance, g_m is the transconductance of the FET, and

e_{pink} is the *pink* or $1/f$ noise term. For this discussion, the key point is that the noise indices A_p and A_s depend on the details of the shaping amplifier.

The Tab. 2.2 shows the noise indices and pulse duration (FWHM) for three common shaping amplifiers, similar to those illustrated in Fig. 2.19. If one holds constant the peaking time, the trapezoidal and the Gaussian have the same parallel noise index, but the digital has lower series noise index and the Gaussian has a longer duration leading to degraded pile-up performance. One must be careful in this comparison, since the time to peak is not really the key parameter. In Fig. 2.19, the pulses all have the same time to peak but quite different durations. The longer duration pulses will exhibit much worse pile-up even with the same time to peak. The key point is that the digital pulse processor, with its true trapezoid, has lower noise indices and a narrower width in the time domain than comparable analog shapers. Therefore, it simultaneously reduces electronic noise and pile-up.

Table 2.2: Noise indices and pulse duration (FWHM) for three common shaping amplifiers. All are written in terms of the peaking time τ_{peak} .

	Step (parallel) noise index	Delta (series) noise index	Duration (FWHM)
	A_p	A_s	
Trapezoid (Digital)	$\frac{2}{3}\tau_{peak} + \tau_{flat}$	$\frac{2}{\tau_{peak}}$	$\tau_{peak} + \tau_{flat}$
7 real pole Gaussian	$\frac{2}{3}\tau_{peak}$	$\frac{2.53}{\tau_{peak}}$	$1.12\tau_{peak}$
CR-RC	$\frac{e^2}{4}\tau_{peak} = 1.87\tau_{peak}$	$\frac{e^2}{4}\tau_{peak} = 1.87\tau_{peak}$	$\frac{e^2}{3}\tau_{peak} = 2.46\tau_{peak}$

Multi Channel Analyzer (MCA) Throughput

There are two sources of dead time in an analog system: some pulses may be lost (not detected) because: (a) the pulses overlap in time or (b) the peak detect and digitizer circuits are busy. Most MCAs use ADCs which require microseconds, and even if the analog pulses do not overlap in time, counts will be lost due to the digitizer's dead time. In the digital processor, there is no dead time associated with the peak digitization. The entire pulse shape is already being digitized, at a fast rate, e.g. 20 MHz. There will be a few clock cycles required to update the histogram memory but this is negligible. So the digital

system has no dead time associated with MCA peak acquisition. It does have a dead time associated with the pulse duration, as discussed above.

Linearity

In the analog system, the non-linearity of the ADC has a major impact on system non-linearity. Since the MCA makes a single measurement of the peak height, any non-linearity in the size of the ADC steps will result in a non-linear pulse height measurement. One common approach to ADC non-linearities is dithering, where random numbers are added to the pulse, the pulse plus these random numbers is digitized, and then the random numbers are subtracted. The result is that several ADC codes are used to measure the voltages of a single pulse height. In the digital system each pulse amplitude is the sum of many different ADC measurements, inherently using many different ADC codes. This gives the digital system much improved linearity.

Configurability

In an analog pulse processor, most parameters are determined by resistors and capacitors. In a pseudo-Gaussian shaper, shaping time is determined by a set of fourteen resistors and capacitors, for example. An analog shaping amplifier with four shaping time constants will require four different sets of all of these components. It is impractical to have many different configuration options in an analog system.

In a digital system, shaping time is set by the number of clock cycles in the digital delay and in the accumulator. One can easily change between shaping times, and with a 20 MHz clock, the step size is 50 ns, giving a very fine adjustment. This permits processing options not possible in the analog approach. For example, some digital processors adjust the peaking time on a pulse-by-pulse basis: if the interval between two pulses is short, then a shorter peaking time is used, adding some noise but eliminating pile-up and count losses. In a digital system, one can easily have many more parameters and configuration options. These parameters include not only the shaping time but baseline restoration parameters, pile-up rejection parameters, etc. A digital system has far more configuration options so the user can readily tailor a system to the needs of an application, resulting in better performance.

Stability and Reliability

Because the analog system relies on resistors and capacitors, its stability is limited to the stability of these components and its reproducibility to their tolerances. The temperature coefficient of the resistors and capacitors will cause gain and shaping to drift with temperature. Tolerances among resistors and capacitors will cause the pulse shape to differ between nominally identical shapers or when changing from one setting to another. Fine gain is usually set by a potentiometer and it is difficult to return to a previous setting, difficult to precisely tune two systems to match.

In a digital system, the stability and reproducibility derive from a few very accurate references, e.g. the crystal oscillator to set timing. Temperature drifts are much lower. Reproducibility is much improved. In a digital system, where fine gain is set digitally, one can return exactly to previous parameters. Moreover, the failure rates of the gates in an FPGA are very low compared with the failure of many discrete components, with their soldered joints.

We can say now, that the digital processor has intrinsic performance advantages compared to analog shapers. It has a finite impulse response, reducing pile-up and baseline shifts; it provides better noise filtering (for the same pulse width); it reduces ballistic deficit and improves linearity; it has better configurability, stability, and reliability.

Its primary disadvantage is that the fast ADC consumes considerably more power than the op-amps and slow ADC used in an analog shaper. However, when the best performance is required, the lowest noise and operation at the highest count rates; the digital processor is clearly the best solution.

CHAPTER 3: ARRAY FOR LIGHT CHARGED PARTICLE DETECTION

In this chapter the array for light charged particle detector that has been developed during this Thesis will be presented. To begin with an introduction to the state-of-the-art gamma ray spectrometers and the advantages of operating them together with charged particle detectors is given. Then the prototype implemented in this work is discussed, including the main characteristics of each component and the description of the analog and digital electronics setups instrumented for processing the pulses coming from the prototype.

The experimental tests performed are mainly related to Heavy-Ion experiments for nuclear Radioactive Ion Beams studies. However, the algorithms presented in this chapter are meant to be general enough to find application in other areas.

3.1 INTRODUCTION

High resolution gamma ray spectroscopy using large arrays of Hyper-Pure Germanium (HPGe) detectors, operated in conjunction with a variety of particle detection systems continues to be one of the most useful experimental techniques for nuclear spectroscopy at Radioactive Ion Beam (RIB) facilities. The state-of-the-art gamma ray spectrometers such as GRETINA in the USA [1], or AGATA Demonstrator Array in Europe [2], also called 4π gamma ray spectrometers, perform on the principle of tracking the interaction sequence of the gamma ray. To fully utilize their capabilities in the study of nuclear reactions, new concepts of auxiliary charged particle detectors that provide better position/angle sensitivity are needed.

Example of a state-of-the-art gamma ray spectrometer: Gamma Ray Energy Tracking In-beam Nuclear Array (GRETINA).

GRETINA consists of 28 highly segmented HPGe crystals to determine the location and energy of every interaction of each gamma ray emitted by a nuclear reaction. The interaction points belonging to a particular gamma ray would then be identified from the position and energy using a procedure called "tracking". The full gamma ray energy is obtained by summing only the interactions belonging to that gamma ray and the problem

of summing two gamma rays is avoided. Tracking makes use of all the information deposited in the detector and of the energy-angle relation given by the Compton scattering equation (Eq. 1.5):

$$E'_\gamma = \frac{E_\gamma}{1 + \frac{E_\gamma}{0.511}(1 - \cos\theta)} \quad (\text{MeV}) \quad (3.1)$$

Tracking Principle

The tracking principle is illustrated in Fig. 3.1 [61]. For a gamma ray with an energy up to about 2 MeV, the dominant interaction modes are photo absorption and Compton scattering. In Compton scattering, the energy of the scattered photon E'_γ (in MeV) is related to the energy of the incident photon E_γ and the scattering angle ϑ by Eq. 3.1.

The energy transferred to the electron which is measured by the detector is $E_e = E_\gamma - E'_\gamma$. If the energy and the direction of the incident photon are known, then there is a definite relation between the scattering angle and the detected energy:

$$\cos\theta_c = 1 + \frac{0.511}{E_\gamma} - \frac{0.511}{E'_\gamma} \quad (3.2)$$

As the photon makes successive Compton scatterings in a detector, this relation is valid for each scattering until a photo-absorption terminates the scattering process. Thus, from the measured position and the energy deposited at each of the Compton interaction point, we can determine uniquely the sequence of the scattering and thus "track" the path of the photon in the detector.

To start the tracking, it is needed to make a first guess of the incident energy. This is done by summing the energy from individual interactions which are assumed to come from a single gamma ray and that it has deposited its *full energy* in the detector. For an event with N interaction points, there are $N!$ possible scattering sequences. They are evaluated, using the angle-energy relation of Compton scattering, to determine the correct sequence. If this sequence is from a full energy gamma ray, then the relation will be satisfied exactly. In practice, it is used a parameter to characterize the deviation from the ideal relation such as the square deviation (Chi-squared) of the measured scattering angle from the predicted scattering angle based on the deposited energy. The correct sequence will have a Chi-squared value of 0. On the other hand, if the gamma ray did not deposit all

of its energy in the detector, the sum energy of the interaction will be less than the true energy and the Compton condition will not be satisfied. In such cases, the Chi-squared value will in general have a non-zero value and, based on this value, these partial-energy (Compton) events can be rejected. This method of Compton rejection has the advantages of a Compton shielded detector (good peak-to-total) and sum spectrometer (high efficiency), but not the disadvantages such as low efficiency and false veto of the Compton shielded detector and false summing of the sum spectrometer.

Tracking has already been used to determine the energy and direction of incident photons. For example, in astronomy Compton telescopes are surveying the sky for gamma ray emitting sources. In laboratory applications such as gamma ray spectroscopy, since the source position is known, the use of tracking will give both the energy and direction of the gamma ray on an event-by-event basis.

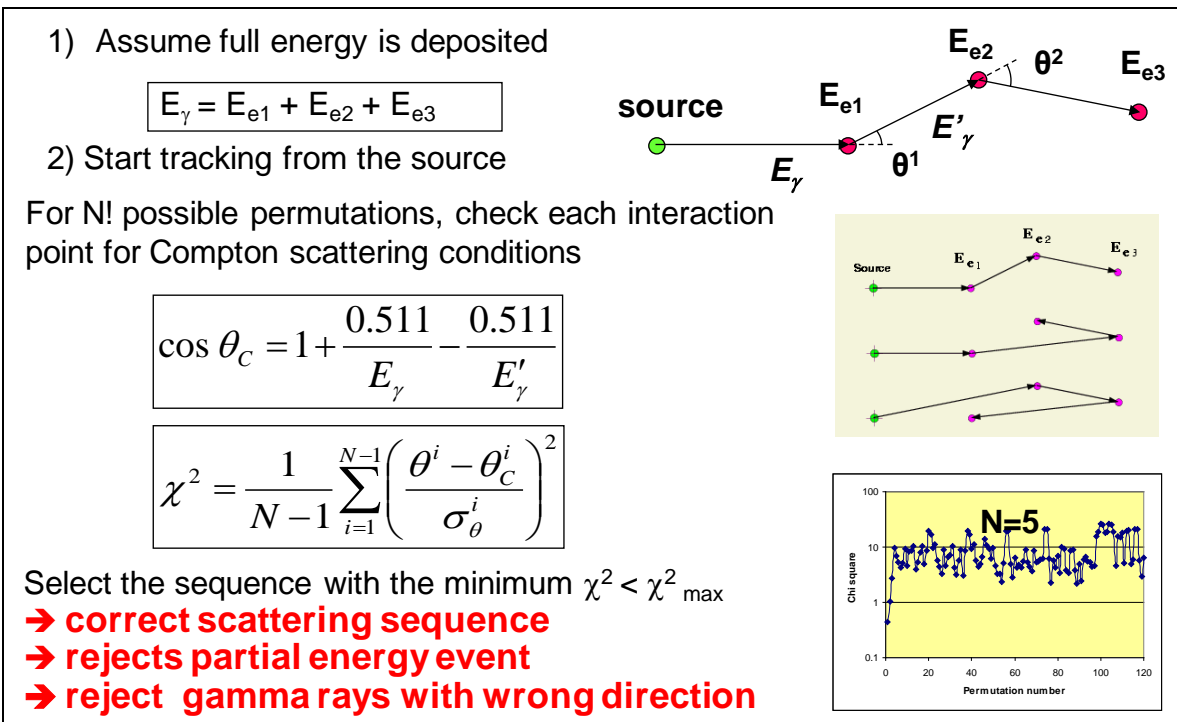


Figure 3.1: Tracking principle assuming that full energy gamma ray is deposited. Source location and interaction points are known.

According to the tracking principle, it is of most importance to detect as accurately as possible both the energy transferred to the electron by a Compton interaction, and the angle of the scattered gamma ray photon. So that, some auxiliary detectors such as charged particle detectors are used in conjunction with the HPGe arrays in order to obtain

further information to satisfy these and other requirements. For example, there is an undesirable effect regarding to the high speeds of the moving nucleus when interacting into a nuclear reaction. Such effect is called the Doppler broadening, and is illustrated in Fig. 3.2. Because of the high velocities of the nucleus within a nuclear reaction, there will always be a spread in speed ΔV of the gamma rays detected by the spectrometer, producing as well a distribution of the direction of the velocity $\Delta\vartheta_N$. Each speed V and position ϑ detected for a single gamma ray photon will produce an energy E_γ as follows:

$$E_\gamma = E_\gamma^0 \frac{\sqrt{1 - \frac{V^2}{c^2}}}{1 - \frac{V}{c} \cos \theta} \quad (3.3)$$

where E_γ is the gamma ray energy measured by the detector (which has suffered a Doppler shift), and E_γ^0 is the gamma ray energy in rest. Because of the spread in speed ΔV , and direction $\Delta\vartheta_N$, there will be a range of values ΔE_γ measured for a single photon, thus having a Doppler broadening effect which produces a considerable deficit on the overall energy resolution of the detector.

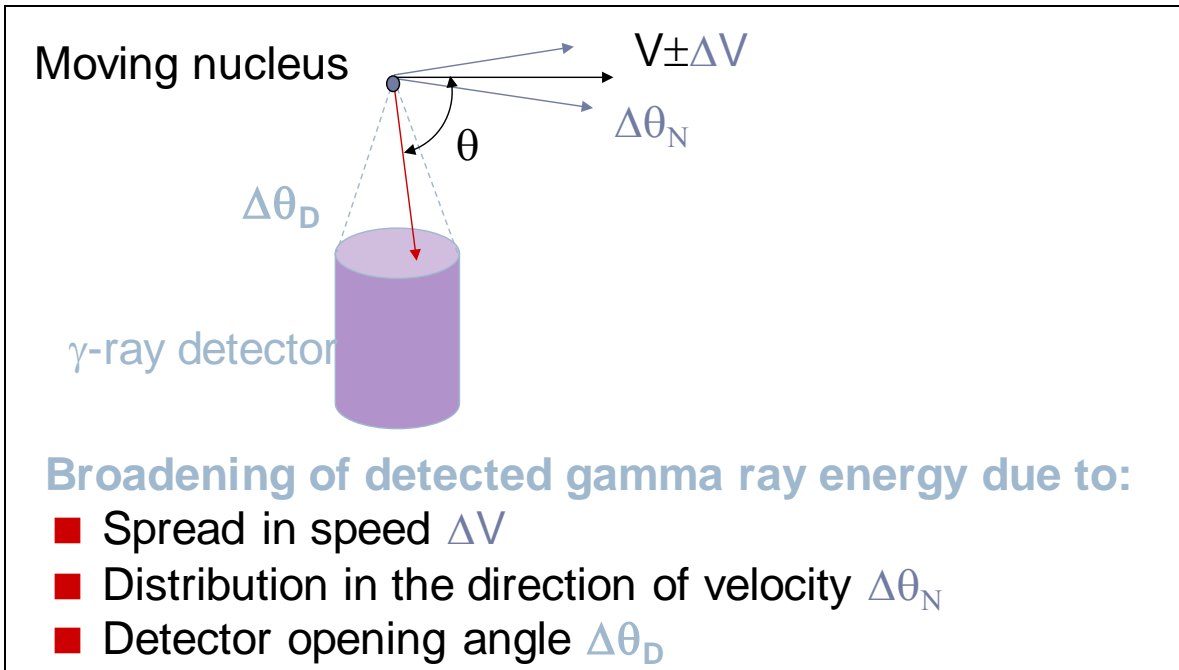


Figure 3.2: Doppler broadening effect due to high speeds of nucleus within a nuclear reaction.

In this case, the accurate determination of the velocity and the angle of both the gamma ray photons and the charged particles emitted by a given nuclear reaction will allow a proper reconstruction of the kinematics of the nuclear reaction, thus making a good correction in the resolution of the detector due to Doppler broadening effect.

In Fig. 3.3, the physical disposition of two gamma ray spectrometers devoted to the study of nuclear structure (see §1.1): GRETINA (left), and Gammasphere [62] (right).

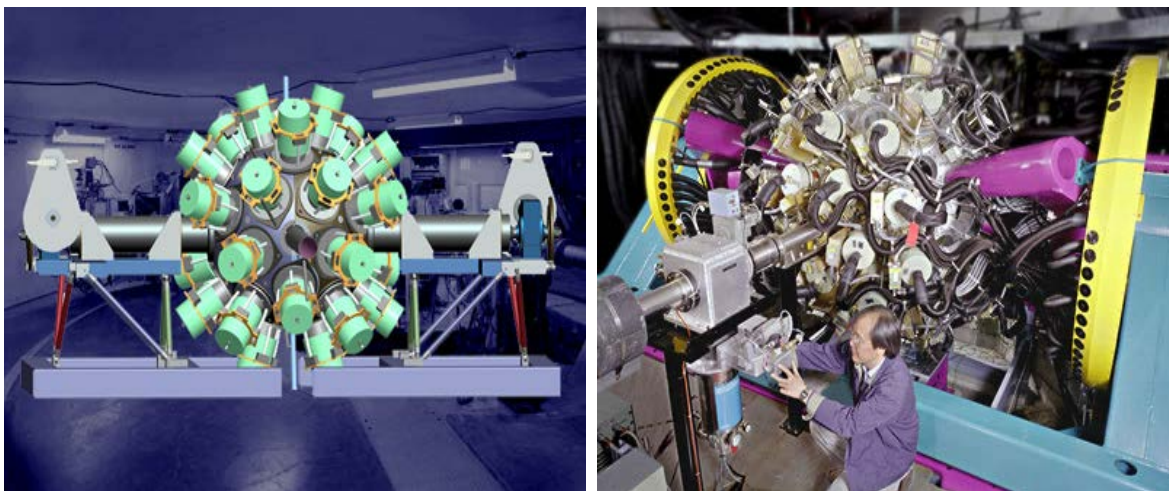


Fig. 3.3: Physical disposition of GRETINA (left) and Gammasphere (right) 4π gamma ray spectrometers.

3.2 4π GAMMA RAY SPECTROMETERS AND CHARGED PARTICLE DETECTORS

Besides the correction of Doppler broadening effect, the use of a 4π -steradians gamma ray spectrometers together with charged particle detectors allows the measurement of a wide range of *decay* properties. A deep discussion about the advantages of combining 4π gamma ray spectrometers and charged particle detectors can be found in [63].

Desirable properties for a charged particle array used with a gamma spectrometer are: low particle-kinetic energy thresholds, good energy resolution and linearity, high count rate capability, stability, angular resolution, immunity to magnetic field, compact size, and resistance to radiation. Additionally it should have the smallest possible influence on the performance of the HPGe detectors.

Several configurations of charged particle detector arrays to work in combination with 4π gamma ray spectrometers have been proposed, based on the use of either solid-state or scintillation detectors. A brief review of some of such configurations is given below.

A. Solid-state detectors for charged particle detection

Since their development as practical detectors in the early 1960's, silicon diodes have become the detectors of choice for the majority of applications in which heavy charged particles are involved (i.e. energy > 10 MeV), because, compared with competing techniques, semiconductor detectors often provides better energy resolution, good stability, excellent timing characteristics, very thin entrance windows, small size, and simplicity of operation. Nevertheless, for the specific purpose of the charged particle detector subject of this Thesis; the use of only a solid-state detector for charged particle detection and identification would provide important disadvantages: first, good energy resolution is needed also for charged particles with energies ≤ 10 MeV, not only for those with higher energies. And secondly, as the charged particle detector is intended to work inside the 4π gamma ray spectrometer, then it is necessary that the detector could be able to stop charged particles but should allow the pass of gamma-ray photons towards the HPGe array. A thin semiconductor detector would allow the pass of some gamma-rays to the gamma-ray spectrometer, but would also allow that charged particles hit the gamma-ray spectrometer, which might, of course, affect the gamma-ray measurements. On the other hand, a thick solid-state detector would stop both kind of radiation and none of the gamma ray photons would be able to reach the gamma ray spectrometer. So that, making use of semiconductor detectors is a bad option to perform as a charged particle detector operating in conjunction into a gamma ray spectrometer, therefore another choice, such as scintillation detectors was explored.

B. Scintillation detectors for charged particle detection

Since mid 1980s, several configurations have been proposed for charged particle detectors to operate as inner balls for gamma ray spectrometers [63]. Most of such configurations were mainly based on the *phoswich* (or *phosphor sandwich*) technique, which consists of the combination of two dissimilar scintillators optically coupled to a single *photomultiplier tube* (PMT). The scintillators are chosen to have different decay times so that the shape of the output pulse form the PMT is dependent of the relative

contribution of scintillation light from the two scintillators. However, the phoswich detectors has limitations because the first scintillator, if thick, reduces the possibility of identification of the low-energy particles and, if thin, the high-energy ones, thus making difficult to adapt detector thicknesses to specific experimental demands. Because of this limitation, during early 1990s, another approach for charged particle detector was proposed, consisting of a CsI(Tl) crystal scintillator with a *PIN photodiode* readout, instead of PMT readout (A. Galindo-Uribarri, 1992), providing a better energy resolution, more compact size, good stability and linearity, and immunity to magnetic fields. However, some disadvantages of the PIN photodiodes like having no amplification at all and radiation damage continued to be a problem for this kind of detectors. Additionally, with the development of new generation 4π gamma ray spectrometers, higher granularity and even better energy resolution and position sensitivity are required than those achieved with PIN diode readout.

Because of the limitations of previous developed charged particle detection arrays, in this Thesis we have proposed and characterized a prototype detector as a building block for an array of charged particle detectors, based on CsI(Tl) scintillators coupled to *silicon photomultipliers* (SiPMs), which might be used as an auxiliary detector with the new generation of 4π gamma ray spectrometers to study the structure and properties of atomic nuclei.

3.3 PROTOTYPE PROPOSED

The array that we have proposed for charged particle detection consists of an inorganic scintillator optically coupled to a SiPM for collection and readout of the light.

Different alpha particles and gamma rays radioisotope sources were used to test the array, and three different electronics instrumentation setups were tested to process the signals coming from the prototype detector:

- Analog electronics setup
- Digital electronics setup
- Gretina digitizer setup

Figure 3.4 schematically shows the idea:



Figure 3.4: Prototype for charged particle detection consisting of a CsI(Tl) scintillator optically coupled to a SiPM for the electronics read out.

3.3.1 WHY USING A CsI(Tl) SCINTILLATOR

As briefly reviewed in §1.4.3, the common material choices in Nuclear Physics for scintillation detection with good efficiency and energy resolution are thallium activated sodium iodide NaI(Tl), sodium activated cesium iodide CsI(Na), and thallium activated cesium iodide CsI(Tl), which main properties are summarized on Tab. 1.1. Here a deeper presentation of such properties is given.

NaI(Tl)

Thallium-activated sodium iodide is an Alkali Halide inorganic scintillator, in which a trace of thallium iodide had been added in the melt, producing an exceptionally light scintillation light output compared with organic materials. Although new organic scintillators offer higher light output, better energy resolution, or faster timing capability, the availability of NaI(Tl) in large volumes at relatively low cost has continued its popularity in a wide range of applications. NaI(Tl) is hygroscopic so crystals must be “canned” into an airtight container for normal use. The light yield from NaI(Tl) for excitation by fast electrons (or gamma rays) is about 38,000 photons per MeV energy deposition. This value ranked the material for many years as the brightest of common scintillators, and many measurements of light yield from other materials historically have been made relative to that of NaI(Tl) as standard. In comparison with other typical organic scintillators NaI(Tl) shows a significant non-proportionality of its scintillation response with deposited electron energy (see Fig. 1.8). Its maximum wavelength of emission is centered at 415 nm.

CsI(Tl) and CsI(Na)

Cesium iodide is another alkali halide. It is commercially available with either thallium or sodium as the activator element with very different scintillation properties in each case. Cesium iodide has a larger gamma ray absorption coefficient per unit size compared to sodium iodide. This advantage is of primary importance for applications such as space instrumentation where size and weight are at a premium. Because it is less brittle than sodium iodide, it can be subjected to more severe conditions of shock and vibration. When cut into thin sheets, cesium iodide may be bent into various shapes without fracturing, and it is reasonably soft and malleable. An extensive bibliography of the properties of cesium iodide (both sodium and thallium activated) can be found in [64].

CsI(Na) has an emission spectrum similar to that of NaI(Tl) with a light yield that is comparable, but its relatively slow decay is a disadvantage. The decay is reported to consist of two components with mean lives of 0.46 and 4.18 μ s and a dependence of the slow to fast component ratio has been shown for various exciting particles [65]. Long-lived phosphorescence components in cesium iodide have also been reported [66]. CsI(Na) is hygroscopic and must be sealed against exposure to ambient atmospheres.

On the other hand, a useful property of CsI(Tl) is its variable decay time for various exciting particles. Pulse shape discrimination techniques can therefore be used to differentiate among various types of radiation [67-72]. Particularly clean separations can be achieved between charged particles such as protons or alpha particles on one hand and electron events on the other hand. The material is less hygroscopic than NaI(Tl) but will deteriorate if exposed to water or high humidity.

The emission spectrum of CsI(Tl) is peaked at a much longer wavelength than that for NaI(Tl) (540nm) and is poorly matched to the response of photo-multiplier tubes with S-11 or bialkali photocathodes. For that reason, the light output is often quoted as being substantially lower in CsI(Tl). However, when measurements are made using photodiodes, and now SiPMs, with extended response into the red region of the spectrum, the scintillations yield is actually higher than that of NaI(Tl) [73]. The absolute light yield at room temperature is measured [74] to be about 54,000 photons/MeV, with a maximum value about 6% higher at -35°C. The yield falls off with temperature change on either side of this maximum, to 64% of the room temperature value at -100°C and to 95% at +50°C.

The luminescent states in CsI(Tl) are populated through an exponential process that results in a rise time of 20ns for the initial appearance of the light. The subsequent decay of these states is among the slowest for the commonly used scintillation materials. The emission for gamma ray excitation shows two primary components [75], with decay times and relative intensities at room temperature of 0.68 μ s (64%) and 3.34 μ s (36%). The best energy resolution is promoted by choosing long shaping times (e.g. 12 μ s in [76]) to fully integrate all the prompt scintillation light. In addition to its primary use as a gamma ray detector, CsI(Tl) has also proven its utility in the spectroscopy of heavy ions [77, 78].

Because of its characteristics, we have concluded that the best choice for our application was the use of a CsI(Tl) scintillator. It has high absolute light output and good capability to discriminate and identify gamma rays and light charged particles by means of pulse-shape analysis. It can stop more energetic particles than solid-state detectors of the same thickness. It is mildly hygroscopic and easy to machine, and also because, as we shall see, the CsI(Tl) peak of maximum emission matches better with the wavelength response of the SiPM selected.

3.3.2 WHY USING A SiPM

As presented in §3.2.2, the readout sensor for scintillation detectors has been for many years the PMT (see details of operation in §1.4.3), substituted later for PIN photodiodes in charged particle detector performing as inner balls for the 4π gamma ray spectrometers. As we shall see in this section, silicon photomultipliers are basically arrays of photodiodes with specific characteristics discussed below, which make them a suitable option as substitutes for PMTs and PIN (conventional) photodiodes for the purposes of this Thesis.

Photodiodes as substitutes for PMTs

Advances in the development of semiconductor photodiodes have led to the substitution of solid-state devices for PMTs in some applications (such as the application subject of this Thesis). In general, photodiodes offer the advantages of higher *quantum efficiency* (i.e. *number of photoelectrons emitted/number of incident photons*); and therefore, the potential for better energy resolution, lower power consumption, more compact size, and improved ruggedness compared with PMTs used in scintillation detection. Photodiodes are also virtually insensitive to magnetic fields and therefore can sometimes be substituted in applications where magnetic fields prevent the use of PMTs. Because the

relatively small dimensions over which charges must move in these devices, their time response is also comparable to that of conventional PM tubes.

There are three general designs that have received attention as possible substitutes for PMTs. Conventional photodiodes (PIN photodiodes) have no internal gain and operate by directly converting the optical photons from the scintillation detector to electron-hole pairs that are simply collected. *Avalanche photodiodes* incorporate internal gain through the use of higher electric fields that increase the number of charge carriers that are collected. A third category is an array of many small-dimension avalanche photodiodes operated in *Geiger* mode, called silicon photomultipliers (SiPMs).

A. PIN photodiodes

When light is incident on a semiconductor, electron-hole pairs are generated in a similar way to that described in §1.4.3. Photons corresponding to typical scintillation light carry about 3-4 eV of energy, sufficient to create electron-hole pairs in a semiconductor with a bandgap of approximately 1-2 eV. The conversion is not limited by the need for charge carriers to escape from a surface as in a conventional photocathode, so the maximum quantum efficiency of the process can be as high as 60-80%, several times larger than in a PMT. This high quantum efficiency also spans a much wider wavelength range than is typical for photocathodes in PMTs, so a much higher primary charge usually is created by the light from the scintillator. However, there is no subsequent amplification of this charge as in a PMT, so the output signal is smaller by orders of magnitude.

In a typical scintillation event, only a few thousand visible photons are produced, so the size of the charge pulse that can be developed is limited at best to no more than the same number of electronic charges. Because of the small signal amplitude, electronic noise is a major problem in pulse mode operation, especially for large-area detectors and low-energy radiations. The noise arises from the two separated sources described in §2.1: series noise, primarily originates from sources within the preamplifier input stage whose relative importance increases with the detector capacitance; and the parallel noise due to fluctuations in the leakage current in the photodiode. The photodiodes overall noise figure can be reduced by cooling the photodiode.

The photodiode quantum efficiency reaches higher values and extends much farther into the long wavelength region than that of typical PMT photocathodes. This extended

spectral response is particularly important for CsI(Tl) scintillators with peak emission spectra at 540nm. Because of the high quantum efficiency of the semiconductor material, the achievable energy resolution is actually superior to that obtainable even with the best photomultiplier tubes.

B. Avalanche photodiodes

The small amount of charge that is produced in a conventional photodiode by a typical scintillation event can be increased through an *avalanche* process that occurs in a semiconductor at high values of the applied voltage. The charge carriers are accelerated sufficiently between collisions to create additional electron-hole pairs along the collection path. Gain is achieved within the semiconductor material (normally silicon) by raising the electric field sufficiently high to enable the migrating electrons to create secondary ionization during the collecting process. Charge carriers within the high-field region will be multiplied by a variable gain, depending on their position relative to the boundaries of the multiplication region.

The internal gain helps pulling the signal up from the electronic noise level and permits good energy resolution in pulse mode at lower radiation energy than possible using conventional photodiodes. Because the gain factor is very sensitive to temperature and applied voltage, avalanche photodiodes require well-regulated high-voltage supplies for stable operation. The gain dependence of temperature is strong compared with that of PMTs, amounting to a decrease in gain of about 2% °C per increase. To maintain good energy resolution when used with scintillators under conditions in which temperature may vary, stabilization schemes have been developed based on using a temperature monitor and making compensating gain adjustments by varying the applied voltage [79] or by other electronic means.

Through the use of antireflective coating on the external surface of the photodiode, quantum efficiencies as high as 80% are achievable at the peak wavelength of the response, typically in the 500-600 nm range. Because of the higher signal/noise provided by the gain, shorter shaping times can be used with avalanche photodiodes that with an equivalent PIN photodiode, permitting higher rate operation and better timing resolution.

The same categories of electronic noise previously mentioned for standard photodiodes are also still present, potentially degrading the energy resolution. On the other hand, the

high quantum efficiency of avalanche photodiodes compared with PMTs helps to offset these disadvantages, and excellent energy resolution has been demonstrated [80-82] in their use with small volume scintillators.

C. The silicon photomultiplier

A Silicon Photomultiplier (SiPM) is a semiconductor photo-detector with many properties similar to that of a photomultiplier tube. A SiPM consists of an array of Geiger-mode Avalanche Photodiodes (APDs) with integrated quenching circuits coupled to a common output. The individual Geiger-mode APDs of a SiPM are often referred to as micro-pixels or micro-cells. Figure 3.5 below shows a schematic diagram of the array of Geiger-mode APDs of a SiPM device. A Geiger-mode APD is a photodiode operated above its breakdown voltage V_{br} . Under these conditions a high electric field exists in the region close to the semiconductor junction interface. In this high-field or avalanche region, carriers gain enough energy that a single carrier can result in the entire junction breaking down to produce a so-called Geiger discharge or pulse. If the single carrier is the result of absorbing a single photon then detecting the Geiger pulse allows single photons to be detected. The Geiger discharge is self-sustaining and must therefore be quenched in order to reset the Geiger-mode APD to its photo-sensitive state.

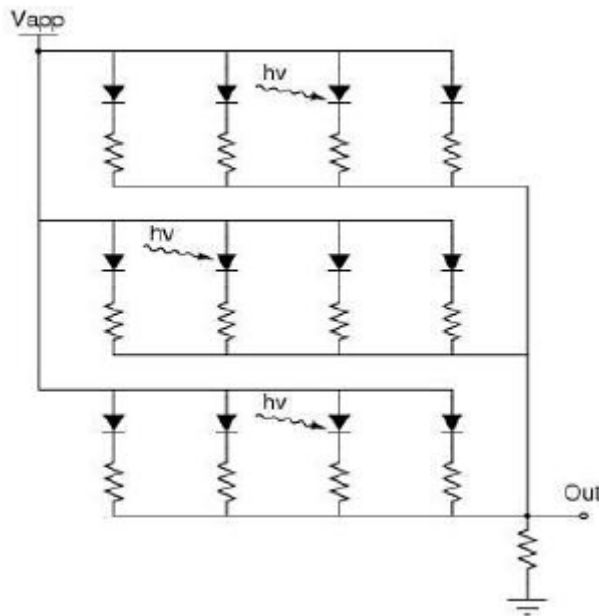


Figure 3.5: Schematic diagram of an array of passively quenched Geiger-mode APDs.

Figure 3.6 shows the quench and reset cycle of a passively quenched Geiger-mode APD. The internal diode RC network sets the quench time while the external RC network dominates the reset time.

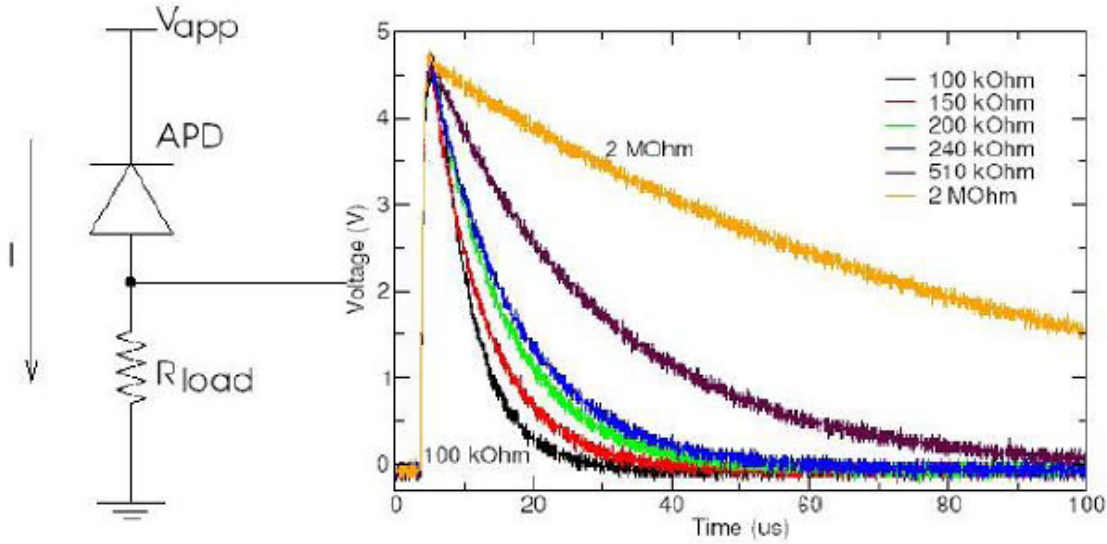


Figure 3.6: Circuit diagram for a passively quenched Geiger-mode APD (left) and the typical quench and reset times of a Geiger pulse calculated for different resistor values R_{load} (right).

While the output from a single Geiger-mode APD is a binary output and independent of the number of photons that trigger the Geiger discharge, the output from a silicon photomultiplier is proportional to the number of Geiger-mode pulses and therefore the number of photons incident on the detector.

Photodetection efficiency

The photodetection efficiency (PDE) is given by the product of the total amount of charge produced per incident photon:

$$PDE = QE * \epsilon_{geom} * \epsilon_{Geiger} \quad (3.4)$$

where:

- QE is the quantum efficiency, defined as the probability that a photon will both enter the device and create a photoelectron. It is a strong function of scintillation

photon wavelength and is related to the optical absorption coefficient of the semiconductor substrate.

- ϵ_{geom} is the fill factor, or geometrical efficiency, i.e. the ratio of the active area per the total area of the device. Bigger pixels improve the geometrical efficiency.
- ϵ_{Geiger} is the Geiger efficiency, i.e. the probability for a photoelectron to trigger an avalanche and is related to the extinction probability for branching processes. That is, some avalanches may begin to form but fail to reach a critical number of electron-hole pairs required to form a full discharge. This loss can be diminished by increasing the bias and thus the electric field.

The PDE is strongly dependant on temperature and voltage. For stable operation, reliable biasing circuitry must be designed to measure or compensate for any fluctuations over the lifetime of the measurement.

Dark pulses and noise

While the SiPM is very sensitive to single photoelectrons, it is equally responsive to thermally generated conduction-band electrons in the silicon. These electrons lead to spurious thermal events that add a random noise component to the scintillation signal. The dark rate observed from a SiPM can be as large as 10^6 pulses/s per mm^2 at room temperature. Most of these events correspond to the firing of a single cell. Thus if the measurement consists of looking for pulses from single photons, the spontaneous dark rate will be very high. However, if a discrimination level is set corresponding to the simultaneous firing of multiple cells (say, 5), the dark rate will be many orders of magnitude lower (see Fig. 3.7b). This level of discrimination would be possible in many applications to scintillation readout where large numbers of photons are registered per pulse. The availability of thermal electrons also can be reduced by cooling the device.

In addition to thermal events, the dark noise of the SiPM includes afterpulsing and optical cross-talk. Afterpulsing occurs when impurities in the silicon lattice act as traps that de-excite exponentially in time. The electrons from these de-excited traps may cause subsequent avalanches within the same cell and increase the number of avalanches per scintillation photons [84]. Optical cross-talk occurs because of avalanche-initiated fluorescence in which photons emitted from the cell trigger avalanches in neighboring cells. As the fill factor (i.e. geometrical efficiency) increases, these avalanche photons are more likely to initiate subsequent avalanches. One solution to this noise mechanism is the fabrication of opaque trenches between pixels. However, when a reflectively wrapped scintillator is mated to the SiPM, avalanche photons may reflect inside the scintillator and

overcome any inter-cell barrier. The statistics of the optical cross-talk noise will then also depend on the optical characteristics of the scintillator. Overall, the noise of a SiPM is a complex interplay of scintillation, thermal, afterpulse, and crosstalk events.

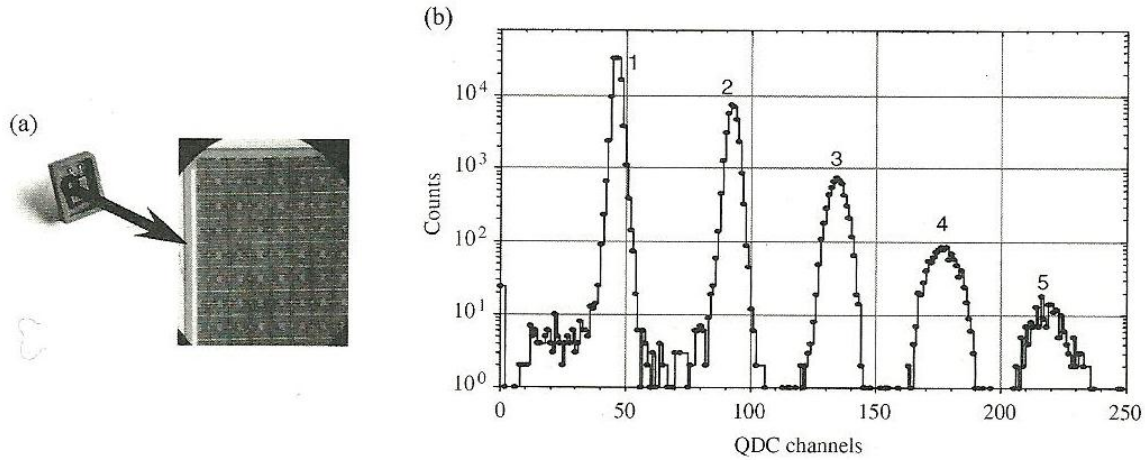


Figure 3.7: (a) A SiPM configuration [83] consisting of 5625 cells arranged in an array with 3 mm X 3 mm overall size. The expanded view shows individual cells. (b) The dark noise amplitude spectrum (the horizontal scale represents pulse amplitude) from the device shown in part (a). The peak on the left corresponds to pulses generated by a single cell, while those to its right correspond to the simultaneous firing of more than once cell, from 2 to 5. The narrow width of the peaks indicates that all cells produce nearly the same output when triggered.

In summary, the choice of using a SiPM as the readout sensor coupled to the CsI(Tl) was made because of its compact size (form factor), high gain (10^6), immunity to magnetic fields, and low operating voltage. As the SiPMs consist of several micro-pixels arranged into different cells, they provide also the capability of having position sensitivity by means of analyzing the signals detected by each individual cell.

3.3.3 SELECTING SPECIFIC CsI(Tl) AND SPECIFIC SiPM

Once it has been chosen to use a CsI(Tl) scintillator coupled to a SiPM, then we proceeded to analyze the matching between CsI(Tl) and some commercially available SiPMs and through an extensive search in the literature, it was found [85] that SiPMs manufactured by the Irish company SensL© [86] achieve the best matching to the CsI(Tl). Table 3.1 summarizes the comparisons made, and the yellow cell points out the maximum signal yield provided, and corresponds to a CsI(Tl)- SensL coupling.

Table 3.1: Relative signal yields of different types of radiation sensors coupled to a CsI(Tl) crystal, compared to an NaI(Tl) scintillator coupled to a Bi-alkali PMT (taken from [85]).

Scintillation crystal	Signal yield of different types of light detectors			
	Bi-alkali PMT	SiPMs		
		Hamamatsu MPPC	SensL SPM	Photonique SSPM
NaI(Tl)	1.00	1.04	0.69	0.30
CsI(Tl)	0.60	0.94	1.44	1.41

By the time of choosing the SiPM for this project, SensL was offering a novel array named SPMArray4: four side tileable large area SPM detector, whose datasheet is available on line in [86]. This SPMArray4 is composed of sixteen pixels, each one is a $3 \times 3 \text{ mm}^2$ SPM3035 (datasheet available in [90]), providing then a 4×4 pixels array. The SPMArray4 is pictured in Fig. 3.8a, and its pixels distribution is shown in 3.8b.

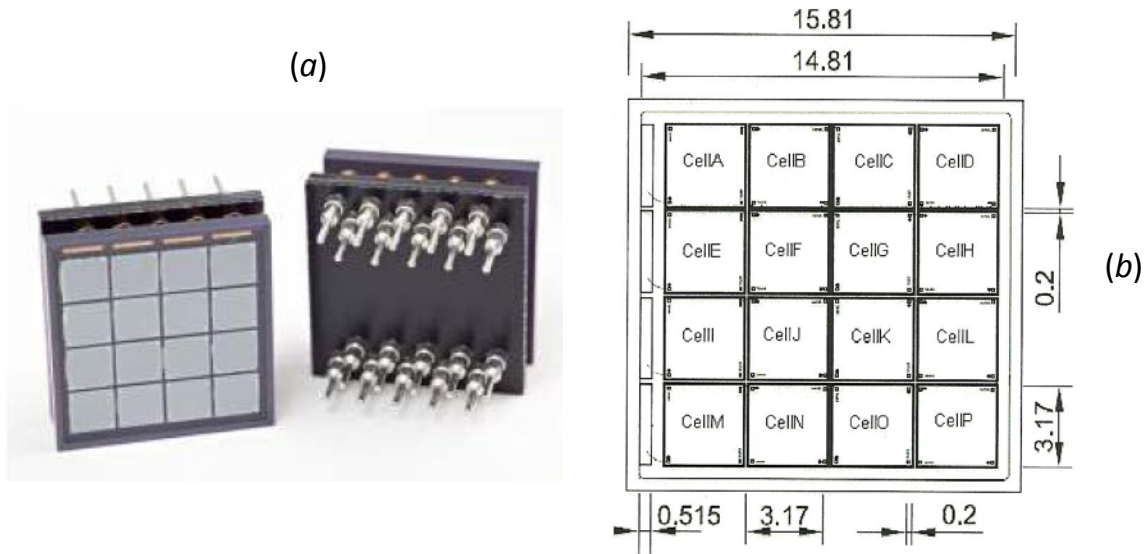


Figure 3.8: (a) 4 side tileable SPMArray mounted onto a pin socket. (b) Top view of the SPM pixel layout in the SPMArray4 package.

For educational purposes, the pre-amplification stage as well as a 16 channel readout electronics evaluation board for the SPMArray4 were also provided by SensL. The entire evaluation kit provided by SensL is described in Tab. 3.2 and it is shown in Fig. 3.9:

Table 3.2: Elements of the evaluation kit provided by SensL

Product	Description
SPMArray4	SPMArray 16 pixel Silicon Photomultiplier Array in 20 pin PGA ceramic package
SPMArray4-A0	Multi-channel preamplification electronic for SPMArray4
SPMArray4-A1	Evaluation board for SPMArray4 for pixellated/summed pixel output

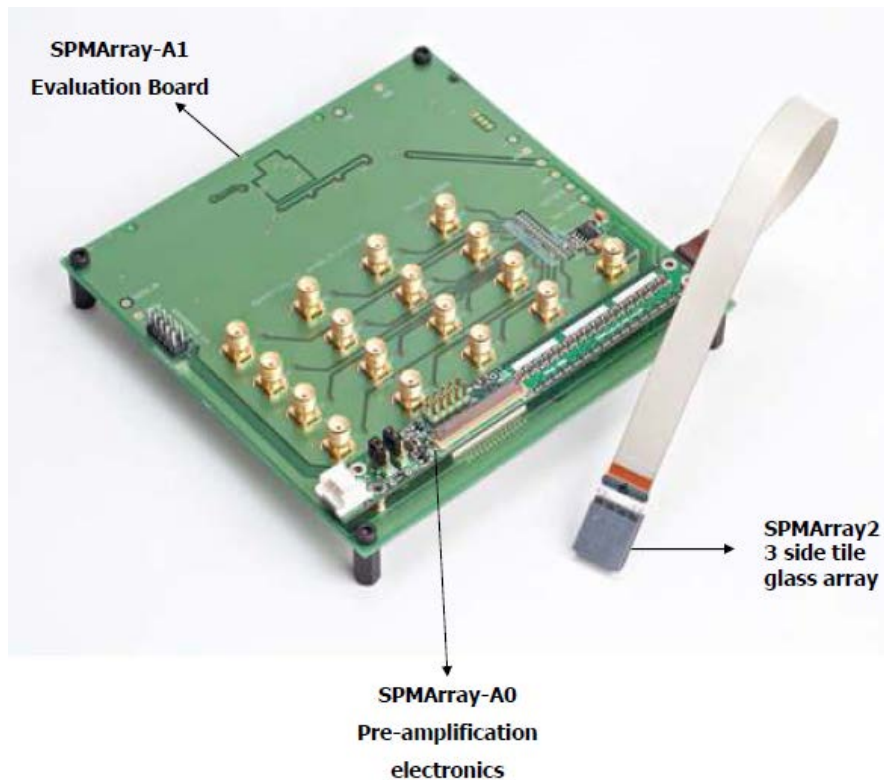


Figure 3.9: SPMArray4 SensL evaluation kit.

Details on the operational characteristics of the SPMArray4 will be given in Chapter 4.

Regarding to the selection of a specific CsI(Tl) crystal, it is important to say that after testing different geometries and reflective characteristics, it was concluded that the scintillator with best *single pixel* response when coupled to the SensL SiPM during the experiments was the CsI(Tl) 11x11x11 mm³ crystal, specifically requested with one face polished and white reflector on the four lateral faces, manufactured by Hilger Crystals® [87].

3.3.4 OPTICAL COUPLING

The CsI(Tl) crystal was optically coupled to the SensL SiPM through a room temperature vulcanizing silicone rubber (*RTV615*) with a refractive index of 1.406 [88] and the following characteristics:

RTV615 silicone rubber compound is clear liquid which cure at room temperature to high strength silicone rubber with the addition of curing agents.

This two-component product is supplied with curing agent in matched kits which are designed for use at a convenient 10:1 ratio by weight as follows:

- RTV615A (10 parts)
- RTV615B (1 part)

The compound is clear and colorless. It is a low viscosity, easily pourable liquid with nominal viscosity ranging between 3000 and 7000 centipoise (cps).

RTV615 silicone rubber compound has been used for protection of electronic components and assemblies against shock, vibration, moisture, ozone, dust, chemicals, and other environmental hazards by potting or encapsulation of the components and assemblies. However, the optical clarity of this silicone rubber compounds suggests evaluation for applications such as optical coupling for maximum light transmission and electronic assemblies where component identification is necessary or desirable.

This 10:1 mixture was processed into a vacuum chamber to extract as much amount of air as possible, then it was heated into an oven and finally it was cut into 15x15 mm² square when cooled down to match the area of the readout light sensor.

3.3.5 RADIOISOTOPE SOURCES TESTED

In order to verify the performance of the charged particle prototype detector, several alpha particles and gamma ray radioactive sources were tested. Such radioisotope sources and their energies are listed in Tab. 3.3.

Table 3.3: Radioisotope sources tested

Radioisotope source	Half-Life [years]	Energy [MeV]	Percent Branching [%]
<i>Alpha particle sources</i>			
²⁵² Cf (Californium-252)	2.65	6.1	97
²⁴¹ Am (Americium-241)	433	5.49	85.2
		5.44	12.8
²⁴⁴ Cm (Curium-244)	18	5.80	76.4
		5.76	23.6
Triple source: ²⁴¹ Am- ²³⁹ Pu- ²⁴⁴ Cm (Americium-241, Plutonium-239, and Curium-244)	433	5.49	85.2
		5.44	12.8
		5.16	73.3
	2.4 x 10 ⁴	5.14	15.1
		5.10	11.5
		5.80	76.4
18	5.76	23.6	
<i>Gamma-ray sources</i>			
¹³⁷ Cs (Cesium-137)	30.17	0.662	93.5
⁶⁰ Co (Cobalt-60)	5.26	1.173	100
		1.332	100

Extensive literature can be found regarding the properties and the mechanisms that lead the production of the radioisotope sources presented, one example is [13].

In common to every radioisotope source, there are some hazards and safety rules to take into account when handling. Some ionizing radiations are more hazardous to human health and environmental issues than others depending on their energy and range of penetration of matter. Next a brief description of alpha particles and gamma rays is presented. Also, in Appendix D, a guide for safe handling of radioactive sources is given.

Alpha particles

Alpha particles don't get very far in the environment. Once emitted, they travel relatively slowly (at approximately one-twentieth the speed of light) due to their electric charge and large mass [89]. *They lose energy rapidly in air, usually expending it within a few centimeters.* Because alpha particles are not radioactive, once they have lost their energy, they pick up free electrons and become helium.

Alpha particles cannot penetrate most matter they encounter. Even a piece of paper or the dead outer layers of human skin is sufficient to stop alpha particles.

The health effects of alpha particles depend heavily upon how exposure takes place. External exposure (external to the body) is of far less concern than internal exposure, because alpha particles lack the energy to penetrate the outer dead layer of skin.

However, if alpha emitters have been inhaled, ingested (swallowed), or absorbed into the blood stream, sensitive living tissue can be exposed to alpha radiation. The resulting biological damage increases the risk of cancer; in particular, alpha radiation is known to cause lung cancer in humans when alpha emitters are inhaled.

Gamma rays

Gamma rays travel at the speed of light and exist only as long as they have energy. Once their energy is spent, whether in air or in solid materials, they cease to exist. Gamma rays can easily travel great distances through air and penetrate several materials.

Because of the gamma rays' penetrating power and ability to travel great distances, it is considered the primary hazard to the general population during most radiological emergencies. In fact, when the term "radiation sickness" is used to describe the effects of large exposures in short time periods, the most severe damage almost certainly results from gamma radiation.

Penetration of matter

Though the most massive and most energetic of radioactive emissions, the alpha particle is the shortest in range because of its strong interaction with matter. The electromagnetic gamma ray is extremely penetrating, even penetrating considerable thicknesses of concrete, as shown in Fig. 3.10.

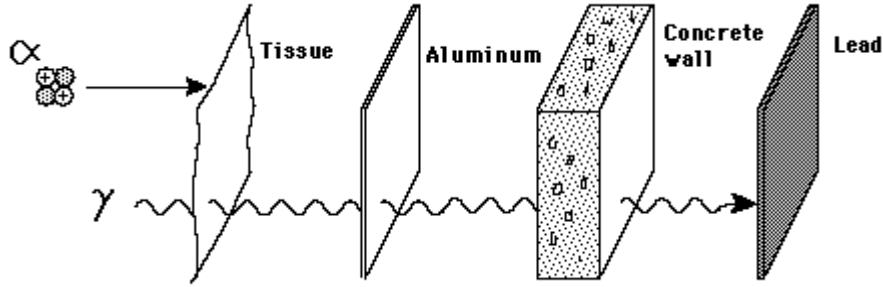


Figure 3.10: Penetration of matter of alpha particles and gamma rays.

3.3.6 CHARGED PARTICLE DETECTION EXPERIMENTAL SETUP

Figure 3.11 illustrates the basic experimental setup implemented for the evaluation of the charged particle prototype detector. As schematically shown, the CsI(Tl) crystal was optically coupled to the SensL SiPM (SPMArray4), which is attached to its pre-amplification stage (SPMArray4-A0) supported by the SensL evaluation board (SPMArray4-A1).

The evaluation board was fixed into a foam rubber surface in order to avoid mechanical variations among experiments.

Each radioisotope source (one at a time) was set on the top of a 50 mm tall Styrofoam glass since, as discussed in the previous section, in air, alpha particles have a range of penetration in matter of few centimeters, whereas gamma rays have further penetration. Finally, the experimental setup was mounted into a dark box in order to avoid external environmental light to alter the measurements.

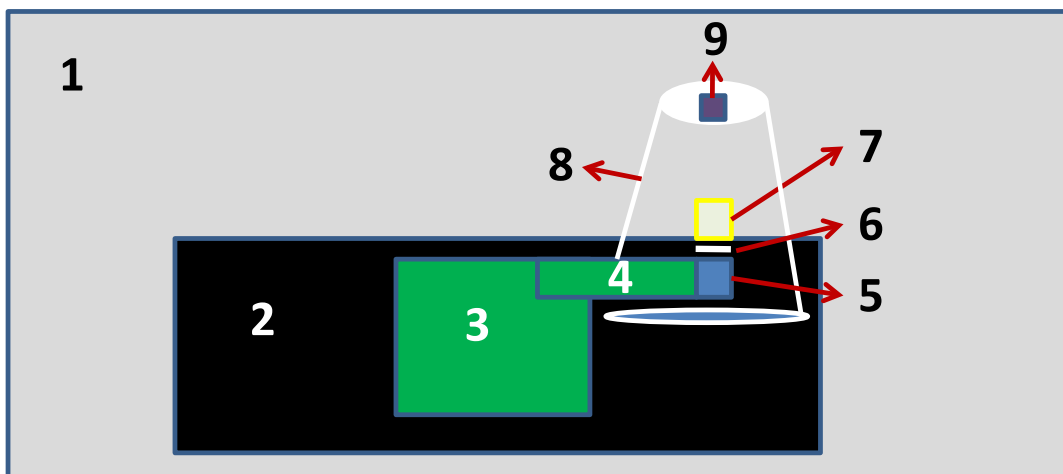


Figure 3.11: Schematic of the experimental setup for charged particle detection

where:

- 1 - Dark box.
- 2 - Foam rubber.
- 3 - SensL SPMArray-A1 Evaluation board.
- 4 - SensL SPMArray-A0 Pre-amplification electronics.
- 5 - SensL SPMArray4 SiPM.
- 6 - RTV optical coupling.
- 7 - 11x11x11 mm CsI(Tl) Hilger Crystal scintillator.
- 8 - 50 mm tall Styrofoam glass.
- 9 - Radioisotope source.

Figure 3.12 pictures numbers 1 to 5 listed above (left), and the dark box which contains the experimental setup (right)

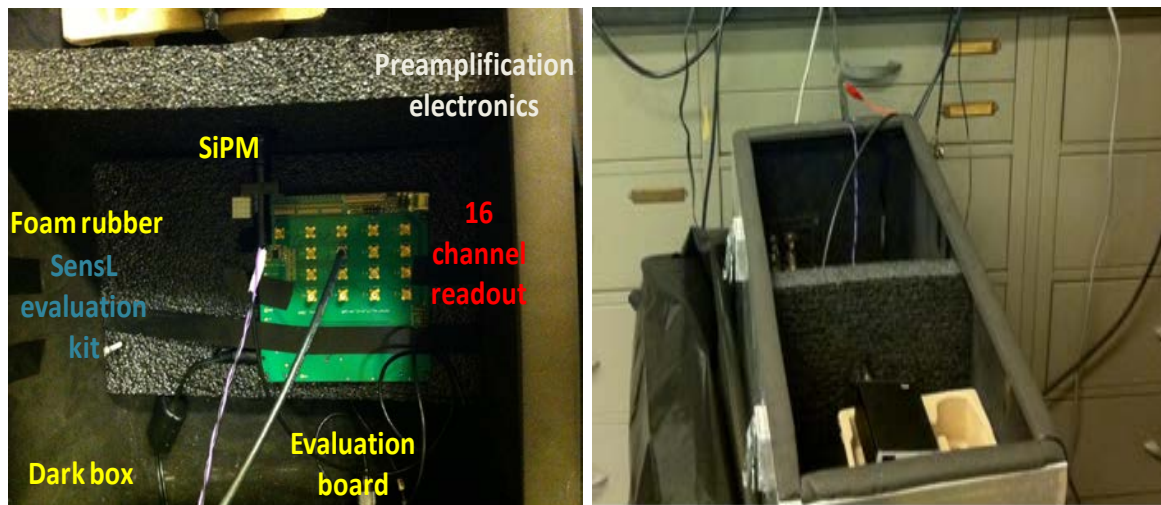


Figure 3.12: (left): SensL evaluation kit fixed to foam rubber into the dark box. (right): Dark box containing the experimental setup.

In order to evaluate the performance of the SensL SiPM, all of the 16 channels (pixels) were tested. However, during the tests carried out for the evaluation of the charged particle prototype array, only one pixel was fully characterized. The channel (pixel) that showed better signal response was the one labeled “cell K” in Fig. 3.8b, so all the tests were done over this pixel.

Once we had the SensL SiPM coupled to the Cs(I)TI, three different electronics setups were used to test the performance of the prototype over a single pixel: an analog electronics setup, a digital electronics setup, and finally, although only for educational purposes, the GRETINA digitizer was explored.

3.3.7 ELECTRONICS: ANALOG FILTERING SETUP

The electronics setup used to acquire pulse height spectra is schematically shown in Fig. 3.13. The output of the scintillation detector was amplified with the SensL transimpedance pre-amplifier, which was then amplified again and shaped with the Ortec 572 spectroscopic amplifier, using the shaping time of 3 μ s. This pulse is then fed to the AMPTEK multichannel analyzer which is connected to the control PC.

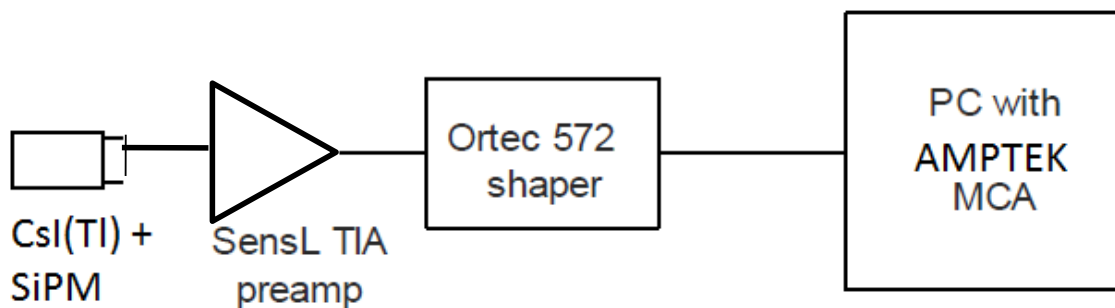


Figure 3.13: Schematic of the analog filtering electronics setup.

A. Pre-amplification Stage:

The pre-amplification of the signals coming from the SiPM was carried out by means of the SPMArray4-A0 board which uses fast charge sensitive (integrating) differential output pre-amplifiers. The pre-amplifiers are implemented using Analog Devices' AD8132 chips. The use of differential output amplifiers allows reducing channel-to-channel crosstalk and sensitivity to ground potential variations across the system compared with a single ended amplification system.

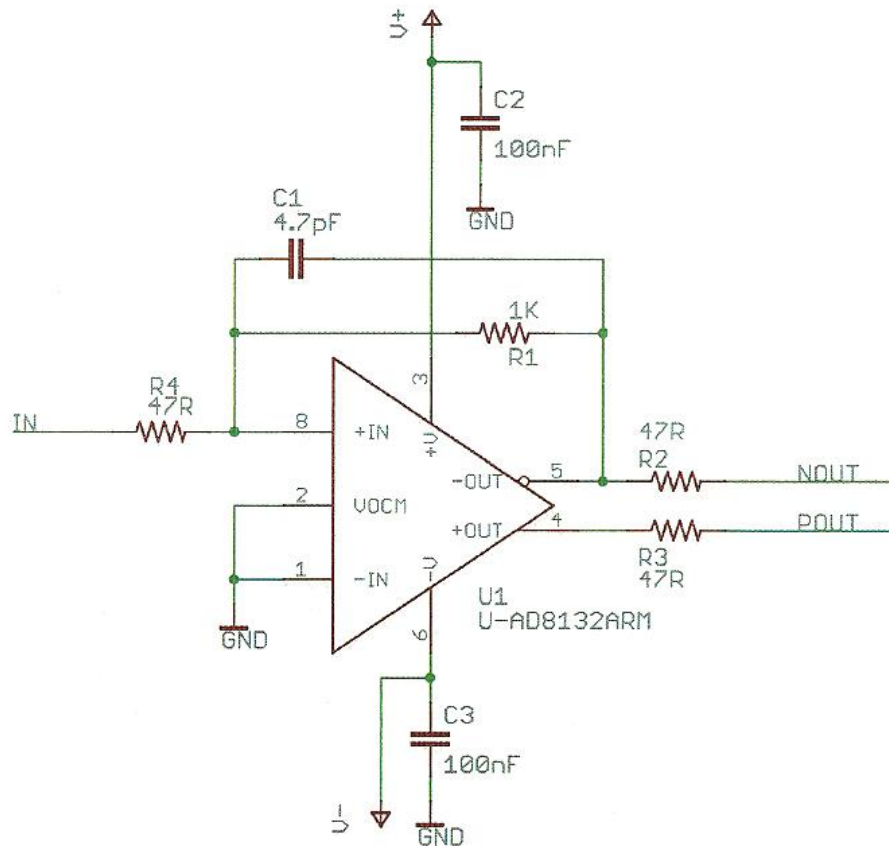


Figure 3.14: Single channel pre-amplification schematic. (The values of the components were taken from the SPMArray4 datasheet only available when purchasing the array).

The pre-amplification of each channel is configured in *transimpedance* mode as shown in Fig. 3.14. The gain is defined by $R1$, while $C1$ and $R4$ provide stability of the transient response. Resistors $R2$ and $R3$ provide matching of the low output impedance of the pre-amplifier to the transmission line impedance, thus providing reflection-free operation. Finally, $R1$ and $C1$ (feedback elements) provide the time constant of the pre-amplifier:

$$\tau_{pre} = RIC1 = 4.7ns$$

Since scintillation pulse light of the CsI(Tl) has a duration of a few μs , the $\tau_{pre} \ll pulse\ duration$. So the output will follow the input shape, that is the shape of the scintillation pulse, as discussed in §1.4.2.2.

The pulses provided by the pre-amplifier are of negative polarity.

As shown in Fig 3.9, the pre-amplification board is mounted onto the evaluation board SPMAArray4-A1, which provides SMA connectors for each one of the pixels output, so that, an SMA-to-BNC coaxial cable was used to feed the pre-amplified signal to the next stage: shaping.

B. Shaping (filtering) stage

In order to shape the pulses coming from the pre-amplifier, an ORTEC 572 spectroscopic amplifier was used. It is an amplifier implemented into a NIM module with an automatic base line restorer and an incorporated pile-up rejection circuit.

The ORTEC 572 has bipolar inputs and outputs, so that it is possible to feed the negative pre-amplified signal and to generate a positive output needed for the next stage.

Table 3.4 summarizes the main characteristics of the ORTEC 572. Further information can be found in [90].

Several tests were performed varying the amplifier's gain and the shaping times, the following values were found to achieve the best performance and signal-to-noise ratio:


Gain: 50

Shaping time: $3\mu\text{s}$

According to Tab. 3.4, using a $\tau = 3\mu\text{s}$ shaping time, then the semi-Gaussian pulse shaping will provide $2.2\tau = 6.6\mu\text{s}$ peaking time pulses.

Finally, the shaped pulse was connected through a BNC-to-LEMO coaxial cable (see Appendix C) onto the AmpTEK pocket multichannel analyzer MCA8000A, which creates a histogram of pulse heights over a particular voltage scale, so that it is a device used to obtain the pulse height spectrum of the radioisotopes sources tested.

Table 3.4: Main characteristics of the ORTEC 572 spectroscopic amplifier.

	<ul style="list-style-type: none"> • Gain Range: Continuously adjustable from 1 to 1500. • Pulse Shape: Semi-Gaussian on all ranges with peaking time equal to 2.2τ and pulse width at 0.1% level equal to 2.9 times the peaking time. • Integral Nonlinearity: For 2 μs shaping time, $<\pm 0.05\%$. • Shaping time: Active pulse-shaping filter network with 0.5, 1, 2, 3, 6, and 10 μs shaping times. <p>INPUTS</p> <ul style="list-style-type: none"> • BNC front- and rear-panel connectors accept either positive or negative pulses with rise times of 10 to 650 ns and decay times of 40 μs to infinity, $Z_{in} \approx 1000 \Omega$ dc-coupled; absolute maximum 20 V. <p>OUTPUTS</p> <ul style="list-style-type: none"> • UNI: Front-panel BNC connector with $Z_o < 1 \Omega$ and rear-panel connector with $Z_o = 93 \Omega$, short-circuit proof; prompt or delayed with full-scale linear range of 0 to +10 V; active filter shaped; dc-restored; dc-level adjustable to ± 100 mV. • BI: Front-panel BNC connector with $Z_o < 1 \Omega$ and rear-panel connector with $Z_o = 93 \Omega$, short circuit proof; prompt output with positive lobe leading and linear range of ± 10 V; active filter shaped.
--	---

C. Pulse discrimination and Pulse height acquisition

MCA8000A Hardware

The MCA8000A incorporates a number of modules. These modules include: (1) Input range selector and linear gate unit; (2) Peak-hold circuitry; (3) Sampling successive approximation ADC; (4) MCA control unit; (5) Microcontroller; (6) RS-232 interface; (7) Power supply; (8) Low level discriminator (LLD); and (9) Nonvolatile memory. A host

computer is used to configure and operate the MCA as well as to manage the obtained spectral data. MCA8000A block diagram:

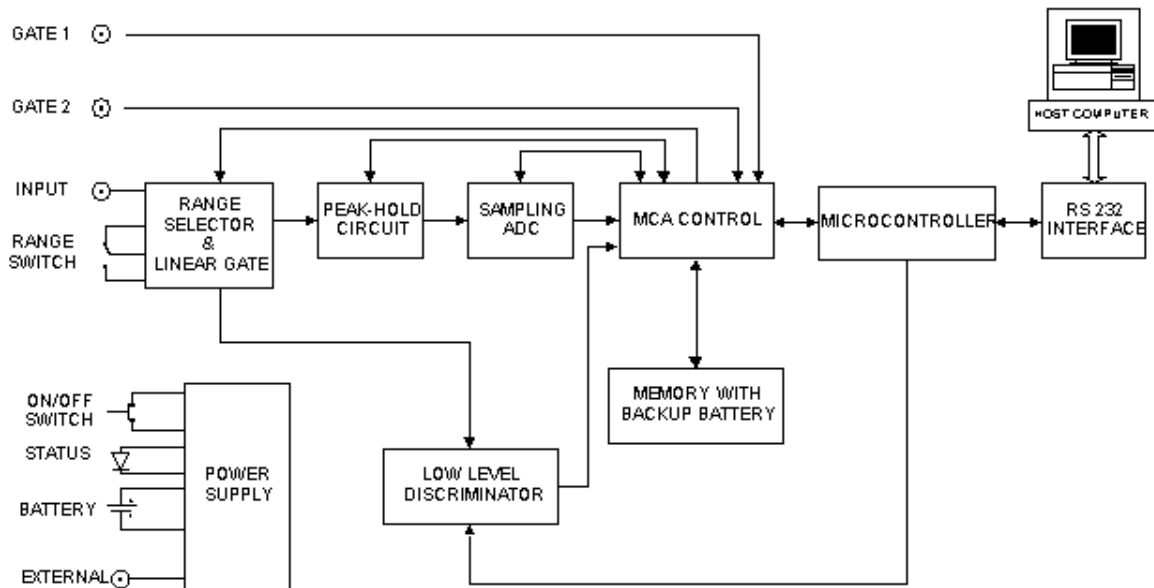


Figure 3.15: MCA800A block diagram, taken from [91].

Input:

The MCA8000 accepts positive, shaped unipolar or bipolar input pulses with peaking times as short as 250 ns. The amplitude range of the input can be either 0 to +5V or 0 to +10V. The input impedance is 200 k Ω for the 0 to +5V range and approximately 2 k Ω for the 0 to +10V range. For our tests, we have used the 0 to +5V input range.

Peak-hold Circuit:

The peak-hold circuit accepts positive pulses with peaking times as short as 250 ns (100 ns shaping times). The peak-hold circuit is based upon the Amptek PH300 hybrid circuit. A peak detect signal is generated when the input pulse peak amplitude is reached. This peak amplitude is then held at the output of the circuit. After approximately 2 μ s following peak detection, the sample-and-hold circuit of the ADC samples the output voltage of the peak-hold circuit. Immediately following this sampling, the peak-hold circuit resets and is ready to accept another pulse for processing.

Analog to Digital Converter (ADC):

The successive approximation 16-bit ADC (with ENOB = 14 bits) can achieve a conversion gain resolution of $2^{14} = 16,384$ channels, thus, over the 0 to 5 V input range selected, a voltage resolution of 0.3 mV is achievable. However, we used a 1024 channel conversion gain, thus obtaining a voltage resolution of 4.88 mV. The ADC digitizes the pulse amplitude in less than 5 μ s. If a second pulse arrives while another pulse is being processed, it is held by the peak-hold circuit. The second pulse is processed after the ADC has completed digitizing the first pulse. Because of this two-stage storage, the dead time following a single pulse can be as short as 2 μ s. The use of the sliding scale technique maintains differential non-linearity to better than $\pm 0.6\%$ from 15mV to full scale and integral non-linearity $< \pm 0.02\%$ over full scale.

The MCA8000A connects to a host computer via an RS-232 interface I/O.

An example of a pulse height histogram obtained by the MCA8000A for a ^{137}Cs source is plotted in Fig. 3.16. In Chapter 4 some other of the pulse height distributions recorded by the MCA in this setup are presented and analyzed.

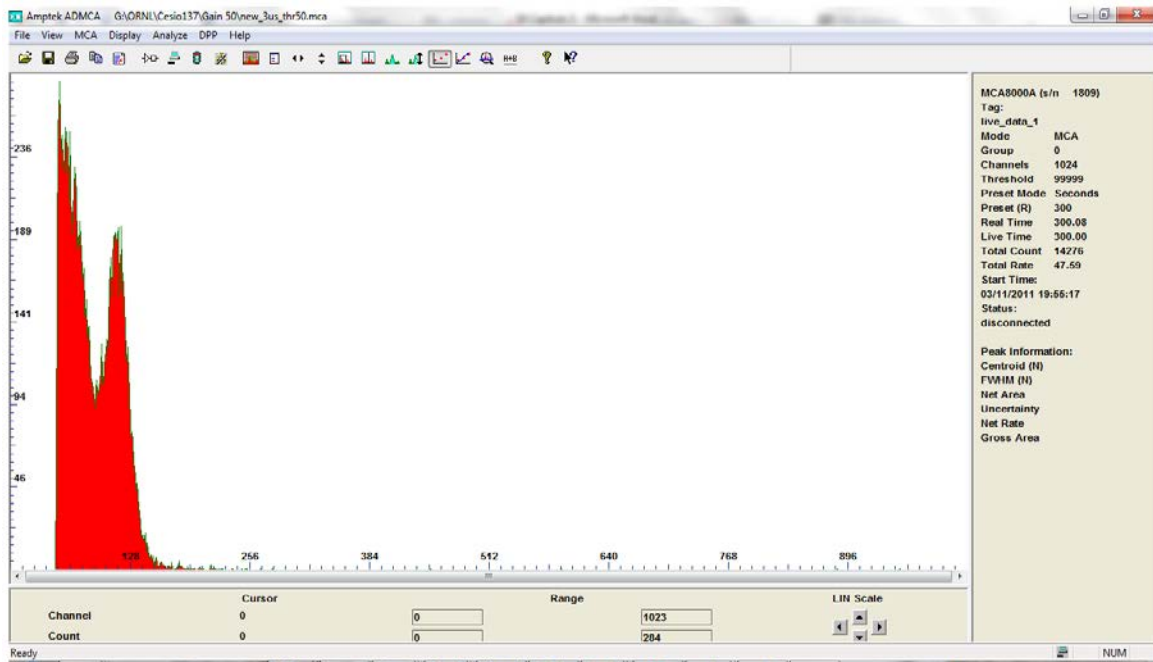


Figure 3.16: Plot of a Cs-137 pulse height distribution taken with the MCA8000A.

3.3.8 ELECTRONICS: DIGITAL FILTERING SETUP

The digital filtering setup schematically shown in Fig. 3.17 consists of the same pre-amplifier stage used in the analog electronics setup, the AD8132 differential amplifier. But instead of using an analog shaping amplifier, the pre-amplified signal was connected to an Agilent Technologies® digital oscilloscope (DSO7104A) which was in charge of digitizing the pulses. Once digitized, the data were loaded into a computer for digital filtering and further analyses. The data acquisition was made by means of both Agilent and MATLAB® software. Finally the data were processed and analyzed through the development of MATLAB® scripts.

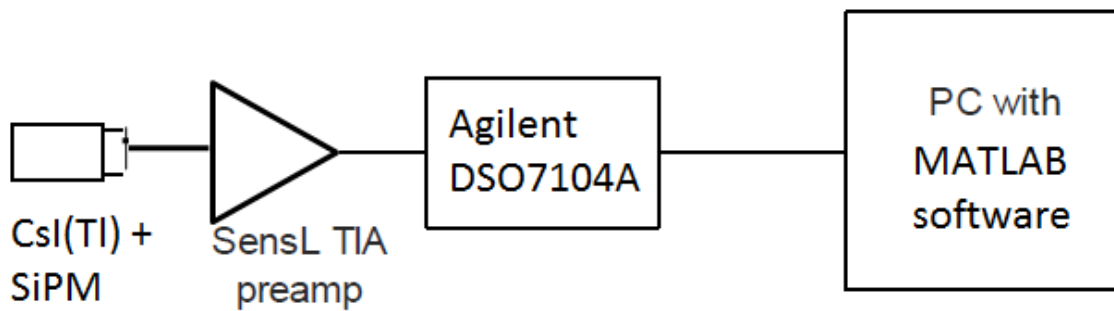


Figure 3.17: Schematic of the digital filtering electronics setup.

A. Agilent DSO7104A oscilloscope for data discrimination and acquisition

DSO7104 is a very sophisticated digital oscilloscope which provides up to 1 GHz bandwidth and 4 GSa/s sample rate. Although it is a very versatile instrument, capable of performing a great number of operations and varying several operational parameters, only the main features and the parameters used in this Thesis will be explained.

Analog Input Impedance (50 Ohm or 1 MOhm)

The input impedance of analog channels can be set to either 50 Ω or 1 M Ω . The 50 Ω mode matches 50 Ω cables and many active probes commonly used in making high frequency measurements. This impedance matching provides the most accurate measurements because reflections are minimized along the signal path.

The 1 M Ω impedance is commonly required for use with most passive probes.

We have selected the 50 ohm impedance since we were using 50 ohm BNC coaxial cables (see Appendix C).

Pulse discrimination

In contrast to the analog electronics, in this setup using the digital oscilloscope, the discrimination of the pulses is carried out at the beginning of the pulse processing chain. Since the pulses detected by the oscilloscope will be downloaded into the computer for further analyses, it is necessary to eliminate as much noise and spurious pulses as possible which might only produce useless acquired data, thus wasting memory space in the processing computer. This pulse discrimination is accomplished by establishing a trigger level that will act as a specific voltage threshold that pulses have to meet in order to be acquired.

Because of the shape and polarity (negative) of the pre-amplified pulses, the trigger used in this case is called “edge trigger”.

Edge Trigger

The Edge trigger type identifies a trigger by looking for a specified edge (slope) and voltage level on a waveform. The slope can be set to rising edge or falling edge.

Sampling Frequency

As already mentioned, the DSO7104 achieves a maximum sampling frequency $f_{Smax} = 4 \times 10^9$ Samples/s, corresponding to a sample period of 250 ps. However, if the sample period is longer, then this maximum sampling frequency will drop. Figure 3.18 shows an example of the pulse resulting from an alpha particle radioactive source compared to the dark noise signal, as we can see, in this example, an acquisition time of 20 μ s (2 μ s/div time scale) was enough to properly record the shape of the alpha pulse. On the other hand, the DSO7104A is capable to save up to 1000 samples per event while an acquisition is running. So that, the sampling frequency performed by the oscilloscope in this example was:

$$f_s = \frac{1000 \text{ Samples}}{20 \mu\text{s}} = 50 \times 10^6 \frac{\text{Samples}}{\text{s}} = 50 \frac{\text{MSa}}{\text{s}}$$

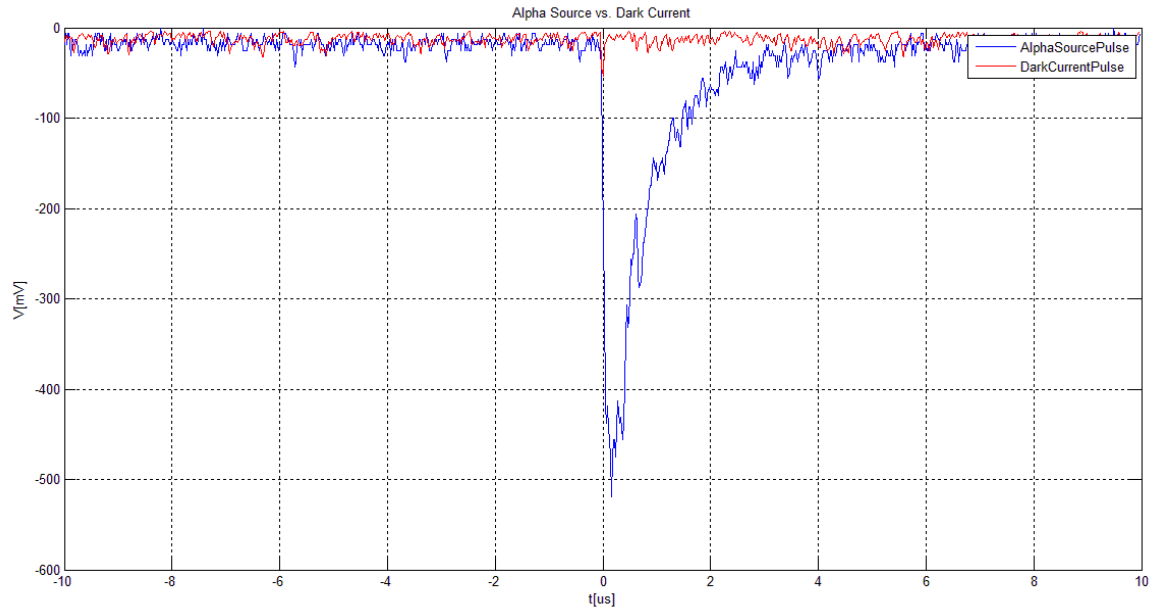


Figure 3.18: Alpha source pulse and dark current pulse taken at a sampling frequency of 50 MSa/s.

Acquisition Mode

The acquisition was carried out in the “Normal” mode, which is the simplest acquisition mode for this scope. The idea was to obtain the pulses’ shape and noise as close as possible to their original characteristics because otherwise important information about the shape of the pulses coming from different radiation sources could be lost. Instead we have developed several algorithms using MATLAB® in order to filtering, restoring baseline shifts and analyzing pulse shapes.

Using *normal* acquisition mode, the analog-to-digital conversion of the oscilloscope is carried out by an 8-bit resolution ADC conversion, so for example, using a 100 mV/div vertical scale, the total input voltage range is 1 V, achieving thus a resolution of $1/256 = 3.9$ mV.

From the example presented in Fig. 3.18 some conclusions were drawn in order to set the operational parameters of the oscilloscope during the data acquisition:

- 1) The dark current pulses are quite above -100 mV voltage level.
- 2) A typical alpha source pulse is above -1 V voltage level.

- 3) The sampling frequency needs to be higher than 50 MSa/s in order to properly reconstruct the rise time of the pulses. According to the Nyquist theorem, the sampling frequency should be at least twice the maximum frequency component of the signal to be sampled. In our case, the maximum frequency component is the rise time of the pulses, which corresponds to 20 ns for CsI(Tl) scintillation photons. Then the sampling frequency should be at least 100 MSa/s. For the Agilent oscilloscope, the sampling frequency corresponds to an acquisition time of 10 μ s, or 1 μ s/div in the horizontal scale.

For most of the radioisotope sources, the following scope parameters work fine:

Threshold level (elimination of dark noise): -70 mV

Voltage scale: 100 mV/div

Time scale: 1 μ s/div

Depending on the intensity of the source tested, the threshold level and the voltage scale might vary to -100 mV and 200 mV/div, respectively.

Once the parameters were set, the oscilloscope was then connected to a PC through an Ethernet LAN connection. The DSO7104A is detected by the computer by means of the Agilent IOsuite software and the acquisition of the pulses is done by the MATLAB® software. This setup then has the following software requirements:

- Agilent IO Libraries to be installed. To get the latest release of the IO Libraries Suite, go to www.agilent.com/find/iosuite
- MATLAB®. The latest release possible with the *Instrument Control* toolbox installed. Go to <http://www.mathworks.com>

Support documentation for using Agilent Instruments with MATLAB® software can be found at:

<http://www.mathworks.com/products/instrument/hardware/agilent.html>

<http://www.home.agilent.com/agilent/editorial.jsp?cc=AW&lc=eng&ckey=1668945&nid=-35802.383408.02&id=1668945>

Once the pulses have been digitized and downloaded to the computer, then several algorithms were performed to process the pulses. Baseline restoration, filtering, pulse height analyzing, and pulse shape discrimination were carried out by means of MATLAB® algorithms.

B. Baseline restoration using MATLAB®

The baseline restoration simply consisted of the subtraction of the noise DC value computed for the first 400 samples of each 1000-sample length pulse. The computation of such DC value was the mean average:

$$DC = \frac{1}{400} \sum_{n=1}^{400} sample(n) \quad (3.5)$$

$$Pulse\ Restored = Original\ Pulse - DC \quad (3.6)$$

Figure 3.19b plots an example of a pulse with baseline restoration using this algorithm.

C. Filtering using MATLAB®

Following the baseline restoration, the pulses were filtered by means of a *moving average filter*.

Moving Average Filter (MA filter)

The moving average filter is a simple low-pass FIR filter commonly used for smoothing an array of sampled data/signal. It takes M samples of input at a time and computes the average of those M-samples producing a single output point. It is a very simple structure used to filter unwanted noisy component from the intended data.

As the filter length increases (more M samples taken) the smoothness of the output increases, whereas the sharp transitions in the data are made increasingly blunt. This implies that this filter has excellent time domain response but a poor frequency response, and we have to be careful because important information regarding to the type of radiation detected might be lost.

The algorithm for the MA FIR filter that we have performed is:

$$y(n) = \frac{1}{M} \sum_{i=n-k}^{n+k} x(i);$$

$$k = \frac{M-1}{2} \quad (3.7)$$

where:

$y(n)$ is the new sample already filtered; $k+1 \leq n \leq \text{pulse length} - k$,

M is the filter length (number of samples to be averaged). For this algorithm M has to be an odd number, and

$x(i)$ is the current sample entering to the filter.

Figure 3.19c plots an example of a filtered pulse using this MA filter over $M = 15$ averaging samples.

D. Pulse height analyzing using MATLAB®

Once the pulses were restored to baseline and filtered, we proceeded to generate the pulse height spectra over each type of radiation detected by the prototype. This was accomplished by simply measuring the peak voltage of each pulse corresponding to each type of radiation and computing the histogram of all of them.

The number of bins used for each histogram corresponds to 256, since the oscilloscope ADC is 8-bit resolution. Figure 3.19d plots an example of one of such histograms.

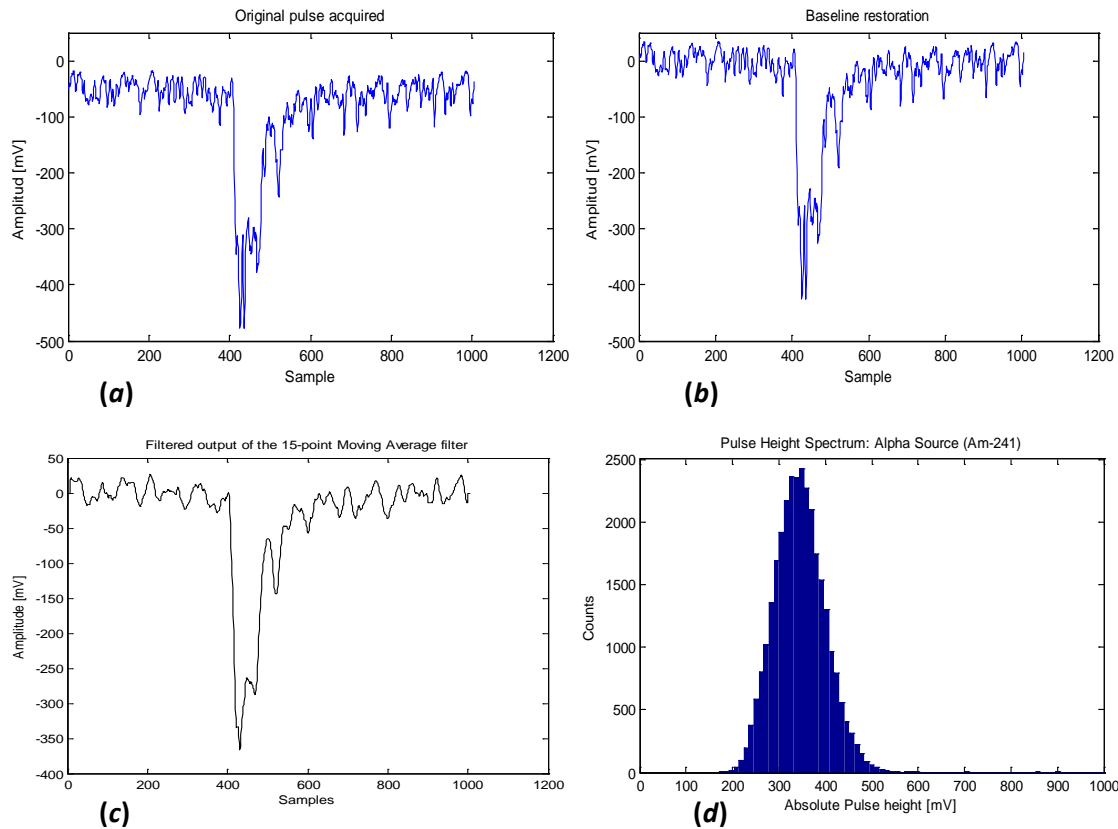


Figure 3.19: Digital Pulse Processing Stages. (a) Original pulse. (b) Baseline restoration. (c) Moving Average Filtering. (d) Pulse height spectrum. These examples correspond to an Am-241 alpha source.

E. Pulse shape discrimination using MATLAB®

The pulse shape discrimination (PSD) techniques exploit the dependence of the output signal from a radiation detector on the particle characteristic (energy, charge and mass). Examples of these techniques are the correlation of the signal rise time (often obtained with zero-crossing after proper shaping) with its amplitude, or the correlation of partial integrals of the signal at different times.

This second technique has often been applied to CsI(Tl) scintillators where a dependence of the fluorescence decay times and amplitudes is observed as a function of the ionization density: CsI(Tl) scintillation pulses decay is a combination of exponentials of different time constants:

$$L(t) = L_s \exp\left(-\frac{t}{\tau_s}\right) + L_f \exp\left(-\frac{t}{\tau_f}\right) \quad (3.8)$$

where $L(t)$ is the light pulse amplitude at time t . L_s and L_f are the total light amplitudes. τ_s and τ_f are the constant time decays for the slow and the fast components respectively ($\tau_s \sim 3.34 \mu s$, $\tau_f \sim 3.34 \mu s$).

Discrimination among particles is then possible because (1) the amplitude ratio of fast and slow components L_f/L_s varies with the particles type; (2) there is a change in decay constant with the density of ionization of the particle, mainly for the short decay constant. A characteristic sampling of the light output at a time t is supplied by measuring the light output $L(t, T)$ obtained by integrating the charge output between times t and $t + T$.

Choosing different values for t and T , related to the slow and fast components, different values of L will be obtained, and it is possible to find different L_f/L_s ratios which will allow the pulse shape discrimination. For example, in [92] the following values are proposed:

$t_1 = 0$ and $T_1 = 400$ ns (fast component)

$t_2 = 1.6 \mu s$ and $T_2 = 1 \mu s$ (slow component)

In analog electronics pulse processing, this technique is implemented by means of properly gated charge to digital converters (QDC) as described in §1.4.8. In the present work, off-line analyses have been developed for PSD based on signal integration at different times once we have digitized and filtered the output pulses from the radiation detector.

The calculation of the charges L_1 and L_2 carried by each pulse was performed by numerically integrating the areas under the processed pulses, strictly, each pulse should be scaled by the output impedance of the amplifier, however, we have computed the area under the pulses in arbitrary units for all radioisotope sources tested.

The algorithm used to calculate the energy of each pulse is as follows:

$$A = \sum_{i=1}^{n-1} (x_{i+1} - x_i)(y_{i+1} + y_i)/2 \quad (3.9)$$

which is known as the trapezoidal rule.

Figure 3.20 plots the PSD achieved between ^{60}Co gamma ray source and ^{241}Am alpha particle source.

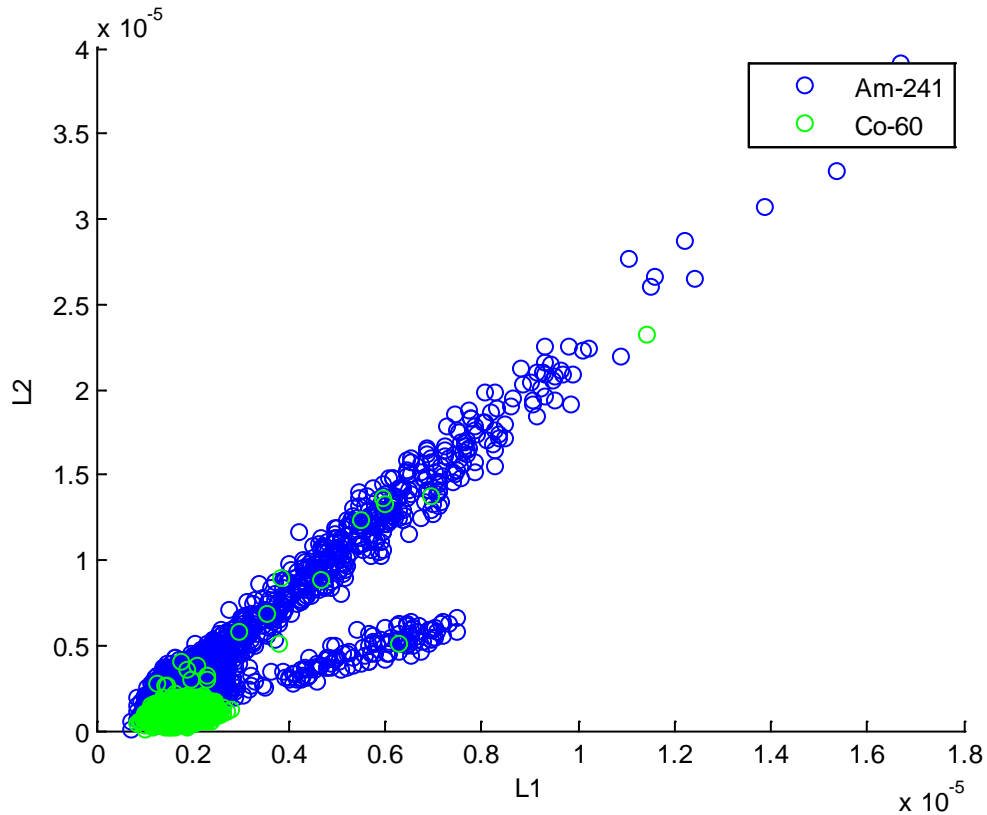


Figure 3.20: Identification of alpha particles and gamma rays with a CsI(Tl) crystal coupled to a SiPM. L_1 and L_2 are the light outputs obtained when integrating the signal within time intervals $T_1 = 400$ ns and $T_2 = 1$ μs at times $t_1 = 0$ and $t_2 = 1.6$ μs .

In fig. 3.21 a picture of the components for both analog and digital electronics are shown.

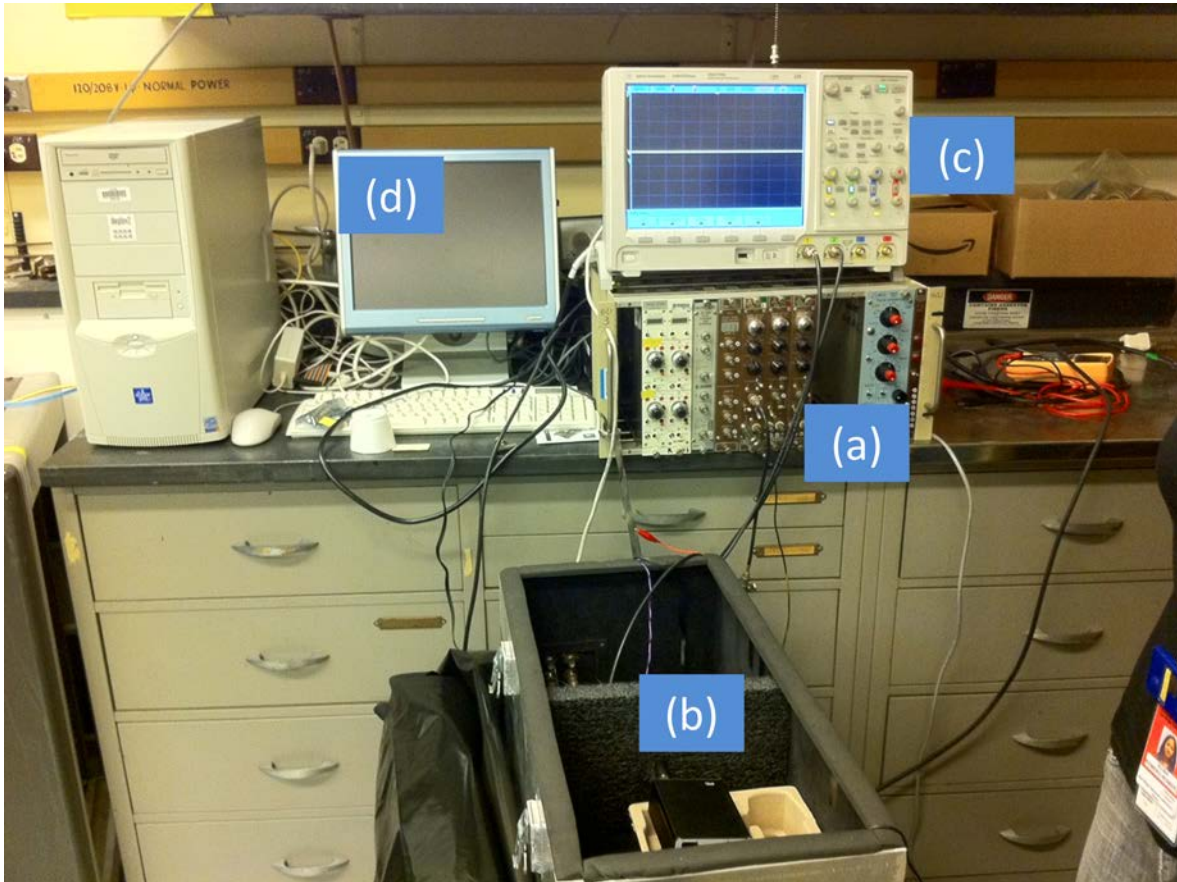


Figure 3.21: Analog and Digital electronics setups: (a) Ortec 572 spectroscopic amplifier; (b) AmpTEK MCA8000A; (c) Agilent DSO7104A oscilloscope and (d) Personal computer for data analyses.

Finally a third electronics setup was explored with educational purposes only, in order to know about the specific purpose digitizers implemented to meet the state-of-the-art, large-scale gamma ray spectrometers requirements. This is the GRETINA digitizer developed by the UCLA Berkeley.

3.3.9 ELECTRONICS: GRETINA DIGITIZER

The GRETINA Digitizer module is a combination of digitizer and digital signal processor based on a FPGA device. It accepts 10 inputs directly from the detector module preamplifiers and digitizes at a nominal frequency of 100 MHz with 14 bits ADC precision. The ADC counts interface to the FPGA, which digitally processes the data.

The GRETINA digitizer communicates to a host computer system through a VMEbus interface using the VME64x protocol. In Fig. 3.22 a picture of the GRETINA digitizer module is presented.

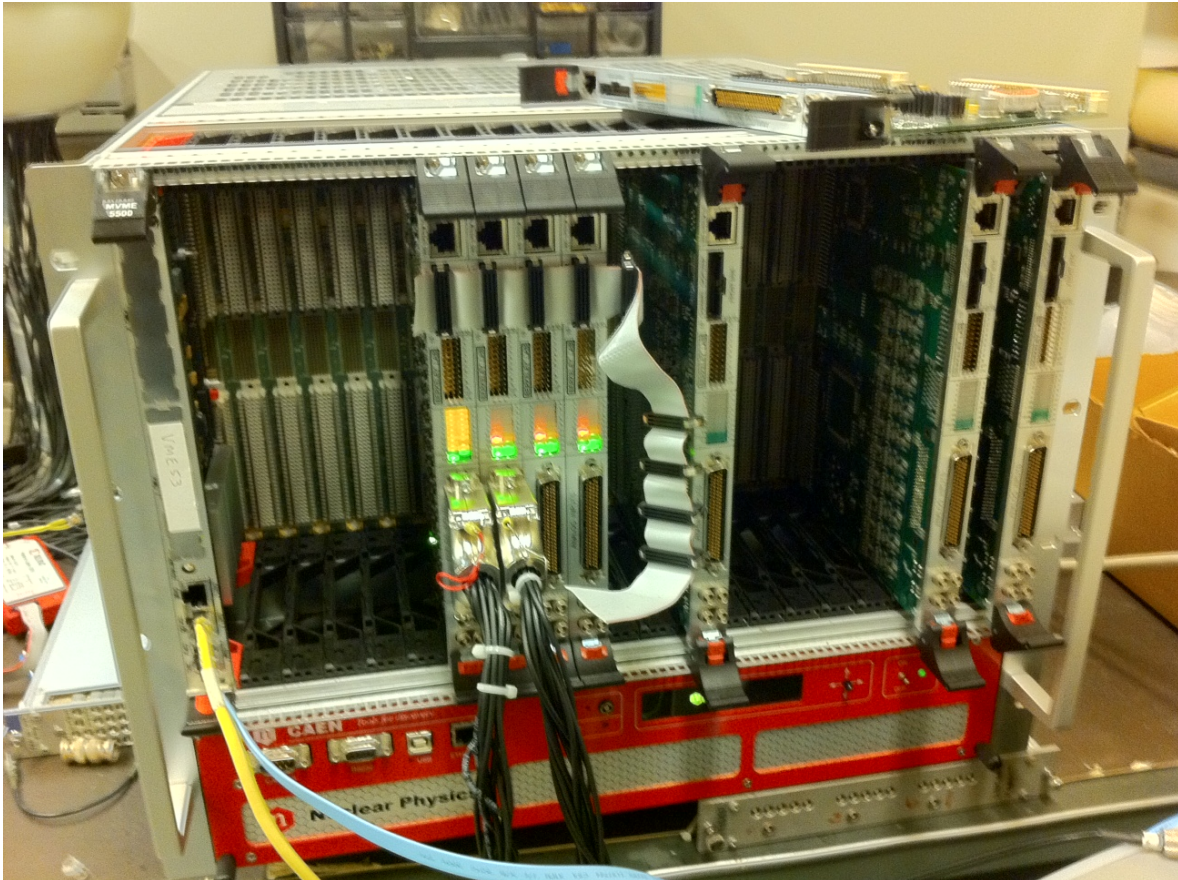


Figure 3.22: Gretina digitizer module into a VMEbus crate.

Few measurements were carried out using the GRETINA digitizer, only the ^{60}Co gamma rays radioactive sources were used in these measurements.

Once digitized and acquired through a Linux operating system host computer, the pulses were processed using MATLAB® in the same way discussed for the digital electronics setup previously presented in this chapter.

The pulse height distribution obtained with the GRETINA digitizer will be presented and discussed in Chapter 4.

CHAPTER 4: RESULTS AND DISCUSSION

Up to now, the theory of operation of radiation detectors used in Nuclear Physics has been reviewed, as well as the pulse processing techniques more commonly used for radiation spectroscopy purposes. Also in Chapter 3, the prototype array for charged particle identification that was developed in this Thesis, together with the instrumentation setups for characterizing it, were presented.

In this chapter, the results obtained in order to evaluate the light charged particle identification as a possible tool to operate in combination with gamma ray spectrometers are discussed.

4.1 SENSL SiPM FEATURES

- The device is sensitive to visible light of 400 nm to 850 nm with a maximum detection peak at 520 nm, which, by the time of the development of our prototype, provided the best CsI(Tl) coupling (540 nm peak emission).
- The SensL SiPM is insensitive to magnetic fields up to 2 T, unlike PMTs, which are very sensitive to even weak magnetic fields (<0.1T). This is because the carriers have a very short path length due to the narrow depletion width of the microcells. This makes SiPM detectors particularly suitable for high-energy physics applications, nuclear medicine, and nuclear physics applications such as the proposed combined CsI(Tl)-SiPM charged particle detection system.
- Number of micro-cells per pixel: 3640. This number will determine the dynamic range of the prototype proposed, as will be presented later on.
- Number of pixels: 16 (4x4 array); this array makes the SiPM suitable for providing position sensitivity to the charged particle detector. Initial research on position sensitivity algorithms using a FPGA has been carried out in this work; however, further development is needed to achieve the implementation required.
- Typical breakdown voltage: $V_{br} = 27.5$ V
- Operating voltage for all the tests: 28.6 V (+1 V above V_{br}). Noise behavior, gain, and photodetection efficiency in SiPM detectors are very sensitive to bias voltage changes, so that it is mandatory to use good regulated power supplies.
- Capacitance: 55 pF per micro-cell.

- Uniformity ratio: 1.18. This ratio is a measure of how similar the pulses coming from different pixels within the SiPM are among each other. The ratio of the max pixel value to the min pixel value is quoted using a constant (DC) light source spot illuminating each pixel.
- Dark rate: 8 MHz per pixel. Since each pixel consists of 3640 micro-pixels, then it can be said that the average dark rate per micro-pixel is about 2kHz. Although this seems to be a high dark rate, for scintillation detectors it can be easily decreased by orders of magnitude by setting good enough thresholds since the scintillation light output is very high compared to the dark noise level.
- Photon detection efficiency: 10 % (@ +1 V above V_{br} , $\lambda = 520$ nm).
- Gain: $>10^6$. Gain comparable to a PMT with the advantages of compactness, insensitivity to magnetic fields, and low bias voltage. All of them important advantages for our application.
- Energy resolution: 14% at 511 keV peak. The energy resolution is a function of the kinetic energy of the incident photons. As we shall see, for higher energy photons, energy resolution improves because more electron-hole pairs in the SiPM are collected, achieving better SN ratios and hence, better energy resolution.

4.2 PERFORMANCE OF THE PROTOTYPE FOR CHARGED PARTICLE DETECTION

4.2.1 CALIBRATION ON DARK NOISE

As described in §3.3.2, in addition to optical generation, in SiPM detectors carriers can also be generated in or near the avalanche region by thermal transitions from the valance band or inter-band gap states. These carriers can also cause Geiger discharge of the diode and are indistinguishable from photo-generated events. The frequency of thermally initiated pulses is referred to as dark rate, and can be determined by counting the number of pulses occurring per second when the SiPM is under dark conditions. As mentioned in the previous section, the dark rate of our SensL SiPM is 8 MHz per pixel corresponding to about 2kHz per micro-pixel (1 micro-pixel = 1 Geiger-mode diode).

Unlike PMTs and linear mode APDs, the gain of a Geiger-mode diode is not defined by the statistical nature of the multiplication process but is set by the diode capacitance and the overbias, V_{over} , which is defined as:

$$V_{over} = V - V_{br} \quad (4.1)$$

where V is the bias applied to the device. This results in a well-defined stable gain and near identical current pulses. The gain then is given by:

$$G_{micro-pixel} = C_{micro-pixel} * \frac{V_{over}}{|q_e|} \quad (4.2)$$

where $C_{micro-pixel}$ is the capacitance of a Geiger-mode diode and q_e is the electronic charge.

In our case:

$$V_{over} = 1.1 \text{ V},$$

$C_{micro-pixel} = 55 \text{ pF}$ (given by the manufacturer); therefore:

$$G_{micro-pixel} = 377.6 \times 10^6$$

The Geiger-mode pulses corresponding to one pixel of the SiPM were observed under dark conditions and digitized on the Agilent oscilloscope. The histogram of the voltage output in response to repeated pulses of dark current incident on the SiPM pixel results in a photoelectron spectrum with well-resolved peaks shown in Fig. 4.1.

The ADC oscilloscope has 8-bit resolution, so that, the histogram is divided into 256 bins, from which only 59 bins are non-zero values and correspond to the peak voltages recorded due to consecutive photoelectrons emitted, which, under dark conditions, are in a 1:1 ratio with the number of micro-pixels fired in the SiPM (M_{fired}). Then up to 59 micro-pixels were fired, from the total 3640 available micro-pixels, it is the 1.6%. Figure 4.2 plots the voltage read on the oscilloscope as a function of the micro-pixels fired in the SiPM. The linear fit gives the following function:

$$Voltage_{osc} = 0.63 (M_{fired}) + 22 \text{ [mV]} \quad (4.3)$$

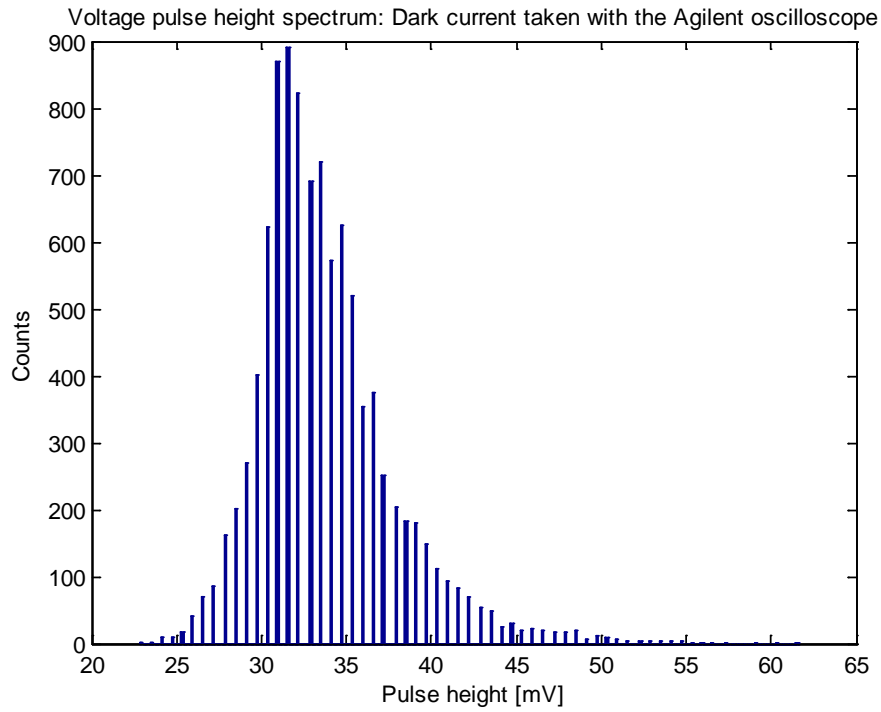


Figure 4.1: Photoelectron spectrum obtained over the peak voltage of dark current pulses.

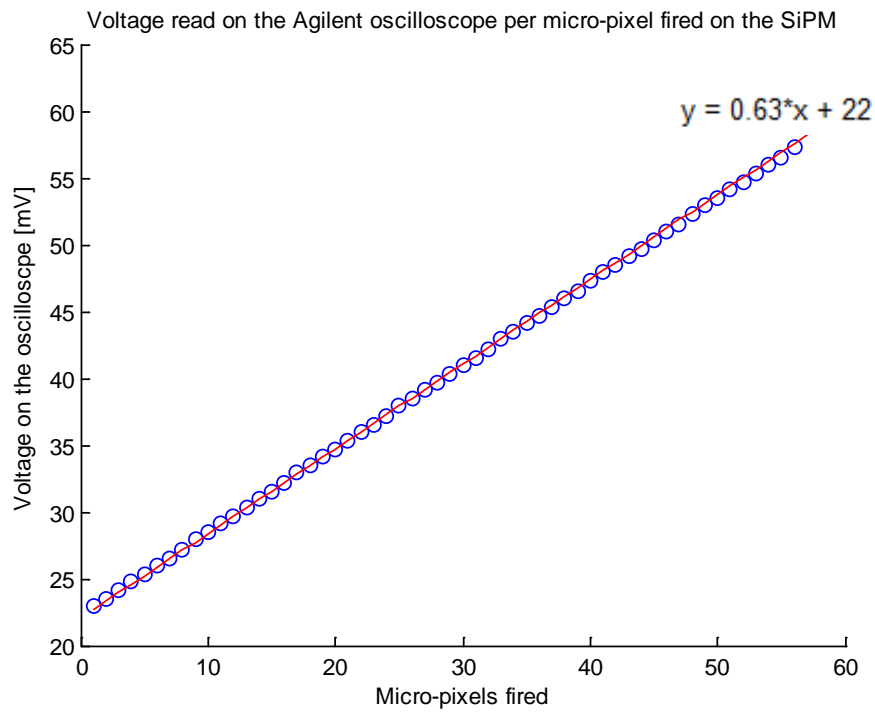


Figure 4.2: Voltage on the oscilloscope as a function of the SiPM micro-pixels fired.

The spectrum plotted in Fig. 4.1 and its voltage calibration (Fig. 4.2), are indicative of the system noise and of the uniform, stable gain of the Geiger-mode APDs. The first peak in the spectrum, often called the pedestal, is a measure of the noise in the system (detector + electronics) and corresponds to instances when no pulses were recorded. This value is 22 mV peak voltage pulse observed on the oscilloscope. The second peak of the spectrum or the first photoelectron peak corresponds to a single pixel fired.

The maximum peak voltage read on the oscilloscope due to dark current pulses in one SiPM pixel is 60mV.

Now, if we divide the peak voltages recorded by 50 ohms (oscilloscope input impedance), then we obtain the current distribution plotted in Fig. 4.3:

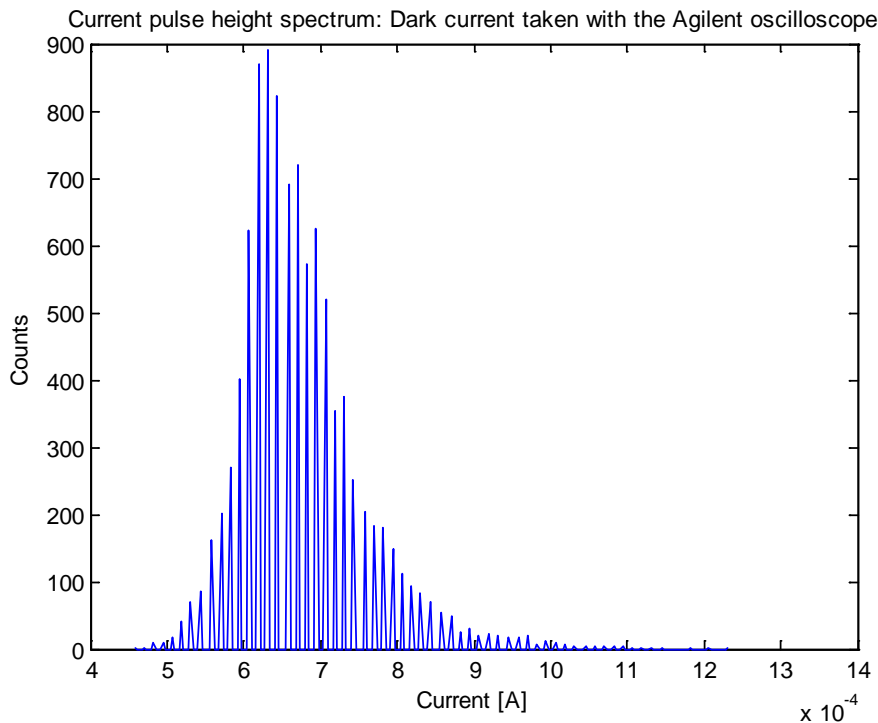


Figure 4.3: Photoelectron spectrum obtained over the peak current of dark current pulses.

This distribution is the same shape of the peak voltage spectrum, only scaled by a 1/50 factor and therefore, the current measured as a function of micro-pixels fired will show the same behavior as well (Fig. 4.4a). The current distribution “seen by the oscilloscope” corresponds to the current carried by the output pulses of the pre-amplification stage

between the SiPM and the oscilloscope. The theoretical current obtained at the output of one SiPM micro-pixel (or the input of the pre-amplifier) is given by:

$$I = N_{photons} * PDE * G_{micro-pixel} * q_e \quad (4.4)$$

where $N_{photons}$ is the number of incident photons per micro-pixel per second (i.e. the dark rate per micro-pixel):

$$I = \frac{8 \times 10^6}{3640} * 0.1 * 377.6 \times 10^6 * 1.602 \times 10^{-19} = 1.3297 \times 10^{-8} \left[\frac{A}{M_{fired}} \right]$$

Figure 4.4 plots both (a) the experimental current at the output of the pre-amplifier (the current seen by the oscilloscope), and (b) the theoretical current at the output of the SiPM as functions of the number of micro-pixels fired in the SiPM.

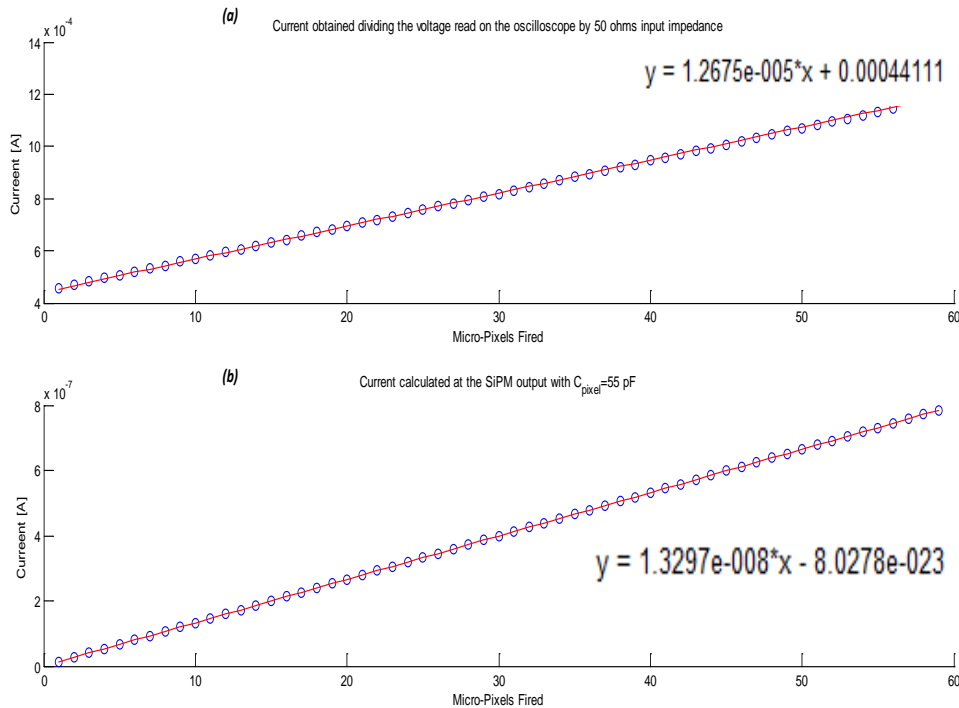


Figure 4.4: (a) Experimental current at the output of the pre-amplifier. (b) Theoretical current at the input of the pre-amplifier.

As shown, the slope of the linear fitting for the experimental current at the output of the pre-amplifier is 1.2675×10^{-5} [A/micro-pixel fired], meanwhile the slope of the linear fitting for the theoretical current at the input of the pre-amplifier (or the output of the SiPM) is 1.3297×10^{-8} [A/micro-pixel fired]. The ratio between both slopes should correspond to no more than the pre-amplifier gain (1000, given by $R1$ on the schematic presented in Fig. 3.14):

$$\frac{slope_a}{slope_b} = \frac{1.2575 \times 10^{-5}}{1.3297 \times 10^{-8}} = 953.22$$

This value represents an error of 4.6% between the theoretical and experimental currents that should be observed at the input-output of the pre-amplifier. And it could come from the tolerances of the capacitance and resistance values or from small changes in the power supply which may affect PDE and gain performance. However, theoretical and experimental results for the calibration on dark noise show very good matching and the well-defined resolvable peaks of the SiPM photoelectron spectrum show that the SiPM has excellent photon counting properties.

4.2.2 DYNAMIC RANGE

The total number of micro-pixels in a SiPM determines its dynamic range. The relationship between the number of micro-pixels fired, (M_{fired}), and the number of incident photons, ($n_{photons}$) can be approximated by [93]:

$$M_{fired} = M_{total} * \left(1 - \exp\left(-\frac{n_{photons} * PDE}{M_{total}}\right) \right) \quad (4.5)$$

where $M_{total} = 3640$ in one pixel of our SiPM.

For our case, the incident photons will be given by the CsI(Tl)-SiPM coupling, which from Tab 3.1 in Chapter 3, is 1.44 times the absolute light yield of a NaI(Tl) scintillator coupled to a bialkali PMT (38,000 ph/MeV). Also, the energies of the charged particles expected to be detected range from 1 to 50 MeV. Then, the maximum number of instantaneous incident photons by the detector will be:

$$Light_Yield_{\max} = 1.44 \left(\frac{38,000 ph}{1 MeV} \right) (50 MeV) = 2.736 \times 10^6 \text{ photons}$$

Figure 4.5 below shows the theoretical dynamic range for a 10% PDE value as a function of the number of instantaneous incident photons for one pixel of the SensL SiPM. The plot shows that the response of the pixel becomes non-linear when more than approximately 900, or a quarter of the total number of micro-pixels, are fired instantaneously. The number of incident photons corresponding to 900 micro-pixels fired is 106,704; which means that using one pixel of the SiPM, the response will become non-linear for energies greater than 2 MeV. This is a very poor value, since it represents only the 4% of the dynamic range required.

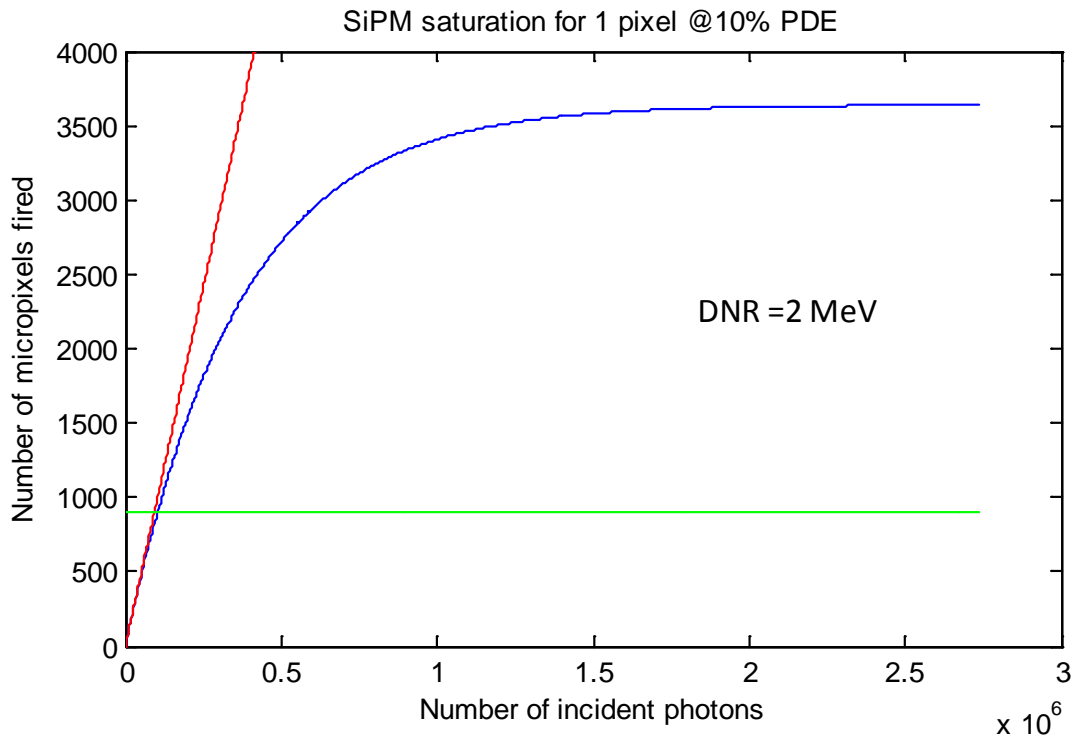


Figure 4.5: Dynamic range for 1 pixel of the SensL SiPM.

On the other hand, if we used the entire 16 pixels of the SiPM (58240) as a large-area detector, then there would be no saturation and the device will be able to detect quasilinearly the number of incident photons corresponding to 50 MeV, as shown in Fig. 4.6.

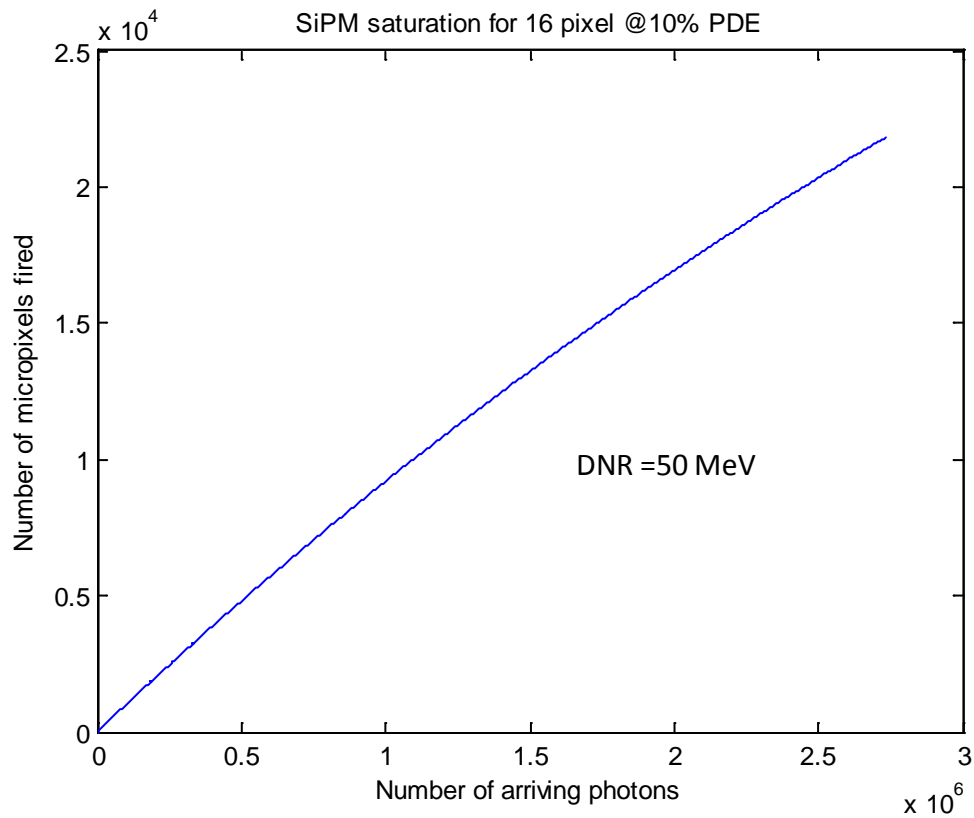


Figure 4.6: Dynamic range for the total 16 pixels of the SensL SiPM.

4.2.3 RESOLUTION AT DIFFERENT ENERGIES

The prototype detector was irradiated with four different alpha particle sources: Cf-252, Cm-244, Am-241, and a triple alpha source; and with two different gamma-ray sources: Cs-137 and Co-60 to enable acquisition of spectra at a number of different energies. The results of the spectra obtained with the Agilent Oscilloscope setup described in §3.3.8 are shown from figures 4.7 to 4.12, and their corresponding energy resolutions summarized in Tab. 4.1:

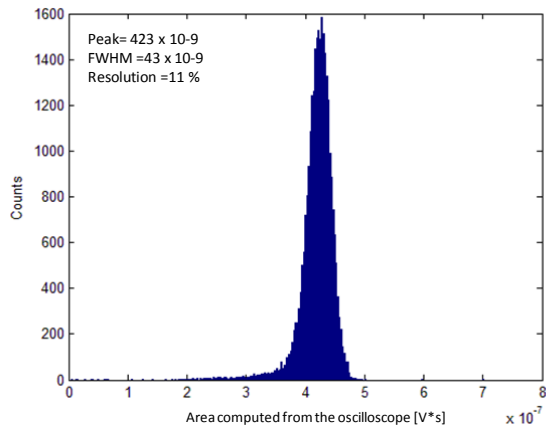


Figure 4.7: Energy spectrum for Cf-252.

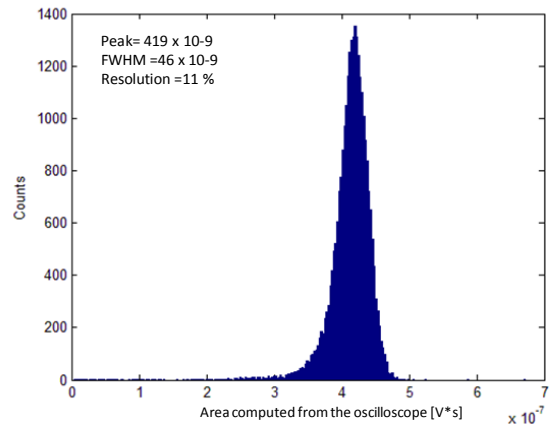


Figure 4.8: Energy spectrum for Cm-244.

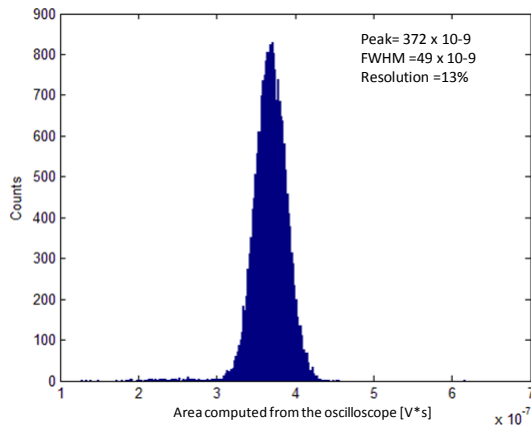


Figure 4.9: Energy spectrum for Am-241.

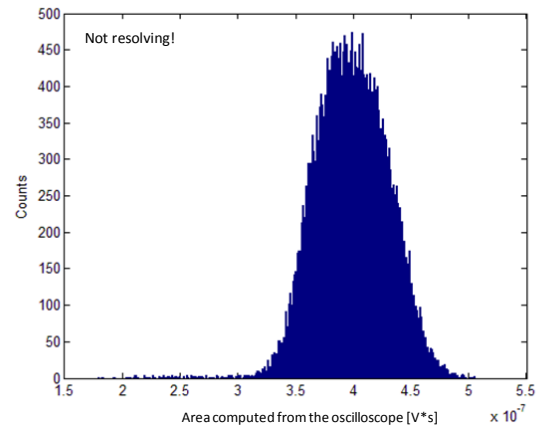


Figure 4.10: Energy spectrum for triple alpha source.

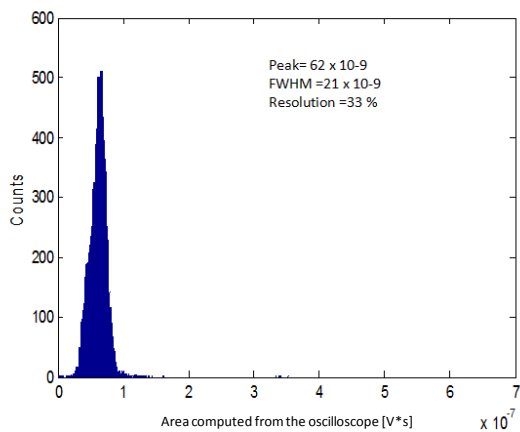


Figure 4.11: Energy spectrum for Cs-137.

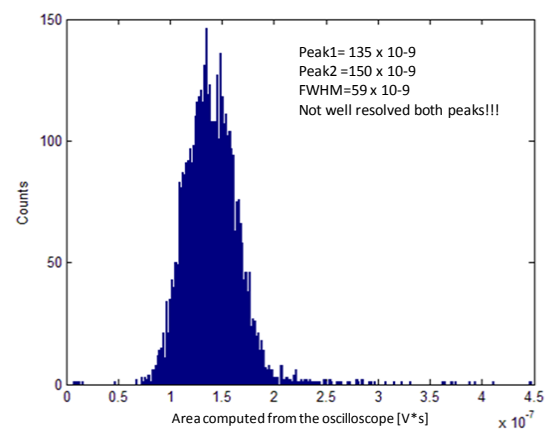


Figure 4.12: Energy spectrum for Co-60.

Table 4.1: Energy resolution for different radioisotope sources.

Radioisotope source	Energy [MeV]	Energy Resolution [%]
Cf-252	6.1	11
Cm-244	5.8	11
Am-241	5.5	13
Triple source: Am-241, Pu-239, and Cm-244	5.5 5.2 5.8	Not resolved!
Cs-137	0.662	33 %
Co-60	1.2 1.3	Not Resolved!

There are a number of potential sources of fluctuation in the response of the detector that affects the energy resolution. These include any drift of the operating characteristics of the detector during the course of the measurements, sources of random noise within the detector and instrumentation system, and statistical noise arising from the discrete nature of the measured signal itself.

As shown in the previous results, the energy of the irradiating source affects the energy resolution. The higher the energy of the source, the larger number of optical photons produced in the scintillator that finally reach the SiPM. Then, as the energy of the source increases, the output of the detector increases too, providing a better signal-to-noise ratio in the measurements and therefore the statistical fluctuations of the signal decrease, resulting in a better energy resolution.

In our case, the best energy resolution was achieved when measuring the alpha sources: Cf-252 (6.1 MeV), Cm-244 (5.8 MeV), both with 11% resolution; and 13% for the Am-241 (5.5 MeV). The triple alpha source irradiates at the same time particles with 5.2, 5.5, and 5.8 MeV. This represents a difference of 300 keV between each other, so that it would be necessary to achieve about 5% energy resolutions (0.3 MeV/5.8 MeV) to resolve these particles from each other.

In the case of the gamma ray sources, the energy resolutions are even poorer because of the lower kinematic energy of their photons, giving a 33% resolution for the Cs-137 and not even determined for the Co-60 source. In analogy with the triple alpha source, the Co-60 source emits photons of two different energies at the same time (1.2 and 1.3 MeV), the difference between them is even lower than that of the triple alpha source: 100 keV. Then an energy resolution of 7% is required to resolve both peaks in the Co-60 source.

For comparison purposes, the energy spectrum of the Cs-137 and the triple alpha sources were obtained using the multichannel analyzer described in §3.3.7. And the Co-60 spectrum was recorded using the GRETINA digitizer (§3.3.9). Figures 4.13-4.15 show such spectra.

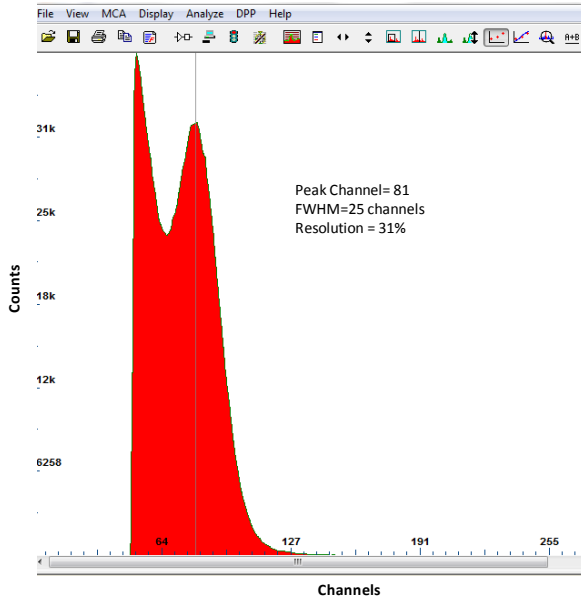


Figure 4.13: Energy spectrum for Cs-137 taken with the MCA8000A.

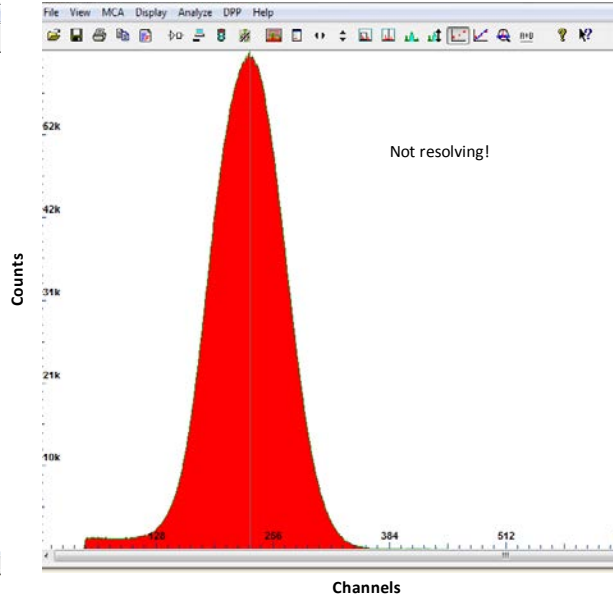


Figure 4.14: Energy spectrum for the triple alpha source taken with the MCA8000A.

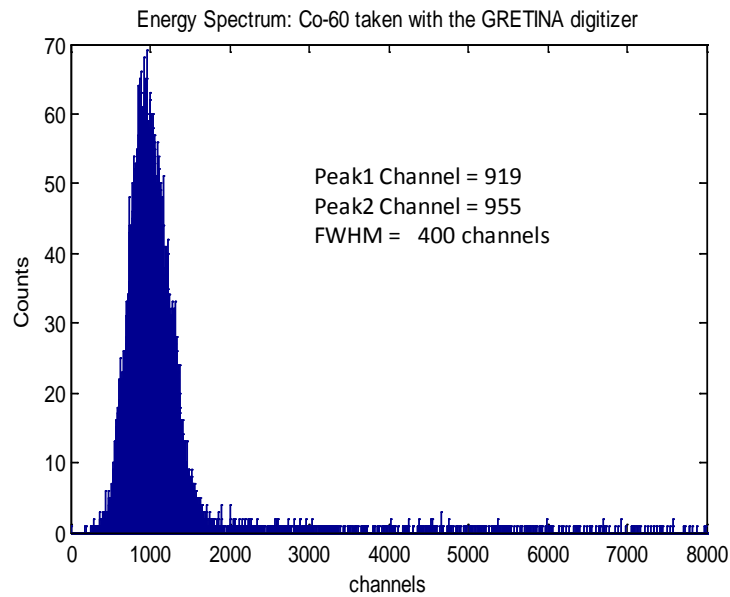


Figure 4.15: Energy spectrum for Co-60 taken with the GRETINA digitizer.

The energy resolution achieved for the Cs-137 gamma source was 30%, and for the triple alpha source, we can see that it is not resolved, as in the case of the previous setup used. Also, the spectrum of the Co-60 gamma source taken with the GRETINA digitizer is not well resolved either using this setup.

These results suggest that the electronics used did not significantly influence the prototype performance. However, the prototype detector does not meet the resolution requirements and several actions should be taken in order to improve its resolution. In the first place, optimization of the readout electronics in order to decrease the overall noise figure has to be done. It is actually future work of this project to implement a custom readout electronics system, based on the digital signal processing techniques explained in Chapter 2, instead of using modular instrumentation. On the other hand, it should be taken into account that the real operation of the charged particle detector within a gamma ray spectrometer will take place under vacuum conditions, where, in the case of alpha or any other charged particles, much better resolution is expected.

4.2.4 LINEARITY

From section §4.2.3, it was shown that a larger number of micro-pixels provides a wider dynamic range and improves the linearity of the detector's response. It was concluded that using only 1 pixel of the SiPM (3640 micro-pixels) the response of the detector begins to become non-linear for incident photons/particles with kinematic energies above 2 MeV. In Fig. 4.16, the kinetic energy of the radioisotope sources as a function of the area computed from the oscilloscope for one pixel of the SiPM is plotted.

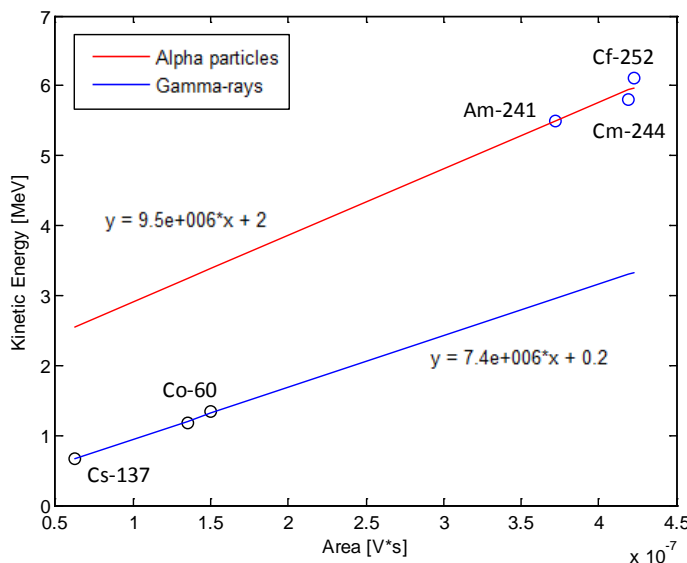


Figure 4.16: Linearity over the gamma rays and alpha particles sources.

Using a linear fit, we studied linearity for the response of the detector over both kinds of radiation sources used. As expected, gamma ray sources present a more linear response compared to the behavior of the alpha particle sources, since the energy of the alpha particles is above 2 MeV, thus the saturation of one pixel of the SiPM produces a non-linear output, meanwhile the gamma rays sources' energies are under 2 MeV and no saturation is reached.

4.2.5 PULSE SHAPE DISCRIMINATION

Pulse shape discrimination was carried out with the technique explained in §3.3.8 by means of MATLAB® software. Data from the Co-60 gamma rays source and from the Am-241 alpha particle source were analyzed and in Fig. 4.17 it can be seen that a well defined discrimination between gamma rays and alpha particle radiation is achieved due to the different decay times that CsI(Tl) scintillators produce depending on the incident particles.

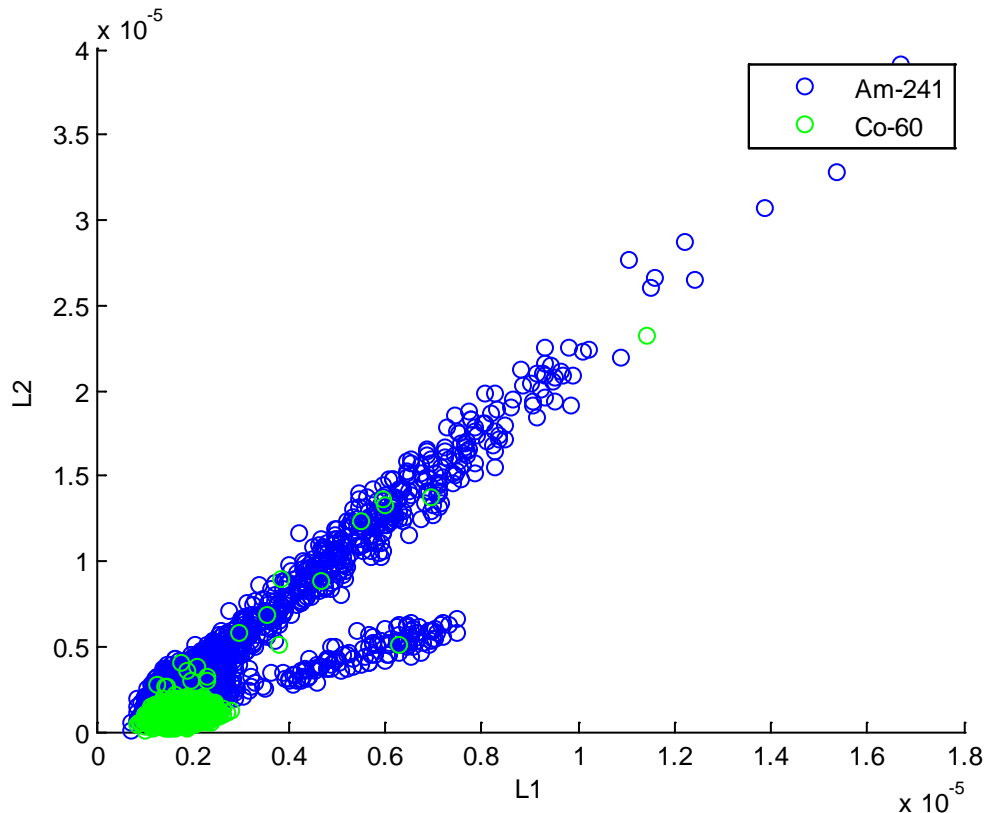


Figure 4.17: Identification of alpha particles and gamma rays detected by the CsI(Tl)-SiPM array. L_1 and L_2 are the light outputs obtained when integrating the signal within time intervals $T_1 = 400$ ns and $T_2 = 1$ μ s at times $t_1 = 0$ and $t_2 = 1.6$ μ s.

However, further analyzes need to be carried on in order to achieve discrimination among pulses from the same type of radiation (i.e. among Am-241, Cm-244, and Cf-252 or between Cs-137 and Co-60), for which the energy resolution for each of them should be improved, since we should lose as less information as possible regarding to the shape of the pulses in order to be accurately identified.

4.2.6 SENSITIVITY TO THE ENVIRONMENT

A. Magnetic field

As already mentioned, the SiPM used is high immunity to magnetic fields up to 2 T, which in consequence will provide immunity to the CsI(Tl)-SiPM array about the same value. This feature will be of special interest when the charged particle detector is placed into a gamma ray spectrometer under the particle accelerator operation conditions.

B. Behavior with temperature

The behavior with temperature of our prototype has to be further investigated since no cooler system has been implemented yet. The cooling setup on which we are about to work is presented in [94], which is supposed to exhibit variations $\ll 0.1\%$ on the SiPM gain and PDE.

C. Radiation damage

Protons, neutrons, and heavy ions are expected to be the major cause of radiation damage in semiconductor detectors. In the present application, the SiPM is protected by the CsI(Tl) crystal from direct detection of most of the charged particles. The thickness of the silicon wafer is small ($< 500\ \mu\text{m}$) and therefore has a reduced efficiency for neutron detection. Although radiation damage is expected to occur, it is also expected to be low enough to not affect the array operation.

CONCLUSIONS AND FUTURE WORK

The identification of particles emitted in nuclear reactions in a wide dynamic range of kinetic energy is an important feature requested by heavy ion experiments. Research in this field is mainly divided in two branches, not necessarily separated, one devoted to the development of new detectors, and the other concerning new methods of analysis.

The work presented in this Thesis has an impact on both research branches: in the first place, the development and characterization of a novel prototype for charged particle detection has been carried out and, in second place, an extensive study about digital processing techniques in Nuclear Physics experiments has been performed.

During the present work we have proposed and characterized a prototype for a charged particle detector based on a CsI(Tl) scintillator coupled to a silicon photomultiplier (SiPM). The use of a SiPM as optical readout sensor for scintillation detectors has become a common choice in gamma ray spectroscopy for medical imaging applications; however we wanted to investigate if this array would be suitable for charged particle detection rather than gamma ray spectroscopy, since it would be a very useful tool in the study of nuclear reactions involving radioactive ion beams (RIBs).

Different alpha particles and gamma ray radioisotope sources were used to test the CsI(Tl)-SiPM array, and three different data acquisition and analysis systems were instrumented for the characterization of the prototype: (1) an analog modular setup consisting of a NIM spectroscopic amplifier followed by a multichannel analyzer, (2) a digital modular setup consisting of a digital oscilloscope connected to a host PC for data analysis using MATLAB custom scripts, and (3) the specific purpose GRETINA digitizer.

By analyzing the energy spectra of different radioisotope sources, it was concluded that performance of the prototype is not significantly affected by the use of either instrumentation setup. However, during the present Thesis, most importance was given to the second setup described since, for the future operation of the charged particle detector the development of a compact, low noise data acquisition and analysis system is required, which will digitally analyze the pulses coming from the detector by means of either DSP or FPGA technology.

The performance of the prototype proposed has to be improved in several aspects in order to operate as an auxiliary detector of gamma ray spectroscopy involving RIBs. Such aspects include:

Dynamic Range: The SiPM used in this work, if used as a large-scale detector (this means using the total 16 pixels available as one output), is capable of providing the 1-50 MeV dynamic range required in experiments with RIBs, but in this case, position sensitivity for the detector would be lost. On the other hand, if we want to use each pixel of the SiPM as independent outputs, then the dynamic range provided by the SiPM falls to only 4% of the dynamic range required. In order to keep position sensitivity, it is possible to increase the dynamic range using SiPMs with higher number of micro-cells per pixel.

Energy resolution: From the results of the resolutions obtained for different energies, it was concluded that the energy of the irradiating source largely affects the energy resolution of the detector. The higher the energy of the source, better the energy resolution achieved. However, it was shown that the SiPM tested does not provide good enough resolution to resolve the radioactive sources under study. To improve the energy resolution, an optimization of the readout electronics in order to decrease the overall noise figure has to be done. On the other hand, the real operation of the charged particle detector within a gamma ray spectrometer will take place under vacuum conditions, where, in the case of alpha or any other charged particles, much better resolution is expected.

Linearity: Because of the limited dynamic range of each pixel of the SiPM, the alpha particle sources under study presented a slightly non-linear output, as in the case of dynamic range, a way to improve linearity is increasing the number of micro-cells per pixel in the SiPM.

Pulse shape discrimination: Good pulse shape discrimination was achieved between gamma rays and alpha particle radiations. However, further analyses need to be carried on in order to achieve discrimination among pulses with similar energies, for which an improvement of the energy resolution is also needed to satisfy this aspect.

In summary, some variations need to be done in order for the CsI(Tl)-SiPM to perform as a charged particle detector operating together with gamma ray spectrometers for the study of RIBs. It is necessary to test different SiPMs with higher number of micro-cells per pixel,

it would also be an option to try with scintillators different from CsI(Tl) that provides lower light yield, such as NaI(Tl).

On the other hand, the advantages that SiPMs present over PMTs or photodiodes as readout sensor for scintillation detectors place them as the very best option for the application subject of this Thesis. Such advantages include small size and mass, immunity to magnetic field, low biasing, excellent photon counting performance, and capability of achieving position sensitivity among others. Then further studies about the correct SiPM for our application will be carried on.

Finally, future work of this project also includes the implementation of the digital pulse processing chain into a portable device such as DSP or FPGA, research on position sensitivity methods, stabilization of temperature by means of an automated cooling system, and the final construction of the charged particle detector to be operated in combination with a gamma ray spectrometer under real-time nuclear reaction conditions.

GLOSSARY

absorption	the process by which radiation imparts some or all of its energy to any material through which it passes.
afterpulse	unwanted pulse (of energy) that follows a signal pulse event.
afterpulsing	the production of afterpulses due to feedback in a photon detector.
alpha particle	bare helium nucleus (two protons plus two neutrons) emitted naturally by many heavy isotopes that can be artificially produced by ionizing and accelerating helium gas
annihilation (electron)	an interaction between a positive and a negative electron in which they both disappear; their energy, including rest energy, is converted into electromagnetic radiation (called annihilation radiation).
annihilation radiation	photons produced when an electron and a positron unite and cease to exist. The annihilation of a positron-electron pair results in the production of two photons, each of 0.511MeV energy.
atom	smallest particle of an element which is capable of entering into a chemical reaction.
atomic mass	the mass of a neutral atom of a nuclide, usually expressed in terms of "atomic mass units." The "atomic mass unit" is one twelfth the mass of one neutral atom of carbon-12, equivalent to 1.6604×10^{-24} gm. (Symbol: u)
atomic number	the number of protons in the nucleus of an atom. (Symbol: Z)
background radiation	radiation arising from radioactive material other than the one directly under consideration. Background radiation due to cosmic rays and natural radioactivity is always present. There may also be background radiation due to the presence of radioactive substances in other parts of the building, in the building material itself, etc.
bandgap	the difference in energy in a substance between electron orbitals in which the electrons are not free to move (the valence band) and orbitals in which they are relatively free and will carry a current (the conduction band).
baseline (of a pulse)	the instantaneous value that the voltage would have had at the time of the pulse peak in the absence of that pulse. In nuclear electronics, pulse heights are measured relative to the baseline, which is not necessarily

	zero.
baseline restoration (BLR)	a method used to keep stabilized the baseline of a shaped pulse.
baseline shift	changes in the pulse baseline. These usually occur due to changes in count rate or to other long term drifts, ie with temperature.
Becquerel	the special name for the unit of activity. One becquerel equals one nuclear transformation per second (abbreviated Bq). (See Curie.) Note that $1\text{Ci} = 3.7 \times 10^{10}\text{Bq}$, and $1\text{Bq} \sim 2.7 \times 10^{-11}\text{Ci}$.
beta particle	charged particle emitted from the nucleus of an atom, having a mass and charge equal in magnitude to that of the electron.
bias (voltage)	the voltage applied to a detector to produce the electric field to sweep out the signal charge.
bipolar pulse	a pulse that has two lobes about the baseline.
breakdown voltage	a reverse bias voltage applied to a photodiode where a small change in voltage causes a relatively large change in current flowing through the diode. A photodiode gets damaged passed this point. Usually defined as the reverse bias for a dark current at $10 \mu\text{A}$. Range: a few Volts to a few hundreds.
Bremsstrahlung	secondary photon radiation produced by deceleration of charged particles passing through matter.
bus	one or more conductors used in common by multiple senders or by multiple receivers.
calibration	(1) the process of using standard values to adjust an instrument so that subsequent readings correspond to their true values. (2) the process of measuring deviations from a set of standard values so that subsequent readings can be converted on their true values.
charge collection time	the time interval, after a radiation interaction, during which the signal current flows between the terminals of the detector.
charge sensitive preamplifier	a preamplifier in which the output voltage signal is proportional to the input charge. Since charge is the time integral of current, a charge sensitive preamplifier provides the time integral of the input current.
charged particle	an elementary particle, such as a proton or electron, with a positive or negative electric charge.

CMOS	Complementary Metal Oxide Semiconductor: one of several semiconductor fabrication technologies and currently the most popular partly because it conserves power by putting p and n type transistors back to back. This is also possible with silicon film TFTCs and ones made using organic semiconducting films. However, achieving both p and n type with polymer films based on printing inks is a relatively recent development.. CMOS advantages for chip cards, tickets and tags are that it has a low power consumption, operates faster and is resistant to electronic noise. CMOS can operate over a wide range of supply voltages. CMOS circuits are susceptible to damage by static electricity so care is required when handling them. They are Field Effect Transistors FETs.
common-mode gain	the gain of a differential amplifier for signals present at both inputs. Expressed as the change in output voltage divided by the change in the common input voltage.
common-mode rejection (CMR)	$20\log_{10}(\text{CMRR})$, where CMRR is the common-mode rejection ratio, or the ratio of differential gain to common-mode gain.
common-mode rejection ratio (CMRR)	ratio of differential gain to common-mode gain.
contamination, radioactive	presence of radioactive material in any place where it is not desired, and particularly in any place where its presence may be harmful. The harm may be in invalidating an experiment or a procedure, or in being a source of unnecessary exposure to personnel.
cosmic rays	high-energy particulate and electromagnetic radiations which originate outside the earth's atmosphere.
crosstalk (optical in SiPMs)	avalanches triggered in neighboring cells due to photons emitted by the fluorescence of the initiated avalanche in the actual illuminated cell.
Curie	the special unit of activity. One curie equals exactly 3.700×10^{10} nuclear transformations per second. (Abbreviated Ci).
cyclotron	a type of particle accelerator in which the particles spiral inside two D-shaped hollow metal electrodes placed facing each other under the effect of a strong vertical magnetic field, gaining energy by a high-frequency voltage applied between these electrodes
dark current (of a photodiode)	current that passes through a biased photodiode in the absence of light.

dead time	the duration of time following a valid event during which a subsequent event will not be measured by a particular electronic system.
decay time constant	the time for a true single exponential waveform to decay to a value $1/e$ of the original height.
decay, radioactive	disintegration of the nucleus of an unstable nuclide by spontaneous emission of charged particles and/or photons.
detector, radiation	any device for converting radiant energy to a form more suitable for observation. An instrument used to determine the presence, and sometimes the amount, of radiation or radioactivity.
disintegration, nuclear	a spontaneous nuclear transformation (radioactivity) characterized by the emission of energy and/or mass from the nucleus. When large numbers of nuclei are involved, the process is characterized by a definite half-life.
Dose Equivalent	the product of the absorbed dose in tissue and various modifying factors. The dose equivalent is used in radiation protection as an indication of the biological effect that will be produced in an irradiated tissue. The unit of dose equivalent is $J.kg^{-1}$. The units of dose equivalent are the sievert (Sv). $1Sv = 1J.kg^{-1}$ and the rem: $1\text{ rem} = 0.01Sv$
dose, absorbed	the mean energy imparted to matter by ionizing radiation per unit mass of irradiated material at a point of interest. The irradiated material is usually specified (e.g., absorbed dose in water, absorbed dose in lead, etc.). The unit of absorbed dose is $J.kg^{-1}$. The units of absorbed dose are the gray (Gy): $1Gy = 1J.kg^{-1}$ and is the rad: $1\text{ rad} = 100\text{ erg.g}^{-1} = 0.01Gy$
dosimeter	instrument to detect and measure accumulated radiation exposure. In common use, a pencil-size ionization chamber with a self-reading electrometer used for personnel monitoring.
dynamic range	Range of input light intensity over which the response is within linearity specification.
dynode	surface in a photomultiplier tube coated with a special semiconductor. When energetic electrons (50-200 eV) strike a dynode, many electrons are released.
efficiency, detector	a measure of the probability that a count will be recorded when radiation is incident on a detector.
electron	a stable elementary particle having an electric charge equal to -1.60210×10^{-19} Coulomb, and a rest mass equal to 9.1091×10^{-31} kg.

electron mobility	the ratio of electron velocity to electric field strength.
electron Volt (eV)	a unit of energy equivalent to the energy gained by an electron in passing through a potential difference of one volt. (Abbreviated: eV, $1\text{eV} = 1.6 \times 10^{-12}$ erg.) Larger multiple units of the electron volt are frequently used: keV for thousand or kilo electron volts, MeV for million or mega electron volts.
energy resolution	the minimum separation between two peaks in the energy spectrum at which the peaks are resolved.
energy spectrum	the distribution of the intensity of the radiation as a function of energy.
equivalent noise charge (ENC)	the value of the noise at the input of an electronic system that would produce the same value of noise at the output as does the actual noise source (regardless of its origin). Also called equivalent noise referred to input.
exposure	(1) being in the same place at the same time as something, as in "exposure to neutrons" for example. (2) a measure of the ionization produced in air by photons. More specifically, it is the sum of the electrical charges in all ions of one sign produced in air when all electrons liberated by photons in a volume element of air are completely stopped in the volume element. The unit of exposure is the roentgen (R): $1\text{R} = 2.58 \times 10^{-4} \text{ C.kg}^{-1}$ (exactly)
external radiation	radiation from a source outside the body. The radiation must penetrate the skin.
fall time (electronics)	time required for the amplitude of a pulse to decrease from a specified value (usually 90%) to another specified value (usually 10%) of its maximum value.
FET	Field-Effect Transistor: A transistor in which the voltage on one terminal (the gate) creates a field that allows or disallows conduction between the other two terminals (the source and drain).
fill factor, SiPM	geometrical efficiency defined as the ratio of the active area per the total area of the device.
film badge	a packet of photographic film used for the approximate measurement of radiation exposure for personnel monitoring purposes. The badge may contain two or more films of differing sensitivity, and it may contain filters which shield parts of the film from certain types of radiation.
form factor	Unique size and shape of a component or device (such as a circuit board, disk drive, or power supply of a computer) that determines its fit

	(physical compatibility) or interchangeability with other components or devices of a system.
Full Width at Half Maximum (FWHM)	the width of a shape at 50% of its peak amplitude. Can refer to the width of a peak in the energy spectrum or to the shape of a pulse or to any other peaked shape. For a Gaussian, the FWHM is 2.35 times its 1σ value.
gamma ray	very penetrating electromagnetic radiation of nuclear origin. Similar properties to x-ray (see X-ray).
granularity	the relative fineness or coarseness by which a measurement can be adjusted.
half-life, radioactive	time required for a radioactive substance to lose 50% of its activity by radioactive decay. Each radionuclide has a unique half-life (also known as physical half-life).
impulse response	output response of a system when given an impulse delta function impulse at its input.
internal radiation	radiation from a source within the body (as a result of deposition of radionuclides in body tissues).
Inverse Square law	the law that states that the intensity of radiation at any distance from a point source varies inversely as the square of that distance.
ion	atomic particle, atom or chemical radical bearing an electrical charge, either negative or positive.
ionization	the process by which a neutral atom or molecule acquires either a positive or a negative charge.
ionizing radiation	any electromagnetic or particulate radiation capable of producing ions, directly or indirectly, in its passage through matter.
isomer (isomeric transition)	a nuclide having the same number of protons and neutrons but a different energy. One isomer is usually less stable and (relatively) quickly transitions to the more stable form, releasing some energy in the process.
isotopes	nuclides having the same number of protons in their nuclei, and therefore the same atomic number, but differing in the number of neutrons and, therefore, in the mass number. Almost identical chemical properties exist between isotopes of a particular element.
leakage current	uncontrolled ("parasitic") current flowing across region(s) of semiconductor structure/device due to thermal generation of carrier-

	hole pairs.
luminiscent	producing electromagnetic radiation as electrons drop from an electronic excited state to a lower excited state. Characterized by a relatively cool temperature and a narrow range of emission wavelengths.
mass number	the number of protons and neutrons in the nucleus of an atom.
monitoring, radiological	periodic or continuous determination of the amount of ionizing radiation or radioactive contamination present in an occupied region as a safety measure for purposes of health protection.
natural radioactivity	the property of radioactivity exhibited by more than 50 naturally occurring radionuclides.
noise, electromagnetic pick-up	unwanted electrical signals received from another circuit due to voltage fluctuations on common conductors or capacitive coupling.
noise, electronic	Undesired spontaneous fluctuations in the output voltage of a system resulting from the physics of the devices and materials making up the system.
noise, Johnson	random voltage generated in an electronic device due to the thermal agitation of electrons within it.
noise, parallel	electronic noise arising from components in parallel with the detector, the signal sources. This is generally equivalent to current noise into the preamplifier and arises primarily from shot noise in the detector and thermal noise in parallel resistances.
noise, pink	also known as $1/f$ noise, Flicker noise, low frequency noise, or excess noise, this is electronic noise with a spectral density that varies as $1/f^\alpha$ with α near unity. Its physical origin is not as clear as shot noise or thermal noise, the other fundamental noise sources: it is clearly associated with the details of fabrication of electronic devices rather than their intrinsic properties. In radiation detector, $1/f$ noise is independent of shaping time constant and therefore often dominates electronic noise at the noise corner.
noise, series	electronic noise arising from components in series with the detector, the signal source. This is generally equivalent to voltage noise into the preamplifier and arises primarily from noise in the input channel of the JFET used at the preamp input.
noise, shot	electric current is the flow of discrete, quantized electric charges. Shot

noise is electronic noise arising from statistical fluctuations in the current through a junction, such as that in a semiconductor detector, where it forms a current or parallel noise source.

noise, thermal electronic noise arising from the random thermal vibrations of charge carriers in a conductor. In radiation detection, thermal noise is most often due to the channel of the input FET, where it is a voltage or series noise source, and to the feedback resistor, where it is a current or parallel noise source.

noise, white random noise with an equal amount of noise power in each frequency interval.

non-ionizing radiation radiation that has lower energy levels and longer wavelengths than ionizing radiation. It is not strong enough to affect the structure of atoms it contacts, but is strong enough to heat tissue and can cause harmful biological effects. Examples include radio waves, microwaves, visible light, and infrared from a heat lamp.

nuclei chart two-dimensional graph in which one axis represents the number of neutrons and the other represents the number of protons in an atomic nucleus. Each point plotted on the graph thus represents the nuclide of a real or hypothetical chemical element. This system of ordering nuclides can offer a greater insight into the characteristics of isotopes than the better-known periodic table, which shows only elements instead of each of their isotopes.

nuclide a species of atom characterized by the constitution of its nucleus. The nuclear constitution is specified by the number of protons (Z), number of neutrons (N) and energy content: or alternatively, by the atomic number (Z) and atomic mass. To be regarded as a distinct nuclide, the atom must be capable of existing for a measurable time. Therefore, nuclear isomers are separate nuclides, whereas promptly-decaying, excited nuclear states and unstable intermediates in nuclear reactions are not so considered.

particle accelerator a machine for accelerating charged elementary particles to very high energies, used for research in nuclear physics

peaking time the time required for a shaped pulse to go from the baseline to the peak. It is related to the shaping time constant of the shaping amplifier, usually approximately 2.4 times as long.

photocathode special semiconductor material placed at the entrance window of a photomultiplier tube to convert photons to electrons by the photoelectric effect.

photon	fundamental quantum of electromagnetic radiation, with zero rest mass, one unit of angular momentum, and an energy E and wavelength λ related by $E = (1.241 \text{ eV/nm})\lambda$.
pile-up	an event in which two (or more) pulses overlap in time.
pulse duration	the time during which the pulse amplitude is non-zero. Because of the difficulty of defining “zero” accurately, it is usually specified as FWHM (full width at half maximum), the time during which the pulse amplitude is greater than or equal to half the peak height.
pulse height	the height of a pulse measured from its peak to the instantaneous baseline. Also called peak height.
pulse height analyzer	circuitry to categorize pulses according to heights. There are two main classes, single channel analyzers and multichannel analyzers.
pulse height distribution	the distribution of the frequency of pulse heights. Usually a histogram, in which the horizontal axis represents the pulse height (in a certain number of pulse height bins, or channels) and the vertical axis represents the number of events with pulse height in each channel. Most often, the pulse height corresponds to deposited energy so the pulse height distribution (PHD) is the energy spectrum. However, the pulse height may also correspond to timing or other properties.
quantum efficiency	the probability of an incident photon to be absorbed (creating a photoelectron). It is a strong function of the photon wavelength and is related to the optical absorption coefficient of the semiconductor substrate. For PMTs: 20-30%. For PIN photodiodes: 60-80%. For APDs and SiPMs ~80%.
rad	the unit of absorbed dose equal to 0.01 J/kg in any medium. (See Absorbed Dose).
radiation	emitted energy in the form of electromagnetic waves (photons) or ionizing particles (electrons, alpha particles or nuclei).
radioactivity	the property of certain nuclides of spontaneously emitting particles or gamma radiation or of emitting x-radiation following orbital electron capture or of undergoing spontaneous fission.
radioisotope (radioactive isotope)	isotopes of an element that have an unstable nucleus. Radioactive isotopes are commonly used in science, industry, and medicine. The nucleus eventually reaches a more stable number of protons and neutrons through one or more radioactive decays. Approximately 3,700 natural and artificial radioisotopes have been identified.

rem	the special unit of dose equivalent. The dose equivalent in rems is numerically equal to the absorbed dose in rads multiplied by the quality factor, distribution factor and any other necessary factors. (See Dose Equivalent)
rise time	the time for the output of a circuit to change from 10 to 90% of its final value after a step input.
secondary electron	an electron ejected from an atom, molecule or surface as a result of an interaction with a charged particle or photon.
self-absorption	absorption of radiation (emitted by radioactive atoms) by the material in which the atoms are located; in particular, the absorption of radiation within a sample being assayed.
sensitivity	smallest amount of a measurable quantity that an instrument can detect.
Signal-to-noise ratio	In analog and digital communications, signal-to-noise ratio, often written S/N or SNR, is a measure of signal strength relative to background noise. The ratio is usually measured in decibels (dB). $S/N = 20 \log_{10}(V_s/V_n)$.
specific activity	total radioactivity of a given radionuclide per gram of a compound, element or radionuclide.
spectrometer	an instrument for obtaining spectra.
spectroscopy	the study of spectra.
spectrum	the distribution of a characteristic of a physical system or phenomenon, or a graphic representation of such a distribution. In most nuclear applications, the energy spectrum is of interest, i.e. one measures the distribution of emitted energies. The timing spectrum, mass spectrum, charge state spectrum, and other spectra are also measured.
spurious count	in a radiation counting device, a count caused by any agent other than radiation.
stable isotope	a non-radioactive isotope of an element.
tail pulse	a pulse having a short rise time and a long, exponential decay.
target	a material bombarded by any radiation.
thermoluminescent dosimeter	a dosimeter made of certain crystalline material which is capable of both storing a fraction of absorbed ionizing radiation and releasing this energy in the form of visible photons when heated. The amount of light

	released can be used as a measure of radiation exposure to these crystals.
time of flight (TOF)	a variety of methods that measure the time that it takes for an object, particle or acoustic, electromagnetic or other wave to travel a distance through a medium.
transimpedance amplifier	An amplifier which converts a current to a voltage.
unipolar pulse	a pulse which is predominantly single sided with respect to its baseline.
valence electron	an electron which is gained, lost or shared in a chemical reaction.
x-rays	penetrating electromagnetic radiation having wavelengths shorter than those of visible light. They are usually produced by bombarding a metallic target with fast electrons in a high vacuum. In nuclear reactions it is customary to refer to photons originating in the nucleus as gamma rays, and those originating in the extranuclear part of the atom as x-rays. X-rays are sometimes called roentgen rays after their discoverer, W. C. Roentgen.

REFERENCES

- [1] <http://grfs1.lbl.gov/>
- [2] <http://agata.pd.infn.it/documents/simulations/demonstrator.html>
- [3] A. Galindo-Uribarri, *AIP Conf. Proc.* Vol. **1271**: 6th Mexican Nuclear Physics School, Mexico City, Mexico, edited by E. Padilla, p.182 (2009).
- [4] D. J. Morrissey and B. M. Sherrill, in *Lecture Notes in Physics*, Springer Verlag, Vol. **651**, 113 (2004).
- [5] G. D. Alton *et al.*, *Nucl. Instrum. and Methods* **B 170**, 515 (2000).
- [6] H. K. Carter *et al.*, *Nucl. Instrum. and Methods* **B 126**, 166 (1997).
- [7] http://www.phy.ornl.gov/hribf/usersgroup/news/jan-03/jan_03.html#RA1.
- [8] A. Galindo-Uribarri, *AIP Conf. Proc.* Vol. **1271**: 6th Mexican Nuclear Physics School, Mexico City, Mexico, edited by E. Padilla, p.186 (2009).
- [9] R.D.Evans, *The Atomic Nucleus*, Krieger, (1982).
- [10] G.F. Knoll, *Radiation detection and measurement*, John Wiley & Sons, p. 31 (1989).
- [11] G.F. Knoll, *Radiation detection and measurement*, John Wiley & Sons, pp. 42-47 (1989).
- [12] G.F. Knoll, *Radiation detection and measurement*, John Wiley & Sons, p. 50 (1989).
- [13] G.F. Knoll, *Radiation detection and measurement*, John Wiley & Sons, (1989).
- [14] C.L. Melcher *et al.*, *IEEE Trans. Nucl. Sci.* **NS-32**(1), 529 (1985).
- [15] E. Sakai, *IEEE Trans. Nucl. Sci.* **NS-34**(1), 418 (1987).
- [16] I. Holl, E. Lorenz, and G. Mageras, *IEEE Trans. Nucl. Sci.* **35**(1), 105 (1988).
- [17] M. Moszynski *et al.*, *IEEE Trans. Nucl. Sci.* **44**(3), 1052 (1997).
- [18] J. D. Valentine, D. K. Wehe, G.F. Knoll, and C. E. Moss, *IEEE Trans. Nucl. Sci.* **40**(4), 1267 (1993).
- [19] J. D. Valentine *et al.*, *Nucl. Instrum. Meth.* **A325**, 147 (1993).
- [20] S. Keszthelyi-Landori and G. Hrehuss, *Nucl. Instrum. Meth.* **68**, 9 (1969).
- [21] G.F. Knoll, *Radiation detection and measurement*, John Wiley & Sons, p. 117 (1989).
- [22] F. N. H. Robinson, *Noise and fluctuations in electronic devices and circuits*, Clarendon Press, (1974).
- [23] Technical proposal for the *Advanced Gamma Tracking Array (AGATA)* project, available on <http://agata.pd.infn.it/>.
- [24] M.A. Deleplanque *et al.*, *Nucl. Instr. and Meth.* **A430**, 292 (1999).
- [25] E. Kowalsky, *Nuclear Electronics*, Springer-Verlag, New York, (1970).
- [26] P. W. Nicholson, *Nuclear Electronics*, Wiley, London, (1974).
- [27] Derenzo
- [28] K. M. Heeger, *IEEE. Trans Nucl. Scie.* **47**(6), 1829 (2000).
- [29] J. M. Adams and G. White, *Nucl. Instrum. Meth.* **156**, 459 (1978).
- [30] J. R. M. Annand, *Nucl. Instrum. Meth.* **A262**, 371 (1987).
- [31] V. T. Jordanov, J. A. Pantazis, and A. C. Huber, *Nucl. Instrum. Meth.* **A380**, 353 (1996).
- [32] J. H. Heltsley *et al.*, *Nucl. Instrum. Meth.* **A263**, 441 (1988).

- [33] M. Moszynski et al., *Nucl. Instrum. Meth.* **A317**, 262 (1992).
- [34] M. Moszynski et al., *Nucl. Instrum. Meth.* **A336**, 587 (1993).
- [35] M. N. Al-Haddad et al., *IEEE Trans Nucl. Sci.* **41**(5), 1765 (1994).
- [36] V. T. Jordanov and G. F. Knoll, *IEEE Trans Nucl. Sci.* **42**(4), 683 (1995).
- [37] A. Jhingan et al., *Nucl. Instrum. Meth.* **A585**, 165 (2008).
- [38] P. A. Södertsröm, J. Nyberg, and R. Wolters, *Nucl. Instrum. Meth.* **A594**, 79 (2008).
- [39] W. K. Warburton et al., *Applied Radiation and Isotopes* **53**, 913 (2000).
- [40] B. Sklar, *Digital Communications, Fundamental and Applications*, Prentice Hall, New Jersey, p. 603 (1988).
- [41] H. B. Crawley et al., *Nucl. Instrum. Meth.* **A342**, 578 (1994).
- [42] Analog Devices, *Fundamentals of Sampled Data Systems*, Application note **AN-282**.
- [43] P. Horowitz, W. Hill, *The Art of Electronics*, Cambridge University Press, (1989).
- [44] H. Taub, *Digital Integrated Electronics*, McGraw-Hill, (1977).
- [45] M. Brendel, *Nucl. Instrum. Meth.* **144**, 357 (1977).
- [46] S. G. Gobbur, D. A. Landis, and F. S. Goulding, *Nucl. Instrum. Meth.* **140**, 405 (1977).
- [47] D. E. Carter and G. Randers-Pehrson, *Nucl. Instrum. Meth.* **199**(3), 497 (1982).
- [48] E. Gatti, A. Geraci, and G. Ripamonti, *Nucl. Instrum. Meth.* **A381**, 117 (1996).
- [49] A. Geraci, G. Ripamonti, and A. Pullia, *Nucl. Instrum. Meth.* **A403**, 455 (1998).
- [50] G. P. Westphal et al., *IEEE Trans. Nucl. Sci.* **48**(3), 461 (2001).
- [51] R. Abbiati, A. Geraci and G. Ripamonti, *IEEE Trans. Nucl. Sci.* **51**(3), 826 (2004).
- [52] A. Pullia and G. Ripamonti, *Nucl. Instrum. Meth.* **A376**, 82 (1996).
- [53] Sen M. Kuo, Woon-Seng Gan, *Digital Signal Processors Architectures, Implementations, and Applications*, PEARSON Education, Inc (2005).
- [54] Altera Inc., available on the internet: <http://www.altera.com>
- [55] Xilinx Inc., available on the internet: <http://www.xilinx.com>
- [56] P. A. Russo, *Comparisons of the Portable Digital Spectrometer Systems*, LA-13895-MS, Los Alamos National Laboratory, USA, (2002).
- [57] C. A. McGrath, R. J. Gehrke, *A comparison of pulser-based analog and digital spectrometers*, *Nucl. Chem.*, **276**, 669 (2008).
- [58] S. N. Bateman et al, *Performance appraisals of digital spectrometry systems for the measurement of bone lead*, *Appl. Rad. Isot.* **53**, 647 (2000).
- [59] Amptek Inc., *AN-DPP-001: "Digital Pulse Processors Theory of Operation"*, www.amptek.com/pdf/dpp_theory.pdf
- [60] F. S. Goulding, *Pulse-shaping in low-noise nuclear amplifiers: A physical approach to noise analysis*, *Nucl. Instrum. Meth.* **100**, 493-504 (1972).
- [61] <http://radware.phy.ornl.gov/greta/>
- [62] <http://www.phy.anl.gov/gammasphere/>
- [63] A. Galindo-Uribarri, *Prog. Part. Nucl. Phys.*, Vol. 28, pp. 463-472, (1992).
- [64] C. J. Crannell, R. J. Kurz, and W. Viehmann, *Nucl. Instrum. Meth.* **115**, 253 (1974).
- [65] S. Keszthelyi-Landori and G. Hrehuss, *Nucl. Instrum. Meth.* **68**, 9 (1969).
- [66] P. E. Francois and D. T. Martin, *Int. J. appl. Radiat. Isotopes* **21**, 687 (1970).
- [67] S. Usuda, A. Mihara, and H. Abe, *Nucl. Instrum. Meth.* **A321**, 247 (1992).
- [68] M. Moszynski et al., *Nucl. Instrum. Meth.* **A336**, 587 (1993).
- [69] B. Ye et al., *Nucl. Instrum. Meth.* **A345**, 115 (1994).

- [70] W. Skulski and M. Momayezi, *Nucl. Instrum. Meth.* **A458**, 759 (2001).
- [71] L. E. Dinca et al., *Nucl. Instrum. Meth.* **A486**, 141 (2002).
- [72] S. C. Wu et al., *Nucl. Instrum. Meth.* **A523**, 116 (2004).
- [73] I. Holl, E. Lorenz, and G. Mageras, *IEEE Trans. Nucl. Sci.* **3**(1), 105 (1988).
- [74] J. D. Valentine, D. K. Wehe, G. F. Knoll, and C. E. Moss, *IEEE Trans. Nucl. Sci.* **40**(4), 1267 (1993).
- [75] J. D. Valentine et al., *Nucl. Instrum. Meth.* **A325**, 147 (1993).
- [76] A. Syntfeld-Kazuch, *IEEE Trans. Nucl. Sci.* **54**(5), 1836 (2007).
- [77] M. Parlog et al., *Nucl. Instrum. Meth.* **A482**, 674 (2002).
- [78] M. Parlog et al., *Nucl. Instrum. Meth.* **A482**, 693 (2002).
- [79] J. Kataoka et al., *Nucl. Instrum. Meth.* **A564**, 300 (2006).
- [80] K. M. James and M. J. Masterson, *Nucl. Instrum. Meth.* **A313**, 196 (1992).
- [81] A. Ochi, Y. Nishi, and T. Tanimori, *Nucl. Instrum. Meth.* **A378**, 267 (1996).
- [82] M. Moszynski et al., *IEEE Trans. Nucl. Sci.* **45**(3), 472 (1998).
- [83] B. Dolgoshein et al., *Nucl. Instrum. Meth.* **A563**, 368 (2006).
- [84] S. Cova, a. Lacaita, and G. Ripamonti, *IEEE Elec. Dev. Let.* **12**, 685 (1981).
- [85] Max Ghelman et al., *Nucl. Instrum. Meth.* **A652**(1), 886 (2010).
- [86] <http://sensl.com/>
- [87] <http://www.hilger-crystals.co.uk/>
- [88] [http://www.dcproducts.com.au/RTV Silicone Solutions/Tech Data Sheets/RTV615_tds.pdf](http://www.dcproducts.com.au/RTV_Silicone_Solutions/Tech_Data_Sheets/RTV615_tds.pdf)
- [89] U.S. Environmental Protection Agency, *Radiation protection*, available on line at: <http://www.epa.gov/radiation/understand/alpha.html>
- [90] <http://www.ortec-online.com/>
- [91] <http://www.amptek.com/mca8000a.html>
- [92] J. Alarja et al., *Nucl. Instr. Meth.* **A242**, 352 (1986).
- [93] SensL, White Paper: *Noise in Silicon Photomultipliers and Vacuum Photomultiplier Tubes*, available on line at: <http://www.photonicsonline.com/article.mvc/Noise-In-Silicon-Photomultipliers-And-Vacuum-0003>
- [94] SensL, Application Note: *Cooled SPMMini Temperature Stability*, available on line at: <http://www.photonicsonline.com/download.mvc/Cooled-SPMMini-Temperature-Stability-0001>
- [95] CAMAC Tutorial Issue, *IEEE Trans. Nucl. Sci.* **NS-20**, No.2 (1973).
- [96] *CAMAC Instrumentation and Interface Standards*, IEEE Document No. SH06437, distributed by Wiley-Interscience, New York, (1976).
- [97] W. D. Peterson, *The VMEbus Handbook*, VMEbus International Trade Association, Scottsdale, Arizona, (1997).
- [98] A. Meza, A. Galindo, R. Ortega, E. Padilla, "Charged-Particle prototype detector to be used in studies with Radioactive Ion Beams", Abstract Book SPIE-ICO-22, 2286138, p. 71 Puebla, Pue, 15 al 19 de agosto del 2011.

APPENDIX A: COUNTING STATISTICS

Radioactive decay is a random process. Consequently, any measurement based on observing the radiation emitted in nuclear decay is subject to some degree of statistical fluctuation. These inherent fluctuations represent an unavoidable source of uncertainty in all nuclear measurements and often can be the predominant source of imprecision or error. The term counting statistics includes the framework of statistical analysis required to process the results of nuclear counting experiments and to make predictions about the expected precision of quantities derived from these measurements.

A.1 CHARACTERIZATION OF DATA

Assume a collection of N independent measurements of the same physical quantity:

$$x_1, x_2, x_3, \dots, x_i, \dots, x_N$$

Now assume that a single typical value x_i from this set can only assume integer values so that the data might represent, for example, a number of successive readings from a radiation counter for repeated time intervals of equal length. Two elementary properties of this data set are:

$$\text{Sum:} \quad \Sigma \equiv \sum_{i=1}^N x_i \quad (\text{A.1})$$

$$\text{Experimental mean:} \quad \bar{x}_e \equiv \Sigma/N \quad (\text{A.2})$$

The experimental mean is written with the subscript to distinguish it from the mean of a particular statistical model.

It is often convenient to represent the data set by a corresponding frequency distribution function $F(x)$. The value of $F(x)$ is the relative frequency with which the number appears in the collection of data. By definition

$$F(x) \equiv \frac{\text{number_of_occurrences_of_the_value_}x}{\text{number_of_measurements}(=N)} \quad (\text{A.3})$$

The distribution is automatically normalized, that is,

$$\sum_{x=0}^{\infty} F(x) = 1 \quad (\text{A.4})$$

As long as we do not care about the specific sequence of the numbers, the complete data distribution $F(x)$ represents all the information contained in the original data set.

Figure A.1 shows the shape of the distribution functions corresponding to two extreme sets of data: one with large amounts of scatter about the mean and one with little scatter. An obvious conclusion is that the width of the distribution functions is a relative measure of the amount of fluctuation or scattering about the mean inherent in a given set of data.

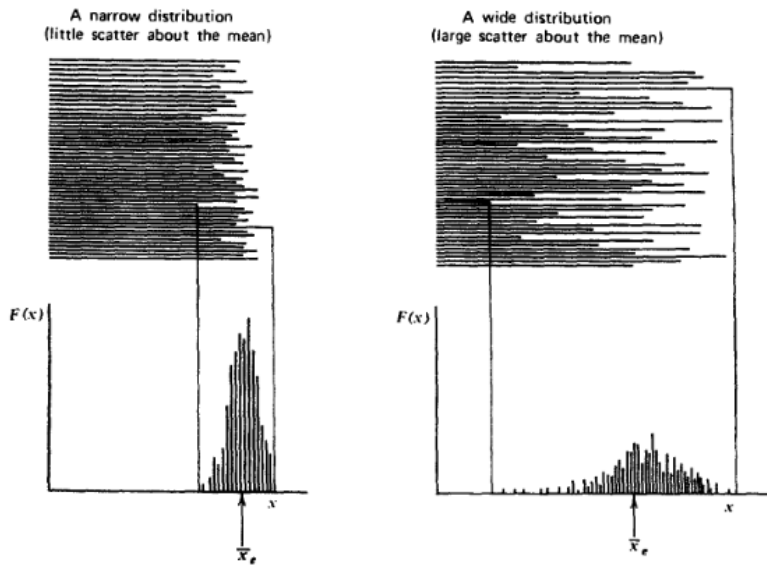


Figure A.1: Distribution function for two sets of data with differing amounts of internal fluctuation.

It is possible to calculate the experimental mean by using the data distribution function, because the mean of any distribution is simply its first moment:

$$\overline{x}_e = \sum_{x=0}^{\infty} xF(x) \quad (\text{A.5})$$

It is also possible to derive another parameter, called the *sample variance*, which will serve to quantify the amount of internal fluctuation in the data set. The first step is to define the residual of any data point as the amount by which it differs from the experimental mean value

$$d_i \equiv x_i - \bar{x}_e \quad (\text{A.6})$$

There must be an equal contribution of positive and negative residuals, so that $\sum_{i=1}^N d_i = 0$

If we take the square of each residual, however, a positive number will always result.

The *deviation* of a given data point as the amount by which it differs from the true mean value \bar{x}

$$\varepsilon_i \equiv x_i - \bar{x} \quad (\text{A.7})$$

It is similar to the residual introduced above, except that the distance from the true mean value \bar{x} is used instead of the experimental mean \bar{x}_e . The sample variance is the average value of each of these deviations after squaring

$$s^2 \equiv \overline{\varepsilon^2} = \frac{1}{N} \sum_{i=1}^N (x_i - \bar{x})^2 \quad (\text{A.8})$$

This definition presents a practical difficulty since it is never possible to know the exact value of the true mean \bar{x} without collecting an infinite number of data points. The best that can be done is to use the experimental mean value \bar{x}_e that have been measured, and thus use residuals rather than deviations. But this process will affect the calculated value of the sample variance, and we cannot simply substitute \bar{x}_e into Eq. A.8. Instead, as shown in [13], the alternative expression

$$s^2 = \frac{1}{N-1} \sum_{i=1}^N (x_i - \bar{x}_e)^2 \quad (\text{A.9})$$

is valid when the experimental mean is used. The sum of squared residuals in the above equation is divided by $N-1$ rather than by N as in Eq. (A.8), a distinction that is significant only when the number of measurements N is small.

The sample variance can be directly calculated from the data distribution function $F(x)$. Since Eq. (A.8) indicates that s^2 is simply the average of $(x - \bar{x})^2$, the same average can be written as:

$$s^2 = \sum_{i=0}^{\infty} (x - \bar{x})^2 F(x) \quad (\text{A.10})$$

An expansion of Eq. (A.10) yields to:

$$s^2 = \overline{x^2} - (\bar{x})^2 \quad (\text{A.11})$$

Two important conclusions about the organization of experimental data are:

1. Any set of data can be completely described by its frequency distribution function $F(x)$.
2. Two properties of this frequency distribution function are of particular interest: the experimental mean and the sample variance.

The experimental mean is given by Eq. (A.5) and is the value about which the distribution is centered. The sample variance is given by Eq. (A.10) and is a measure of the width of the distribution, or the amount of internal fluctuation in the data.

A.2 STATISTICAL MODELS

Under certain conditions, it is possible to predict the distribution function that will describe the results of many repetitions of a given measurement. We define a measurement as counting the number of successes resulting from a given number of trials. Each trial is assumed to be a binary process in that only two results are possible: success or not a success. For the following it will be also assumed that the probability of success is a constant for all trials. For example, in the case of observing a given radioactive nucleus for a time t the number of trials is equivalent to the number of nuclei in the sample under observation, and the measurement consists of counting those nuclei that undergo decay. We identify the probability of success of any one trial as p . In the case of radioactive decay, that probability is equal to $(1 - e^{-\lambda t})$, where λ is the decay constant of the radioactive sample.

Three specific statistical models are introduced:

1. The *Binomial Distribution*. This is the most general model and is widely applicable to all constant- p processes. It is, unfortunately, computationally cumbersome in radioactive decay, where the number of nuclei is always very large, and is used only rarely in nuclear counting applications.
2. The *Poisson Distribution*. This model is a direct mathematical simplification of the binomial distribution under conditions that the success probability p is small and constant. In practical terms, this condition implies that we have chosen an observation time that is small compared with the half-life of the source. Then the number of radioactive nuclei remains essentially constant during the observation, and the probability of recording a count from a given nucleus in the sample is small.
3. The *Gaussian or Normal Distribution*. It is a further simplification if the average number of successes is relatively large (say, greater than 25 or 30). This condition will apply for any situation in which we accumulate more than a few counts during the course of the measurement. This is most often the case so that the Gaussian model is widely applicable to many problems in counting statistics.

All the above models become identical for processes with a small individual success probability p but with a large enough number of trials so that the expected mean number of successes is large.

A. The Binomial Distribution

The binomial distribution is the most general of the statistical models discussed. If n is the number of trials for which each trial has a success probability p , then the predicted probability of counting exactly x successes is:

$$P(x) = \frac{n!}{(n-x)!x!} p^x (1-p)^{n-x} \quad (\text{A.12})$$

$P(x)$ is the predicted probability distribution function, and is defined only for integer values of n and x .

Some properties of the binomial distribution are important. First, the distribution is normalized:

$$\sum_{x=0}^n P(x) = 1 \quad (\text{A.13})$$

The average or mean value of the distribution is given by

$$\bar{x} = \sum_{x=0}^n xP(x) \quad (\text{A.14})$$

By substituting Eq. (A.12) for $P(x)$ and carry out the summation, a remarkably simple result is derived:

$$\bar{x} = pn \quad (\text{A.15})$$

A *predicted variance* σ^2 is defined as a measure of the scatter about the mean predicted by a specific statistical model $P(x)$:

$$\sigma^2 = \sum_{i=0}^n (x - \bar{x})^2 P(x) \quad (\text{A.16})$$

Conventionally, σ^2 is called the *variance*, and it is associated with a predicted probability distribution function by calling it a *predicted variance*. It is also conventional to define the standard deviation as the square root of σ^2 .

Carrying out the summation indicated in Eq. (A.16) for the specific case of $P(x)$ given by the binomial distribution, the following result is obtained:

$$\sigma^2 = pn(1 - p) \quad (\text{A.17})$$

or,

$$\sigma^2 = \bar{x}(1 - p) \quad (\text{A.18})$$

$$\sigma = \sqrt{\bar{x}(1 - p)} \quad (\text{A.19})$$

B. The Poisson Distribution

Many categories of binary processes can be characterized by a constant and small probability of success for each individual trial. Included are most nuclear counting experiments in which the number of nuclei in the sample is large and the observation time is short compared with the half-life of the radioactive species. Similarly in particle beam

experiments, many particles from accelerator might strike a target for every recorded reaction product. Under these circumstances, the binomial distribution reduces to the Poisson form:

$$P(x) = \frac{(pn)^x e^{-pn}}{x!} \quad (\text{A.20})$$

Because $\bar{x} = pn$ holds for this distribution as well as for the parent binomial distribution,

$$P(x) = \frac{(\bar{x})^x e^{-\bar{x}}}{x!} \quad (\text{A.21})$$

This is a very useful simplification because now we need only to know the mean value of the distribution in order to reconstruct its amplitude at all other values of the argument. This a great help for processes in which we can in some way measure or estimate the mean value, but for which we have no idea of either the individual probability of the size of the sample. Such is usually the case in nuclear measurements.

Some properties of the Poisson distribution follow directly. The distribution is also normalized:

$$\sum_{x=0}^n P(x) = 1 \quad (\text{A.22})$$

The average or mean value of the distribution is given by

$$\bar{x} = \sum_{x=0}^n xP(x) = pn \quad (\text{A.23})$$

The predicted variance σ^2 differs from that of the binomial and can be evaluated from the prior definition Eq. (A.16):

$$\sigma^2 = \sum_{i=0}^n (x - \bar{x})^2 P(x) = pn \quad (\text{A.24})$$

Then,

$$\sigma^2 = \bar{x} \quad (\text{A.25})$$

and the predicted standard deviation is:

$$\sigma = \sqrt{\bar{x}} \quad (\text{A.26})$$

C. The Gaussian or Normal Distribution

The Poisson distribution holds as a mathematical simplification to the binomial distribution in the limit $p \ll 1$. If in addition, the mean value of the distribution is large (say, greater than 25 or 30), additional simplifications lead to the Gaussian distribution:

$$P(x) = \frac{1}{\sqrt{2\pi\bar{x}}} \exp\left(-\frac{(x-\bar{x})^2}{2\bar{x}}\right) \quad (\text{A.27})$$

This is again a distribution function defined only for integer values of x . It shares the following properties with the Poisson distribution:

1. It is also normalized:

$$\sum_{x=0}^n P(x) = 1 \quad (\text{A.28})$$

2. The distribution is characterized by a single parameter $\bar{x} = np$.
3. The predicted variance is $\sigma^2 = \bar{x}$.

Two important characteristics of the Gaussian distribution are:

1. The distribution is symmetric about the mean value \bar{x} . Therefore, $P(x)$ depends only on the absolute value of the deviation of any value x from the mean, defined as $\varepsilon \equiv x - \bar{x}$.
2. Because the mean value \bar{x} is large, values of $P(x)$ for adjacent values of x are not greatly different from each other. In other words, the distribution is slowly varying.

These two observations suggest a recasting of the distribution as an explicit function of the deviation ε (rather than of x) and as a continuous function (rather than a discrete function). These changes are accomplished by rewriting the Gaussian distribution as:

$$G(\varepsilon) = \sqrt{\frac{2}{\pi\bar{x}}} e^{-\varepsilon^2/2\bar{x}} \quad (\text{A.29})$$

Where $G(\epsilon)d\epsilon$ is now defined as the differential probability of observing a deviation in $d\epsilon$ about ϵ . Comparing Eq. (A.29) with Eq. (A.27), there is a factor of 2 that has entered in $G(\epsilon)$ because there are two values of x for every value of the deviation ϵ .

Because we are now dealing with a continuous function, some properties of the distribution must be redefined as shown in Fig. A.2.

If we substitute $\sigma^2 = \bar{x}$ in Eq. (A.29), the value of the exponential factor now depends only on the ratio of ϵ to σ . Formally defining this ratio as:

$$t \equiv \frac{\epsilon}{\sigma}$$

The Gaussian distribution can be rewritten in terms of this new variable t :

$$G(t) = \sqrt{\frac{2}{\pi}} e^{-t^2/2} \tag{A.30}$$

where $0 \leq t \leq \infty$.

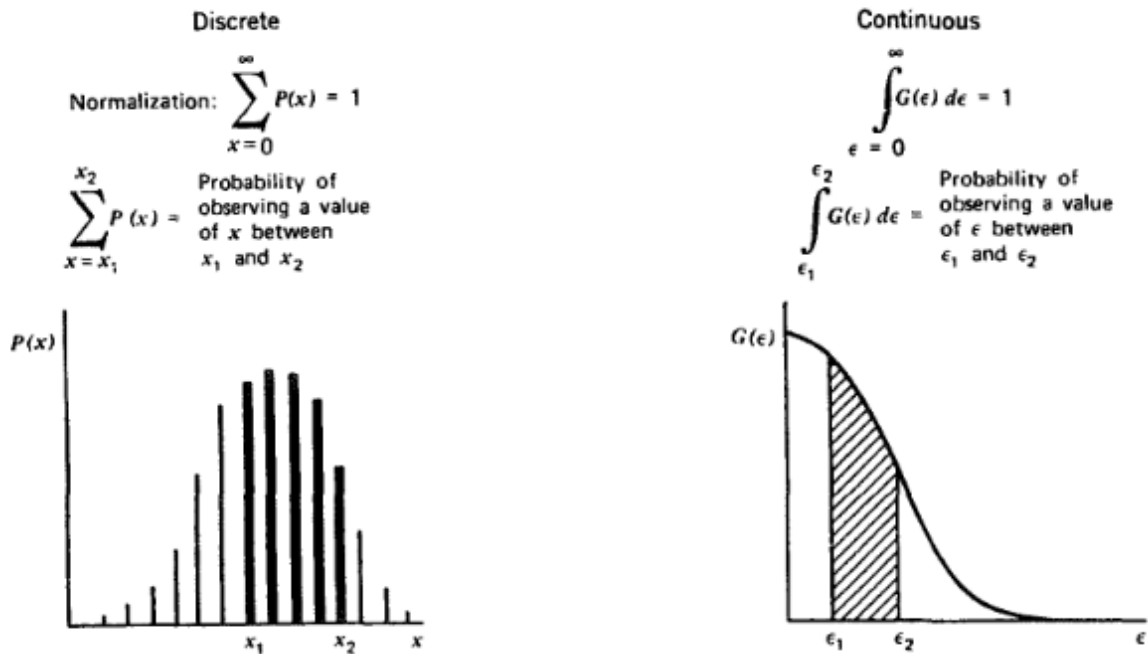


Figure A.2: Comparison of the discrete and continuous forms of the Gaussian distribution.

From the definitions illustrated in Fig. A.2, the probability that a typical normalized deviation t predicted by a Gaussian distribution will be less than a specific value t_0 is given by the integral

$$\int_0^{t_0} G(t) dt \equiv f(t_0)$$

The value of $f(t_0)$ gives the probability that a random sample from a Gaussian distribution will show a normalized deviation t that is less than the assumed value t_0 . As shown in Fig. A.3. Tabulated values of this function can be found in most collections of statistical tables.

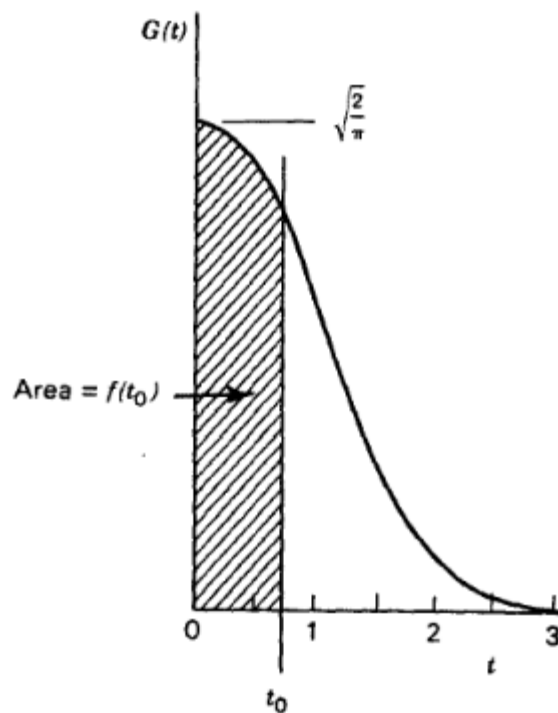


Figure. A.3: A plot of the general Gaussian curve.

APPENDIX B: COAXIAL CABLES

A. Cable construction

Virtually all interconnection of components in a traditional signal chain for radiation detector pulses is carried out using a shielded coaxial cable. A diagram of a typical cable construction is shown in Fig. B.1.

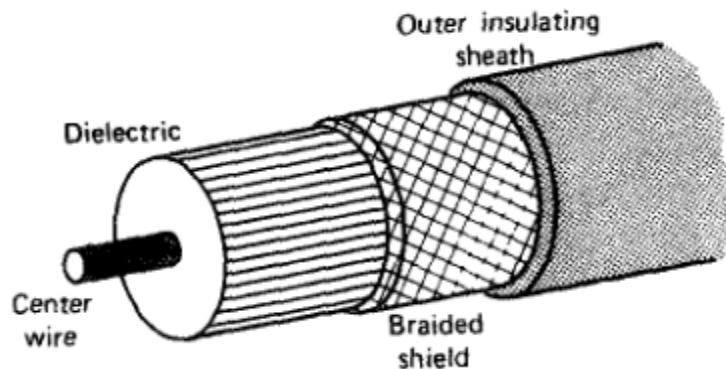


Figure B.1 Construction of a standard coaxial cable.

The shielded construction is designed to minimize pickup of noise from stray electric and electromagnetic fields. To preserve the flexibility of the cable, the outer shield is usually made of braided strands of fine copper wire. The effectiveness against low-frequency electric fields is determined primarily by the tightness of the braided shield. High frequency electromagnetic fields are shielded by virtue of the skin effect. At frequencies at which the skin depth is comparable to or smaller than the braid strand thickness (say, greater than 100 kHz), the shielding is quite effective but will become less at lower frequencies. Under extreme conditions, it is sometimes necessary to surround the braid with a second shield to fully exclude the effects of very strong fields through which the cable must pass. Doubly shielded coaxial cables are commercially available (see Tab. B.1) in which a second braided shield is provided, but a better solution for difficult cases is to run a conventional cable inside tubing made of a solid conductor. For most routine applications, single-shielded cable provides entirely satisfactory isolation from unwanted signal pick up.

Table B.1: Properties of coaxial cables^a.

	Insulating Material	Cable Diameter (cm)	Characteristic Impedance (ohms)	Signal ^b Propagation	HV Rating	Cable Capacitance (pF/m)	Signal Attenuation per Meter	
							MHz	dB
RG-8/U	Polyethylene	1.03	52	0.659	5000	96.8	100 400	0.066 0.154
RG-11/U	Polyethylene	1.03	75	0.659	5000	67.3	100 400	0.066 0.138
RG-58/U	Polyethylene	0.50	53.5	0.659	1900	93.5	100 400	0.135 0.312
RG-58C/U	Polyethylene	0.50	50	0.659	1900	100.1	100 400	0.174 0.413
RG-59/U	Polyethylene	0.61	73	0.659	2300	68.9	100 400	0.112 0.233
RG-62/U	Semisolid polyethylene	0.61	93	0.840	750	44.3	100 400	0.102 0.207
RG-174/U	Polyethylene	0.25	50	0.659	1500	101.0	100 400	0.289 0.656
RG-178/U	TFE teflon	0.18	50	0.694	1500	95.1	400	0.951
Double Shielded Coaxial Cables								
RG-9/U	Polyethylene	1.07	51	0.659	5000	98.4	100 400	0.062 0.135
RG-223/U	Polyethylene	0.52	50	0.659	1900	101.0	100 400	0.157 0.328

^aTaken from [13].^bFraction of speed of light in a vacuum (3.00×10^8 m/s).

B. Cable properties

The velocity of propagation for pulses through a coaxial cable is a function only of the dielectric materials separating the central conductor and the outer shield and is inversely proportional to the square root of the dielectric constant. Cables using air or some other gas as a dielectric have a propagation velocity very close to the velocity of light in vacuum. Some especial-duty cables with polyethylene foam dielectric have a somewhat higher velocity of propagation. At the other extreme, special delay cables with helically wound central conductors can reduce the velocity of propagation by factors of 100 or more.

Table B.1 lists important properties of coaxial cable types commonly used for nuclear instrumentation. The “RG/U” designation arose originally as a military specification and the numbers were assigned to various cable types in order of approval. Consequently, they bear no relation to specific cable properties. The RG/U designation implies adherence

to certain quality standards not usually found in lower-cost coaxial cables intended for consumer electronics applications. The historical trend has been to replace the older large-diameter signal cables (such as RG-8/U) with smaller-sized cables such as RG-59/U or RG-62/U, or with miniature types such as RG-178/U. In signal cables, the important specifications are usually the characteristic impedance and the capacitance per unit length. In cables intended to carry bias voltage to detectors, the maximum voltage rating is also important.

No real cable is a perfect transmission line. There will always be dissipative losses caused by imperfect dielectrics and resistance of the center conductor that will result in some attenuation and distortion of the transmitted pulse, especially its high-frequency components. For most applications, these effects are small and can often be neglected for cables shorter than a few tens of meters. However, for demanding situations involving the transmission of fast rise time pulses, some attention should be paid to the high-frequency attenuation specifications of the cable to prevent deterioration of the fast characteristics of the transmitted pulse.

C. Noise pickup and component grounding

The key to minimizing noise pickup is to recognize that interference always involves (1) a source, (2) a couple medium, and (3) a receiver. As an example, the source could be transient current on a power supply, the coupling could be the impedance between ground nodes in a circuit, and the receiver could be the preamplifier input. As another example, the source could be the fast edges on a clocked digital line, the coupling medium could be the capacitance to a signal node, and the receiver could be the shaping amplifier's input. Interference problems depend sensitively on the details of a particular setup and often upon parasitic circuit elements. The best solution for one setup may make problems worse in another setup.

Many problems arise from grounding, because the "ground" in a circuit serves many functions. Implicitly, one usually assumes that all of the "ground" points in a circuit are the same potential. This can only be the case if the ground nodes have zero resistance and/or no current flows between the ground points. Consider the simple example shown in Fig. B.2. A preamplifier is located some distance from the shaping amplifier, with a single ground connection between them. The preamp produces an output signal referenced to the "ground" voltage of the preamp. The preamp dissipates power, so a power supply

current flows into the preamp and then returns along the ground connection to the shaping amplifier. This current generates a voltage between the ground of the preamp and that of the amplifier whose magnitude is simply the product of the return current and the path resistance. Potential problems arise because the “ground” is serving both as a signal reference and as a path for the return of the supply current.

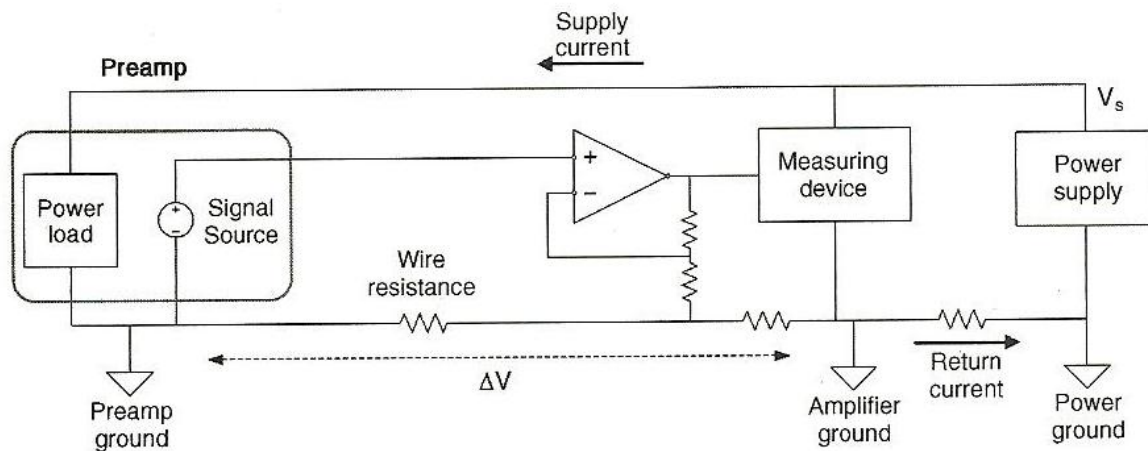


Figure B.2: Sketch illustrating ground connections in a simple system.

The outer shields of coaxial cables interconnect the chassis ground of each component with that of the next. Some current may flow in the shield to maintain the common ground potential. In many routine applications, this ground current is small enough to be of no practical consequence. However, if components are widely separated and internally grounded under widely different conditions, the shield current can be large and its fluctuations may induce significant noise in the cable. Such ground loops should be eliminated by ensuring that all components are internally grounded to a single common point for the entire system.

A technique known as common mode rejection is sometimes helpful in reducing the effects of noise pickup on interconnecting cables. The basic idea is to separate the signal reference from other ground connections. The receiving device (often the linear amplifier) is designed with a differential input so that the signal is measured on one input relative to a reference voltage at the second input. Connection to the two inputs is made by identical cables that are run side-by-side to the signal source (often the pre-amplifier). Only the first cable is connected to the signal source, whereas the cable from the reference input is left open at the sending end. In principle, much of the pickup will appear on both cables and will therefore be eliminated by the differential input.

Undesirable transient signals can also be induced in cable shields (especially loop configurations) if nearby equipment involves the fast switching of large currents. Computers are a potential source of high-frequency noise pickup and may need to be kept at a distance from detectors and pre-amplifiers where signal levels are low.

The first step to solving grounding issues is to recognize that the concept of “ground” includes three distinct and important notions. In the first place, there must be a common connection to earth ground. This connection has a very important safety role: it provides a low-impedance path to earth. (Users have been killed when their body became the lowest impedance path from their instruments to their lab bench.) In the second place, “ground” is the return path for power supply current. Power supplies will be sending a current into the circuits, and by continuity, this current has to return to the supply. In the third place, “ground” is a reference for signals. A signal source generates an output voltage relative to its reference.

To minimize ground noise, these functions should be separated as much as possible. For example, the power return current should flow along a different path than the signal reference currents. Digital circuits are inherently noisy, since their current flows for brief intervals at the clock edge, so separation of the return path for digital components from those of low-noise analog components is often desirable. Using a “star” ground requires connecting signal reference grounds so that all signal voltages are measured with respect to a single point. This approach can be helpful, but the user must identify all the ground paths. When using benchtop systems, where several modules are all plugged into a single outlet strip, the separate earth grounds on each module will lead to many ground paths. Serial connections to a computer may also add ground paths.

D. Characteristic Impedance and cable reflections

A general discussion of pulse transmission through coaxial cables is best divided into two extremes: cases in which low-frequency or slow pulses are transmitted, or those in which high-frequency or fast pulses are involved. The distinction of whether a given application involves fast or slow pulses depends on a comparison of the fastest pulse component (usually the rise time) with the transit time of the pulse through the cable. For cables with solid polyethylene dielectric, the transit time is about 5.1 ns/m. Pulses having rise times that are large compared with the transit time are slow pulses, whereas those having a rise time comparable to or shorter than the transit time are fast pulses. For cables of a few

meters in length, only the pulses from very fast detectors will qualify as fast pulses, whereas even relatively slow detector outputs must be considered as fast pulses if the cable is several hundred meters long.

For slow pulses, the cable acts much like a simple conductor interconnecting components. Its important properties then are simply its series resistance and capacitance to ground. The resistance of the central conductor is very small for cables less than a few hundred meters in length, so the most significant parameter usually is the cable capacitance. This capacitive loading will increase linearly with cable length, but is seldom a practical problem except between the detector and preamplifier. Because the noise characteristics of a typical pre-amplifier will deteriorate with increasing input capacitance, there is a premium on keeping the additional capacitive loading to a minimum. In most other aspects, the choice of cable for slow pulse applications is not critical, and virtually any of the cables listed in Tab. B.1 will suffice for routine interconnection of components.

For fast pulses, a number of other considerations become important. Prominent among these is the characteristic impedance of the cable. It is a property that depends on the dielectric material and diameters of the inner conductor and outer shield of the cable but is independent of the cable length. To illustrate the physical meaning of characteristic impedance, imagine that the voltage generator shown in Fig. B.3 is capable of generating a step voltage change from zero to some finite value V_0 at a time $t = 0$. If this voltage step is applied to the input of a coaxial cable, it will travel down the length of the cable with the velocity of propagation discussed in the previous section. During the time this voltage step is traveling down the cable, current is being drawn from the signal source because a finite charge per unit length of the cable is required to raise the central conductor voltage from zero to V_0 . If the cable were infinitely long, this current drain would be continuous because the step voltage would propagate indefinitely and continue to draw current from the source. In this example, the characteristic impedance of the cable is simply given by the ratio of the step voltage V_0 divided by the current drawn by the infinitely long cable.

For cables of finite length, we must pay some attention to the conditions that exist at the far end of the cable. The cable is terminated by the effective resistance R_t that appears between the central conductor and outer shield of the cable at the far end. If the cable is connected to an electronic component, then the termination resistance is effectively just the input impedance of that component. If the cable is simply left unconnected, its termination resistance is infinite, or it may be terminated by connecting a resistor

between the central conductor and the outer shield. When it is desired to terminate a cable that is connected to a component with high input impedance with a lower termination resistance, a resistor-to-ground (called shunt terminator) can be inserted parallel to the input of the device so that the effective termination is the parallel combination of the input impedance and the shunt terminator resistance.

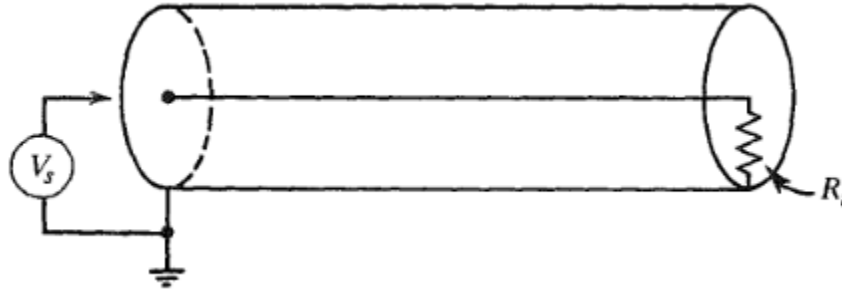


Figure B.3: Application of a step voltage V_s to a coaxial cable terminated in R_t .

Now consider what happens when a cable is terminated in its own characteristic impedance. For the sake of example, assume a long cable with 50-ohm characteristic impedance that is terminated by connecting a 50-ohm resistor across the far end. If a 5V step input is applied to the sending end, then during the time the step is propagating along the length of the cable, a current of 100 mA is drawn from the source. The current simply goes into charging successive segments of the cable as the voltage step propagates. During this period the 50-ohm resistor does not draw current because the center conductor voltage at the far end of the cable remains at zero. When the voltage step finally reaches the far end, the situation changes. Current no longer goes into charging up the cable because it is already fully charged over its entire length. However, the 50-ohm resistor now feels a 5 V potential and will therefore begin to draw a current of 100 mA current to the cable from the instant the step is applied, and it must maintain this current even after the step has propagated along the entire length of the cable. Therefore, as far as the signal generator is concerned, a coaxial cable terminated in its own characteristic impedance behaves like an infinitely long cable of the same impedance.

Other conditions prevail if the cable is not terminated in its characteristic impedance. There will then be an abrupt change in the properties of the medium through which the step is propagating, and reflections from the end of the cable will therefore be generated. If the cable is shorted (R_t is made equal to zero), then the step is inverted and reflected back down the cable toward the sending end with an amplitude equal to the original step.

If the end of the cable is simply left unterminated (R_t is infinite), then a reflection of the same polarity and amplitude will propagate back toward the sending end. Only when the cable is terminated in its own characteristic impedance are reflections completely avoided. Table B.2 shows the reflection conditions for a step voltage of amplitude A for termination conditions between the extremes of zero and infinity.

When transmitting fast pulses through coaxial cables, these reflections can be very undesirable and may lead to distortions of the transmitted pulse form. In these applications, therefore, the user must pay careful attention to the impedance of the cable and the termination conditions at each end. Because the majority of cables used for nuclear pulse applications have characteristic impedances of either 50 or 93 ohms (see Tab. B.1), many of the commercial circuits intended for fast pulse applications are designed with input and/or output impedances of 50 or 93 ohms as well. It is usually sufficient to properly terminate only the receiving end of the cable because, in principle, all reflections are thereby avoided. If slight mismatches occur, however, a small reflected component will be propagated back to the sending end where the termination conditions now become important. The output impedance of the generating device determines this termination value, and if is also equal to the characteristic impedance of the cable, further reflections are suppressed. Instrument systems in which all the input, output, and cable impedances are the same value can therefore be rather generally interconnected without fear of significant reflections.

Table B.2: Reflection conditions created by various terminations at the end of a coaxial cable with characteristic impedance Z_0 . Step Input waveform with amplitude A is assumed.

Termination Resistance R	Reflected Step Amplitude
0	$-A$
Between 0 and Z_0	Between $-A$ and 0
Z_0	0
Between Z_0 and ∞	Between 0 and $+A$
∞	$+A$

Taken from [13].

If the device impedance does not match the cable impedance and reflections must be avoided, external termination resistors may be used at the point where the cable connects to the device in order to create proper termination conditions. A termination resistor

added in series will add its resistance value to the device impedance at either end of the cable, while a shunt resistor added in parallel to the output or input will lower the device impedance to the equivalent resistance of the parallel combination.

E. BNC connectors

The **BNC connector (Bayonet Neill–Concelman)** is a common type of RF connector used for coaxial cable. It is used with radio, television, and other radio-frequency electronic equipment, test instruments, video signals, and was once a popular computer network connector. BNC connectors are made to match the characteristic impedance of cable at either 50 ohms or 75 ohms. It is usually applied for frequencies below 3 GHz and voltages below 500 Volts. Similar connectors using the bayonet connection principle exist, and a threaded connector is also available.

The BNC connector is used for signal connections such as:

- analog and serial digital interface video signals
- amateur radio antennas
- aviation electronics (avyonics)
- test equipment.

F. LEMO connectors

LEMO is both the name of an electronic and fiber optic connector manufacturer based in Switzerland, and the name commonly used to refer to push-pull connectors made by that company, which are used in medical, industrial, audio/visual, telecommunications, military, scientific research and measurement applications. The best known LEMO connectors are high quality push-pull circular types.

LEMO 00-compatible connectors are often used in physics and engineering applications for interconnection between NIM/CAMAC modules. They are typically used with RG-174 cable.

This cable assembly has a characteristic impedance of 50 ohms. 50 ohm coax cable, connectors, and adapters are commonly used in fi (802.11 wireless LAN) antennas, ham

transceivers, and other radio frequency (RF) analog and digital signaling, microwave, radar, hi-fidelity professional audio, non-destructive testing (NDT), oil and petroleum production, ultrasonic transducers, accelerometers, strain gauges, and some professional video applications.

APPENDIX C: THE NIM, CAMAC, AND VME INSTRUMENTATION STANDARDS

C.1 THE NIM (NUCLEAR INSTRUMENT MODULE) SYSTEM

The NIM bin is designed to fit into the standard 19-inch relay rack and is subdivided into 12 individual module positions across its width. A NIM module occupies a unit width of 34.4 mm, although integral multiples of this width are permitted corresponding to modules of double width, triple width, and so on. Each of the 12 bin locations is provided with a 42-pin connector that matches with a corresponding connector at the back of each module. Pin assignments and functions are illustrated in Fig. C.1. Primary dc supply voltages provided by the bin are ± 12 V and ± 24 V. Some NIM bins also provide ± 6 V, mostly for modules using integrated circuits, but these voltages are not strictly required by the NIM rules. The NIM bin and modules can be of two standard heights: $5 \frac{1}{4}$ inches (133 mm) or $8 \frac{3}{4}$ inches (222 mm), but the larger of these sizes is by far the more common.

Although some limited logic and switching operations can be performed through designated connector pins, the primary means of transmitting linear and logic pulses between NIM modules is by coaxial cables connected to appropriate jacks on either the back or front panel of the module. BNC connectors are specified for signal jacks, whereas SHV connectors are standard for high-voltage connections.

The NIM standard also recommends that shaped linear pulses correspond to one of three specific dynamic ranges:

- 0 to +1 V (primarily for integrated circuits)
- 0 to +10 V (primarily for transistor-based circuits)
- 0 to +100 V (primarily for vacuum-tube-based circuits and largely obsolete)

NIM modules designed for the processing of linear pulses are signal compatible only if they share a common classification for the dynamic range of the signals.

Logic signal levels are also specified in the NIM standard. Standard logic levels for logic states and the transmission of digital data are given in Tab. C.1. Fast logic pulses on 50-ohm impedance systems are separately specified in Tab. C.2.

Detailed specifications for NIM systems are contained in USAEC Report TID-20893, which was first issued in July 1964. This report has subsequently undergone revision every few years.

Table C.1: NIM Standard Logic Levels.

	Output (Must Deliver)	Input (Must Respond to)
Logic 1	+4 to +12 V	+3 to +12 V
Logic 0	+1 to -2 V	+1.5 to -2 V

Table C.2: NIM Fast Logic Levels for 50 ohm Systems.

	Output (Must Deliver)	Input (Must Respond to)
Logic 1	-14 to -18 mA	-12 to -36 mA
Logic 0	-1 to +1 mA	-4 to 20 Ma

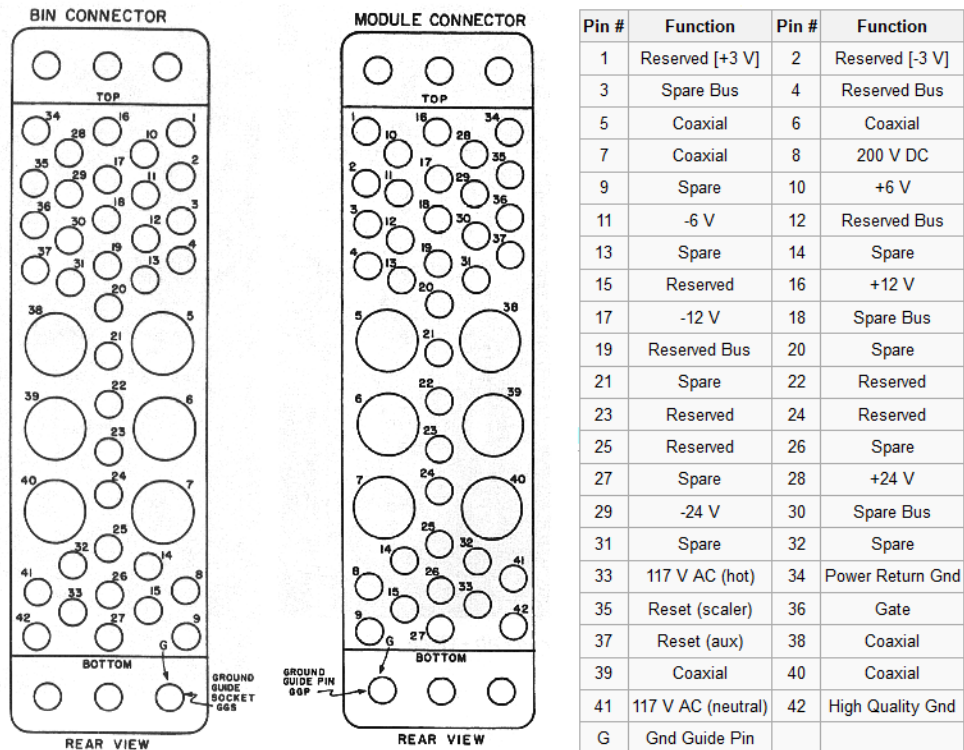


Figure C.1: Pin assignments for the NIM standard connector between bin and module.

The NIM standard does not adapt easily to situations in which large volumes of digital data must be processed. Furthermore, the basic module width is needlessly large for many digital units that do not require large numbers of front panel controls. These considerations, together with the desire for standard interfacing with digital computers, has led to the development of the CAMAC standard described next.

C.2 THE CAMAC (COMPUTER AUTOMATED MEASUREMENT AND CONTROL) STANDARD

The CAMAC standard is based on a crate, which also fits the standard 19-inch relay rack but which is subdivided into 25 individual module stations spaced 17.2 mm apart. Electrical connection between each module and the crate is made by a printed circuit board edge connector with 86 contacts. The width of the CAMAC station accommodates many modules consisting of a single printed circuit board with mounted integrated circuits. When modules must involve bulkier equipment or more than one board, multiples of the basic width can be used, and the double-width or triple-width module will occupy two or three standard slots.

Within the crate, each connector provides access to the *dataway*, which is a data highway consisting of conductor busses for digital data, control signals, and power. One of the basic design features of CAMAC is that digital communication between plug-in modules within a crate occurs over this dataway. It replaces external interconnection of modules for many digital functions, but some coaxial cable connections must be retained for linear signals and other purposes. These signals can be coupled to either the front or back of a module using the type 50CM connector recommended in the CAMAC standard.

The extreme right-hand station within the crate is different from the remaining 24 and is called the control station. It is intended that this station will be occupied by a crate controller plug-in module. The crate controller is usually a double-width module that occupies one normal station (usually the 24th) as well as the control station. The crate controller provides all the control functions necessary for the transfer of data between modules in a crate and serves as the interface between the crate and any external equipment. No CAMAC system is complete without a crate controller, and none will function without one, except on an individual module basis. In order to communicate properly over the dataway, each individual module must have sufficient internal coding and decoding to read digital data from the dataway and to supply such data from its own internal circuits when requested by the crate controller.

A diagram of the dataway is shown in Fig. C.2. The power busses are connected to all 25 stations and provide ± 6 V and ± 24 V for module power. Although not required by CAMAC, ± 12 V may also be available, depending on the specific crate design, and connections are reserved for these voltages. Except for the control station, all normal stations are also interconnected by 24 parallel read lines and 24 write lines. These lines can be used to transmit 24 parallel bits of data from a module along the read lines and to a module along the write lines. The control station is connected to each of the normal stations by separate private lines. Twenty-four of these are *station lines* (N lines), one of which corresponds to each normal station and must be activated to communicate with that specific station. An additional 24 are *look-at-me lines* (L lines), one for each station, by means of which each individual normal station may signal to the control station that it requires attention.

Modules cannot communicate directly with each other but must do so only through the crate controller. In providing a command to a given station, the controller, in addition to activating the corresponding N line, must also complete the command by providing a coded subaddress and function. These are communicated via five *function lines* (F lines) and four *subaddress lines* (A lines), which are fully bussed to all stations. Two *strobe lines* (S_1 and S_2) are also fully bussed and must be activated to initiate operations or to transfer data. The remaining busses shown in Fig. C.2 have fairly descriptive names that indicate their functions.

In addition to managing the internal module-to-module communication within a crate, the crate controller must also serve to interface the dataway with external equipment that is to be part of the overall system. Because CAMAC systems are of greatest interest when large volumes of digital information must be handled in a given application, the crate controller is often required to interface with the I/O structure of a computer. Standard crate controllers can be obtained for interfacing the more common types of laboratory computers, as well as to interface with the *branch highway* (type A controller) and *serial highway* (type L controller) described below.

If the number of CAMAC modules that must be used in a given application exceeds the room available in a single crate, or if several crates in different remote areas must be linked to a common data system, then a method must be provided to couple together more than one CAMAC crate. The arrangement can be either a parallel interconnection (a branch highway) consisting of 66 pairs of signal and ground wires, or a series chain (a serial highway) in which only two pairs of conductors are used. In the latter case, data are

sent serially and it is therefore slower, but costs are often much lower than for a branch highway interconnection.

Detailed specifications for CAMAC can be found in IEEE Documents 583-1975, 596-1976, and 595-1976, as well as in Ref. [95, 96].

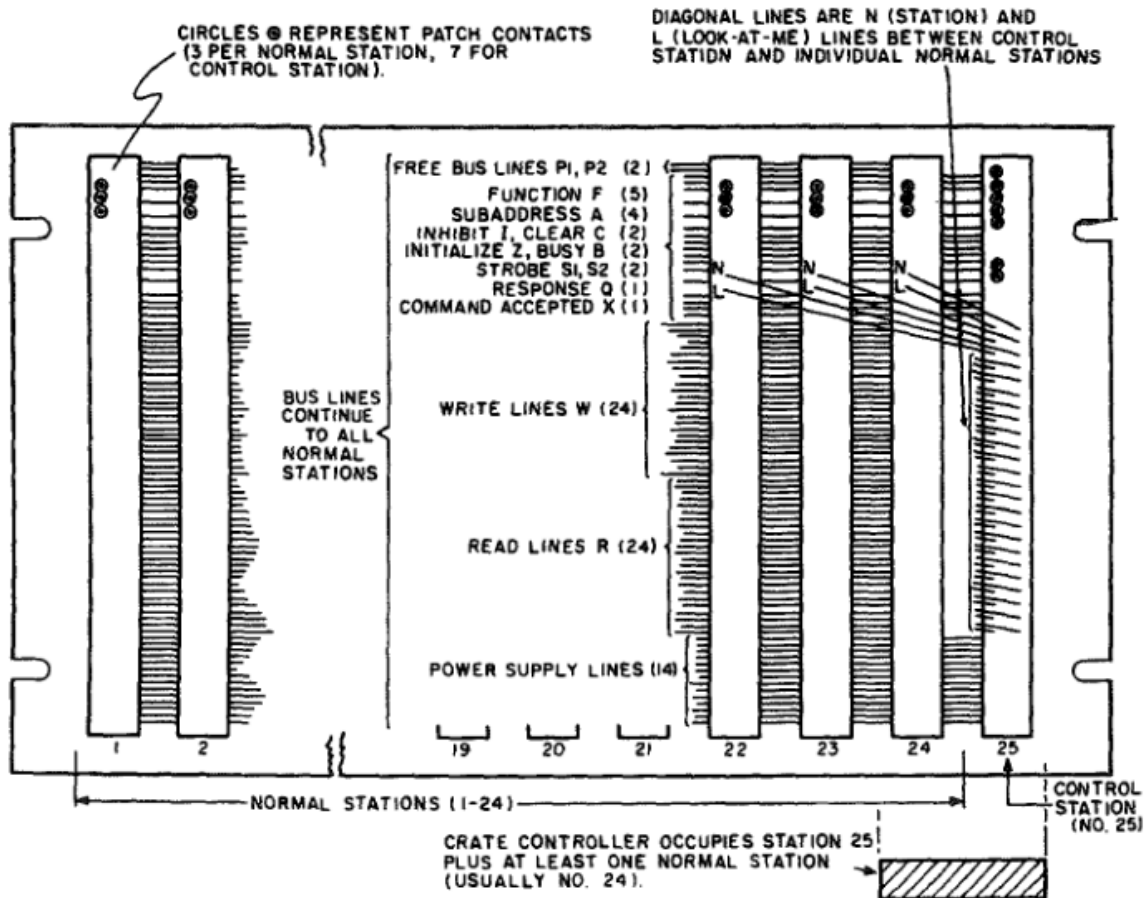


Figure C.2: Diagram of the CAMAC dataway.

C.3 THE VMEBUS STANDARD

Originally developed as a computer bus, VMEbus has been adapted for use in many applications, including nuclear instrumentations. It has gained popularity as an alternative to the CAMAC standard for systems that require digital data processing or computer control and interfacing.

VMEbus modules offer the same utility as NIM and CAMAC modules, including power supplies, discriminators, scalers, and amplifiers, but parameters are more often set through software control rather than rotary knobs and switches, allowing automated or remote control of parameters. User-interface software may reside directly on an embedded computer within a VMEbus module. Interfacing with PCs by means of USB, PCI, or other connections is also possible. VMEbus can be extended to multi-crate systems through bridge cards connected between subracks. Other protocols such as Ethernet connections can be used to link subracks into a common network or with a single PC. In addition to providing measurement functions, VMEbus modules can also be used to control mechanical systems.

Three major versions of the VMEbus standard are commonly used: VME (IEEE 1014-1987), VME64 (ANSI/VITA 1-1994), and VME64x (ANSI/VITA 1.1-1997). An introduction to these standards is also found in [97]. Each version is backward compatible with previous standards, so modules can always communicate with each other using a base set of features. The less common VMEbus Extensions for Instrumentation (VXIbus) standard is based on the VMEbus standard but aims for greater standardization in hardware and software. It also provides additional features, including electromagnetic shielding, additional power, and message-passing ability.

The VMEbus standard recommends subracks that fit within the standard 19-inch relay rack. Each subrack holds up to 21 VMEbus modules spaced 0.8 inches (20.32 mm) apart that plug into the backplane of the subrack. Each module is a printed-circuit board that connects to the backplane with sets of pins. Associated pins connect between modules through the backplane to create a bus. The backplane supplies the modules with DC voltages of +5 V and ± 12 V. One pin supplies standby +5 V even when the crate power is off. Some of the additional VME64x pins provide +3.3 V and nominal ± 48 V (between 38 and 75 V).

VMEbus modules communicate with each other through digital signals bussed over the backplane and all data transfers occur in terms of direct memory access. However, necessary analog input and output may occur through the front panel, often using LEMO00 (see Appendix C) or ribbon connectors because of space constraints.

The VMEbus is an asynchronous bus; there is no predefined rate at which transfers occur. Instead, requests and data transfers over the backplane can occur as fast as the slowest

module involved, subject to signal propagation. Conceptually, the bus is composed of four subbuses: the data transfer bus, the priority interrupt bus, the data transfer arbitration bus, and the utility bus, as shown in Fig. C.3.

Within each subrack, the left-most slot must contain a module acting as a system controller. The system controller provides bus arbitration, timeout errors for unresponsive modules, and utility functions such as a system clock and often and activity monitor. At any time, a module may act as either a master or slave. Masters are able to request access to the data transfer bus using the data transfer arbitration bus.

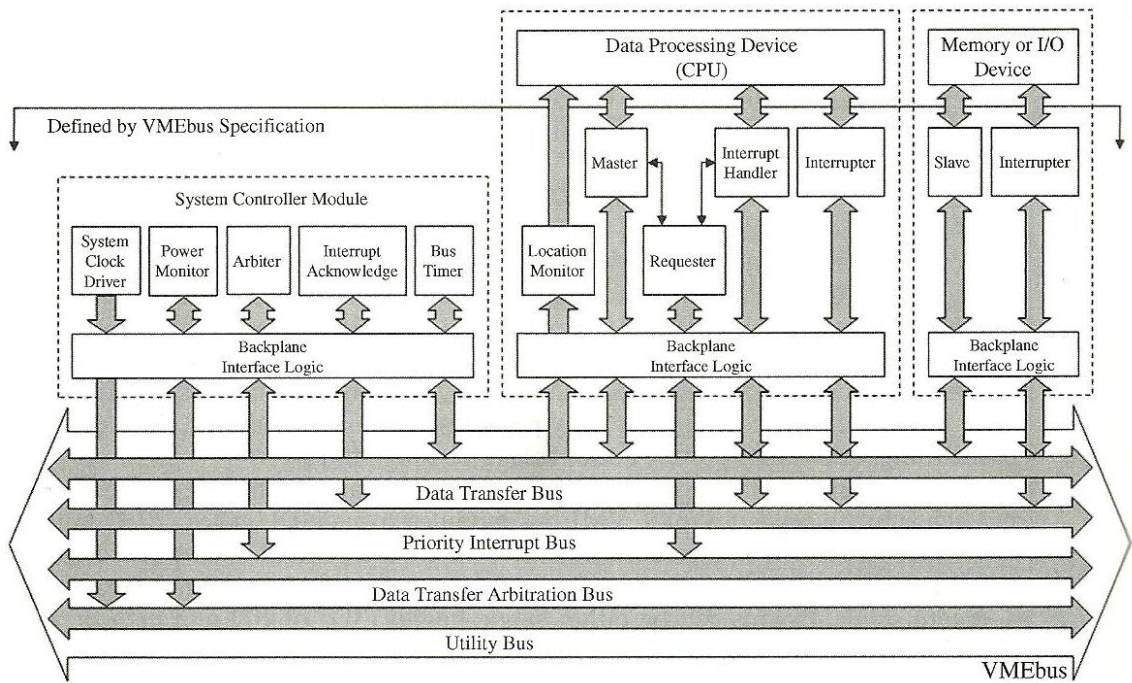


Figure C.3: Functional modules and busses defined by the VMEbus standard.

The system controller arbitrates these requests and grants access to the bus to one module at a time. Upon receiving ownership of the bus, the master drives address and address-modifier bus lines to specify the address of a slave module and the type of transfer that will occur. The slave with this address replies, and data transfer occurs over the data bus lines. For 64-bit data, the address lines are used in conjunction with the data lines in data transfers. After the data transfer is complete, the master vacates the bus. In some cases, slave modules must gain the attention of masters, such as when new input has been sent to an I/O module. The slave does this by driving one of seven interrupt bus lines. A master monitoring this interrupt line will then request the bus, acknowledge the interrupt, and apply the appropriate response.

Several types of addressing schemes and data transfers are available. The user must ensure compatible addressing and data-transfer capabilities between masters and slaves. To simplify these comparisons, the VMEbus standards specify a set of *mnemonics* for the addresses and data lengths that masters and slaves can produce and decode. Address mnemonics begin with “A” followed by the address length the module supports, and basic data transfer mnemonics begin with “D” followed by the data transfer sizes available. For example, A16 modules can only produce and respond to 16-bit addresses. Standards developed since VME include 64-bit data transfer ability through multiplexed transfers.

APPENDIX D: GUIDE TO THE SAFE HANDLING OF RADIOACTIVE MATERIALS IN RESEARCH

To establish appropriate controls on the use of radioactive materials, it is important to know the basic characteristics of these materials.

Radioactive materials have certain characteristics, such as the types of radiations emitted and the rate of emission. Knowledge of these characteristics is helpful in establishing protective controls for the use of the material.

D.1 CHARACTERISTICS OF RADIOACTIVE MATERIALS

The manner in which a radionuclide will emit radiation is well defined and very characteristic. The term “manner” refers to the type, energy and intensity of the radiation.

The major types of radiation are:

- **Alpha particles** – massive charged particles, identical in mass and charge with 4He nuclei, that are emitted from the nucleus with discrete energies (for example, ^{238}U alpha particles).
- **Beta particles** – light charged particles that come in positive (positron) and negative (negatron) forms, have the same mass as an electron and are emitted from the nucleus with a continuous range of energies up to some maximum energy (for example, ^{22}Na emits positrons, ^{32}P , ^3H , ^{14}C , ^{35}S and ^{131}I all emit negatrons).
- **Gamma rays** – electromagnetic radiation emitted from the nucleus with discrete energies (for example, ^{131}I , ^{125}I , ^{60}Co , ^{51}Cr , ^{137}Cs).
- **X-rays** – electromagnetic radiation emitted from the electron shells of an atom with discrete energies (for example, ^{131}I , ^{125}I).

Two other types of radiation are generated in the material surrounding the radioactive atoms rather than by the radioactive atoms themselves. These are external bremsstrahlung and annihilation radiation:

- **External bremsstrahlung** consists of photons created by the acceleration of charged particles in the electromagnetic field of the nucleus. The photons are emitted with a continuous range of energies up to the maximum energy of the charged particle. For example, when phosphorous-32 (^{32}P) beta particles interact with certain materials, for example, lead, significant external bremsstrahlung radiation fields can be generated.
- **Annihilation radiation** consists of two 0.511 MeV photons formed by the mutual annihilation of a positive beta particle and an electron. For example, when sodium-22 (^{22}Na) positive beta particles interact with matter, annihilation radiation is emitted.

D.1.1 SOURCES OF RADIOACTIVE MATERIAL

Radioactive material can be

- reactor-produced (by-product) material
- accelerator-produced material
- naturally-occurring material

Radioactive material produced in nuclear reactors (i.e., by the fission process itself or by the neutrons emitted) is called reactor-produced or by-product material. By-product material is regulated by the United States Nuclear Regulatory Commission or an agreement state. Many of the radionuclides commonly used in biological research, ^3H , ^{14}C , ^{35}S , ^{32}P , ^{125}I , ^{33}P and ^{131}I , are by-product materials.

Radioactive materials produced by charged particle accelerators are called accelerator-produced materials (e.g., ^{22}Na , ^{57}Co and ^{111}In).

A naturally-occurring radioactive material is any radioactive material that occurs naturally on earth. All naturally-occurring radioactive material is regulated by each state, with the exception of the following, which are regulated by the United States Nuclear Regulatory Commission: “source” material (uranium, thorium and ores that contain greater than 0.05% uranium or thorium by weight) and “special nuclear material” (uranium enriched in ^{233}U or ^{235}U). A good example of state-regulated naturally-occurring radioactive material is radium-226.

Some sources are stored in containers that are meant to be opened to permit the material to be removed. These are called “unsealed” sources. Other sources, not designed to be opened, are appropriately called “sealed” sources. Working with unsealed sources presents a much higher risk of contamination than working with sealed sources. Therefore, special precautions must be observed.

D.2 WHY IONIZING RADIATION IS POTENTIALLY HAZARDOUS

To work safely with radioactive materials, it is necessary to have an understanding of the potential hazards they pose and how to avoid these hazards.

Ionizing radiation imparts energy to living cells. In large enough doses, this energy can damage cellular structures, such as chromosomes and membranes. If not repaired, this damage can kill the cell or impair its ability to function normally. Whether this damage is harmful depends on many factors, including the type of cell, the absorbed dose and the rate of absorption.

D.2.1 EFFECTS OF HIGH DOSES OF RADIATION

Individuals and populations exposed to high doses of radiation display various types of detrimental effects. In some cases, the severity of these effects in an individual is proportional to the dose delivered – the higher the dose the greater the severity. Examples of such proportional effects are erythema (reddening of the skin), epilation (loss of hair), cataracts and “acute radiation syndrome.” These are known as deterministic effects and they all display a threshold: below a certain dose, no effects are observed.

Serious birth defects caused by irradiation of the fetus or embryo appear to exhibit a threshold at approximately 5 rem, the incidence of birth defects is not significantly different from the normal incidence. To prevent the occurrence of radiation-induced birth defects, the United States Nuclear Regulatory Commission requires radiation exposures for pregnant workers to be kept under 0.5 rem for the pregnancy period.

Another important type of effect is radiation carcinogenesis. The incidence of radiation-induced carcinogenesis in a population is assumed to be proportional to dose. It is assumed that these effects occur without threshold and that there are no effects only when the dose is zero. This has been observed in heavily irradiated populations such as

the survivors of the Hiroshima and Nagasaki bombings, where an increase in cancer has occurred.

Radiation mutagenesis is the induction of changes in hereditary traits caused by radiation damage to the chromosomes. All such hereditary changes are assumed to be detrimental to the survival of a person's descendants. Radiation mutagenesis has never been observed in any irradiated human population. This does not mean that no genetic damage has occurred. In fact, data from animal studies suggest otherwise.

Rather, the absence of observable effects in humans suggests that the genetic effects of radiation are too subtle to detect amidst the normal background of mutations in the human population.

D.2.2 OCCUPATIONAL EXPOSURE TO RADIATION

Occupational dose limits are tens to hundreds of times lower than the threshold doses for deterministic effects. Therefore, such effects occur only as a result of accidents, radiation therapy and acts of war.

Radiation mutagenesis and carcinogenesis are assumed to occur without threshold. In other words, these effects are assumed to occur to some degree in any irradiated population, not just highly irradiated populations. The primary hazards of occupational exposure to radiation are assumed to be an increase in the incidence of radiation mutagenesis and carcinogenesis in the worker population.

It is important to note that no statistically significant increase in these effects has ever been observed in a regulated worker population. Statistics show that the risk, if any, is small compared to the other health or safety hazards of the workplace.

D.3 RELATIVE RISKS OF LOW-LEVEL RADIATION

As with any chemical, the small quantities of radioactive materials used in medicine and research demand care in handling, but the risk to human health is surprisingly small when compared to experiences in everyday life.

As simple an act as crossing the street carries some risk. Certainly, all work situations carry some risk of personal injury. Working with radioactive materials is not hazard-free, but when placed in the proper perspective of other living and working environments, the occupational dangers are seen to be slight.

D.3.1 THE MATHEMATICAL CONCEPT OF RISK

A risk is the mathematical probability that an injury, damage or other detrimental event will occur. Risks are usually calculated by observing a group of people and counting the number of times a detrimental effect occurs. The risk of the detrimental effect occurring is the number of events divided by the number of people in the group.

For example, assume that there are 150 million drivers in the United States and that 50,000 are killed in automobile accidents each year. The average risk of death from automobile accidents for each driver is $150,000,000 \div 50,000$, or one in three thousand per driver per year.

However, calculating the risk of contracting cancer as a result of working with radioactive materials cannot be done in such a simple way. At the low levels associated with medical and research applications, no link between cancer and occupational exposure has been observed. In other words, people who work with radiopharmaceuticals and comparable materials show about the same rate of cancer as the population in general. That is not to say no risk is present. It means that the risk from occupational radiation exposure is so small that it cannot be measured directly. Instead the risk is estimated from observations of people who have been exposed to high doses of radiation. These estimates are intended to be conservative; the actual risk may be much lower.

D.3.2 COMPARISON OF RISKS

Another way to express the risk of an action is to compute the extent to which one's life may be shortened as a result of that action. This is done by a formula that compares average life expectancy with life expectancy given the occurrence of certain events. In general, the assumption is that the less an event shortens one's life, the less the risk.

D.4 PROCEDURES AND DEVICES FOR MEASURING PERSONAL DOSE

In working with radioactive materials, careful monitoring of the amount of ionizing radiation delivered to your body allows you to verify that safe practices are being followed.

The risks of working with radioactive materials are reduced to acceptable levels by engineered and procedural controls. The monitoring of personal dose equivalents is an important method to verify that these controls are effective.

Radiation protection dosimetry can be divided into two categories:

- External dosimetry, where the radiation source is outside the body and the biological properties of the source do not influence the dose equivalent received.
- Internal dosimetry, where the radiation source is inside the body and the dose equivalent received depends on the biological properties of the source.

D.4.1 EXTERNAL DOSIMETRY

External dosimetry is commonly performed by one or both of the following methods:

- You wear an integrating dosimeter (a “personal” dosimeter) that indicates the dose equivalent at a point on the body.
- The dose equivalent is estimated by considering the dose equivalent rate in the area and how long you worked there. The dose equivalent rate might be measured or calculated.

D.4.2 PERSONAL DOSIMETERS

The most common personal dosimeters are a film dosimeter, thermoluminescent dosimeter (TLD), optically stimulated luminescent dosimeters (OSLD) and pocket ionization chamber (PIC or “pencil dosimeter”).

Film dosimeters consist of a small piece of photographic film in a light-proof package. Filters are placed over the film to obtain information about the type and energy of the incident radiation. This information is needed to adjust the dose equivalent indicated by

the film because the film does not respond to radiation in exactly the same way as tissue. Film dosimeters fade and are sensitive to heat. They have the advantages of being relatively inexpensive and providing a permanent record of the dose equivalent received.

TLDs are small inorganic crystals that, when heated, emit a quantity of light. Under certain conditions, the light emitted is proportional to the energy deposited in the crystal. TLDs are small, rugged, re-usable and respond to most types of radiation in the same way as tissue. However, TLDs are more expensive than film dosimeters and do not provide a permanent record of the dose equivalent.

OSLDs are similar to TLDs except that the absorbed radiation energy is released by laser light instead of heat. These dosimeters are also small and rugged, can be reanalyzed and are more sensitive than TLDs.

PICs are small ionization chambers that are relatively expensive and not very rugged. Direct reading PICs may be read in the field without erasing the accumulated dose. This provides an immediate reading of the dose equivalent being received during an operation, which is very helpful in reducing doses.

Personal dosimeters should be worn on the part of your body that receives the greatest dose in relation to its dose limit. Preferably, several dosimeters should be worn at key locations. Dosimeters should be stored in an area where there is a low, constant background. They should be kept free of contamination.

D.4.3 ESTIMATING DOSE EQUIVALENTS

The dose equivalent you receive can be estimated by measuring the dose rate with a survey meter and multiplying by the length of time you stay in the radiation field. This method is useful for estimating the magnitude of the dose likely to be received. However, problems can arise when the dose equivalent rate is incorrectly measured; the dose equivalent rate measured is not representative of the radiation fields where you work or the time you will spend in the field is underestimated.

D.4.4 INTERNAL DOSIMETRY

The distribution and retention of a radioactive material will influence the dose equivalent received once it is inside the body. Therefore, in internal dosimetry, you don't try to directly measure dose; instead, you characterize the distribution and retention of the radioactive material. Once this is known, the dose equivalent can be readily calculated using standard internal dosimetry methods.

The distribution and retention of radioactive material in the body is commonly estimated in three ways:

1. The quantity of radioactive material that enters your body is monitored, and Reference Man biokinetic models are used to estimate the distribution and retention of the radioactive material.
2. The rate at which radioactive material is excreted from your body is monitored over a period of time, and Reference Man models are used to estimate the distribution and retention of the radioactive materials.
3. The quantity of radioactive material in a particular region or organ of your body is directly monitored over a period of time and the dose equivalent to that organ is estimated.

D.4.5 MONITORING METHODS

Air sampling near the breathing zone is an acceptable method of monitoring the intake of radioactive material. To produce reasonable results, it is important to obtain a representative sample of the air you breathe. For example, if the room air concentration is not uniform, the air should be sampled as close to the "nose" as possible.

A practical method of monitoring the excretion of a radioactive material is urine bioassay. This method is not very useful for those radioactive materials that are not readily excreted. Steps should be taken to keep bioassay samples free from extraneous contamination. For example, bioassay samples should be submitted away from the workplace in a contamination-free area.

Thyroid monitoring for radioiodine is one of the best examples of directly determining the quantity of a radioactive material in an organ. Direct monitoring for radioactivity in a

specific organ or the whole body can be effective, provided that the radioactive material emits radiation that can be easily detected from outside of the body and when there is no external contamination of the body.

D.4.6 MONITORING REQUIREMENTS

The Nuclear Regulatory Commission regulations require that occupationally exposed individuals must be monitored for external or internal dose if it is likely that they will receive an external or internal dose exceeding ten percent of the applicable regulatory limits.

If the licensee is required to monitor any individual for both internal and external dose, then these doses must be summed to determine compliance with the applicable dose limit.

D.4.7 DOSE LIMITS

Nuclear Regulatory Commission occupational dose limits are specified for a calendar year as follows:

Whole body – 5 rem

Any individual organ, skin or extremity – 50 rem

Lens of the eye – 15 rem

Occupation dose limits for minors are set at 10% of the above limits.

The dose limits for an embryo/fetus of an occupational exposed woman who declares in writing that she is pregnant is 500 millirem for the entire duration of the pregnancy.

Members of the public are limited to 100 millirem per year. Members of the public may be exposed to an additional 500 millirem per year, occasionally, from radiation from a patient who has been administered radioactive material.

All the above limits do not include exposure to radiation to patients from medical procedures or exposure to radiation in the environment due to consumer products, fallout or naturally-occurring radionuclides.

D.5 CONTROLLING EXPOSURE TO EXTERNAL RADIATION

Time, distance and shielding are the critical elements that must be controlled to ensure the protection of people who work with radioactive material that emit penetrating radiation.

External exposure is the irradiation of live tissue from sources outside the body. The following examples list some ionizing radiations that are capable of penetrating the dead outer layer of skin to reach live tissue:

- gamma rays (e.g. from ^{22}Na , ^{51}Cr , ^{125}I , ^{131}I)
- photons from positron annihilation (e.g. from ^{22}Na)
- beta particles with energies greater than about 100 keV (e.g. from ^{32}P , ^{90}Y)
- bremsstrahlung (e.g. from ^{32}P , ^{90}Y)
- x-rays (e.g. from ^{125}I)

The primary objective in controlling external exposure is to minimize the accumulated radiation dose. The committed dose may be reduced by reducing either the dose rate or the time of exposure. The dose rate can be reduced by placing shielding material between the source and you or by placing the source at a greater distance from you.

D.5.1 TIME

The time of exposure to penetrating radiation can be reduced by planning operations or by using special procedures during operations.

Planning Operations

- Review the safety aspects of the operation in detail.
- Carry out trial runs with no or low levels of radioactivity.
- Design operations to be a sequence of simple steps that can be accomplished quickly and safely.
- Adjust equipment to ensure that you are comfortable when handling radioactivity.

During the Operation

- Equipment should be assembled before introducing the radiation source.
- The dose rates at various steps in the operation should be monitored or known to ensure that effort is concentrated to reduce time of working in high radiation fields.
- Operations that do not require proximity to radioactive materials – for example, paperwork or resting – should be carried out away from the radiation areas.
- Work with a sequence of sources, one at a time rather than in the presence of large sources of penetrating radiation.
- Regularly monitor and promptly remove contaminated gloves.

D.5.2 DISTANCE

Ionizing radiation spreads through space like light or heat. Generally, the farther you are from a source of radiation the lower your dose rate.

Distance is very useful for protection when handling physically small sources. The dose rate from a small source is inversely proportional to the square of the distance from the source.

This “inverse square law” means, for example, that if the distance from the source is doubled, the dose rate will be one fourth.

If you get too close to a source, the dose rate can increase substantially. The dose rate at 0.1 inch from a small source will be 10,000 times higher than 10 inches from the source.

Since detectors used to measure dose rates tend to average the dose rate over the sensitive volume of the detector, large detectors will tend to underestimate dose rates close to a small source. A small detector such as a thermoluminescent dosimeter chip can be used to give a more accurate estimate of dose rates near a small source.

Methods for Reducing Exposure

The following methods can reduce exposure by increasing the distance between the operator and the source:

- Avoid direct handling of sources of penetrating radiation. Never directly handle unshielded multi-millicurie sources.
- Use forceps, tongs, custom-designed holders and spacers to maintain distance between your hand and the source.
- Design simple tools for securely handling sources (e.g. a Lucite block with cylindrical holes to hold a vial).
- Routinely store sources at the back of benches and ventilated enclosures remote from normal access.

D.5.3 SHIELDING

There is a variety of shielding materials that can be placed between you and the source to absorb most of the radiation that would otherwise reach you.

The choice of shielding material depends on the type of radiation and other functions served by the shields (such as containment, transparency or structural support). Dense materials with high atomic numbers, such as lead, form the most effective and compact shields for small sources of penetrating radiation. Because beta rays are less penetrating than other rays, pure beta ray emitters can be effectively shielded by lighter materials such as glass, water or Lucite.

When high energy beta rays are emitted and absorbed, secondary x-rays and bremsstrahlung radiation are generated. The intensity of this secondary radiation increases if the beta rays are absorbed in high-atomic-number shielding material. This secondary radiation is more penetrating than the beta rays. When large quantities (i.e. greater than 100 mCi, or 3.7 GBq) of a pure beta emitter like ^{32}P are used, the quantity of secondary radiation may be excessive unless shielded.

The best shielding configuration in this case is to use a 1/2-inch-thick Lucite acrylic sheet, or similar material, adjacent to the ^{32}P to absorb the beta rays, while minimizing the creation of secondary radiation. Use sheets of lead foil outside the shields of Lucite to absorb the more penetrating bremsstrahlung and x-rays.

Methods for Reducing Exposure

Methods to reduce exposure by using shielding materials include the following:

- When planning an operation, calculate the shielding needs using half-value layers and gamma-ray constants or dose-rate measurements.
- Check the adequacy of shields in all directions accessible to personnel by monitoring around (and especially beneath and behind) the operation.
- Store radioactive materials emitting penetrating radiation in lead containers with lead lids.
- Where space permits, concrete blocks may be used to enclose a radioactive storage area.
- Use mirrors, periscopes or transparent shields – for example, lead glass windows – to view operations. Avoid direct viewing by peering around shadow shields.
- Use a rigid frame to secure potentially-unstable shielding materials.
- Use custom-designed shields for syringe barrels when millicurie quantities are being handled.
- Avoid direct exposure to high-energy, beta-emitting sources. The dose rate to the skin from beta rays is 10 to 100 times as high as for gamma rays of the same energy and intensity.
- Whenever practical, use dilute solutions of high energy beta-emitting radionuclides since the larger volume of liquid will effectively absorb more of the beta rays.

D.6 PREVENTION OF INTERNAL RADIOACTIVE CONTAMINATION

The better the procedures for preventing contamination, the lower the risk to everyone working with low-level radioactive materials.

The main objective of controlling radioactive contamination is to prevent internal doses to workers. The primary means of contamination control is to prevent it by containing the radioactive materials during all handling phases. Other procedures should be followed when containment is impractical or as additional safety measures.

Radioactive contamination can enter the body by ingestion, inhalation or absorption through intact or damaged skin. To prevent internal exposure, it is necessary to intercept each of these contamination routes.

D.6.1 PREVENTING INGESTION

Intake through ingestion can be minimized by ensuring that potentially-contaminated objects are not placed in the mouth. In areas where unsealed radioactive materials are handled, do not eat, drink, smoke, apply cosmetics, pipette by mouth or place fingers, pens and pencils in your mouth. Physical barriers can prevent accidental ingestion due to explosion or splashing.

D.6.2 PREVENTING INHALATION

Inhalation intakes can be prevented by ensuring that radioactive materials are secured in sealed containers. Suitable containers include NENSure™ vials, crimp-sealed vials, flame-sealed ampules or vacuum systems and vessels vented through traps or filters.

When sealed systems are impractical or additional precautions are necessary, radioactive materials that could become airborne should be handled in ventilated enclosures, such as fume hoods. Fume hoods provide protection by drawing air past the worker into an enclosure and safely exhausting it. In this process, small releases are diluted to negligible concentrations by the air flow.

D.6.3 PREVENTING SKIN ABSORPTION

Skin contamination is best prevented by using tools to avoid direct contact with potentially-contaminated objects and to prevent submersion in airborne radioactivity. Additional protection can be provided by using splash guards and by wearing gloves, a lab coat and other protective clothing.

Avoid sharp objects and handle syringes carefully to prevent inadvertent self-injection. Special considerations should be given to protecting damaged skin. Open wounds or rashes should be covered or you should consider postponing operations until your skin has healed.

Regular checks should be made to ensure that skin contamination is quickly recognized. In the event of contamination of the skin, exposure of the skin and absorption can be minimized by promptly decontaminating the affected area.

D.6.4 OTHER INTERNAL EXPOSURE CONSIDERATIONS

Other internal exposure considerations include:

- Minimize the quantity of radioactivity in process by designing operations appropriately.
- Remain aware of your internal exposure by performing appropriate bioassays. For operations where small quantities of radioactivity are handled, this may only be necessary as an initial check to show that exposure is negligible.
- Make sure safety procedures address accident potential and specify appropriate action, since the risk of internal exposure may increase under accident conditions. When large sources are spilled or released, personnel should leave the immediate vicinity. Proper recovery operations should be planned with the radiation safety staff to maintain exposure controls.
- Contamination controls are necessary for all unsealed sources, including low-energy beta emitters such as ^3H , ^{14}C , ^{35}S and ^{63}Ni . Unlike external exposure where skin and clothing can shield the body from non-penetrating radiation, all radioactive materials can contribute to an internal dose when taken into the body.

D.7 PROTECTIVE CLOTHING WHEN HANDLING RADIOACTIVE MATERIALS

The best way to control potentially hazardous materials is at the source. However, protective clothing provides a good level of secondary protection.

If protective clothing is to be effective, it must be worn at all times. It must be worn properly, it must be the right fit and it must be in good condition.

D.7.1. PROTECTING YOUR BODY AND CLOTHING

Any time you are in an area where unsealed sources of radioactive material are being used, wear a lab coat. A lab coat, properly fastened, will protect against casual contamination. However, it is not effective against spills or splashing and it does not protect your head, neck, hands or feet.

Disposable lab coats are best for working around long-lived radionuclides. Reusable lab coats are acceptable when handling short-lived radionuclides, provided they are stored for a sufficient time to permit decay of any contamination prior to being washed.

Both cloth and disposable lab coats may be reused if they are free from contamination and in good condition. They should be stored in a controlled area and you should monitor lab coats both during operations and after removing them. Particular attention should be paid to the sleeves, pockets and lower front surfaces of the coat.

All lab coats should be fire-resistant. Waterproof aprons, full-body jump suits and hoods provide additional protection in environments where the potential for more severe contamination is present.

D.7.2 GLOVES

Whenever your hands are near unsealed radioactive material, you should wear gloves.

Gloves are secondary protection only. They should not be used to handle radioactive materials directly. When you no longer need gloves, they should be carefully removed, monitored and disposed or stored appropriately.

Rips or holes make gloves ineffective. Be careful working around hot surfaces, sharp objects or chemicals that can attack the glove material.

Periodic changes of gloves are recommended. The greater the potential hazard, the more frequent a change of gloves is needed. Wearing two pair of gloves and frequently changing the outer pair is also a good safety practice.

Gloves should be monitored frequently. Don't use contaminated gloves or gloves that may be contaminated. If you are wearing gloves and they are exposed to radionuclides that emit penetrating radiation, remove the gloves as quickly as possible to minimize skin exposure. This is particularly important when handling high-energy beta emitters.

D.7.3 FOOTWEAR

Don't wear sandals or open-toe shoes. Comfortable, sturdy footwear should be selected that will protect against contamination or injury due to broken glass or corrosive materials.

In some cases, steel-toed shoes may be desirable to protect against physical hazards. In controlled areas where low-level floor contamination is a potential hazard, a separate pair of work shoes for use only in that area is a good idea. Disposable shoe covers of plastic or paper are available to prevent contamination of ordinary shoes. However, these can wear through rapidly and can be slippery.

D.7.4 EYE AND FACE PROTECTION

Safety glasses provide protection for your eyes and face; however, remember that this is secondary protection only.

Safety glasses are of some use in protecting against low penetration radiation, such as low-energy x-rays and medium-energy beta particles but provide little protection from penetrating gamma radiation.

D.7.5 RESPIRATORY PROTECTION

Contain operations that create radioactive dust, vapor or gases. Vented enclosures with protective filters are available for such operations.

In cases where entering a contaminated zone is unavoidable or in emergency situations, respiratory protection may be necessary. It may also be useful for certain decontamination operations.

If you wish to use respiratory protection, you first must have a medical examination. Also, you must be trained in the proper selection, fitting, operation and maintenance of the devices. Safety and medical departments within your organization are responsible for issuing authorizations to use respiratory protection and for maintaining records.



15 - 19 August 2011, William O. Jenkins Convention Centre, Puebla, Mexico

ACKNOWLEDGMENT

of the Attendance of:

AVRIL MEZA OLIVO

to the 22nd General Congress of the International Commission for Optics (ICO)

Fernando Mendoza Santoyo
General Conference Chair

Alejandro Cornejo
Conference Co-Chair



Development and characterization of a charged-particle prototype detector to be used in studies with radioactive ion beams

A. Meza-Olivo^{1,2,3}, A. Galindo-Uribarri^{1,2}, R. Ortega-Martínez⁴, E. Padilla-Rodas⁵
¹Physics Division, Oak Ridge National Laboratory, Oak Ridge TN 37831, USA
²Department of Physics and Astronomy, University of Tennessee, Knoxville TN 37996, USA
³Facultad de Ingeniería, UNAM, México City 04510, México
⁴Centro de Ciencias Aplicadas y Desarrollo Tecnológico, UNAM, México City 04510, México
⁵Instituto de Ciencias Nucleares, UNAM, México City 04510, México



Introduction:

High-resolution γ -ray spectroscopy using large arrays of HP-Ge detectors operated in conjunction with a variety of particle detection systems continues to be one of the most useful experimental techniques for nuclear spectroscopy at Radioactive Ion Beam (RIB) facilities. The new generation γ -ray spectrometers (GRETINA and the AGATA Demonstrator Array) operate on the principle of tracking the interaction sequence of the γ -ray. To fully utilize their capabilities in the study of nuclear reactions, new concepts of auxiliary charged-particle detectors that can provide better position/angle sensitivity are needed.

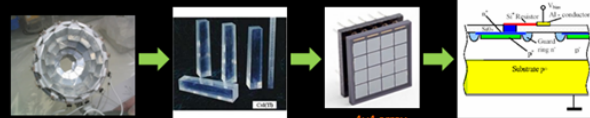
Exciting developments have taken place in the last few years concerning the silicon photomultipliers (SiPM), this technology consists of a multi-pixel silicon photodiode with a large number of micro-pixels, combined on a common substrate and working into a common load. Each pixel is operated in Geiger mode. These detectors exhibit high quantum efficiency, immunity to magnetic fields, good resolution and a gain of 10^6 (i.e. comparable to PMTs). We report on the characterization of a silicon photomultiplier coupled to various scintillators for charged particle detection and identification processing the signals using digital techniques.

Objective:

To characterize a prototype detector as a building block for an array of charged-particle detectors based on scintillators coupled to SiPMs. This array could be used as an auxiliary detector with the new generation of 4π -Gamma-ray spectrometers, such as GRETINA [1], to study the structure and properties of atomic nuclei.

Charged-particle detector

Array of CsI(Tl) coupled to SiPM



SiPM detectors are mounted onto a low profile ceramic package.

For CoulEx:

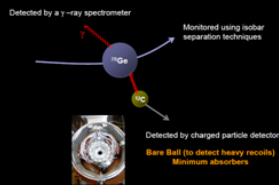
Detection of both reaction products: target-like and projectile-like with an angular resolution of $\sim 1^\circ$ in the lab frame (in θ and ϕ) will be crucial.

Since CoulEx reactions are binary in nature, the range of Q-values will be very small relative to the kinetic energy of the fragments, accurate kinematic reconstruction sufficient for a precise Doppler correction will be possible.

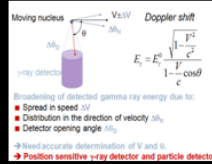
For Transfer Reactions:

Detection of target-like reaction products with an angular resolution of $\sim 4^\circ$ in the lab frame (or better) will be crucial. This is also the need of being able to clearly distinguish target-like recoils, e.g. carbon ions, from protons and alphas.

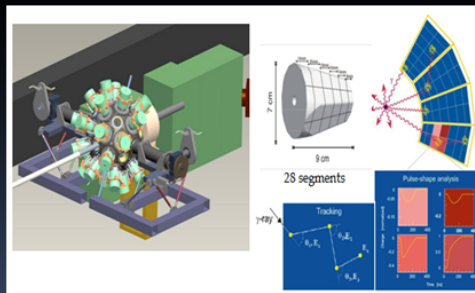
CoulEx in Inverse Kinematics with RIBs



Doppler Broadening Correction



Gamma Ray Tracking Principle



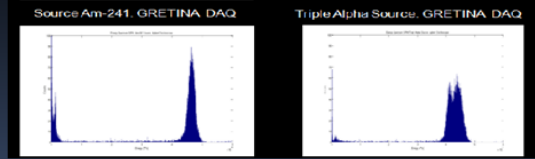
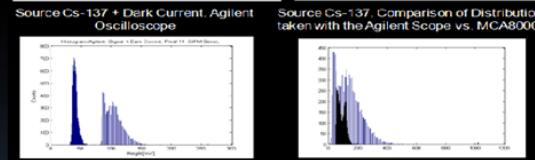
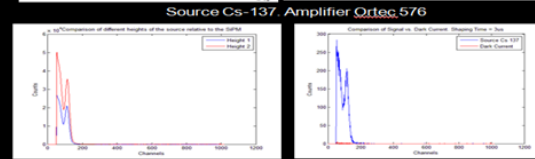
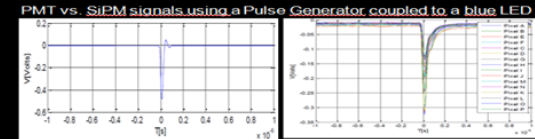
References:

- [1] <http://grfs1.lbl.gov>
- [2] J.R. Beane et al., "ISOL science at the Holifield Radioactive Ion Beam Facility", J. Phys. G: Nucl. Part. Phys. 38 (2011) 024002
- [3] A. Galindo-Uribarri, "Experiments with a 4 π Charged-Particle Detector and the 8 π Spectrometer", Prog. Part. Nucl. Phys. 46(2), pp. 463-472, 1992.

Acknowledgements:

- Research sponsored by the Office of Nuclear Physics, U.S. Department of Energy.
- Physics Division, Oak Ridge National Laboratory.
- Department of Physics and Astronomy, University of Tennessee Knoxville.
- Universidad Nacional Autónoma de México.
- Consejo Nacional de Ciencia y Tecnología, México.

Preliminary Results



Conclusions:

Up to now we have successfully tested a Sensi. SiPM using three different Data Acquisition Systems. The results obtained have shown that we are on the right way to develop a Charged-Particle detector based on CsI(Tl) scintillators coupled to SiPM's and to be able to make particle identification due to the properties of the CsI(Tl) crystals. Future work involves the characterization of some others silicon photomultipliers to be done into a vacuum chamber in order to improve the sensors resolution and sensitivity.